Turbidity and Light Attenuation in Coastal Waters of the Great Barrier Reef

Thesis submitted by

Rachael K. Macdonald

for the degree of Doctor of Philosophy Ph.D. (by research) Physics

in the College of Science, Technology and Engineering,

James Cook University, Townsville, Queensland,

Australia

December 2015

Primary Supervisor: Professor Peter V. Ridd

Email: rachael.macdonald@my.jcu.edu.au

Acknowledgments

I would firstly like to express my immense gratitude to Professor Peter Ridd. As a sharp-minded, passionate scientist and an absolute credit to his field, I was very fortunate to tackle this research under his supervision. Peter's enthusiasm for oceanography (and science in general) made a lasting impression upon me as an undergraduate physics student. He has since become an exemplary mentor, and advisor. Thank you Peter, for going above and beyond the call of duty, to ensure I could return to this research after the births of my two children. Thank you for knowing precisely when a little encouragement (pressure) was required, and conversely, when I needed support and understanding. And most of all, thank you for teaching me how to argue like a physicist!

A huge thank you to co-supervisor, Doctor James Whinney. Your attention to detail and enormous patience saw me through the most frustrating of equations and derivations. Your research experience and guidance was a priceless contribution to my work. Also, to the past and present employees of the Marine Geophysics Laboratory. Thank you for your assistance in field deployments, instrument calibrations and equipment preparation. Thank you for innumerable animated conversations (scientific or otherwise), your encouragement and friendship.

Last but not least, to my wonderful husband Simon. Words cannot properly convey my gratitude for all the hard work you have put in, during my time as a Ph.D. student. Thank you for the countless meals prepared, housework taken care of, words of encouragement, smiles of confidence and total support and for keeping our children happy, healthy and loved. Thank you also for all your help with my research and field work, particularly the boat driving (and trailer backing!)

I dedicate this thesis to my two beautiful children, Thomas and Piper. Always remember, you can do anything you put your mind to. Reach for the stars!

Statement of Access to Thesis

I, the undersigned, the author of this thesis, understand that James Cook University will make it available for use within University Library and, by microfilm or other means, allow access to users in other approved libraries.

All users consulting this thesis will have to sign the following statement:

> In consulting this thesis, I agree not to copy or closely paraphrase it in whole or in part without the written consent of the author; and to make proper public written acknowledgement for any assistance, which I have obtained from it.

Beyond this, I do not wish to place any other restriction on access to this thesis.

……………………………….. ………………………..

(Signature) (Date)

Declaration

I declare that this thesis is my own work and has not been submitted in any form for another degree or diploma at any university or other institution of tertiary education. Information derived from the published or unpublished work of others has been acknowledged in the text and a complete list of references is given.

R. K. Macdonald

14th December 2015

Statement of the Contribution of Others

Nature OF Assistance	Contribution	Names, Titles and Affiliations of Co-Contributors
Intellectual support	Supervisory support	Peter Ridd, James Whinney
Financial support	Field research Stipend School Top-up Grant	Marine Geophysics Laboratory Australian Postgraduate Award School of Science, Engineering and Technology
Data collection	Field assistance Instrumentation	Marine Geophysics Laboratory Marine Geophysics Laboratory

Included Publications

Chapter No.	Details of publication(s) on which chapter is based	Nature and extent of the intellectual input of each author, including the candidate
2	Macdonald R. K., Ridd P., Whinney J., Larcombe P., Neil D. (**2013**) *Towards environmental management of water turbidity within open coastal waters of the Great Barrier Reef*, Marine Pollution Bulletin, Volume 74, Issue 1, 15 September 2013, Pages 82-94.	The authors co-developed the research question. Macdonald assembled historical dataset, performed analysis and wrote the first draft of the paper which was revised with editorial input from Ridd, Whinney, Larcombe and Neil. Macdonald developed the figures and tables.
5	Macdonald R. K., Whinney J., Ridd P. (**submitted**) *Light attenuation and vertical turbidity profiles of coastal GBR waters*, Marine Pollution Bulletin, Submitted July 2015	Macdonald developed the research question, collected the data, performed analysis and wrote the first draft of the paper which was revised with editorial input from Ridd and Whinney. Macdonald developed the figures and tables.
4	Macdonald R. K., Whinney J., Ridd P. (**unpublished**) *The search for secondary turbidity drivers in coastal GBR waters*.	Macdonald developed the research question, assembled dataset, performed analysis and wrote the first draft of the paper which was revised with editorial input from Whinney and Ridd. Macdonald developed the figures and tables.

Abstract

Investigations were made into light attenuation and turbidity in coastal waters of the Great Barrier Reef (GBR). Turbidity and suspended sediment concentrations (SSC) cause increased light attenuation throughout the water column and can influence the location, nature and health of coral reefs and other marine biota. As a result, turbidity and light form an important part of marine monitoring and water quality plans. In the first part of this research (Chapter 2), typical inshore turbidity regimes were characterised using exceedance curves and derivatives, for 61 sites, representing the data-set with the largest spatial extent of any previously used for the GBR. Prior to this study, little published work documented 'typical' ranges of turbidity for reefs within coastal waters. The highest median turbidity (at 50% exceedance (T_{50})) was 15.3 NTU and at 90% exceedance (T_{90}) was 4.1 NTU. The GBRMPA guideline for mean annual concentration of total suspended solids (SSC) for open coastal waters is 2.0 mg l^{-1}. However, comparisons between mean and median turbidity showed large differences (up to a factor of 3), consistent with a strongly skewed temporal turbidity distribution. Exceedance results indicated strong spatial and temporal variability in water turbidity across inter/intraregional scales. Characterisation of turbidity regimes should contribute to the understanding of turbidity and SSC in the context of environmental management of coastal reefs.

The second part of this research explored the dominant (Chapter 3) and secondary (Chapter 4) drivers of turbidity. Wave-induced shear stress is a known dominant driver of inshore reef turbidity and resuspension of sediment occurs when critical bed shear-stress is reached. Wave-induced shear-stress was calculated from nephelometer-obtained pressure measurements, near the seabed in Cleveland Bay. Comparisons with concurrent turbidity measurements indicated the critical stress values required to induce sediment resuspension. A critical stress value of ~1 N/m^2 was found to be sufficient to produce turbidities in excess of 20 mg l^{-1} within Cleveland Bay. This was the first time shear stress had been calculated and related back to turbidity, using such instrumentation. The result is now being applied to water quality monitoring for consultancy, within the Marine Geophysics Laboratory. Using exceedance data, potential secondary turbidity drivers: water depth, distance to shore and distance to river were also investigated. Multiple linear regression and

stepwise quadratic/interaction regression analyses were implemented. No significant relationship was found between any of the potential secondary drivers and turbidity at 10, 50 and 90% exceedance levels. Results indicate that at these sites, the effect of rivers was too small to be measurable.

The final part of this research investigated the greatly overlooked relationship between turbidity and light (Chapter 5). Vertical light and turbidity (*T*) profiles were obtained and linked for the first time, at inshore GBR locations. Attenuation coefficients (k_d) were calculated over water-column intervals, producing linear relationships between k_d and turbidity ($R^2=0.91$). Site-specific, average diffuse attenuation coefficients are presented ($k_d^{AVG} = 0.43\ \mathrm{m}^{-1}$) and deconstructed into their clear-water ($k_d^{cl} = 0.3\ \mathrm{m}^{-1}$) and turbidity-based attenuation ($\alpha = 0.076\ \mathrm{m}^{-1}/\mathrm{NTU}$) components. A site-specific model predicting depth-averaged turbidity (T_{pred}) using light was implemented, producing a new method of measuring inshore, depth-averaged turbidity. Model results correlated well to measured turbidity (T_{avg}); T_{pred} = 1.0(T_{avg}) and $R^2=0.78$ (Cleveland Bay), and T_{pred} = 0.77(T_{avg}) and $R^2=0.68$ (Tully coast). The euphotic depth of Cleveland Bay was found to be 10 m for a depth-averaged turbidity of 2.5 NTU. Turbidity data is generally obtained near the seabed, due to the difficulty obtaining long-term depth profiles. However, strong linear relationships between depth-averaged turbidity and seabed turbidity were discovered. Depth-averaged turbidity was between 0.3-0.4 times seabed turbidity at all sites. Importantly, this finding may be extrapolated and used to infer depth-averaged values for all other (near seabed) data in the GBR. Finally, as an extension to the PAR light attenuation study, spectral attenuation coefficients were compared for inshore-offshore and shallow/deep waters of Cleveland Bay (Chapter 6). A hyperspectral radiometer was deployed to obtain exploratory light profiles. This enabled the behaviour of light across a spectrum of 137 individual wavelengths (from 300 ~ 800nm) to be measured. Results depict the variation of light attenuation coefficients across individual wavelengths. Spectral attenuation coefficients were compared to the PAR clear water attenuation component for Cleveland Bay. In Chapter 5, this component was calculated to be $k_d^{cl} = 0.3\ \mathrm{m}^{-1}$ and this was validated across the colour spectrum at offshore sites. This work has contributed to a broader understanding of light and turbidity in waters of the coastal Great Barrier Reef.

Table of Contents

Acknowledgments iii

Statement of Access to Thesis iv

Declaration v

Statement of the Contribution of Others vi

Included Publications vii

Abstract viii

Table of Contents x

Table of Figures xvii

Table of Tables xxi

Chapter 1. INTRODUCTION AND LITERATURE REVIEW 1

1.1 Introduction 1

1.2 Turbidity in the inshore GBR 2

1.3 Adverse effects of very high turbidity 5

1.4 External sediment supply to the inshore GBR 7

1.5 Wave-induced sediment resuspension 8

1.6 Turbidity levels may not be increasing in the inshore GBR 11

1.7 Environmental management of GBR turbidity 12

1.8 Light attenuation and turbidity 14

Chapter 2. MEASURING TURBIDITY AND EXCEEDANCE ANALYSIS 22

2.1 Abstract 22

2.2 Introduction 23

2.2.1 Turbidity and the Great Barrier Reef 23

2.2.2 Relationship of turbidity to suspended sediment concentration 24

2.2.3 Turbidity and SSC in environmental management 26

2.3 Materials and methods 28

2.3.1 Instrumentation and data collection 28

2.3.2 Data handling methods 29

2.4 Site locations 31

2.4.1 Region 1: Moreton Bay 31

2.4.2 Region 2: Hay Point 32

2.4.3 Region 3: Cleveland Bay and Magnetic Island 33

2.4.4 Region 4: Paluma Shoals and Rattlesnake Island 33

2.4.5 Region 5: Mission Beach and Family Group Islands 34

2.4.6 Region 6: Frankland Islands 34

2.4.7 Region 7: Port Douglas and Alexandra Shoals 35

2.4.8 Region 8: Princess Charlotte Bay and region 35

2.5 Results 44

2.5.1 Turbidity time series 44

2.5.2 Mean and median (T_{50} Exceedance) turbidity 45

2.5.3 Overview of turbidity exceedance patterns 46

2.5.4 Weighted means and exceedance low-high ranges 48

2.5.5 Exceedance for Nelly Bay sites wet and dry seasons 51

2.5.6 Nelly Bay and Princess Charlotte Bay 2011-2002 wet season comparison.... 53

2.6 Discussion.. 55

Chapter 3. WAVE SHEAR STRESS – DOMINANT TURBIDITY DRIVER 63

3.1 Introduction 63

3.2 Calculation of maximum bottom shear-stress.. 67

3.2.1 Above the wave boundary layer 69

3.2.2 Inside The Wave Boundary Layer 69

3.2.3 Calculation of Friction Factor and Effective Drag Coefficient 71

3.3 Calculation of wave-induced shear-stress from pressure 74

3.4 Results.. 75

3.5 Discussion.. 79

Chapter 4. THE SEARCH FOR SECONDARY DRIVERS OF TURBIDITY 82

4.1 Abstract.. 82

4.2 Introduction 83

4.2.1 Turbidity and suspended sediment.. 84

4.2.2 Dominant turbidity drivers.. 85

4.2.3 Turbidity exceedance 86

4.3 Methods 87

4.3.1 Water depth 88

4.3.2 Distance to mainland and river 88

4.3.3 Multivariable Regression 89

4.4 Site locations 90

4.5 Data table 93

4.6 Results 95

4.6.1 Turbidity and distance to mainland 96

4.6.2 Turbidity and distance to river mouth 99

4.6.3 Turbidity and water depth 101

4.6.4 Region typing 103

4.7 Analysis 105

4.8 Discussion 110

4.8.1 Multivariable regression 110

4.8.2 Region Typing 111

4.8.3 Concluding remarks 112

Chapter 5. LIGHT ATTENUATION AND VERTICAL TURBIDITY PROFILES 116

5.1 Abstract 116

5.2 Introduction 117

5.3 Theory 119

5.3.1 Calculation of the diffuse attenuation coefficient (*k_d*) 119

5.3.2 Euphotic depth calculations 121

5.4 Methods 122

5.4.1 Instrumentation 122

5.4.2 Sites and data collection 124

5.5 Results 126

5.5.1 Time series 126

5.5.2 Relationship between k_d and turbidity 127

5.5.3 Relationship between depth-averaged and seabed turbidity 130

5.5.4 Use of light and depth data to infer turbidity 132

5.5.5 Coral photic depth thresholds for the coastal GBR 135

5.6 Discussion 137

5.6.1 Attenuation coefficient as a function of turbidity 137

5.6.2 Investigating turbidity and depth 138

5.6.3 Predicting turbidity from light data 139

5.6.4 Coral photic depth thresholds 141

5.6.5 Extreme weather events 142

Chapter 6. SPECTRAL IRRADIANCE ATTENUATION COEFFICIENTS 147

6.1 Introduction 147

6.2 Theory 150

6.2.1 Calculation of the spectral diffuse attenuation coefficients ($kd\lambda$) 150

6.3 Methods 151

6.3.1 Location 151

6.3.2 Instrumentation 152

6.4 Results 153

6.4.1 Variation of attenuation coefficient with depth 153

6.4.2 Variation of attenuation coefficient with site and wavelength 158

6.4.3 Comparing Attenuation Coefficients for PAR and depth 159

6.5 Discussion 161

Chapter 7. CONCLUDING REMARKS 164

Appendix A – The Inner Continental Shelf 167

Appendix B – Linear Wave Theory 170

Surface gravity wave propagation – Basic theory 170

Assumptions 171

Mathematical Formulation: 172

Appendix C - Orbital Wave Motion and Shear Stress Theory 176

Orbital wave motion – Basic theory 176

i) Deep water waves 177

ii) Shallow water waves 178

iii) Intermediate depths 179
iv) Graphing bottom orbital velocity 179
Shear stress - basic theory 184
i) Constant shear stress contours 189
Appendix D – Matlab Programs: 191
resuspension.m (see Chapter 3) 191
turbidityFACTORS.m (see Chapter 4) 198
exceedanceProg3.m (see Chapter 2) 210
Appendix E - Light Attenuation Theory and Derivations 214
Introduction 214
(i) The scattering coefficient 215
(ii) The absorption coefficient: 215
(iii) Total Attenuation and the attenuation coefficient 216
Derivations of irradiance 217
(i) Case 1: SPC not dependant on depth (derivation of Beer-Lambert's Law) 219
(ii) Case 2: Concentration as a linear function of depth 221
(iii) Case 3: Concentration as an exponential function of depth 222
REFERENCES 226

Table of Figures

Figure 1 Locations of the eight regions used in this paper 36

Figure 2 (a-g) Locations of turbidity monitoring sites across eight study regions. (a) Moreton Bay, (b) Hay Point and Mackay, (c) Cleveland and Halifax Bay, (d) Mission Beach and Family group, (e) Frankland Islands, (f) Alexandra Shoals and Port Douglas, (g) Princess Charlotte Bay 39

Figure 3 Turbidity data acquisition time periods, for 8 regions across the Great Barrier Reef and Moreton Bay. Data was acquired between 1993 to 2009.Apr)) 44

Figure 4 Turbidity time series for Nelly Bay3 (site 14) during February 2002 45

Figure 5 Turbidity time series for June Reef2 (site 59) during February 2002. 45

Figure 6 Mean turbidity and T50 exceedance data for all 61 sites. 46

Figure 7 Exceedance curves for all regions. Curves presented are those for the site with the lowest T_{50} value in each region. 47

Figure 8 Exceedance curves for all regions. Curves presented are those for the site with the highest T_{50} value in each region. 48

Figure 9 Lowest T_5 value, highest T_5 value and mean T_5 value (weighted by length of deployment) for each region. 49

Figure 10 Lowest T_{10} value, highest T_{10} value and mean T_{10} value (weighted by length of time series), for each region. 49

Figure 11 Lowest T_{50} value, highest T_{50} value and mean T_{50} value (weighted by length of deployment), for each region. 50

Figure 12 Lowest mean turbidity, highest mean turbidity and mean of mean-turbidity (weighted by length of deployment) for each region. 50

Figure 13 Nelly Bay1 (site12) exceedance curves for the wet and dry seasons of 2001 and 2002. 51

Figure 14 Nelly Bay2 (site13) exceedance curves for the wet and dry seasons of 2001 and 2002. 52

Figure 15 Nelly Bay3 (site14) exceedance curves for the wet and dry seasons of 2001 and 2002. 52

Figure 16 Nelly Bay4 (site15) exceedance curves for the wet and dry seasons of 2001 and 2002. 53

Figure 17 Wet season exceedance for PCB (solid lines) and Nelly Bay (dotted blue lines) across 2001 & 2002. 54

Figure 18 Picture of a Nephelometer. This water quality monitoring instrument logs turbidity (using an optical backscatter sensor), pressure, light and temperature. Featuring Campbell logger hardware. 65

Figure 19 Relationship of RMS pressure fluctuations to turbidity. 66

Figure 20 Calculated significant wave height and turbidity time series for the Cleveland Bay dataset. Each H_{sig} value is calculated from 10 individual pressure measurements, the sensor height from the bed (0.3 m) and sampling frequency of 1 Hz. 77

Figure 21 Significant wave height (m) and RMS wave height (m) calculated from calibrated pressure measurements (Average water depth (m)). Data from Cleveland Bay 2013. 78
Figure 22 Calculated wave-induced bottom shear stress and concurrent turbidity time series for Cleveland Bay. Site specific constants include mean depth = 12 m, bottom roughness = 0.0025, mean current = 0.1 m/s and mean period = 4.9 s (Orpin 1999). Critical stress limit for resuspension shown (1 N/m^2) (Orpin 1999). ... 78
Figure 23 Maximum shear-stress calculated using various sig wave heights (H_{sig}) vs. wave period. H_{sig} of 2.29 m and 0.5 m are calculated from measured data during high and low turbidity event respectively. Other wave heights taken from the literature for mean turbidity (0.66 m) and a cyclonic event (2.34, 3.58 m) (Justin - Cat 0). Critical stress limit taken from the literature (1 N/m^2). Mean wave period in Cleveland Bay is 4.9 s. Results show during high turbidity events, bottom shear stresses exceed critical stress limit, realistic wave period..... 79
Figure 24 Map showing: 7 turbidity regions across the inshore Great Barrier Reef (top). Numbered sites within Cleveland Bay region (bottom) (see Table 4). 91
Figure 25 Turbidity (NTU) vs. distance to mainland (km) across all sites. Turbidity is displayed at 10 %, 50, % and 90 % Exceedance. 97
Figure 26 Cleveland Bay deployments showing turbidity exceedance vs distance to mainland at 10 % turbidity exceedance (top), 50 % turbidity exceedance (middle) and 90 % turbidity exceedance (bottom). 98
Figure 27 Turbidity (NTU) vs. distance to closest major river (km) across all sites. Turbidity is displayed at 10 %, 50, % and 90 % Exceedance.. 99
Figure 28 Cleveland Bay deployments showing turbidity exceedance vs distance to closest major river at 10 % turbidity exceedance (top), 50 % turbidity exceedance (middle) and 90 % turbidity exceedance (bottom)..... 100
Figure 29 Turbidity (NTU) vs. average water depth (m) across all sites. Turbidity is displayed at 10 %, 50, % and 90 % Exceedance. 101
Figure 30 Cleveland Bay deployments showing turbidity exceedance vs average water depth at 10 % turbidity exceedance (top), 50 % turbidity exceedance (middle) and 90 % turbidity exceedance (bottom). 102
Figure 31 Exceedance curves grouped by type. Type 1: Shore-attached fringing reefs including Paluma Shoals, Alexandra Shoals and Port Douglas sites. Wide variation in turbidity is seen across this type......................... 104
Figure 32 Exceedance curves grouped by type. Type 2: Muddy Embayment – all Cleveland Bay sites. Wide variation in turbidity is seen across this type and the generalised turbidity regime follows an exponential decay curve until flattening out around 10 NTU... 104
Figure 33 Exceedance curves grouped by type. Type 3: All other sites. Very wide variation in turbidity is seen with generalised turbidity regime exceeding 1 NTU about 65% of the time. The type also follows a weak linear decay curve... 105
Figure 34 Measured median turbidity vs. multivariable linear regression model... 106
Figure 35 Stepwise linear regression model with inverted, quadratic term. Model R^2 value is 0.099 and P-value is 0.012. No physically significant linear correlation is found between measured turbidity and combinations of interaction and quadratic terms... 108
Figure 36 Measured turbidity (T50) vs. colourmap model generated from stepwise regression. Combining depth and distance to shore terms, (top). Combining depth and Distance to river terms (bottom)................ 109

Figure 37 Schematic of instrument setup defining instrument numbers and intervals used in light attenuation calculations. 123

Figure 38 Section of North Queensland Coastline depicting portion of Great Barrier Reef and locations for quad-nephelometer deployments, Cleveland Bay (CB) and Tully coast (T1 and T2). 125

Figure 39 Time series data at Tully site T1. Top image: Water depth. Instrument 1 is located closest to the surface, followed by instruments 2 and 3. Instrument 4 is located closest to the seabed. Middle image: Turbidity (labelled with high and low turbidity event) nb. turbidity plotted on a log scale. Bottom: Light. 127

Figure 40 Light attenuation coefficients (calculated for depth interval 4) versus depth-averaged turbidity. Data are between 10am-2pm and hourly averaged. a: CB, $\alpha = 0.07\ m - 1/NTU$), $kdcl = 0.3\ m - 1$ and $R^2 = 0.91$. b: T1, $\alpha = 0.04\ m - 1/NTU$, $kdcl = 0.41\ m - 1$ and $R^2 = 0.66$. c: T2, $\alpha = 0.037\ m - 1/NTU$, $kdcl = 0.40\ m - 1$ and $R^2 = 0.79$. 129

Figure 41 Light attenuation coefficients (calculated for depth intervals 1, 2 and 3) versus depth-averaged turbidity. Data are between 10am-2pm and hourly averaged. a: CB b: T1 c: T2. 130

Figure 42 Depth-averaged turbidity (averaged over all four instruments) versus seabed turbidity. Data are hourly averages. a: CB, $Tavg = 0.40Tbed + 2.1$ and $R^2 = 0.96$. b: T1, $Tavg = 0.30Tbed + 0.92$ and $R^2 = 0.99$. c: T2, $Tavg = 0.38Tbed + 0.26$ and $R^2 = 0.99$. 131

Figure 43 Predicted (depth-averaged) turbidity (T_{pred}) vs. measured (depth-averaged) turbidity (T_{avg}). Light data < 0.5 $\mu E\ m - 2s - 1$ are omitted. T_{pred} constants: $\alpha = 0.076\ m - 1NTU - 1$ and $kdcl = 0.3\ \mathrm{m} - 1$ calculated from CB data. a: (Training) CB data segment (10 am – 2 pm). b: Remainder of CB dataset (2pm-10am), T_{pred} = 1.0(T_{avg}) and $R^2 = 0.77$. c: T1 dataset, T_{pred} = 0.61(T_{avg}) and $R^2 = 0.64$. d: T2 dataset T_{pred} = 0.56(T_{avg}) and $R^2 = 0.69$. 134

Figure 44 Predicted (depth-averaged) turbidity (T_{pred}) vs. measured (depth-averaged) turbidity (T_{avg}). Light data < 0.5 $\mu E\ m - 2s - 1$ are omitted. T_{pred} constants: $\alpha = 0.041\ \mathrm{m} - 1\mathrm{NTU}$ and $kdcl = 0.4\ \mathrm{m} - 1$ calculated from T1 data. a: T1 data segment (2 pm - 10 am), T_{pred} = 0.77(T_{avg}) and $R^2 = 0.68$. b: T2 data segment (2 pm – 10 am), T_{pred} = 0.65(T_{avg}) and $R^2 = 0.78$. 135

Figure 45 Irradiance curves for Cleveland Bay depicting euphotic depths for depth-averaged turbidities. Light curves are modelled (equation 1), I_0(maxima) = 1925 $\mu\mathrm{E\ m} - 2s - 1$. Photic limit is 1% of I_0(maxima). Close-up inset: For depth-averaged turbidity of 2.5 NTU, photic depth is 10 m. For depth-averaged turbidity of 5 NTU and 10 NTU, photic depths are 6.7 and 4.3 m respectively. 136

Figure 46 (The author) Rachael and Simon Macdonald performing exploratory research with hyperspectral radiometer, on the RV James Kirby in Cleveland Bay, September 2015. 148

Figure 47 Routes 1 and 2 depicting data collection waypoints (light and depth) across Cleveland Bay. 152

Figure 48 Measured irradiance uW/cm^2/nm) vs wavelength (nm) for offshore site 10 in Cleveland Bay (total depth ~ 11m). 154

Figure 49 Measured irradiance uW/cm^2/nm) vs wavelength (nm) for offshore site 9 in Cleveland Bay (total depth ~ 10m). 154

Figure 50 Attenuation coefficient vs. wavelength for offshore site 10 in Cleveland Bay (total depth ~ 11m). Kd is calculated over 2 m intervals from the surface to (near) seabed. 155

Figure 51 Attenuation coefficient vs. wavelength for offshore site 9 in Cleveland Bay (total depth ~ 10m). Kd is calculated over 2 m intervals from the surface to (near) seabed. 156
Figure 52 Attenuation coefficient vs depth for a selection of wavelengths offshore site 10 (Cleveland Bay). .. 157
Figure 53 Attenuation coefficient vs depth for a selection of wavelengths at offshore site 9(Cleveland Bay). 157
Figure 54 Attenuation coefficients (surface-2m) vs wavelength for both inshore and offshore sites. The general variation of kd with wavelength is also observed. 158
Figure 55 Attenuation coefficient for 6-8 m depth interval vs wavelength for several deep water/offshore sites. The general variation of k_d with wavelength is observed. 159
Figure 56. Water depth (hourly averaged) versus attenuation coefficient k_{dPAR}. k_{dPAR} is calculated using hourly averaged light and depth data, over 3 depth intervals and appended (Chapter 5). 160
Figure 57 PAR Attenuation coefficient and turbidity (both hourly averaged) vs. water depth for 3 days of "low turbidity" conditions (data taken from 10am-2pm only). January 2013. The turbidity regime is similar to that during the spectral radiometry dataset (September 2015) (although turbidity measurements were not obtained on this later field trip). Attenuation coefficients approximate 0.3 m^-1 as calculated for the clear water component in Chapter 5. 161
Fig 58 Depiction of the continental shelf. 167
Figure 59 Fluid particles in orbital motion 176
Figure 60 Horizontal Bottom Orbital Velocity Vs. Wave Period - For a depth of 10 m and Wave Heights of 0.5, 1.5 and 3 m respectively. 182
Figure 61 Horizontal Bottom Orbital Velocity Vs. Wave Period - For a depth of 50 m and Wave Heights of 0.5, 1.5 and 3 m respectively. 182
Figure 62 Horizontal Bottom Orbital Velocity Vs. Wave Period - For a depth of 200 m and Wave Heights of 0.5, 1.5 and 3 m respectively. 183
Figure 63 Constant wave-induced bottom shear stress theoretical contours. 189
Figure 64 Constant current-induced bottom shear stress theoretical contours. 190
Figure 65 Constant maximum bottom shear stress theoretical contours. 190
Figure 66 diagram showing attenuation of monochromatic light beam. 218

Table of Tables

Table 1 Site and region data and location information 39

Table 2 Mean turbidity and turbidity exceedance values (T_5, T_{10}, T_{50} and T_{90}) for each site. 41

Table 3 Timings of Nelly Bay and Princess Charlotte Bay data. Wet season is defined as November to April (inclusive). 43

Table 4 Site Information taken from Macdonald et al. (2013). 93

Table 5 Mean turbidity, exceedance (T_{10}, T_{50}, T_{90}), depth, distance to mainland, distance to river data. 95

Table 6 Stepwise regression analysis of independent variables, depicting ten independent variables and the generated statistics. 106

Table 7 Site locations for light attenuation study 125

Chapter 1. INTRODUCTION AND LITERATURE REVIEW

1.1 Introduction

This chapter covers a review of the current literature related to suspended sediment, water turbidity and light attenuation in the inshore Great Barrier Reef (GBR). The review is divided into eight sections. Section 1.2 defines turbidity and describes its variability across the inshore GBR. Section 1.3 covers documented adverse biological effects of high turbidity and suspended sediment. Section 1.4 discusses the contribution of riverine sediment supply to turbidity. Section 1.5 covers existing research on the correlation between wave-induced sediment resuspension and turbidity. In section 1.6, the argument that turbidity levels are not increasing in the GBR is explored. Section 1.7 covers current environmental management of turbidity in the GBR. Finally, Section 1.8 explores the current literature connecting light attenuation and turbidity on the inshore GBR.

In Chapter 2, an analysis of the largest turbidity data set across the Great Barrier Reef (GBR) is presented, which aims to define typical turbidity regimes, using exceedance curves and derivatives. Wave-induced shear stress is a known dominant driver of inshore turbidity. The aim of Chapter 3, is to calculate shear stress from pressure measurements near the seabed. Comparisons with concurrent turbidity measurements are presented, depicting critical stress levels required for sediment resuspension. The aim of Chapter 4 is to investigate the relationship of turbidity to several potential underlying factors such as proximity to rivers, water depth and distance to shore. Chapter 5 introduces light attenuation and describes how vertical profiles of light and turbidity were obtained. The aim of this chapter is to mathematically link light attenuation to turbidity for the first time, for inshore GBR locations. A site-specific model predicting depth-averaged turbidity using light was implemented. A relationship between water column turbidity and seabed turbidity is described. Findings are presented that can be used to infer depth-averaged values for all other seabed turbidity data in the GBR. Lastly in Chapter 6, spectral irradiance attenuation coefficients were obtained as an extension to the light study which utilised PAR. Results are presented for 137 individual wavelengths at inshore/offshore locations, over various depths and compared to the PAR attenuation component for clear water.

1.2 Turbidity in the inshore GBR

The Great Barrier Reef (GBR) is the largest and most bio-diverse coral reef eco-system in the world, extending over 14 degrees of latitude (Maxwell 1968; Hopley 1982; Hopley et al. 2007). Water turbidity is a transient phenomenon which is largely spatially and temporally variable (Orpin et al. 2004). Turbidity in the inshore or coastal region of the GBR is a major focus for research due to land proximity, exposure to catchment runoff, dredging activities and coastal development (Furnas 2003; Brodie et al. 2005; Fabricius 2005; GBRMPA 2010; REEFPLAN 2013).

Turbidity measures the cloudiness of water and is measured by detecting scattering of light. Scattering is predominantly caused by suspended sediment in the water column, but is also related (to a lesser degree) to algae, micro-organisms and other particulate matter. Turbidity is often closely related and 'calibrated' to suspended sediment concentration (SSC) (Larcombe et al. 1995b) but is also dependent upon a wide range of sedimentary variables, especially those related to grain size and type (Ludwig and Hanes 1990; Conner and De Visser 1992; Wolanski et al. 1994; Bunt et al. 1999).

Natural or background concentrations of suspended sediment refer to concentrations that are not directly caused by anthropogenic activity. Background SSCs on inshore fringing reefs of the GBRL have not been thoroughly investigated, which is partly due to the difficulty in disassociating natural and anthropogenic effects. However, background concentrations vary with factors such as bed type, and the nature of waves and currents experienced, so that that variation is often locally and seasonally controlled. A mean estimate for fringing reefs near Magnetic Island and around Cleveland Bay is ca. 5 mg l^{-1} (Larcombe et al. 1995b), where concentrations were generally less than this in a 4 month-long period (Larcombe et al. 1995b). These are, it should be noted, measurements of turbidity calibrated to SSC. However, within this location, sediment resuspension frequently results in SSCs > 20 mg l^{-1} (Gilmour 1999; Anthony et al. 2004). SSCs at soft-bottomed sites within Cleveland Bay and Halifax Bay (inshore GBR) are regularly in excess of 100 $^{mg\ l-1}$ for 2-3 day periods (Larcombe et al. 1995b; Larcombe et al. 2001) and during strong swell wave events these concentrations exceeded 200 mg l^{-1}. In Nelly Bay, a fringing reef setting in Cleveland Bay, turbidity varied by four orders of magnitude (0.1 to >100 NTU) over a 37-day period, and high turbidity events occurred simultaneously with high winds and associated high sea states, whereas during calm weather, turbidity was <1 NTU (Orpin et al. 2004).

Turbidity is intricately connected to irradiance. Variations to irradiance are caused by turbidity. In a two year study (Anthony et al. 2004), contributions of turbidity, clouds and tides to variations in irradiance were examined and used to predict benthic primary productivity. The study site is located within Cockle Bay, Townsville; on a turbid-zone fringing coral reef in the GBR lagoon. Benthic irradiance was shown to follow major and minor cycles, where turbidity is a primary driving force. It was reported that 74-79% of the total annual irradiance variation may be attributed to attenuation by suspended solids i.e. turbidity. As depth is increased, irradiance variation caused by turbidity increased asymptomatically to 95%. Clouds are found to account for 14-17% relative irradiance variation and tides for 7-10%. This pattern is compared to predictions of physiologically optimal irradiance for the coral, *Turbinaria mesenterina.* It is suggested that the coral oscillate between states of photoinhibition (light stress) and energy deficiency (light limitation), and that this cycle is governed strongly by turbidity variations. A dynamic photosynthesis-irradiance model was employed to analyze the effect of this benthic irradiance pattern on temporal patterns of photoinhibition of primary producers.

Spatial and temporal variations in light are connected to cloud formation patterns as well as turbidity levels. These variations affect energy balances of many aquatic primary producers, in particular benthos. In general, the combined effect of cloud, turbidity and tide variations on the weekly-monthly light patterns is unknown for coastal benthic habitats. This work by Anthony et al (2004) was the first to examine and quantify the relative contributions of the environmental factors causing temporal variation in irradiance and then make predictions based on this analysis on benthic primary productivity.

1.3 Adverse effects of very high turbidity

Although sediment plays a vital role in and around inshore reefs, very high levels of suspended sediment in the water column can adversely affect coral growth and reproduction (Goatley et al. 2013). Laboratory and field experiments were performed on the coral *Acropora digitifera* and it was found that suspended sediment can inhibit fertilisation, larval survival and settlement (Gilmour 1999). Extreme turbidity levels are a contributing stress factor for many benthic organisms (Rodgers 1990; Brown 1997). The reduction of light in turbid water can hinder coral (Anthony and Fabricius 2000) and seagrass photosynthesis (Stafford-Smith 1993). Transplanted eelgrass was studied in nutrient and turbidity gradients by Moore et al. (1996). Poor long-term eelgrass survival is found to be related to seasonally high levels of water column light attenuation (Moore et al. 1996). An important study by Anthony and Fabricius (2000) involved an experimental analysis on suspended particulate matter (SPM) and contrasting light effects on coral energy budgets. They examined two zooxanthellate corals, *Goniastrea retiformis* and *Porites cylindrical*. It was shown that periods of high turbidity resulted in energy deficiency in *P. cylindrical*. Interestingly, under the same conditions *G. retiformis* thrived. This particular coral appears to possess an ability to offset such stresses from very high particle loads (Anthony and Fabricius 2000).

Potential stress thresholds for some coastal corals were quantified by Cooper et al. (2008) using an 18 month data set of water turbidity at Horseshoe Bay on the northern side of Magnetic Island, a continental island located within Cleveland Bay, a soft-bottomed embayment off Townsville with water depths ranging from about 3-13 m. Shallow areas were defined as being 2 m below LAT. The site is also occasionally influenced by river plumes and lies 100 km north of the mouth of the Burdekin River, the largest single riverine source of sediment to the GBRL (Belperio 1983). Turbidity greater than 20 NTU occurred mostly during high wind events and was interpreted as caused by wave resuspension within Cleveland Bay, with subsequent advection to Horseshoe Bay by tidal currents. Turbidity exceeded 50 NTU during Tropical Cyclone Larry in March 2006 and during a high wind event in February 2007. Flooding of the Burdekin River was also recorded during the period of February 2007. This was commented upon by Orpin and Ridd (using the same data set) who showed that there was no relationship between the Burdekin plume and the turbidity at Horseshoe Bay (Orpin and Ridd 2012). Analysing coral bioindicators for water quality, the study concluded that long-term (ca. 2 years) turbidity >3 NTU leads to sub-lethal coral stress and >5 NTU may represent a threshold for severe stress on corals in shallow areas (Cooper et al. 2008).

Sedimentation in large amounts may also smother the surface of corals and other organisms (Rodgers 1990; Fabricius and Wolanski 2000; Orpin et al. 2004). This can cost the coral energy, as mucous is excreted to remove the deposition, and may be lethal in some cases. In particular, high levels of muddy sediment and bio-nutrients may mix to produce large sticky aggregate particles, known as marine snow (Fabricius and Wolanski 2000). The increased size and viscoid nature of marine snow may well increase the chances of coral smothering as it is far more difficult for the corals to remove than fine sediment. Smothering can eventually lead to coral death (Fabricius and Wolanski 2000).

1.4 External sediment supply to the inshore GBR

It is widely accepted that terrigenous sediment supply to the Queensland coastline over the last two hundred years is increasing due to anthropogenic impact on Central Queensland catchments (Moss et al. 1993; Fabricius and Wolanski 2000; McCulloch et al. 2003a; Pandolfi et al. 2003; Orpin and Ridd 2012). There is significant concern within the scientific community regarding whether the increase in external sediment supply (e.g. terrestrial sediment supplied by rivers) is having a significant impact on the reef and has led to the hypothesis that riverine sediment discharge is a significant driver of turbidity levels (Wolanski et al. 2004; Brodie et al. 2005; Wolanski and De'Ath 2005; Wolanski et al. 2008; Lambrechts et al. 2010; De'ath et al. 2012; Fabricius et al. 2012).

Establishing a causal relationship between the increase in terrestrial runoff and the degradation of the GBR is difficult. Fabricius (2005) discussed the direct effects of terrestrial runoff on coral and other reef organisms; growth, survival and reproduction (Fabricius 2005). The high variability of parameters were well recognized in this study and it was noted that the severity of responses to terrestrial runoff depends on a number of factors including the physical, hydrodynamic, spatial and biological properties of the location.

A recent paper examined the main determinants of inshore turbidity using 3 years of almost continuous turbidity data (Fabricius et al. 2012). Effective wave height was found to be the major driver and secondary turbidity signals were also found for river distance and river discharge. In the study wave resuspension was also confirmed as the dominant turbidity driver and it was the first study to document secondary turbidity drivers on the GBR (Fabricius et al. 2012). The greatest source of external nutrients to the Great Barrier Reef (GBR) is river runoff (Fabricius and Wolanski 2000). Sediment and nutrients are discharged into the inner lagoon of the GBR during flood events via plumes. Turbid river flood plumes can appear quite impressive, but carry minimal sediment loads and have short term, local effects on inner shelf turbidity (Orpin and Ridd 2012; Fabricius et al. 2014). In terms of direct sedimentation and compared to suspended sediment concentrations (SSC) caused by waves, it has been proposed that river plumes do not substantially impact mid and outer sites of the GBR shelf (Larcombe and Woolfe 1999a). Instead, wave-induced resuspension of sediment is be the predominant mechanism facilitating SSC on inshore reefs (Orpin and Ridd 2012).

1.5 Wave-induced sediment resuspension

It is well established that wave-induced resuspension of pre-existing bed sediment is the dominant driver of turbidity in coastal reef waters (Larcombe et al. 1995b; Larcombe et al.

2001; Anthony et al. 2004; Orpin et al. 2004; Cooper et al. 2008; Orpin and Ridd 2012). Turbidity is correlated to wave height, wave period and tidal range and also wind speed (Larcombe et al. 1995b; Fabricius et al. 2012). Regular resuspension of large amounts of sediment is likely to have always occurred around reefs as frequent SE winds around inshore reefs cause waves to exert high shear stresses on the seabed. This in turn stirs fine sediment on the seabed up into the water column, causing periods of high turbidity/SSC (Orpin et al. 1999). It is probable that the wind events and sediment availability on the seabed have not significantly altered since European settlement. Larcombe and Woolfe (1999a,b) were the first to recognise that SSC in the GBR is predominantly caused by sediment resuspension and not by river plumes. Until very recently, this theory was not universally acknowledged and there is still significant concern that terrigenous supply is causing reef degradation (Larcombe and Woolfe 1999a,b; GBRMPA 2010; REEFPLAN 2013; Fabricius et al. 2014).

There are many examples in the literature indicating a correlation between high wave events and increased turbidity. Orpin et al. (2004) presented data from Geoffrey Bay and Nelly bay, showing high turbidity levels exceeding 100 NTU, and remained elevated above 10 NTU for several days (Orpin et al. 2004) .

A substantial study of water turbidity at Horseshoe Bay on Magnetic Island was presented by Cooper et al. (2008). This site is occasionally affected by the river plume of the Burdekin River. It lies 100km from the mouth of the Burdekin River, the largest external source of sediment to the GBRL. High levels of turbidity (greater than 20 NTU) recorded in Cooper et al. (2008), occurred predominantly during high wind events and interpreted as caused by wave resuspension. The peak turbidity measured greater than 50 NTU, occurring during Tropical Cyclone Larry in March 2006 and a high wind event in February 2007. Burdekin river flooding was also recorded during this period (Cooper et al. 2008). This can be a contentious issue, since there is some difficulty in resolving the influence of flood plumes from resuspension events. This arises because flood plumes often occur around high wind and storm activity, which generally also cause elevated sea states. Therefore, resuspension events are likely to occur simultaneously with river flood plumes. However, most high turbidity events in the study by Cooper et al. (2008) were associated with high winds rather than flooding, implying that wave induced re-suspension is the primary mechanism involved. Conversely, the influence of concurrent visible plumes must not be disregarded entirely (Ridd 2010; Orpin and Ridd 2012) .

Results from the study by Anthony et al (2004) demonstrated that daily seabed irradiances frequently fall to less than 10% of the irradiance maxima and remain so for up to two weeks. There were considerable irradiance fluctuations throughout the two year period of this study, with two primary cycles identified; a strong 8 week cycle and a weaker 3-4 week. As mentioned above, this appears to be predominantly turbidity driven and secondarily affected by cloud changes. The strong 8-week cycle is thought to reflect the large scale pressure systems in the tropics – the Madden-Julian atmospheric oscillation. Tides were also important, producing a two-week irradiance cycle. Based around prior work (Larcombe et al. 1995b) it was concluded in the study that the key mechanism driving turbidity in Cleveland bay is wave resuspension, and that tidal currents are of some minor influence. This is further substantiated by a strong fit of predicted irradiance fluctuations to observed wind speeds (Anthony et al. 2004).

1.6 Turbidity levels may not be increasing in the inshore GBR

Recent geological data and assessments of sedimentary processes on the *central* section of the GBR shelf have demonstrated that it is not obvious that sedimentation accumulation rates and turbidity levels at most coral reefs would be increasing despite the higher sediment loads delivered by rivers (Larcombe and Woolfe 1999a; Orpin and Ridd 2012). Larcombe and Woolfe (1999 a,b) use geological data and hydrodynamic theory to show that elevated SSC is generally caused by seabed-sediment resuspension, due to waves and not by flood plumes. They conclude that increased sediment supply to the GBRL will not increase SSC at most coral reefs because there is already more than sufficient easily suspended sediment on the sea bed which is available for suspension (Larcombe and Woolfe 1999a,b).

In GBR coastal regions, the seabed commonly houses shore attached wedges of fine sediment (Belperio 1988). For example, Bowling Green Bay and Cleveland Bay contain sediment sourced from the Burdekin River. Sediment has been delivered to these bays since the rise in sea level after the last glaciation. Larcombe and Woolfe (1995) argue that extra terrigenous sediment supplied to these bays has little influence on sediment availability, only contributing a few millimetres of thickness to the sediment layer, which is already several metres thick (Larcombe et al. 1995b). In addition, sediment can be removed from the greater system and become trapped in such northward facing embayment. This occurs when south easterly trade winds drive coastal currents to the north, transporting suspended sediment and depositing into areas with less energetic wave conditions (Larcombe and Woolfe 1999a,b). Alongside the process of embayments trapping sediment, there is suggestion that over geological timescales, some measure of terrigenous sediment is transported in a small but constant flux over the continental margin (Dunbar et al. 2000) This glacio-eustatically controlled process across the inner continental shelf has been documented as occurring over the last 300 KY via sediment cores, and the most rapid rates of sediment accumulation, in the Queensland trough are found to occur during periods of rapid sea-level rise and shoreline transgression (Dunbar and Dickens 2003).

1.7 Environmental management of GBR turbidity

One of the critical issues cited for management of the Great Barrier Reef World Heritage Area (GBRWHA) is protection of the ecological systems from water-borne contaminants such as sediment and nutrients (GBRMPA 2010). It is well established that export of sediments to the GBRL has increased over the last 150 years, primarily due to anthropogenic disturbance of soils in the catchments (Belperio 1983; Neil et al. 2002; Furnas 2003; McCulloch et al. 2003b), but this does not necessarily mean that regimes of turbidity or sedimentation are altered (Larcombe and Woolfe 1999a). Suspended sediments may act as a limiting factor to coral reef health, primarily by reducing available light for photosynthesis, and being a source of material that subsequently settles onto the corals and bed. Safe turbidity levels in the GBR lagoon are an important consideration in the management of the Great Barrier Reef system (GBRMPA 2010).

Environmentally-based trigger values for water quality contaminants are currently in place, which would trigger a management response if exceeded. The water quality guidelines for the Great Barrier Reef Marine Park ((REEFPLAN 2013)) define the purpose of such trigger values (GBRMPA 2010). This includes; providing support for target setting for water quality that is leaving catchments, initiating a management response upon exceedance of a trigger value, supporting strategies that minimize contaminant release and enabling future research into impacts of contaminants as well as cumulative ecosystem impacts at local and regional levels (GBRMPA 2010). It is stressed within this document that the defined trigger levels are not targets, but instead are guideline values that, upon exceedance, are a trigger for management action.

Trigger values within REEFPLAN 2010 for open coastal water bodies (as well as mid-shelf and offshore) are derived from the analysis of over ten years of sediment and nutrient data, obtained by the Australian Institute of Marine Science (AIMS) using discrete spot water sampling. Water quality parameters used for suspended sediment are Secchi depth and suspended solids concentration (other parameters include chlorophyll, particulate, dissolved and total nitrogen and particulate, dissolved and total phosphorous) (De'ath and Fabricius 2008). Two water-quality methods were combined to define guideline trigger values, the first being modeled relationships between reef biota condition and each water quality parameter. The second method involved analysis of the distribution of water quality in waters off Cape York, which waters are taken in REEFPLAN 2010 as a reference site because the Cape was considered subject to land use of relatively low intensity. However, it is acknowledged by GBRMPA that uncertainties still exist with applying Cape York water quality data to other waters of the GBR. Accordingly, the proposed application of guideline trigger values considers this point (GBRMPA 2010). The GBRMPA guideline trigger value for mean annual concentration of total suspended solids (SSC) for open coastal waters has been set to 2.0 mg l^{-1} (GBRMPA 2010) based at least partly on water quality data acquired over the last decade.

1.8 Light attenuation and turbidity

Light availability is a dominating survival factor for many marine organisms and plants and there is no exception for the Great Barrier Reef (GBR). Sunlight penetrates the upper layer of ocean (the euphotic zone) enabling photosynthesis to occur within the solar wavelength band 400-700 nm (photosynthetically active radiation (PAR))(Wright 1995). The depth of the euphotic zone depends upon water turbidity and varies with location (Wright 1995). Light attenuation in the GBR affects biota by reducing light penetration for photosynthesis and reducing visual range for sighted marine organisms (Davies-Colley and Smith 2001). The diffuse attenuation coefficient (k_d) is an apparent optical property related to light attenuation, that cannot be measured directly. However, it can be very useful, i.e. to obtain penetration depths for photosynthetic coral in GBR waters. k_d has a strong linear relationship to suspended particle matter (SPM) and good predictions of k_d have been made previously from single depth light and SPM measurements in the literature (Devlin et al. 2008; Liu et al. 2010). Previously reported values of k_d for Cleveland Bay are K_d = 0.147-0.439 m^{-1}) (Anthony et al. 2004; Kirk 2010) and other examples around Australia are k_d values of 0.4 m^{-1} (Swan River, WA), 0.55 m^{-1} (Lake Macquarie, NSW) 0.18 m^{-1} (Tasman Sea, NSW) (Kirk 2010).

Within coastal regions of the GBR (i.e. located within the 20 m isobath (Wright 1995; Cooper et al. 2008; Macdonald et al. 2013), SPM is a major influence on water turbidity, with minor influences being phytoplankton and dissolved organic matter / yellow substance (Furnas 2003). SPM is variable with depth and this variation can affect penetration depths and bottom production. Therefore, obtaining vertical profiles of water turbidity is important to understand how light changes throughout the entire water column. Little is known about the interactions between light and turbidity in this context. Direct measurements of turbidity are easily obtainable. However, for the GBR, these are generally only measured near the seabed (Fabricius et al. 2012; Macdonald et al. 2013). Restricting measurements to the benthos may not provide a complete picture, as a great deal of marine biota also inhabit the water column above the seabed. However, obtaining a depth profile of turbidity, and a depth averaged turbidity value, is complicated and potentially expensive, because multiple measurements and instruments are required. Coastal GBR turbidity also has high temporal variability; therefore a vertical turbidity profile can be difficult to model (Orpin and Ridd 2012).

Light is a key resource for marine ecosystems, as it controls growth for the many groups of phototrophic organisms (Anthony et al. 2004). However, the role of light limits in shaping GBR ecosystems is not well understood (GBRMPA 2010). Aside from the commonly defined photic depth (being 1% of surface irradiance (Kirk 2010). There are several other varying limits for coral growth within the literature (between 50-450 $\mu E\ m^{-2}s^{-1}$) (Kleypas 1999). Inshore corals on the GBR are often exposed to intermittent periods of very low light, due to waves causing periods of sediment resuspension. Therefore these limits may not be as applicable to inshore corals (Dubinsky 1990; Larcombe et al. 1995b) (Conner and De Visser 1992; Logan et al. 2013).

Euphotic depth (Z_{eu}) is generally defined to be a measure of the depth where only 1 % of the surface irradiance remains (Wright 1995; Kleypas 1999; Devlin et al. 2008; Kirk 2010; Fabricius et al. 2012; Weeks et al. 2012; Fabricius et al. 2014). Most photo-autotrophic organisms cannot achieve positive net daily production below depths of this threshold. The definition of the euphotic depth as being 1 % of surface is equivalent to defining Z_{eu} = 4.6/k_d , assuming k_d is approximately constant with depth (Kirk 2010; Saulquin et al. 2013). Further, the mid-point of the euphotic depth (1/2 Z_{eu}) can be approximated as 2.3/k_d and corresponds to the depth at which downward irradiance is reduced to 10 % of the value just below surface (Kirk 2010). However, the definitions of photic limits for coral reef are not well defined and significant differences between various authors exist in the literature. For example, Chalker (1981) suggests a photic band exists between 50-450 $\mu E\ m^{-2}s^{-1}$ using a range of I_k for individual coral, where I_k is a measure of coral adaption to light (Chalker 1981). This value is potentially much larger than the photic limit of 1% of the surface value which is 20 $\mu E\ m^{-2}s^{-1}$ for the GBR region where typical maximum surface irradiance is *ca.* 2000 $\mu E\ m^{-2}s^{-1}$. Hard coral colonies on Middle Reef are commonly observed and monitored at depths of 5 m (Schaffelke et al. 2009). Also hard coral cover and richness in the near-shore GBR peaks around 5-7 m (DeVantier et al. 2006).

REFERENCES

Anthony KRN, Fabricius KE (2000) Shifting roles of heterotrophy and autotrophy in coral energetics under varying turbidity. Journal of Experimental Marine Biology and Ecology 252:221-253

Anthony KRN, Ridd PV, Orpin AR, Larcombe P, Lough J (2004) Temporal variation of light availability in coastal benthic habitats: Effects of clouds, turbidity, and tides. Limnology and Oceanography 49:2201-2211

Belperio AP (1983) Terrigenous sedimentation in the central Great Barrier Reef lagoon: a model from the Burdekin region. BMR Journal of Australian Geology and Geophysics 8:179-190

Belperio AP (1988) Terrigenous and carbonate sedimentation in the Great Barrier Reef province. Elsevier, Amsterdam

Brodie J, Fabricius K, De'ath G, Okaji K (2005) Are increased nutrient inputs responsible for more outbreaks of crown-of-thorns starfish? An appraisal of the evidence. Marine Pollution Bulletin 51:266-278

Brown BE (1997) Disturbances to reefs in recent times. In: Birkeland C (ed) Life and Death of Coral Reefs. Chapman and Hall Inc., New York, pp354-385

Bunt J, Larcombe P, Jago CF (1999) Quantifying the response of optical backscatter devices and transmissometers to variations in suspended particulate matter (SPM). Continental Shelf Research 19:1199-1220

Chalker BE (1981) Simulating light-saturation curves for photosynthesis and calcification by reef-building corals. Marine Biology 63:135-141

Conner CS, De Visser AM (1992) A laboratory investigation of particle size effects on an optical backscatterance sensor. Marine Geology 108:151-159

Cooper TF, Ridd PV, Ulstrup KE, Humphrey C, Slivkoff M, Fabricius KE (2008) Temporal dynamics in coral bioindicators for water quality on coastal coral reefs of the Great Barrier Reef. Marine and Freshwater Research 59:703-716

Davies-Colley RJ, Smith DG (2001) Turbidity, suspended sediment, and water clarity: A review. Journal of the American Water Resources Association 37:1085-1101

De'ath G, Fabricius K (2008) Water Quality of the Great Barrier Reef: Distributions, Effects on Reef Biota and Trigger Values for the Protection of Ecosystem Health

De’ath G, Fabricius KE, Sweatman H, Puotinen M (2012) The 27–year decline of coral cover on the Great Barrier Reef and its causes. Proceedings of the National Academy of Sciences

DeVantier LM, De’ath G, Turak E, Done TJ, Fabricius KE (2006) Species richness and community structure of reef-building corals on the nearshore Great Barrier Reef. Coral Reefs 25:329-340

Devlin MJ, Barry J, Mills DK, Gowen RJ, Foden J, Sivyer D, Tett P (2008) Relationships between suspended particulate material, light attenuation and Secchi depth in UK marine waters

Dubinsky Z (1990) Evolution and zoogeography of coral reefs. In: Dubinsky Z (ed) Ecosystems of the World - Coral Reefs. Elsevier, Amsterdam; New York, pp1-9

Dunbar G, Dickens G (2003) Massive siliciclastic discharge to slopes of the Great Barrier Reef Platform during sea-level transgression: constraints from sediment cores between 15°S and 16°S latitude and possible explanations. Sedimentary Geology 162:141-158

Dunbar GB, Dickens GR, Carter RM (2000) Sediment flux across the Great Barrier Reef Shelf to the Queensland Trough over the last 300 ky

Fabricius KE (2005) Effects of terrestrial runoff on the ecology of corals and coral reefs: Review and synthesis. Marine Pollution Bulletin 50:125-146

Fabricius KE, Wolanski E (2000) Rapid smothering of coral reef organisms by muddy marine snow. Estuarine, Coastal and Shelf Science 50:115-120

Fabricius KE, Logan M, Weeks S, Brodie J (2014) The effects of river run-off on water clarity across the central Great Barrier Reef. Marine Pollution Bulletin 84:191-200

Fabricius KE, De'ath G, Humphrey C, Zagorskis I, Schaffelke B (2012) Intra-annual variation in turbidity in response to terrestrial runoff on near-shore coral reefs of the Great Barrier Reef. Estuarine, Coastal and Shelf Science

Furnas M (2003) Catchments and corals: terrestrial runoff to the Great Barrier Reef. Australian Institute of Marine Science, Townsville, Qld

GBRMPA (2010) Water quality guidelines for the Great Barrier Reef Marine Park. Great Barrier Reef Marine Park Authority, Townsville

Gilmour J (1999) Experimental investigation into the effects of suspended sediment on fertilisation, larval survival and settlement in a scleractinian coral. Marine Biology 135:451-462

Goatley CHR, James Cook University. School of M, Tropical B (2013) The ecological role of sediments on coral reefs.

Hopley D (1982) The geomorphology of the Great Barrier Reef: Quaternary development of coral reefs. John Wiley, New York

Hopley D, smithers S, Parnell KE (2007) The geomorphology of the Great Barrier Reef: development, diversity, and change. Cambridge University Press, Cambridge

Kirk JTO (2010) Light and Photosynthesis in Aquatic Ecosystems. Cambridge University Press, Cambridge

Kleypas JA (1999) Environmental Limits to Coral Reef Development: Where Do We Draw the Line? American Zoologist 39:146-159

Lambrechts J, Humphrey C, McKinna L, Gourge O, Fabricius KE, Mehta AJ, Lewis S, Wolanski E (2010) Importance of wave-induced bed liquefaction in the fine sediment budget of Cleveland Bay, Great Barrier Reef. Estuarine, Coastal and Shelf Science 89:154-162

Larcombe P, Woolfe KJ (1999a) Increased sediment supply to the Great Barrier Reef will not increase sediment accumulation at most coral reefs. Coral Reefs 18:163-169

Larcombe P, Woolfe KJ (1999b) Terrigenous sediments as influences upon Holocene nearshore coral reefs, central Great Barrier Reef, Australia. Australian Journal of Earth Sciences: An International Geoscience Journal of the Geological Society of Australia 46:141 - 154

Larcombe P, Costen A, Woolfe KJ (2001) The hydrodynamic and sedimentary setting of nearshore coral reefs, central Great Barrier Reef shelf, Australia: Paluma Shoals, a case study. SEDIMENTOLOGY 48:811-835

Larcombe P, Ridd PV, Prytz A, Wilson B (1995b) Factors controlling suspended sediment on inner-shelf coral reefs, Townsville, Australia. Coral Reefs 14:163-171

Liu W-C, Wu R-S, Wu EM-Y, Chang Y-P, Chen W-B (2010) Using water quality variables to predict light attenuation coefficient: case study in Shihmen Reservoir. Paddy and Water Environment 8:267-275

Logan M, Fabricius K, Weeks S, Canto M, Noonan S, Wolanski E, Brodie J (2013) The Relationship between Burdekin River discharges and photic depth in the central Great Barrier Reef. Report to the National Environmental Research Program. Reef and Rainforest Research Centre Limited, Cairns 29pp

Ludwig KA, Hanes DM (1990) A laboratory evaluation of optical backscatterance suspended solids sensors exposed to sand-mud mixtures. Marine Geology 94:173-179

Macdonald RK, Ridd PV, Whinney JC, Larcombe P, Neil DT (2013) Towards environmental management of water turbidity within open coastal waters of the Great Barrier Reef. Marine Pollution Bulletin 74:82-94

Maxwell WGH (1968) Atlas of the Great Barrier Reef. Elsevier, Amsterdam

McCulloch M, Fallon S, Wyndham T, Hendy E, Lough J, Barnes D (2003a) Coral record of increased sediment flux to the inner Great Barrier Reef since European settlement. Nature 421:727-730

McCulloch M, Fallon S, Wyndham T, Hendy E, Lough J, Barnes D (2003b) Coral record of increased sediment flux to the inner Great Barrier Reef since European settlement

Moore KA, Neckles HA, Orth RJ (1996) Zostera marina (eelgrass) growth and survival along a gradient ofnutrients and turbidity in the lower Chesapeake Bay. Marine Ecology Progress Series 142:247-259

Moss A, Queensland. Dept. of E, Heritage, Queensland. Dept. of Primary I (1993) A Preliminary assessment of sediment and nutrient exports from Queensland coastal catchments. Queensland Dept. of Environment and Heritage, Brisbane

Neil DT, Orpin AR, Ridd PV, Yu B (2002) Sediment yield and impacts from river catchments to the Great Barrier Reef lagoon. Marine and Freshwater Research 53:733-752

Orpin AR, Ridd PV (2012) Exposure of inshore corals to suspended sediments due to wave-resuspension and river plumes in the central Great Barrier Reef: A reappraisal. Continental Shelf Research 47:55-67

Orpin AR, Ridd PV, Thomas S, Anthony KRN, Marshall P, Oliver J (2004) Natural turbidity variability and weather forecasts in risk management of anthropogenic sediment discharge near sensitive environments. Marine Pollution Bulletin 49:602-612

Pandolfi JM, Bradbury RH, Sala E, Hughes TP, Bjorndal KA, Cooke RG, McArdle D, McClenachan L, Newman MJH, Paredes G, Warner RR, Jackson JBC (2003) Global trajectories of the long-term decline of coral reef ecosystems. Science 301:955-958

REEFPLAN (2013) Reef water quality protection plan 2013 - For the Great Barrier Reef World Heritage Area and adjacent catchments. In: Cabinet DoPa (ed). Reef Water Quality Protection Plan Secretariat, Brisbane

Ridd P (2010) A Review of the Exposure of Corals to Suspended Sediments in the inshore Great Barrier Reef. School of Engineering and Physical Sciences, James Cook University, Townsville, QLD

Rodgers CS (1990) Responses of coral reefs and reef organisms to sedimentation. Marine Ecology Progress Series 62:185-202

Saulquin B, Hamdi A, Gohin F, Populus J, Mangin A, d'Andon OF (2013) Estimation of the diffuse attenuation coefficient KdPAR using MERIS and application to seabed habitat mapping. Remote Sensing of Environment 128:224-233

Schaffelke B, Thompson A, Carleton J, Davidson J, Doyle J, Furnas M, Gunn K, Skuza M, Wright M, Zagorskis I (2009) Reef Rescue Monitoring Program Final Report of AIMS Activities 2008/2009. Australian Institute of Marine Science

Stafford-Smith MG (1993) Sediment-rejection efficiency of 22 species of Australian scleractinian corals. Marine Biology 115:229-243

Weeks S, Werdell P, Schaffelke B, Canto M, Lee Z, Wilding J, Feldman G (2012) Satellite-Derived Photic Depth on the Great Barrier Reef: Spatio-Temporal Patterns of Water Clarity. Remote Sensing 4:3781-3795

Wolanski E, De'Ath G (2005) Predicting the impact of present and future human land-use on the Great Barrier Reef. Estuarine, Coastal and Shelf Science 64:504-508

Wolanski E, Delesalle B, Gibbs R (1994) Carbonate mud in Mataiva Atoll, French Polynesia: Suspension and export. Marine Pollution Bulletin 29:36-41

Wolanski E, Richmond RH, McCook L (2004) A model of the effects of land-based, human activities on the health of coral reefs in the Great Barrier Reef and in Fouha Bay, Guam, Micronesia. Journal of Marine Systems 46:133-144

Wolanski E, Fabricius KE, Cooper TF, Humphrey C (2008) Wet season fine sediment dynamics on the inner shelf of the Great Barrier Reef. Estuarine, Coastal and Shelf Science 77:755-762

Wright LD (1995) Morphodynamics of Inner Continental Shelves. CRC Press, Boca Raton

Chapter 2. MEASURING TURBIDITY AND EXCEEDANCE ANALYSIS

This chapter was published as a research paper in Marine Pollution Bulletin – September 2013

Macdonald R. K., et. Al (2013) *Towards environmental management of water turbidity within open coastal waters of the Great Barrier Reef*, Marine Pollution Bulletin, Volume 74, Issue 1, 15 September 2013, Pages 82-94. **http://www.sciencedirect.com/science/article/pii/S0025326X1300413X**

2.1 Abstract

Water turbidity and suspended sediment concentration (SSC) are commonly used as part of marine monitoring and water quality plans. Current management plans utilise threshold SSC values derived from mean-annual turbidity concentrations. Little published work documents typical ranges of turbidity for reefs within open coastal waters. Here, time-series turbidity measurements from 61 sites in the Great Barrier Reef (GBR) and Moreton Bay, Australia, are presented as turbidity exceedance curves and derivatives. This contributes to the understanding of turbidity and SSC in the context of environmental management in open-coastal reef environments. Exceedance results indicate strong spatial and temporal variability in water turbidity across inter/intraregional scales. The highest turbidity across 61 sites, at 50% exceedance (T_{50}) is 15.3 NTU and at 90% exceedance (T_{90}) 4.1 NTU.

Mean/median turbidity comparisons show strong differences between the two, consistent with a strongly skewed turbidity regime. Results may contribute towards promoting refinement of water quality management protocols.

2.2 Introduction

2.2.1 Turbidity and the Great Barrier Reef

The Great Barrier Reef (GBR) is the world's largest coral reef province, stretching along 2600 km of Australia's eastern coastline from 10º to 25º south latitude (Maxwell 1968; Hopley 1982; Hopley et al. 2007). The continental shelf is composed of three main shore-parallel zones, inner shelf, middle shelf and outer shelf, initially defined by the predominant sediment type (Maxwell 1968) and subsequently more formally defined by a combination of sediment type, bathymetry and topography (Belperio 1983,1988). The inner shelf of the GBR or Great Barrier Reef Lagoon (GBRL) is a focus for research due in part to its proximity to land, and thus exposure to coastal development, dredging and runoff from adjacent catchments (Furnas 2003). Open coastal water or the 'inshore' region of the inner shelf is defined here as being located within the 20 m isobath (Wright 1995; Cooper et al. 2008).

It is unclear what constitutes a typical mean suspended sediment concentration (SSC) or typical temporal variability in SSC across the GBRL. SSC is variable, both spatially and temporally (Larcombe and Woolfe 1999a; Cooper et al. 2008) and quantitative measurements are limited during extreme weather events, when levels are likely to be high.

Furthermore, high-frequency time series of SSC, lasting longer than a few months are generally very expensive to implement. As a result, the role of frequency, magnitude and duration in determining the impact that elevated SSCs have on corals in the GBRL is not well understood (Orpin and Ridd 2012). However, a recent study investigated determinants of inshore turbidity using ~3 years of almost continuous *in-situ* turbidity logger data on 14 reefs (Fabricius et al. 2012).

2.2.2 Relationship of turbidity to suspended sediment concentration

Turbidity is a measure of light scattering which, in the ocean, is caused mainly by suspended material in the water column, consisting of sediment, algae, micro-organisms and other particulate matter. Turbidity can be 'calibrated' to SSC (Larcombe et al. 1995b) however the conversion is not absolute, because the relationship varies in response to a wide range of sediment characteristics, particularly those related to grain size and type, which also change with time (Ludwig and Hanes 1990; Conner and De Visser 1992; Wolanski et al. 1994; Bunt et al. 1999; Anthony et al. 2004). In many cases, SSC (C) can be related to turbidity (T) by a linear relationship C=mT where m varies between 1 and 4 (Orpin and Ridd 2012).

Natural or background concentrations of suspended sediment refer to concentrations that are not caused by anthropogenic activity. Background SSCs on inshore fringing reefs of the GBRL have not been thoroughly investigated, which is partly due to the difficulty in disassociating natural and anthropogenic effects. However, background concentrations vary with factors such as bed type, and the nature of waves and currents experienced, so that

that variation is often locally and seasonally controlled. An estimate for fringing reefs near Magnetic Island and around Cleveland Bay is ca. 5 mg l^{-1} (Larcombe et al. 1995b), where concentrations were generally less than this in a 4 month-long period (Larcombe et al. 1995b). These are, it should be noted, measurements of turbidity calibrated to SSC. However, within this location, sediment resuspension frequently results in SSCs > 20 mg l^{-1} (Gilmour 1999; Anthony et al. 2004). SSCs at soft-bottomed sites within Cleveland Bay and Halifax Bay (inshore GBR) are regularly in excess of 100 mg l^{-1} for 2-3 day periods (Larcombe et al. 1995b; Larcombe et al. 2001) and during strong swell wave events these concentrations exceeded 200 mg l^{-1}. In Nelly Bay, a fringing reef setting in Cleveland Bay, turbidity varied by four orders of magnitude (0.1 to >100 NTU) over a 37-day period, and high turbidity events occurred simultaneously with high winds and associated high sea states, whereas during calm weather, turbidity was <1 NTU (Orpin et al. 2004).

Potential stress thresholds for some coastal corals were quantified by Cooper (2008) using an 18 month data set of water turbidity at Horseshoe Bay on the northern side of Magnetic Island, a continental island located within Cleveland Bay, a soft-bottomed embayment off Townsville with water depths ranging from about 3-13 m. Shallow areas were defined as being 2 m below LAT. The site is also commonly influenced by river plumes and lies 100 km north of the mouth of the Burdekin River, the largest single riverine source of sediment to the GBRL (Belperio 1983). Turbidity greater than 20 NTU occurred mostly during high wind events and was interpreted as caused by wave resuspension within Cleveland Bay, with subsequent advection to Horseshoe Bay by tidal currents. Turbidity exceeded 50 NTU during Tropical Cyclone Larry in March 2006 and during a high wind event in February 2007.

Flooding of the Burdekin River was also recorded during the period of February 2007. Analysing coral bioindicators for water quality, the study concluded that long-term (ca. 2 years) turbidity >3 NTU leads to sub-lethal coral stress and >5 NTU may represent a threshold for severe stress on corals in shallow areas (Cooper et al. 2008).

2.2.3 Turbidity and SSC in environmental management

One of the critical issues cited for management of the Great Barrier Reef World Heritage Area (GBRWHA) is protection of the ecological systems from water-borne contaminants such as sediment and nutrients (GBRMPA 2010). It is well established that export of sediments to the GBRL has increased over the last 150 years, primarily due to anthropogenic disturbance of soils in the catchments (Belperio 1983; Neil et al. 2002; Furnas 2003; McCulloch et al. 2003b), but this does not necessarily mean that regimes of turbidity or sedimentation are altered (Larcombe and Woolfe 1999a). Suspended sediments may act as a limiting factor to coral reef health, primarily by reducing available light for photosynthesis, and being a source of material that subsequently settles onto the corals and bed. Safe turbidity levels in the GBRL form a factor in the management of the Great Barrier Reef system (GBRMPA 2010).

Environmentally-based trigger values for water quality contaminants are currently in place, which would trigger a management response if exceeded. The water quality guidelines for the Great Barrier Reef Marine Park (REEFPLAN 2010) define the purpose of such trigger values (GBRMPA 2010). This includes; providing support for target setting for water quality that is leaving catchments, quick management response upon exceedance of a trigger value, supporting strategies that minimize contaminant release and enabling future research into impacts of contaminants as well as cumulative ecosystem impacts at local and regional levels (GBRMPA 2010). It is stressed within this document that the defined trigger levels are not targets, but instead are guideline values that, upon exceedance, are a trigger for management action.

Trigger values within REEFPLAN 2010 for open coastal water bodies (as well as midshelf and offshore) are derived from the analysis of over ten years of sediment and nutrient data, obtained by the Australian Institute of Marine Science (AIMS) using discrete spot water sampling. Water quality parameters used for suspended sediment are Secchi depth and suspended solids concentration (other parameters include chlorophyll, particulate, dissolved and total nitrogen and particulate, dissolved and total phosphorous) (De'ath and Fabricius 2008). Two water quality monitoring methods were combined to define guideline trigger values, the first being modeled relationships between reef biota condition and each water quality parameter. The second method involved analysis of the distribution of water quality in waters off Cape York, which waters are taken in REEFPLAN 2010 as a reference site because the Cape was considered subject to land use of relatively low intensity. However, it is well acknowledged by GBRMPA that uncertainties still exist with applying Cape York water quality data to other waters of the GBR. Accordingly, the proposed application of guideline trigger values considers this point. The guideline trigger value for SSC in open coastal waters is 2.0 mg l^{-1} (GBRMPA 2010).

This paper presents turbidity data from a range of coral reef sites throughout open coastal waters within the GBR and Moreton Bay, during a period of one and a half decades. These data enable the examination of turbidity and SSC characteristics for these waters, in the context of ecological processes and environmental management. This is undertaken by exploring the potential uses of means, medians and exceedance curves of turbidity. We present one of the most comprehensive datasets for the region in terms of temporal density, geographic coverage and the total number of sites, and in terms of the data having been acquired using consistent instrumentation and modes of deployment.

2.3 Materials and methods

2.3.1 Instrumentation and data collection

Turbidity measurements from 61 sites along the GBRL were collated from previously unpublished data gathered between 1993 and 2009 (Table 1). These sites extend from Moreton Bay (27^{o}S) to Princess Charlotte Bay (14^{o}S). Some of the data were collected as part of commercial work associated with water-quality monitoring of dredging activities (not during dredge phase). As such, much of the data has not yet been fully analysed and represents a valuable untapped resource.

The turbidity data were collected using optical backscatter turbidity loggers (nephelometers) with identical optics and which include a wiper blade mounted on the optical aperture (Ridd and Larcombe 1994). Behind the aperture are optical fibres, which transmit and receive infra-red light. The automatic wiping system allows the nephelometer to be deployed in tropical waters for periods as long as one month without bio-fouling (Ridd and Larcombe 1994; Orpin et al. 2004). All instruments ran under the same basic logging parameters, averaging 10 second readings every 10 minutes and calibrated to the same standard. Instruments were placed approximately 30 cm from the sea floor, and turbidity data were recorded for approximately one month before being downloaded. Exceptions to this deployment depth were Paluma Shoals (Table 1, *sites 37, 38*; instruments deployed at 0.9 m and 1.7 m depths respectively) and two sites at Middle Reef (Table 1, *sites 10, 11*; instruments deployed at 0.7 m and 2.2 m depths respectively). The sensors were programmed to record one ten-second average measurement of turbidity every ten minutes. The sensors were also programmed to self-clean every 120 minutes. Prior to deployment, the sensors were calibrated to a turbidity standard. The loggers used in this study have a potential zero error of 0.5 NTU and as such, data recorded below this value is reported as < 0.5 NTU.

2.3.2 Data handling methods

Exceedance curves were developed for turbidity at all sites and the values for T_{10}, T_{50}, T_{90} were determined i.e. the turbidity which is exceeded 10%, 50% and 90% of the time, respectively. T_{50} values represent median turbidity and T_{10} and T_{90} represent turbidity values at the 90th and 10th percentiles respectively. Exceedance curves have been used previously to present GBR turbidity data (Larcombe et al. 2001) and have demonstrated the bimodal turbidity regimes at Paluma Shoals and other inner shelf ‘turbid-zone' reefs and allowed inferences to be made of repeated volumes of material resuspended and temporarily accumulated (Larcombe et al. 2001). Subsequently, the potential effect these turbidity and sedimentation regimes have on coral physiology has been analysed (Anthony et al. 2004).

Comparisons between data sets of different duration, obtained in different years and at different times of year must be done with caution because of the seasonality involved (Fabricius et al. 2012) and the episodic nature of many significant driving factors, such as river floods or cyclonic waves and currents (Orpin and Ridd 2012). Some of our datasets are too short to include the effects of some of these factors and/or allow their statistical assessment. Nevertheless, because some of the data derive from regions where no other instrumental data are available, even these short datasets contain valuable information. For example, one month of data, sampled at 10-minute intervals, contain over 4000 measurements of turbidity, which number probably around 2 orders of magnitude greater than what is typically available from discrete Secchi depth measurements, such as those used in REEFPLAN 2010. Furthermore, continuous nephelometer sampling enables the measurement of turbidity data in rough weather and elevated sea states, which are rarely well represented by discrete water samples, because of safety considerations surrounding manual sampling.

2.4 Site locations

Turbidity measurements were obtained from 8 regions between Moreton Bay in southeast Queensland and Princess Charlotte Bay in far North Queensland (Figs. 1 and 2(a-g)). Sites were segmented in terms of Regions, which were chosen based on their geographic locations. All sampling sites are located at or adjacent to inshore coral reefs or coral communities. Sites are mostly in the central section of the GBR, spanning both dry tropics and wet tropics regions. The site locations range from areas of human activity in the marine environment, such as the Hay Point region, to relatively undisturbed areas, such as Princess Charlotte Bay.

2.4.1 Region 1: Moreton Bay

Moreton Bay is a subtropical embayment between 27^{o}S and 28^{o}S, which is approximately 110 km from north to south, with a 15.5 km wide entrance at the north, and three narrow entrances between the sand islands that define its eastern shoreline (Neil, 1998). Moreton Bay is not part of the GBRL, but the data are relevant as part of documenting turbidity regimes on inshore reefs. Water depth in Moreton Bay increases gradually from the west coast to maximum depths of ca. 20 to 30 m in the central eastern Bay. The mean range of the semi-diurnal tides is 1.48 m (springs) and 0.84 m (neaps) in the eastern Bay and 1.71 m and 0.97 m, respectively, in the western Bay. Moreton Bay is ca. 1500 km^2 in area and river catchments totalling ca. 23 000 km^2 drain into it along the western shoreline. The dominant land use in the catchment is grazing (ca. 65%), with cropping (5%) and urban areas (ca. 10%) and < 25% remnant natural vegetation (Capelin et al. 1998).

Coral communities in Moreton Bay have existed episodically during the Holocene sea-level highstand (Lybolt et al. 2011) with a transition from Acroporid- to Favid-dominated species assemblages (Johnson and Neil, 1998; Lybolt et al. 2011). Modern coral communities, characterised as 'marginal' (Lybolt et al. 2011), occur adjacent to island and mainland sites in central Moreton Bay, varying in characteristics (e.g. cover, species composition) in relation to gradients in factors such as water quality (Abal and Dennison 1996; Capelin et al. 1998; Johnson and Neil 1998; Neil 1998; Lybolt et al. 2011) and sedimentation rates (Johnson and Neil 1998).

2.4.2 Region 2: Hay Point

Hay Point is located approximately 40 km south of Mackay, on the central Queensland coast. The Port of Hay Point is a coal exporting facility, with initial development and subsequent expansion occurring over the last two decades and a major dredging operation between May and October 2006. The turbidity data presented here were acquired in 2008, 2 years after the cessation of dredging (Chartrand et al. 2008). Victor Island (*Site 7*) is the closest site to the port, at a distance of approximately 3.5 km. Fringing coral reef communities are distributed around Victor, Round Top and Flat Top Islands. Seagrass and algal communities are distributed with low to moderate cover around the Port of Hay Point. Sediments in the Hay Point area consist of mainly silts and fine sands of variable thickness (1-30 cm) with stiff clays beneath (Trimarchi and Keane 2007).

2.4.3 Region 3: Cleveland Bay and Magnetic Island

Cleveland Bay, adjacent to Townsville is at 19^{o}S, partially sheltered from southeasterly waves and open to the north with a maximum depth of ca. 15 m. The granitic body of Magnetic Island lies at the entrance to the bay and the fringing reefs on the Island are about 10 km from the mainland coast. Fringing coral reefs with a diverse range of hard and soft coral species occur around its margins. Platypus Channel is a 12-13 m deep artificial channel allowing shipping access to the Port of Townsville, and dredge spoil has historically been dumped in the northern part of the bay around the 10 m isobath (Perry et al. 2012). Bottom sediments in Cleveland Bay are mainly soft and silty and easily resuspended (Belperio 1979) containing between 20% and 45% material finer than coarse silt (~40 µm; (Lou and Ridd 1997). The sediments largely comprised a mixture of four dominant grain sizes; terrigenous grains at sizes of 7, 30 and 110 µm and coarse carbonate sand at ~900 µm (Larcombe et al. 1995b). Of relevance to the turbidity data presented here, dredging work took place in Cleveland Bay for two months from the end of January 1993 and construction related to harbour and marina development was also occurring on the fringing reef at Nelly Bay throughout the period of data acquisition at sites 12-15 (Table 1).

2.4.4 Region 4: Paluma Shoals and Rattlesnake Island

Paluma Shoals are located between Townsville and Ingham and contains a shore-attached turbid-zone coral reef (Larcombe et al. 2001). It is relatively unusual compared to other inner-shelf reefs in the GBR in that it has vertically accreted to sea level and formed a well-developed reef flat (Smithers and Larcombe 2003; Hopley et al. 2007; Perry et al. 2008; Palmer et al. 2010) although there is increasing recognition of similar reefs elsewhere (e.g.

Lugger Shoal; Middle Reef) (Perry et al. 2009b; Browne et al. 2012; Perry et al. 2012). The sediments on the reef flats of Paluma Shoals consist of terrigenous and calcareous gravel and sand (Perry et al. 2010). The reef slope sediments consist of muddy gravelly quartz sands (Larcombe et al. 2001). Rattlesnake Island is a 2.5 km long outcrop of igneous rock, situated 11 km offshore of Paluma Shoals. Most of the island is surrounded by narrow fringing reefs of maximum width of 350 m off the southern and western shores, and a sand spit is located on the western reef flat. The outer reef flat has a thin veneer of living coral, whereas the inner flat has a field of dead microatolls (Hopley et al. 1983).

2.4.5 Region 5: Mission Beach and Family Group Islands

Dunk Island is located approximately 4 km off the coast of Mission Beach, midway between Townsville and Cairns. The island is mainly composed of granitic and metamorphic rocks and has an area of 9 km^2. The fringing reef on the southern and western sides of the island reaches a maximum width of 900 m (Hopley et al. 1983). Lugger Bay, on Dunk Island has a small reef platform, Lugger Shoal (Perry and Smithers 2006; Perry et al. 2009b). The seafloor sediment around Mission Beach on the mainland coast is predominantly terrigenoclastic and the main riverine sediment sources come from the Tully, Hull and Murray Rivers (Neil 1996; Perry et al. 2009b).

2.4.6 Region 6: Frankland Islands

The Frankland Islands are located ~40 km southeast of Cairns and ~8 km offshore. Although the Frankland Islands are a popular tourist destination, little information is available on the sediment type or distribution around the Frankland Island fringing reefs, although it is likely that they lie outside the terrigenous inner shelf sedimentary wedge (e.g. Johnson and Searle, 1984; Gagan et al., 1980), and so are probably dominated by carbonate sediments.

2.4.7 Region 7: Port Douglas and Alexandra Shoals

Alexandra Shoals are a series of fringing coral reefs approximately 30 km north of Cairns. The reefs consist of a wide, low relief reef flat that extends for about 5 km along the mainland coast, in close proximity to a sandy mangrove-fringed tidal flat. Coarse, sandy sediment is predominant. The mouth of the Mowbray River is at the southern end of the northern-most fringing reef. The adjacent coastal plain is used for sugar cane cropping and housing development. Port Douglas is located approximately 60 km north of Cairns and has a high concentration of tourism activities. The nearest estuary to Port Douglas is Dickson's Inlet.

2.4.8 Region 8: Princess Charlotte Bay and region

Princess Charlotte Bay is a 50 km wide bay located on Cape York Peninsula. The shelf at Princess Charlotte Bay has a semi-continuous barrier at the shelf edge which separates the oceanic circulation and dampens ocean swell. The Normanby, Marrett, Bizant and North Kennedy Rivers discharge into the bay, causing large sediment plumes during the wet season (Bryce et al. 1998). Sediments in Princess Charlotte Bay are more terrigenous near the river mouths, with coarse sandy sediments of high carbonate content close to the outer reef tract (Sahl and Marsden 1987).

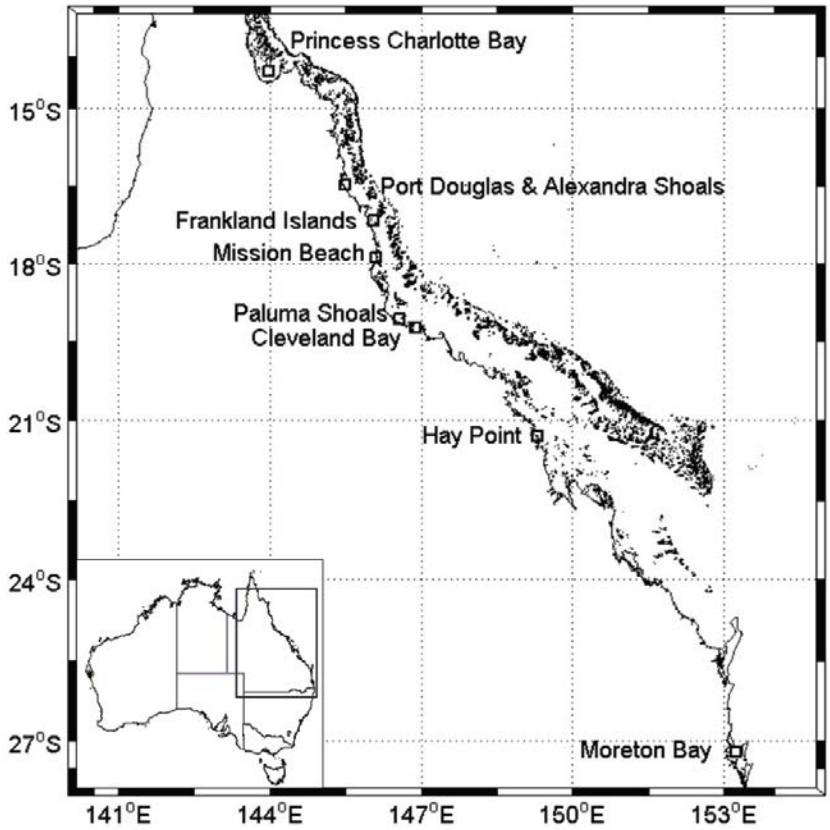

Figure 1 Locations of the eight regions used in this paper

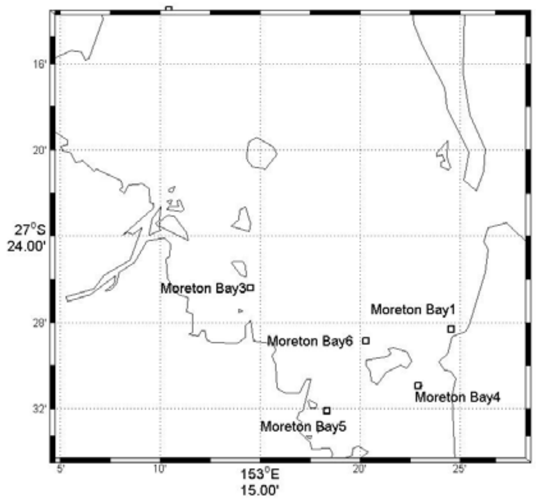

Figure 2a

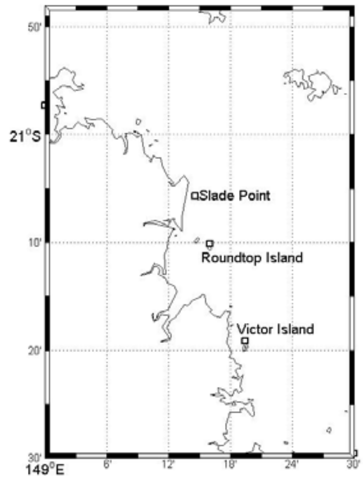

Figure 2b

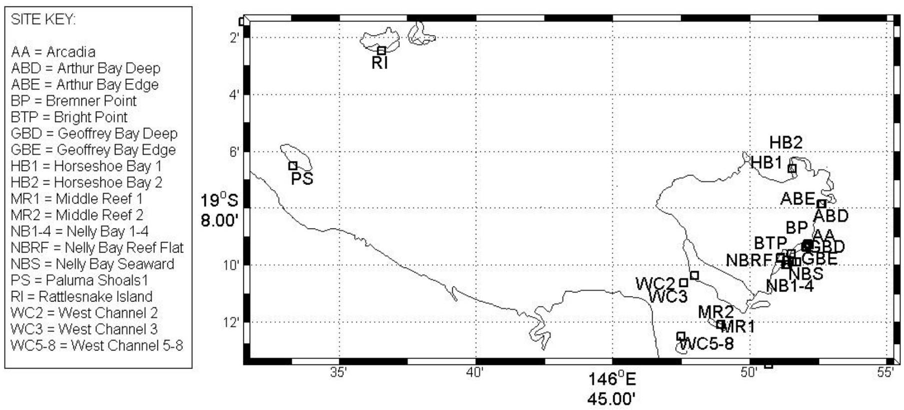

Figure 2c

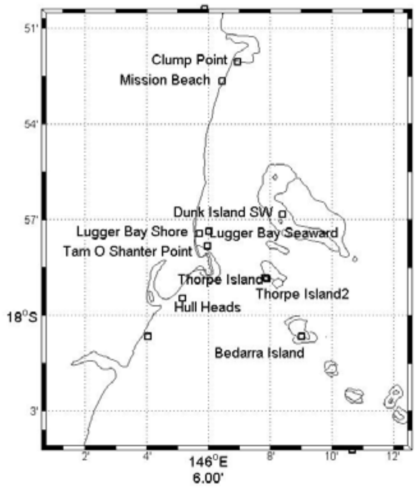

Figure 2d

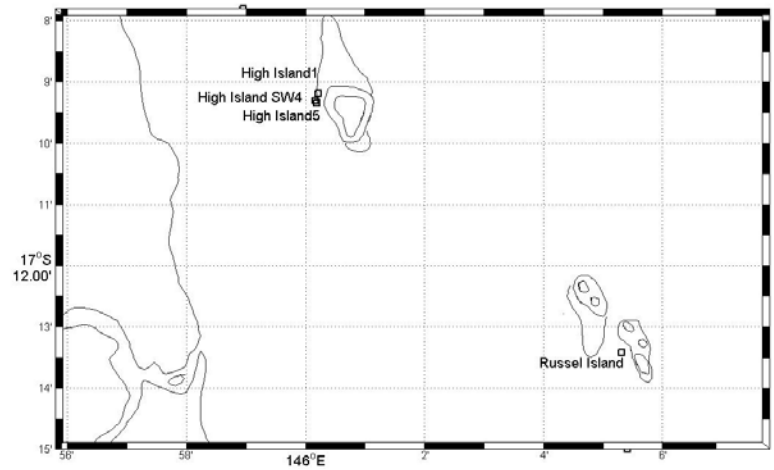

Figure 2e

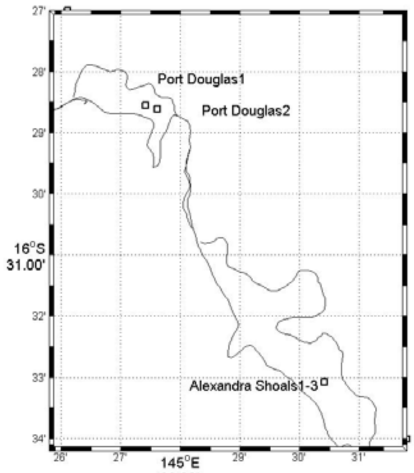

Figure2f

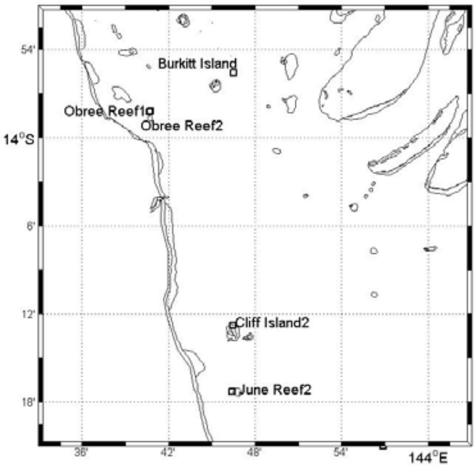

Figure2g

Figure 2 (a-g) Locations of turbidity monitoring sites across eight study regions. (a) Moreton Bay, (b) Hay Point and Mackay, (c) Cleveland and Halifax Bay, (d) Mission Beach and Family group, (e) Frankland Islands, (f) Alexandra Shoals and Port Douglas, (g) Princess Charlotte Bay

Table 1 Site and region data and location information

Region	Site #	Site Name	Days of data	Year	Latitude	Longitude
Moreton Bay	1	Moreton Bay1	37	2003	-27.47	153.41
	2	Moreton Bay3	38	2003	-27.44	153.24
	3	Moreton Bay4	38	2003	-27.52	153.38
	4	Moreton Bay5	52	2003	-27.53	153.31
	5	Moreton Bay6	37	2003	-27.48	153.34
Hay Point	6	Slade Point	31	2008	-21.10	149.24
	7	Victor Island	31	2008	-21.32	149.32
	8	Roundtop Island	31	2008	-21.17	149.27
Cleveland Bay / Magnetic Island	9	Middle Reef1	104	1993	-19.20	146.82
	10	Middle Reef2 0.7m	21	2009	-19.20	146.82
	11	Middle Reef2 2.2m	16	2009	-19.20	146.82
	12	Nelly Bay1	620	2001-2002	-19.17	146.86
	13	Nelly Bay2	589	2001-2002	-19.17	146.86
	14	Nelly Bay3	589	2001-2002	-19.17	146.86
	15	Nelly Bay4	589	2001-2002	-19.17	146.86
	16	Arthur Bay Edge	121	1993	-19.13	146.88
	17	Arthur Bay Deep1	121	1993	-19.13	146.88

	18	Arthur Bay Deep2	121	1993	-19.13	146.88
	19	Geoffrey Bay Edge	120	1993	-19.16	146.87
	20	Geoffrey Bay Deep	121	1993	-19.16	146.87
	21	Nelly Bay Seaward	37	2000	-19.16	146.86
	22	Bright Point	22	2000	-19.16	146.86
	23	Arcadia	37	2000	-19.15	146.87
	24	Bremner Point	37	2000	-19.16	146.87
	25	Nelly Bay Reef Flat a	14	2000	-19.16	146.85
	26	Nelly Bay Reef Flat b	14	2000	-19.16	146.85
	27	Horseshoe Bay2	789	2005-2007	-19.11	146.86
	28	Horseshoe Bay1	116	1993	-19.11	146.86
	29	West Channel2a	28	2004	-19.18	146.79
	30	West Channel2b	28	2004	-19.18	146.79
	31	West Channel3	28	2004	-19.17	146.80
	32	West Channel5	12	2004	-19.21	146.79
	33	Virago Shoal	15	2004	-19.21	146.79
	34	West Channel7	15	2004	-19.21	146.79
	35	West Channel8	15	2004	-19.21	146.79
Paluma Shoals	36	Rattlesnake Island	92	1993	-19.04	146.61
	37	Paluma Shoals0.9m	29	2009	-19.11	146.56
	38	Paluma Shoals1.7m	29	2009	-19.11	146.56
Mission Beach and Islands	39	Mission Beach	39	2000	-17.88	146.11
	40	Dunk Island SW	39	2000	-17.95	146.14
	41	Thorpe Island	39	2000	-17.98	146.13
	42	Lugger Bay Shore	30	2003/2004	-17.96	146.10
	43	Bedarra Island	30	2003/2004	-18.01	146.15
	44	Lugger Bay Seaward	36	2003/2004	-17.96	146.10
	45	Clump Point	30	2003/2004	-17.87	146.12
	46	Thorpe Island2	31	2003/2004	-17.98	146.13
	47	Tam O Shanter Pt	30	2003/2004	-17.96	146.10
Frankland Islands	48	Russel Island	23	2000	-17.22	146.09
	49	High Island1	13	2000	-17.15	146.00
	50	High Island SW4	40	2000	-17.16	146.00
	51	High Island5	40	2000	-17.16	146.00

Port Douglas / Alexandra Shoals	52	Port Douglas1	67	2004	-16.48	145.46
	53	Port Douglas2	65	2004	-16.48	145.46
	54	Alexandra Shoals1	32	2000	-16.55	145.51
	55	Alexandra Shoals2	33	2000	-16.55	145.51
	56	Alexandra Shoals3	33	2000	-16.55	145.51
Princess Charlotte Bay	57	Obree Reef1	78	2001	-13.97	143.68
	58	Obree Reef2	69	2001	-13.97	143.68
	59	June Reef2	68	2001	-14.29	143.77
	60	Burkitt Island	48	2001	-13.93	143.78
	61	Cliff Island2	48	2001	-14.21	143.77

Table 2 Mean turbidity and turbidity exceedance values (T_5, T_{10}, T_{50} and T_{90}) for each site.

Site #	Site Name	Mean T (NTU)	T_5 (NTU)	T_{10} (NTU)	T_{50} (NTU)	T_{90} (NTU)
1	Moreton Bay1	1.4	3.4	2.3	1.0	<0.5
2	Moreton Bay3	0.6	1.5	1.3	<0.5	<0.5
3	Moreton Bay4	0.8	2.0	1.1	<0.5	<0.5
4	Moreton Bay5	3.4	9.8	5.9	2.1	1.2
5	Moreton Bay6	0.4	0.7	0.6	<0.5	<0.5
6	Slade Point	4.3	11.3	6.4	2.5	1.3
7	Victor Island	25.0	106.8	43.7	9.3	1.4
8	Roundtop Island	2.6	10.2	6.2	0.7	<0.5
9	Middle Reef1	9.1	27.3	19.2	5.3	2.3
10	Middle Reef2 0.7m	1.7	5.6	3.7	0.8	<0.5
11	Middle Reef2 2.2m	3.0	9.2	7.6	1.4	<0.5
12	Nelly Bay1	1.9	6.2	3.0	0.9	<0.5
13	Nelly Bay2	4.4	7.5	4.0	1.0	<0.5
14	Nelly Bay3	1.8	5.1	3.3	1.3	<0.5
15	Nelly Bay4	1.5	4.6	3.0	0.9	<0.5
16	Arthur Bay Edge	6.2	16.8	12.8	3.7	1.7
17	Arthur Bay Deep1	5.3	16.2	12.0	3.1	1.2
18	Arthur Bay Deep2	6.0	16.8	12.3	3.1	1.2

19	Geoffrey Bay Edge	7.3	23.4	16.1	3.4	1.5
20	Geoffrey Bay Deep	12.5	51.1	23.5	3.7	1.3
21	Nelly Bay Seaward	14.9	70.6	47.1	3.9	1.5
22	Bright Point	10.8	45.6	20.0	2.1	0.7
23	Arcadia	3.2	7.8	5.5	1.9	1.6
24	Bremner Point	8.9	40.3	22.3	2.4	<0.5
25	Nelly Bay ReefFlat a	4.7	21.8	13.6	0.8	<0.5
26	Nelly Bay ReefFlat b	8.5	32.9	22.5	2.9	0.5
27	Horseshoe Bay2	3.3	13.9	9.4	1.1	<0.5
28	Horseshoe Bay1	9.5	26.5	15.6	4.6	1.1
29	West Channel2a	6.4	13.6	10.7	5.2	3.0
30	West Channel2b	5.3	11.3	8.8	4.3	2.4
31	West Channel3	3.8	7.4	5.6	2.3	1.2
32	West Channel5	7.2	32.2	19.0	2.5	<0.5
33	Virago Shoal	5.3	20.4	13.7	2.0	<0.5
34	West Channel7	4.9	16.3	11.9	2.7	1.0
35	West Channel8	5.1	17.7	11.1	2.7	1.3
36	Rattlesnake Island	3.8	9.1	6.4	2.9	1.3
37	Paluma Shoals 0.9m	8.8	21.6	17.8	7.3	1.1
38	Paluma Shoals 1.7m	12.3	36.1	28.5	8.0	0.7
39	Mission Beach	3.9	13.5	9.2	2.1	0.8
40	Dunk Island SW	7.0	20.6	11.5	1.2	<0.5
41	Thorpe Island	2.8	11.8	7.5	1.2	<0.5
42	Lugger Bay Shore	8.0	39.1	28.7	1.2	<0.5
43	Bedarra Island	5.3	10.7	7.1	3.9	1.6
44	Lugger Bay Seaward	8.5	43.2	27.4	2.1	1.1
45	Clump Point	2.4	13.1	7.1	0.8	<0.5
46	Thorpe Island2	1.9	6.7	4.6	0.8	<0.5
47	Tam O Shanter Pt	3.9	15.0	9.4	1.8	0.7
48	Russel Island	1.3	5.0	2.5	<0.5	<0.5
49	High Island1	3.1	14.5	8.9	<0.5	<0.5
50	High Island SW4	0.8	1.3	0.8	<0.5	<0.5
51	High Island5	1.2	1.3	0.8	<0.5	<0.5
52	Port Douglas1	13.3	28.2	23.3	11.4	4.1

53	Port Douglas2	7.0	14.1	12.1	6.5	2.1
54	Alexandra Shoals1	10.3	35.2	23.9	5.2	<0.5
55	Alexandra Shoals2	17.4	44.3	38.1	15.3	1.1
56	Alexandra Shoals3	5.8	21.5	15.5	2.7	<0.5
57	Obree Reef1	2.8	6.4	4.9	2.2	0.9
58	Obree Reef2	2.3	5.6	4.0	1.7	0.9
59	June Reef2	3.6	11.6	8.2	2.2	<0.5
60	Burkitt Island	1.0	1.9	1.2	0.6	<0.5
61	Cliff Island2	1.7	7.0	4.6	0.5	<0.5

Table 3 Timings of Nelly Bay and Princess Charlotte Bay data. Wet season is defined as November to April (inclusive).

Site name	Region	Date from	Date to	Season	length (days)	Year
Nelly Bay1	Cleveland bay	29/03/2001	9/12/2002	dry - wet - dry	620.00	2001-2002
Nelly Bay2	Cleveland bay	2/04/2001	12/11/2002	dry - wet - dry	589.00	2001-2002
Nelly Bay3	Cleveland bay	2/04/2001	12/11/2002	dry - wet - dry	589.00	2001-2002
Nelly Bay4	Cleveland bay	2/04/2001	12/11/2002	dry - wet - dry	589.00	2001-2002
Obree Reef1	Princess Charlotte Bay	25/12/2001	13/03/2002	wet	78.00	2001
Obree Reef2	Princess Charlotte Bay	25/12/2001	5/03/2002	wet	69.00	2001
June Reef2	Princess Charlotte Bay	31/12/2001	9/03/2002	wet	68.00	2001
Burkitt Island	Princess Charlotte Bay	31/12/2001	17/02/2002	wet	48.00	2001
Cliff Island2	Princess Charlotte Bay	31/12/2001	17/02/2002	wet	48.00	2001

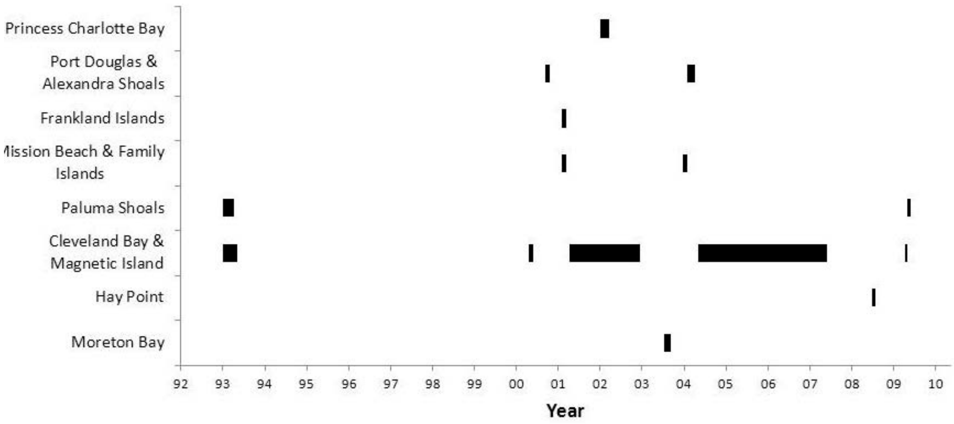

Figure 3 Turbidity data acquisition time periods, for 8 regions across the Great Barrier Reef and Moreton Bay. Data was acquired between 1993 to 2009.

2.5 Results

2.5.1 Turbidity time series

Space does not permit the graphical presentation of all of the 61 time-series. However the time series for Nelly Bay3 (*site 14*) and June Reef2 (*site 59*) (Figs. 4, 5) show the general patterns of turbidity which are typical of many of the 61 sites, although the magnitudes of the turbidity recorded vary between sites. For example, at Nelly Bay (Figure 4), throughout this time period of roughly 24 days, turbidity ‘events’ occur around day 14 and 20 as well as a significant long term increase during day 13-17. Between days 7 and 13 there are tidally-driven turbidity oscillations between 2 and 8 NTU and there are also other variations at time scales of minutes and hours that cannot be seen at this resolution.

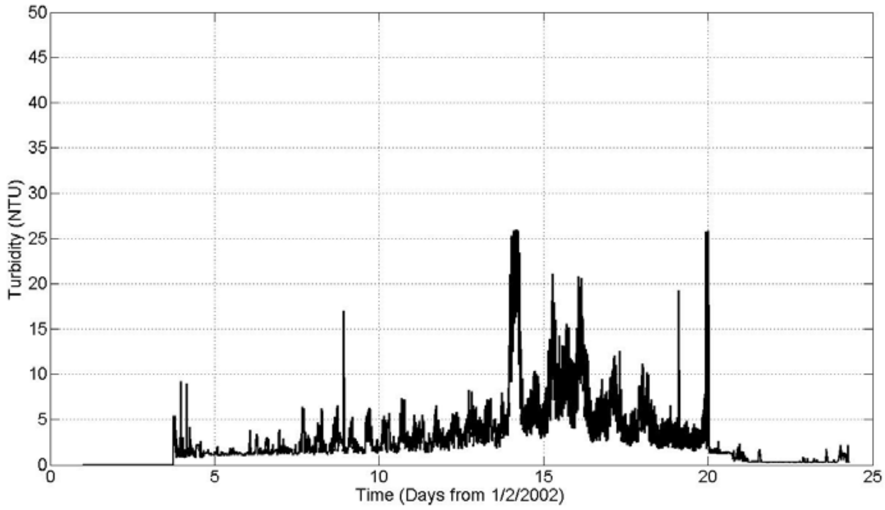

Figure 4 Turbidity time series for Nelly Bay3 (site 14) during February 2002 .

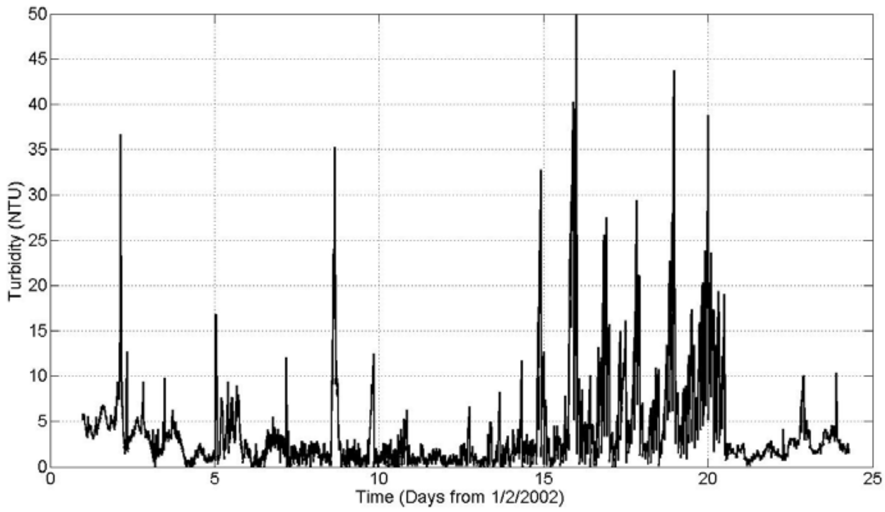

Figure 5 Turbidity time series for June Reef2 (site 59) during February 2002.

2.5.2 Mean and median (T_{50} Exceedance) turbidity

REEFPLAN currently uses the annual mean value, because exposure to high concentrations is considered ecologically important. Mean and median (T_{50}) turbidity for each (Figure 6) vary between 0.4 and 25.0 NTU (mean) and 0.3 and 15.3 NTU (median). The within-site turbidity distribution is strongly skewed, often with a factor of 5 difference between mean and T_{50}. This is directly related to the episodic nature of some of the key processes driving turbidity, and raises an important issue when considering either mean or median turbidity data to calculate threshold levels. At present the physiological response of corals is not sufficiently well understood to determine whether the mean or the median is most relevant.

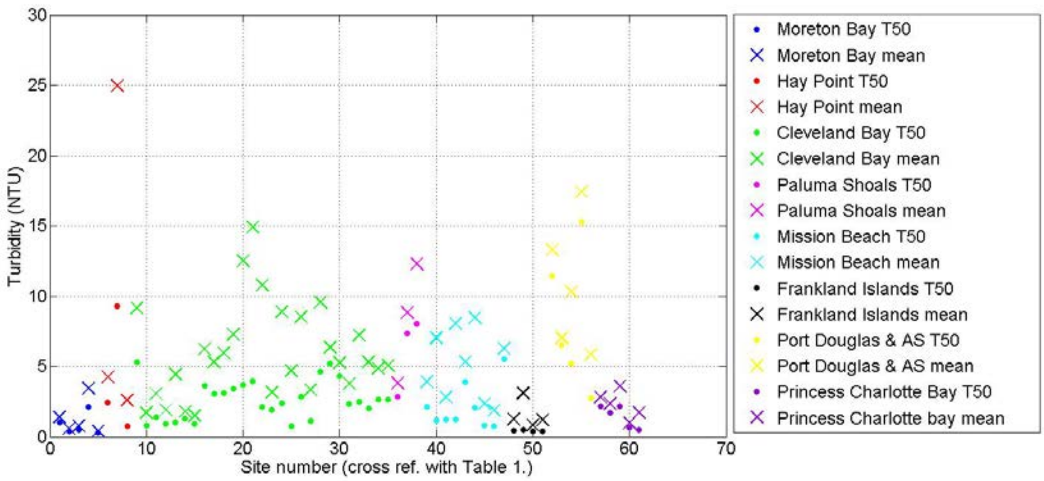

Figure 6 Mean turbidity and T50 exceedance data for all 61 sites.

2.5.3 Overview of turbidity exceedance patterns

Exceedance curves were generated for all sites and the T_{10}, T_{50}, and T_{90} values calculated (Table 2). Selected exceedance curves are presented in Figs 7 and 8. All 61 sites exhibit a T_{50} value of less than 16 NTU. The highest T_{50} values occurred throughout Port Douglas/Alexandra Shoals and Hay Point, which were; 15.3, 11.4 and 9.3 NTU for sites 55, 52 and 7, respectively (Table 1). The lowest T_{50} values occurred in Moreton Bay and the Frankland Islands, which were; 0.3, 0.4 and 0.4 NTU for sites 5, 2 and 50, respectively (Table 1). The highest T_{90} value was 4.1 NTU at site 52 in the Port Douglas region (Table 1). The lowest T_{90} values were negligible (<0.5 NTU i.e. below the zero point accuracy of the instruments) for 26 of the 61 sites. (Table 1) and there appear to be no shared site characteristics within this set of negligible T_{90} values. The highest T_{10} value was 47.1 NTU from site 21, Cleveland Bay (Table 1) and the lowest T_{10} value was found in Moreton Bay, site 5 at 0.6 NTU. The median value for all T_{10} is 8.9 NTU, for all $T_{50\ is}$ 2.1 NTU and for T_{90} is 0.5 NTU.

Exceedance curves for the sites with the lowest and highest T_{50} values for each of the 8 regions (Figure 7 and 8 respectively) show considerable within-region difference. The most pronounced differences are for the Moreton Bay, Hay Point/Mackay, Cleveland/Halifax Bay and Mission Beach/Family Group regions. For example, at Moreton Bay site 4 (Figure 8) over 95% of the values exceed 1 NTU, while for site 5 (Figure7) less than 5% exceed 1 NTU. Similarly, at Hay Point site 7 (Figure 8) over 70% of the values exceed 5 NTU while at site 8 (Figure 7) less than 10% of the values exceed 5 NTU.

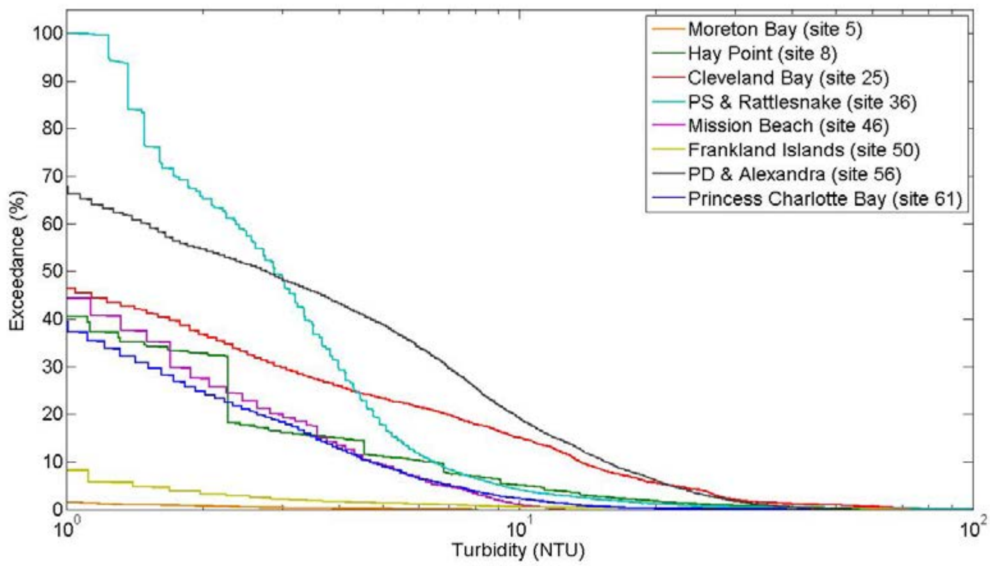

Figure 7 Exceedance curves for all regions. Curves presented are those for the site with the lowest T_{50} value in each region.

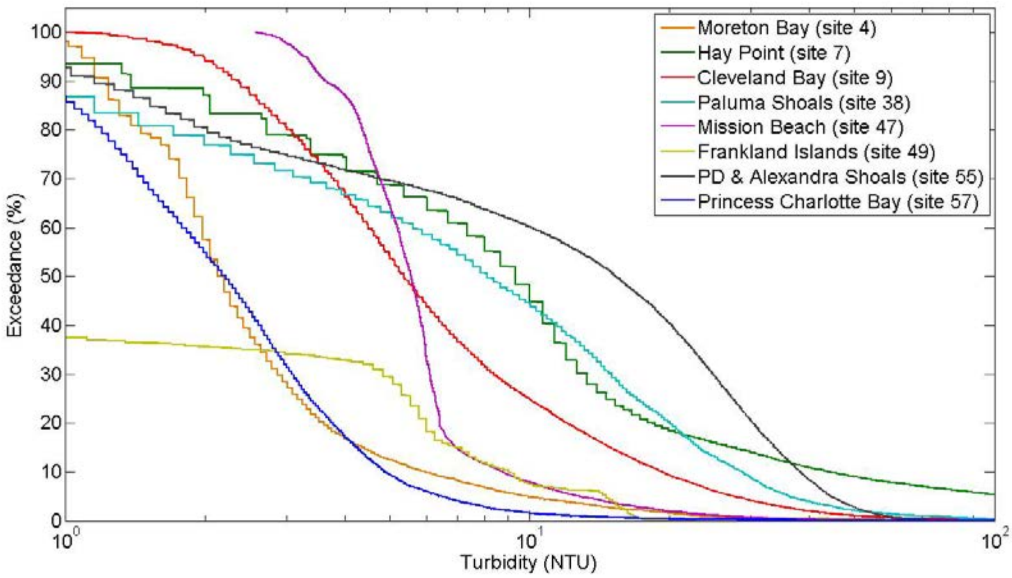

Figure 8 Exceedance curves for all regions. Curves presented are those for the site with the highest T_{50} value in each region.

2.5.4 Weighted means and exceedance low-high ranges

The ranges of T_5, T_{10} and T_{50} are depicted in Figs. 9, 10, 11, respectively. The mean T_5, T_{10} and T_{50} exceedances per region are weighted according to the length of the time series, which accounts for the variability in site deployment lengths within each region. For example, assuming the average of all T_5 values was calculated in the usual way (i.e. sum of T_5 values/number of sites), if the data acquisition period for one of the sites in that region is much longer than the others, then the average T_5 will be dominated by that particular site's T_5 value. Therefore, the weighted average method for each region is performed by taking the sum-product (i.e. the sum of the products of both the T_5 values and the number of days per site). This is then divided by the total number of days. This is repeated for T_{10} and T_{50} values. The mean turbidity (Figure 12) shows the lowest and highest averages per site for each region. This is then weighted according to length of deployment as described above.

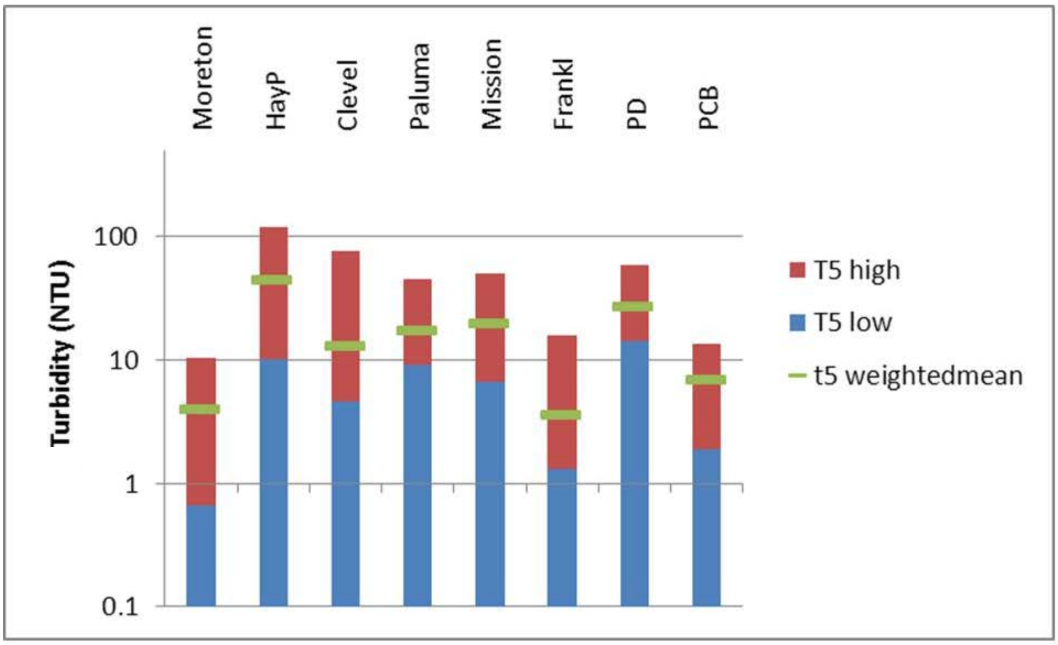

Figure 9 Lowest T_5 value, highest T_5 value and mean T_5 value (weighted by length of deployment) for each region.

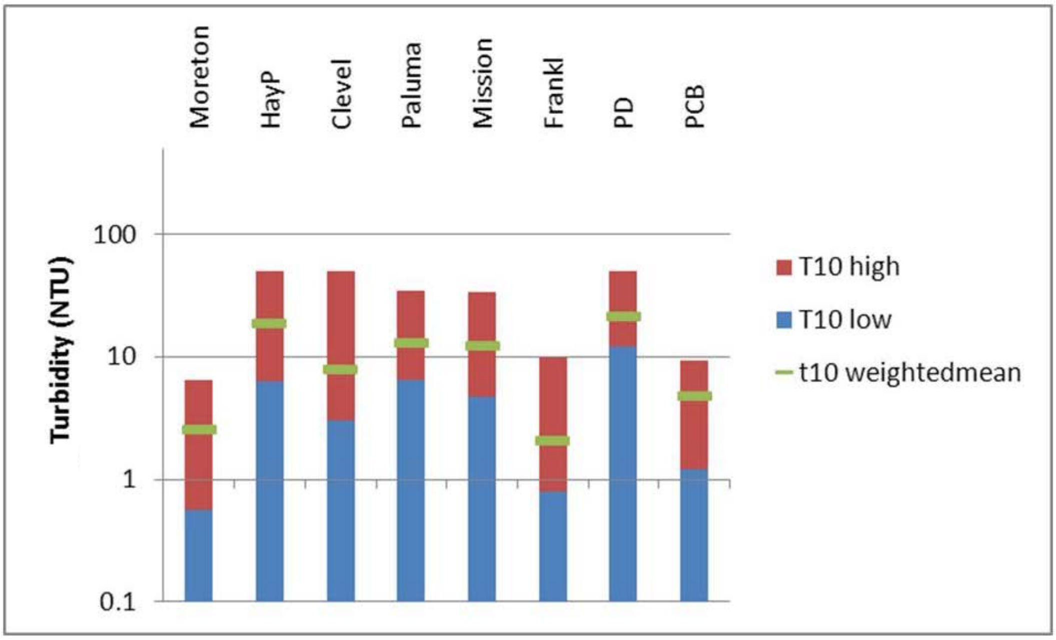

Figure 10 Lowest T_{10} value, highest T_{10} value and mean T_{10} value (weighted by length of time series), for each region.

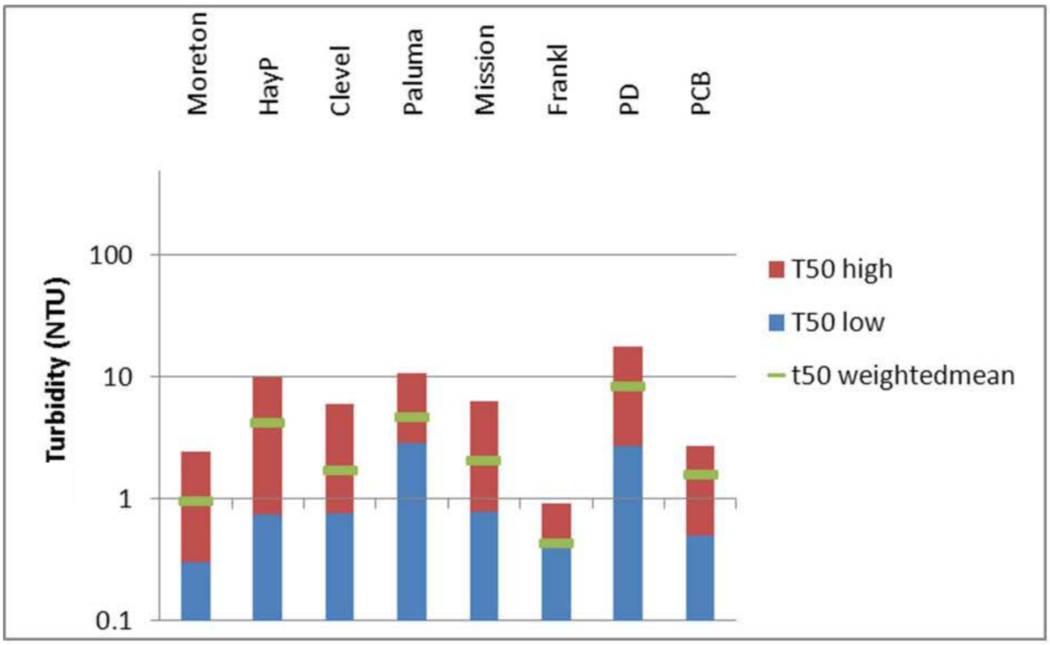

Figure 11 Lowest T_{50} value, highest T_{50} value and mean T_{50} value (weighted by length of deployment), for each region.

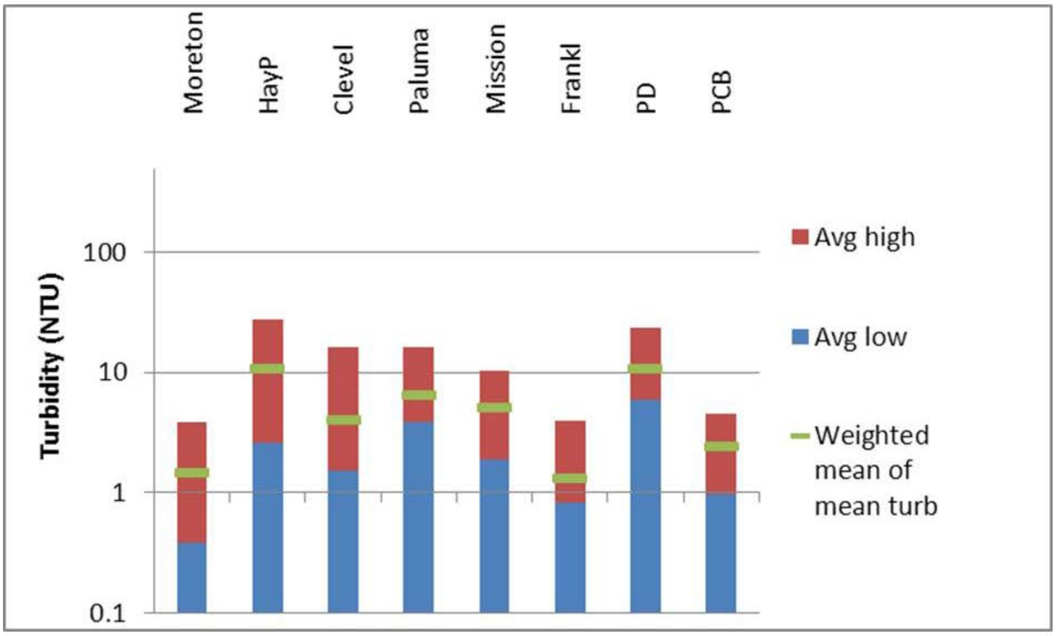

Figure 12 Lowest mean turbidity, highest mean turbidity and mean of mean-turbidity (weighted by length of deployment) for each region.

2.5.5 Exceedance for Nelly Bay sites wet and dry seasons

The sites denoted as Nelly Bay 1-4 within the Cleveland Bay region are approximately 200 m apart, and represent a turbidity record of almost 2 years, enabling investigation of both seasonal variation and small-scale spatial variation. The variation across these sites is broad. For example, Nelly Bay1 (site 12) exceedance curves for the wet and dry seasons are very similar (Figure 13), whereas in Nelly Bay2 (site 13) the dry season exceedance curve shows distinctly higher turbidities-than the wet (Figure 14).

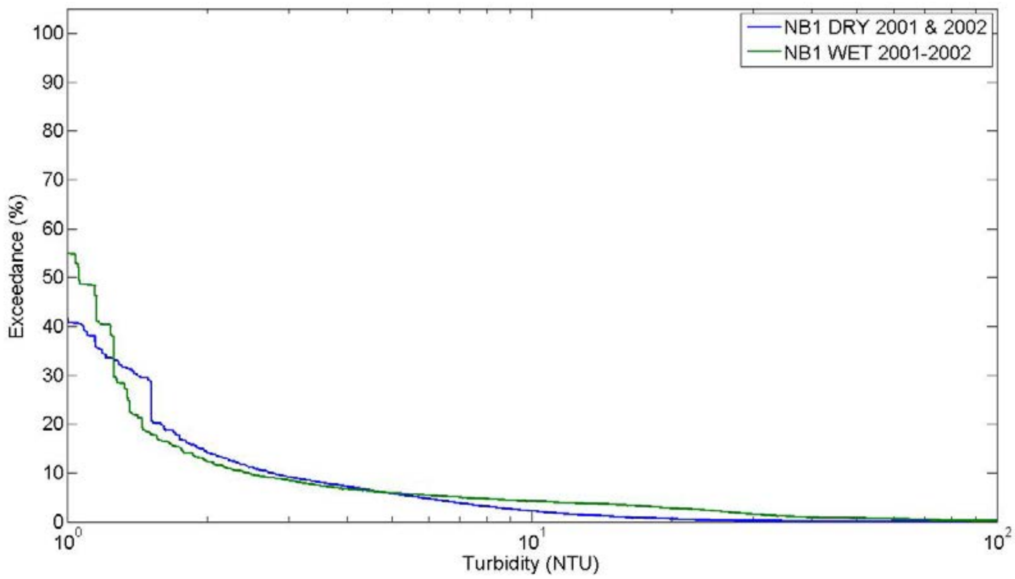

Figure 13 Nelly Bay1 (site12) exceedance curves for the wet and dry seasons of 2001 and 2002.

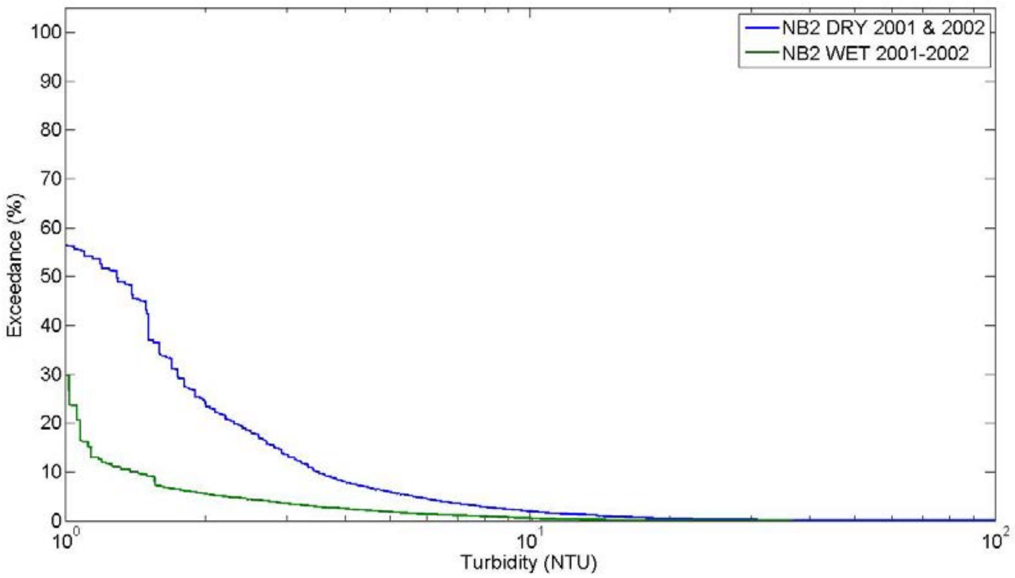

Figure 14 Nelly Bay2 (site13) exceedance curves for the wet and dry seasons of 2001 and 2002.

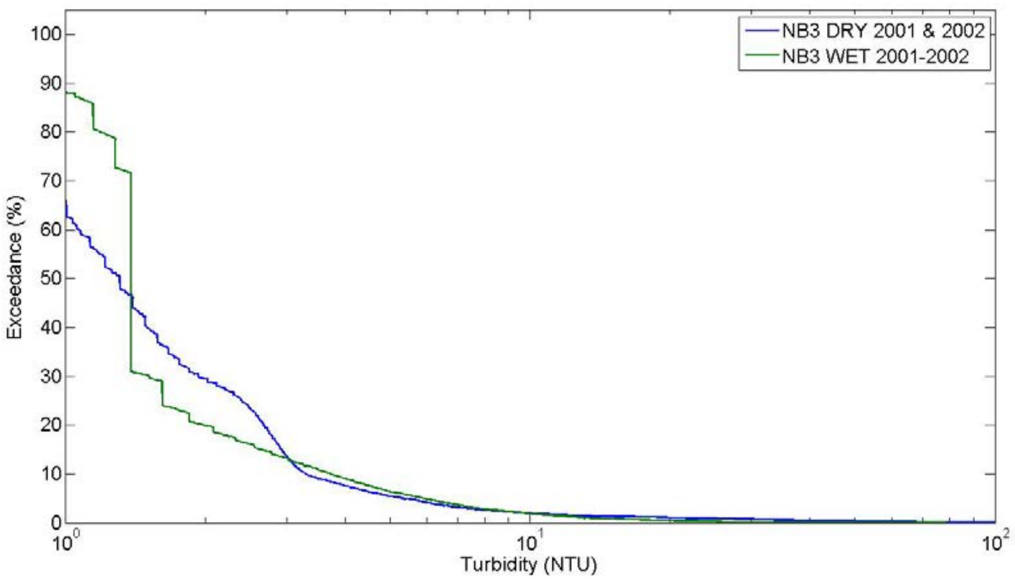

Figure 15 Nelly Bay3 (site14) exceedance curves for the wet and dry seasons of 2001 and 2002.

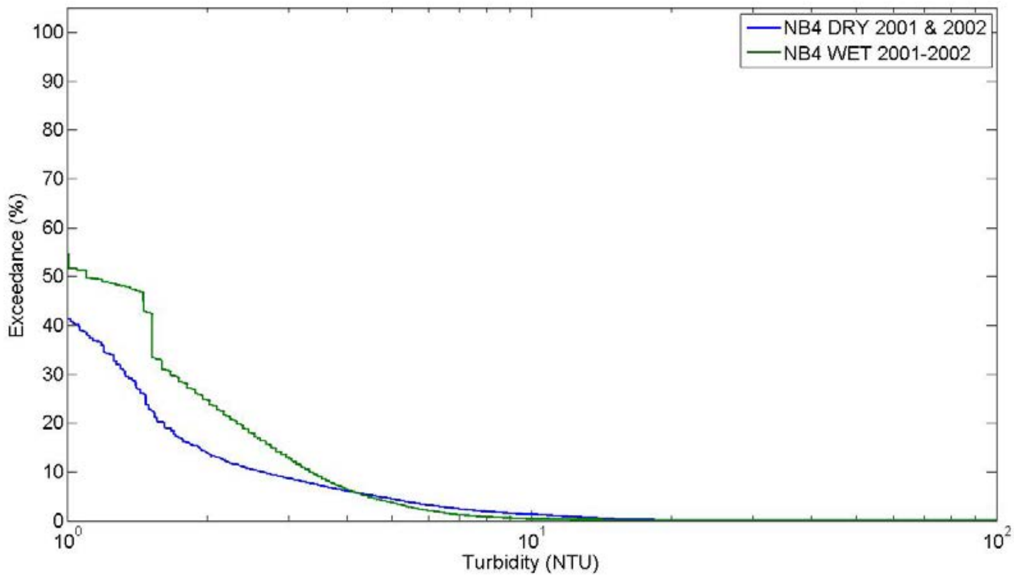

Figure 16 Nelly Bay4 (site15) exceedance curves for the wet and dry seasons of 2001 and 2002.

2.5.6 Nelly Bay and Princess Charlotte Bay 2011-2002 wet season comparison

Presented below are turbidity data for two geographically different locations within the same wet season (2001-2002; Figure 3). Turbidity exceedance curves are presented for four Nelly Bay sites in Cleveland Bay and five Princess Charlotte Bay (PCB) sites (Fig 17). PCB data were recorded over the same wet season as Nelly Bay. PCB is also of particular interest because the Cape York area is used as a reference site for 'pristine' water quality in the GBRL (GBRMPA 2010).

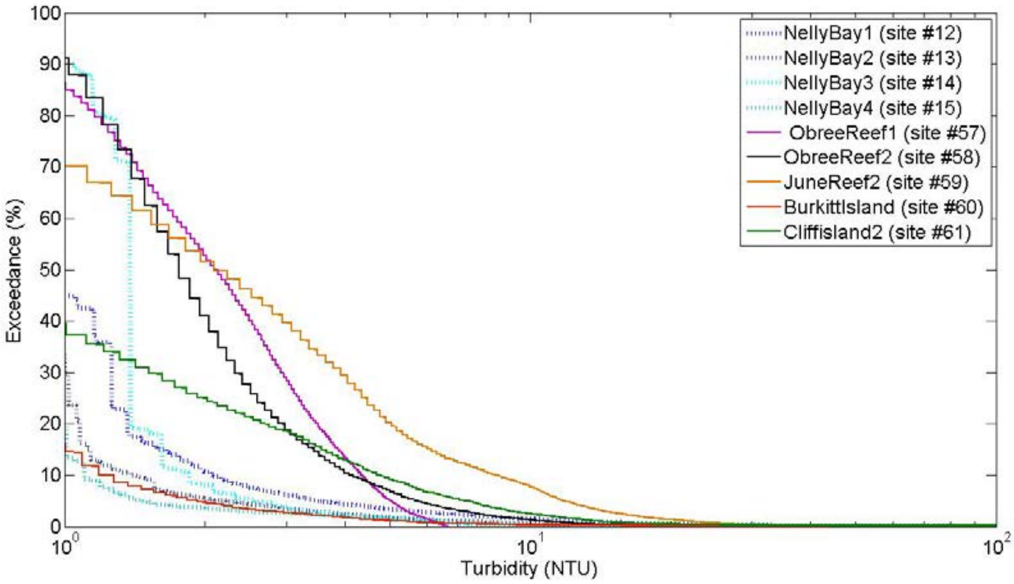

Figure 17 Wet season exceedance for PCB (solid lines) and Nelly Bay (dotted blue lines) across 2001 and 2002.

Turbidity exceedance parameters vary markedly across the Princess Charlotte Bay region. Some sites within this region compare very closely, such as ObreeReef1 (site 57) and ObreeReef2 (site 58). Both of these sites have approximately 60% of values exceeding 2 NTU, contrasting with just 5% of turbidity values exceeding 2 NTU at Burkitt Island (site 60). The variability between sites in Nelly Bay is lower, although Nelly Bay1 (site 12) and Nelly Bay4 (site 15) depict between 4 and 14 % of values exceeding 2 NTU. When comparing the two regions for values at 2 NTU, the Nelly Bay sites all fall within 5-15% exceedance, whereas the PCB sites vary from 25-70% exceedance. However, for a slightly higher turbidity value the differences between the two regions are small. For example at 5 NTU the difference across all Nelly Bay and Princess Charlotte Bay sites is around 10% exceedance, with the exception of JuneReef2 (site59), which is higher. At 10 NTU, all but JuneReef2 are within 5% exceedance.

2.6 Discussion

The GBRMPA guideline for mean annual concentration of total suspended solids (SSC) for open coastal waters has been set to 2.0 mg l^{-1} (GBRMPA 2010) based at least partly on water quality data acquired over the last decade. The additional data presented in this paper may be useful to refine any future guideline values as it is based on >800,000 data points across 61 reef sites. For many of these sites, there are no previously published turbidity data.

Care must be taken when interpreting these data as many of the sites have been affected by human activity and are thus less suitable as a basis for establishing turbidity guideline values. In addition, while the data sets are mostly at least a month in length, a longer data series would be useful to ensure that important wind events that may generate highly turbid conditions occur within the data.

A notable aspect of the data is the large difference in turbidity between some sites within the same region and time period, emphasizing the high level of spatial variability in water turbidity in these areas. For example, within the Hay Point region, Victor Island (site 7) has a mean and median turbidity of 25 and 9.3 NTU respectively. However Roundtop Island (site 8) has a mean and median turbidity of 2.6 and 0.7 NTU, which is a factor of 10 and 14 greater respectively. Even sites extremely close together can have very different turbidity characteristics. For example, Alexandra Shoals3 (site 56) which is only 300m from Alexandra Shoal2 has a mean turbidity of 6 NTU and a median of 2.7, which are less by factors of 3 and 6 respectively than the corresponding values for Alexandra Shoals2.

In examining cross-region turbidity, it should be noted that the various sites in a region are not necessarily representative of all conditions within that region. It is possible that some regions are over-represented by either low or high turbidity sites. Thus no attempt is made to compare the turbidity levels between whole regions, other than to say that the median values can vary by an order of magnitude. For example, the T_{50} for the Moreton Bay and the Frankland Islands are around 1 NTU compared with 9 NTU for Port Douglas. A consistent feature amongst all regions is the high variability between sites within the regions. The ratio between the highest and lowest T_{50} value within a region can reach 10 e.g. Cleveland Bay.

Another important feature of the data is that there is often a very large difference between the mean and median (T_{50}) turbidity. This is a consequence of the distribution being highly skewed, so that a relatively small number of very high turbidity values can have a large effect on the mean turbidity but not on the median. In the extreme case of Victor Island (site 7) the mean is almost 3 times higher than the median. In 28 out of the 61 sites, the mean was more than double the median value. REEFPLAN uses the mean value since exposure to high concentrations is considered ecologically important and De’ath and Fabricius (2008) argue that percentiles (e.g. medians) do not adequately reflect acute high values. However, based on the data presented here, the use of median data has the potential to greatly influence guideline levels.

Before a comparison can be made between guideline values and the data presented here, the issue of converting turbidity data to SCC values (the parameter used in REEFPLAN) must be addressed. The most accurate way to measure SSC is to take water samples for laboratory analysis. The obvious problem with this method is that long term time series of SSC are prohibitively expensive and safety considerations dictate that very rough weather conditions, when SSC is likely to be very high, cannot be sampled. Turbidity is a surrogate measure of SSC but the calibration from NTU to SSC is site specific and may well change with time because light scattering (essentially turbidity) depends strongly on grain size which may change with time, especially during extreme weather events. We do not have calibration equations for the majority of the sites in our data set so no attempt has been made to convert all of the data into SSC values. However, one of the best calibrations between NTU and SSC was done in 2003 by pumping water from the reef flat on Nelly Bay through a long pipe whilst simultaneously measuring turbidity (Dupont 2003). It was a very good calibration because it was performed over a rough weather event so a wide range of turbidity readings were obtained. This yielded a calibration equation where the NTU needed to be multiplied by a factor of 5 in order to produce TSS. Other calibrations have yielded multiplication factors of as low as 1.0.

One issue with turbidity sensors, particularly in relatively low turbidity GBR waters, is that the zero point error is often large. For example modern sensors such as the Campbell OBS 3 has a potential zero error of 0.5 NTU and the YSI 6136 has a zero error of 0.3 NTU. A zero error of 0.5 NTU would give a minimum error in the TSS value of 0.5 mg l^{-1} using an NTU to TSS factor of 1.0 but this could rise to 2.5 mg l^{-1} for a worst case scenario of a calibration factor of 5. Thus the zero point error for many sensors is large relative to the 2.0 mg l^{-1} guideline value.

The REEFPLAN guideline value of 2 mg l^{-1} endeavours to provide a reasonable figure that might be representative of typical undisturbed conditions for open coastal waters, however the data presented here are from sites for which are affected by human disturbance. Thus no comment about the validity of the guideline value can be made.

To summarise, half of the 61 sites have mean turbidities of greater than 4.7 NTU and 47 sites had mean turbidities greater than 2 NTU. The median T_{10} value was 9 NTU, the median T_{50} value was 2.1 NTU, and the median T_{90} value was 0.5 NTU. There was no systematic pattern of variation in mean or median turbidity at sites sampled along the Queensland coast, with the lowest mean, T_{50}, T_{10}, and T_5 turbidities observed in Moreton Bay, the Frankland Group and Princess Charlotte Bay. Across most parameters, the highest turbidities observed were at Hay Point and Port Douglas. Using the minimum NTU to SSC conversion factor of 1.0, the above values could thus also be used as minimum SSC values. With this assumption, half of the sites have a median turbidity (T_{50}) which is greater than the REEFPLAN guidelines and 47 sites (77%) have a mean turbidity greater than 2 mg l^{-1} using the lowest reasonable conversion factor of 1.0.

REFERENCES

Abal EG, Dennison WC (1996) Seagrass depth range and water quality in southern Moreton Bay, Queensland, Australia. Marine and Freshwater Research 47:763-771

Anthony KRN, Ridd PV, Orpin AR, Larcombe P, Lough J (2004) Temporal variation of light availability in coastal benthic habitats: Effects of clouds, turbidity, and tides. Limnology and Oceanography 49:2201-2211

Belperio AP (1979) The combined use of wash load and bed material load rating curves for the calculation of total load: An example from the Burdekin River, Australia. Catena 6:317-329

Belperio AP (1983) Terrigenous sedimentation in the central Great Barrier Reef lagoon: a model from the Burdekin region. BMR Journal of Australian Geology and Geophysics 8:179-190

Belperio AP (1988) Terrigenous and carbonate sedimentation in the Great Barrier Reef province. Elsevier, Amsterdam

Browne NK, Smithers SG, Perry CT (2012) Coral reefs of the turbid inner-shelf of the Great Barrier Reef, Australia: an environmental and geomorphic perspective on their occurrence, composition and growth. . Earth-Science Reviews 115:1-20

Bryce S, Larcombe P, Ridd PV (1998) The relative importance of landward-directed tidal sediment transport versus freshwater flood events in the Normanby River estuary, Cape York Peninsula, Australia. Marine Geology 149:55-78

Bunt J, Larcombe P, Jago CF (1999) Quantifying the response of optical backscatter devices and transmissometers to variations in suspended particulate matter (SPM). Continental Shelf Research 19:1199-1220

Capelin M, Kohn P, Hoffenberg P (1998) Land use, land cover and land degradation in the catchment of Moreton Bay. The University of Queensland, School of Marine Science, Brisbane

Chartrand KM, Rasheed MA, Sankey TL (2008) Deepwater seagrass dynamics in Hay Point - measuring variability and monitoring impacts of capital dredging: Final Report. Ports Corporation of Queensland 43

Conner CS, De Visser AM (1992) A laboratory investigation of particle size effects on an optical backscatterance sensor. Marine Geology 108:151-159

Cooper TF, Ridd PV, Ulstrup KE, Humphrey C, Slivkoff M, Fabricius KE (2008) Temporal dynamics in coral bioindicators for water quality on coastal coral reefs of the Great Barrier Reef. Marine and Freshwater Research 59:703-716

De'ath G, Fabricius K (2008) Water Quality of the Great Barrier Reef: Distributions, Effects on Reef Biota and Trigger Values for the Protection of Ecosystem Health

Dupont L (2003) Development of an in-situ fluorometer for the study of organic materials on a fringing reef. James Cook University,

Fabricius KE, De’ath G, Humphrey C, Zagorskis I, Schaffelke B (2012) Intra-annual variation in turbidity in response to terrestrial runoff on near-shore coral reefs of the Great Barrier Reef. Estuarine, Coastal and Shelf Science

Furnas M (2003) Catchments and corals: terrestrial runoff to the Great Barrier Reef. Australian Institute of Marine Science, Townsville, Qld

GBRMPA (2010) Water quality guidelines for the Great Barrier Reef Marine Park. Great Barrier Reef Marine Park Authority, Townsville

Gilmour J (1999) Experimental investigation into the effects of suspended sediment on fertilisation, larval survival and settlement in a scleractinian coral. Marine Biology 135:451-462

Hopley D (1982) The geomorphology of the Great Barrier Reef: Quaternary development of coral reefs. John Wiley, New York

Hopley D, Smithers S, Parnell KE (2007) The geomorphology of the Great Barrier Reef: development, diversity, and change. Cambridge University Press, Cambridge

Hopley D, Slocombe AM, Muir F, Grant C (1983) Nearshore fringing reefs in north Queensland. Coral Reefs 1:151-160

Johnson PR, Neil DT (1998) The corals of Moreton Bay: living with extremes. The University of Queensland, School of Marine Science, Brisbane

Larcombe P, Woolfe KJ (1999a) Increased sediment supply to the Great Barrier Reef will not increase sediment accumulation at most coral reefs. Coral Reefs 18:163-169

Larcombe P, Costen A, Woolfe KJ (2001) The hydrodynamic and sedimentary setting of nearshore coral reefs, central Great Barrier Reef shelf, Australia: Paluma Shoals, a case study. Sedimentology 48:811-835

Larcombe P, Ridd PV, Prytz A, Wilson B (1995b) Factors controlling suspended sediment on inner-shelf coral reefs, Townsville, Australia. Coral Reefs 14:163-171

Lou J, Ridd PV (1997) Modelling of Suspended Sediment Transport in Coastal Areas Under Waves and Currents. Estuarine, Coastal and Shelf Science 45:1-16

Ludwig KA, Hanes DM (1990) A laboratory evaluation of optical backscatterance suspended solids sensors exposed to sand-mud mixtures. Marine Geology 94:173-179

Lybolt M, Neil D, Zhao J, Feng Y, Yu K-F, Pandolfi J (2011) Instability in a marginal coral reef: the shift from natural variability to a human-dominated seascape. Frontiers in Ecology and the Environment 9:154-160

Maxwell WGH (1968) Atlas of the Great Barrier Reef. Elsevier, Amsterdam

McCulloch M, Fallon S, Wyndham T, Hendy E, Lough J, Barnes D (2003b) Coral record of increased sediment flux to the inner Great Barrier Reef since European settlement. Nature. 13;421(6924):727-30

Neil DT (1996) Sediment concentrations in streams and coastal waters in the North Queensland humid tropics: Land use, rainfall and wave resuspension contributions. In: Hunter HM, Eyles AG, Rayment GE (eds) Downstream effects of land use. Dept. Natural Resources, Brisbane, pp97-101

Neil DT (1998) Moreton Bay and its catchment: landscape and seascape, development and degradation. The University of Queensland, School of Marine Science, Brisbane

Neil DT, Orpin AR, Ridd PV, Yu B (2002) Sediment yield and impacts from river catchments to the Great Barrier Reef lagoon. Marine and Freshwater Research 53:733-752

Orpin AR, Ridd PV (2012) Exposure of inshore corals to suspended sediments due to wave-resuspension and river plumes in the central Great Barrier Reef: A reappraisal. Continental Shelf Research 47:55-67

Orpin AR, Ridd PV, Thomas S, Anthony KRN, Marshall P, Oliver J (2004) Natural turbidity variability and weather forecasts in risk management of anthropogenic sediment discharge near sensitive environments. Marine Pollution Bulletin 49:602-612

Palmer SE, Perry C, Smithers SG, Gulliver P (2010) Internal structure and accretionary history of a nearshore, turbid-zone coral reef: Paluma Shoals, central Great Barrier Reef, Australia. Marine Geology 276:14-29

Perry CT, Smithers SG (2006) Taphonomic signatures of turbid-zone reef development: examples from Paluma Shoals and Lugger Shoal, inshore central Great Barrier Reef, Australia. Coral Reefs 28:941-948

Perry CT, Smithers SG, Johnson KG (2009b) Long-term coral community records from Lugger Shoal on the terrigenous inner-shelf of the central Great Barrier Reef, Australia. Coral Reefs 28:941-948

Perry CT, Gulliver P, Palmer SE, Smithers SG (2010) Internal structure and accretionary history of a nearshore, turbid-zone coral reef: Paluma Shoals, central Great Barrier Reef, Australia. Marine Geology 276:14-29

Perry CT, Smithers SG, Gulliver P, Browne NK (2012) Evidence of very rapid reef accretion and reef growth under high turbidity and terrigenous sedimentation. Geology 40:719-722

Perry CT, Smithers SG, Palmer SE, Larcombe P, Johnson KG (2008) 1200 year paleoecological record of coral community development from the terrigenous inner shelf of the Great Barrier Reef. Geology 36:691-694

Ridd P, Larcombe P (1994) Biofouling control for optical backscatter suspended sediment sensors. Marine Geology 116:255-258

Sahl LE, Marsden MAH (1987) Shelf sediment dispersal during the dry season, Princess Charlotte Bay, Great Barrier Reef, Australia. Continental Shelf Research 7:1139-1159

Smithers S, Larcombe P (2003) Late Holocene initiation and growth of a nearshore turbid-zone coral reef: Paluma Shoals, central Great Barrier Reef, Australia. Coral Reefs 22:499-505

Trimarchi S, Keane J (2007) Port of Hay Point apron area and departure path capital dredging project: environmental review. Ports Corporation of Queensland, Brisbane

Wolanski E, Delesalle B, Gibbs R (1994) Carbonate mud in Mataiva Atoll, French Polynesia: Suspension and export. Marine Pollution Bulletin 29:36-41

Wright LD (1995) Morphodynamics of Inner Continental Shelves. CRC Press, Boca Raton

Chapter 3. WAVE SHEAR STRESS – DOMINANT TURBIDITY DRIVER

3.1 Introduction

It is well established that wave-induced resuspension of pre-existing bed sediment is the dominant driver of turbidity in coastal reef waters. Resuspension is well correlated to wave height, wave period and tidal range and also wind speed (Larcombe et al. 1995b; Larcombe et al. 2001; Anthony et al. 2004; Orpin et al. 2004; Cooper et al. 2008; Fabricius et al. 2012; Orpin and Ridd 2012). This process is initiated by frequent south easterly winds around the inshore GBR. These trade winds generate waves, which exert shear-stresses on the seabed and if the shear-stress reaches a critical limit, sediment is resuspended into the water column. The maximum bottom shear stress in most coastal regions is caused by oscillatory wave-induced currents (Wright 1995). Although waves and tidal currents can work conjointly to re-suspend bed sediments, in general for most of the GBR tidal currents alone are too weak (Grant and Madsen 1979; Orpin et al. 1999).

The dominance of waves in controlling sediment resuspension, turbidity and ultimately light levels has been ascertained. Therefore, any field measurements of water turbidity close to coral reefs should ideally be supplemented by measurements of the wave condition, so that high turbidity events caused by waves can be attributed to the correct cause. To this end, much environmental monitoring work (especially that related to coastal dredging operations) benefits from wave measurements in addition to turbidity and light measurements (Waltham et al. 2015).

Much of the measurements of waves and turbidity close to corals on the Great Barrier Reef (and a considerable proportion of that reported in Chapter 2) have utilised instrumentation developed by the Marine Geophysical Laboratory at James Cook University. In addition to measuring turbidity and light, these nephelometers also produce a crude measure of wave-induced pressure fluctuations, by monitoring water pressure every second, over a period of 10 seconds (Figure 18). The RMS (root mean squared) fluctuation in pressure is then reported and increased RMS water pressure is often related to increased turbidity events (Figure 19). One major problem with this methodology is that measuring pressure fluctuations at 1 Hz over 10 seconds would generally be regarded as grossly insufficient, both in terms of frequency and total period, to describe the wave field. For most work measuring waves, one could expect a sampling frequency of a few Hertz over a period of many minutes (Tucker 1991). Unfortunately the high sampling rate that is generally used requires very large memory capacity, which is not available on the Campbell Scientific (CR1000) data loggers used in these instruments. The question thus arises, can the very small quantity of wave data be used to make meaningful calculations about bottom shear stress? This had not been attempted previously, despite the instrument being used in dredge monitoring operations over the last decade in locations such as: Barrow Island (WA), Abbot Point, Hay Point, Townsville, Roslyn Bay and many other locations on the Queensland coast. As such a very large amount of pressure data is available, that has possibly not been used to its full extent and this is the subject of this chapter.

Figure 18 Picture of a Nephelometer. This water quality monitoring instrument logs turbidity (using an optical backscatter sensor), pressure, light and temperature. Featuring Campbell logger hardware.

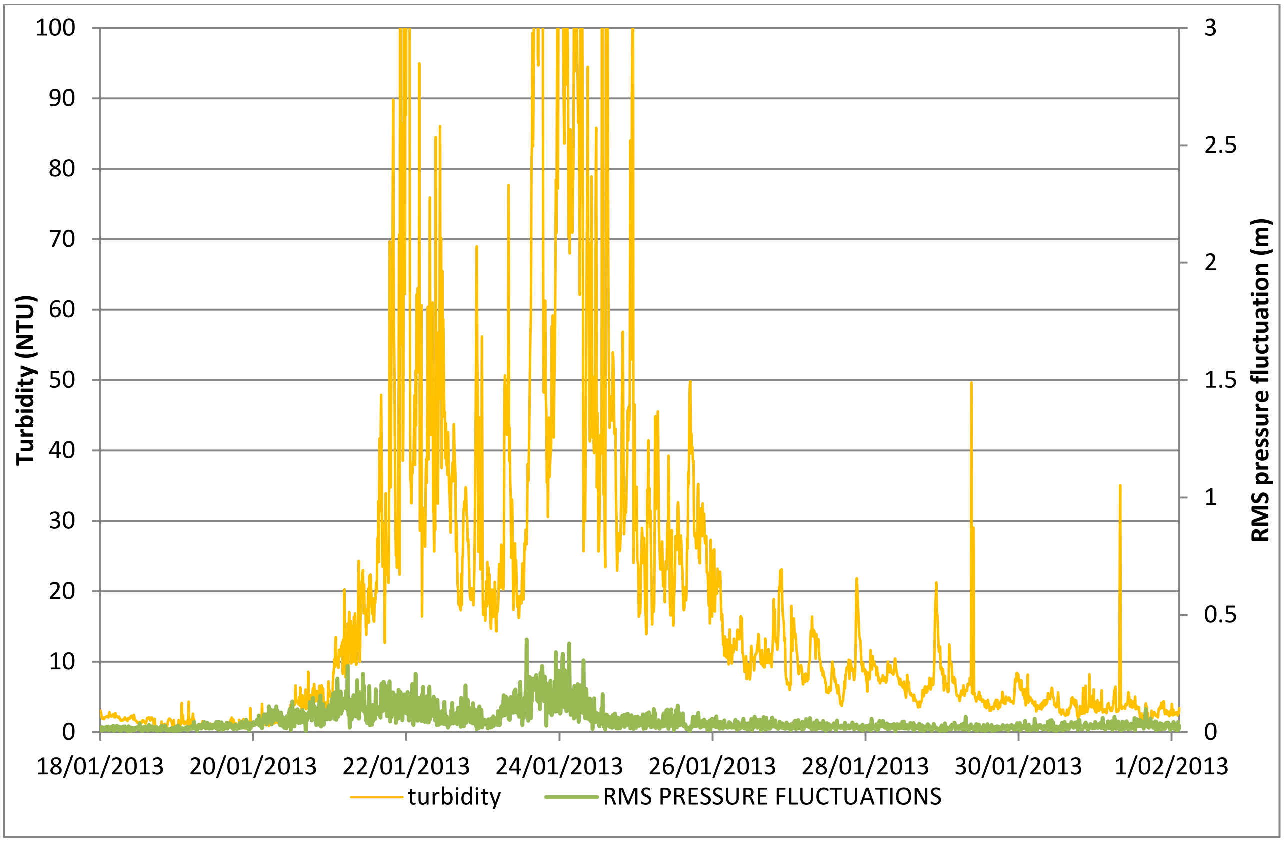

Figure 19 Relationship of RMS wave height (pressure fluctuations) to turbidity.

Bottom water pressure data (10 readings at 1 Hz) were collected along with turbidity data at Cleveland Bay (18/01/2013-1/2/2013). A Matlab routine, waveps.m was utilised which calculates the significant wave height H_{sig} after correcting the attenuation of pressure variations for depth. *Wavesp.m* uses standard calculations, as described in (Tucker 1991). Average significant wave heights were also calculated by the same method for two 12 hour periods of low (<10 NTU) and high (>50 NTU) turbidity.

The resultant significant wave height was used to calculate wave-induced bottom shear-stress (τ_w). Maximum shear stress was also derived and calculated in terms of its components, current-induced shear stress and wave-induced shear stress (Basic mathematical treatment of shear stress is provided in Appendix C). A Matlab program was written (Appendix D), which solves these equations for any given significant wave heights and depths in Cleveland Bay.

3.2 Calculation of maximum bottom shear-stress

The maximum bottom shear-stress for co-linear flow is given by;

$$\tau_{bmax} = \tau_c + \tau_w \tag{1}$$

as described by (Signell et al. 1990) and (Orpin et al. 1999). Here τ_w is the maximum oscillatory (unsteady) component (due to the wave) and τ_c is the steady component (due to the current) (Grant and Madsen 1979). Both components are actually functions of waves and currents. However, the shear stress components are partitioned into two parts for mathematical simplicity. In other words, equation (1) is not a simple linear addition of shear stresses due to pure waves and pure currents.

Following Signell et al. (1990), the effect of the steady current on the wave-induced shear stress (τ_w) is small and thus can be neglected. τ_w is controlled by a straightforward friction factor, f_w as defined below (section 3.2.3). However, the current-induced shear stress (τ_c) is a strong function of both waves and currents. The non-linear interaction is controlled by the effective drag coefficient (C_{de}), which is calculated by an iterative process also defined below (section 3.2.3).

The governing equation for instantaneous boundary shear stress (τ_b) is defined in Appendix C and can be used to obtain maximum bottom shear stress (τ_{bmax}), where the magnitude is given as,

$$|\tau_{bmax}| = \frac{1}{2}\rho C_{de}\alpha|u_b|^2 \tag{2}$$

where $|u_b|$ is the maximum near-bottom orbital velocity (also derived in Appendix C) as $u_b = \frac{\omega a}{\sinh(kh)}$, and

$$\alpha = 1 + (|u_c|/|u_b|)^2 + 2(|u_c|/|u_b|)\cos\phi_c \tag{3}$$

where $|u_c|$ is the magnitude of the steady current velocity at reference height above the bed and ϕ_c is the angle made by u_c with the direction of wave propagation. This angle only needs to be defined from 0° to 90° in accordance with linear wave theory. Magnitudes of the two partitioned shear stress components are thus calculated separately (equations (4) and (6) below).

3.2.1 Above the wave boundary layer

In the upper region above the boundary layer, wave-induced motions and current induced motions are able to be resolved separately. Here shear stress is only related to the steady current. Disregarding direction, the magnitude of this current induced shear stress is given by,

$$|\tau_c| = \frac{1}{2}\rho C_{de}|u_b|^2 = \rho {u_{*c}}^2$$

4

And the current-induced shear velocity, u_{*c} (derived in Appendix C) is given as,

$$u_{*c} = \sqrt{\frac{\tau_c}{\rho}}$$

5

3.2.2 Inside The Wave Boundary Layer

Inside the wave boundary layer, close to the seabed, a nonlinear interaction between the two flows occurs where shear stress is associated with both the wave and the current motions. Therefore the calculation of maximum bottom shear stress will require the solution to the component equation (1)

To begin, the magnitude of the wave-induced component of shear stress, τ_w is given by,

$$|\tau_w| = \frac{1}{2}\rho f_w|u_b|^2 = \rho {u_{*w}}^2$$

6

And the wave-induced shear velocity, u_{*w} (derived in Appendix C) is given as,

$$u_{*w} = \sqrt{\frac{\tau_w}{\rho}}$$

7

In equation (6), f_w is the wave friction factor, defined below. The equation for wave height, $a = H/2$ is substituted into this equation to give,

$$u_b = \frac{H\omega}{2\sinh kh}$$

8

Squaring equation (8) and substituting into equation (6) gives,

$$\tau_w = \frac{\rho f_w H^2 \omega^2}{8\sinh^2(kh)}$$

9

and similarly,

$$\tau_c = \frac{\rho C_{de} H^2 \omega^2}{8\sinh^2(kh)}$$

10

and

$$\tau_{bmax} = \frac{\rho C_{de} H^2 \omega^2}{8\sinh^2(kh)}$$

11

In the Matlab program (Appendix D), using equations (9, 10 and 11), separate shear stresses may be graphed directly as plots of τ_w, τ_c or τ_{bmax} vs. wave period, T. However, rearranging equation (9) for wave height, H produces an equation that may be used to contour wave-induced shear stresses based on a graph of wave height, H_w vs. period, T,

$$H_w = \sqrt{\frac{8\tau_w \sin^2(kh)}{\rho f_w \omega^2}}$$

12

Similarly an expression can be produced from equation (10) that can be used to contour current-induced shear stress based on a graph of wave height, H_c vs. period, T,

$$H_c = \sqrt{\frac{8\,\tau_c \sin^2(kh)}{\rho C_{de} \omega^2}}$$

13

Finally, a summation of the wave-induced and current-induced shear stresses is implemented into the Matlab routine (Appendix D) to provide contours of maximum bottom shear stress using the following equation,

$$H_{bmax} = \sqrt{\frac{8\,\tau_{max} \sin^2(kh)}{\rho C_{de} \omega^2}}$$

14

3.2.3 Calculation of Friction Factor and Effective Drag Coefficient

In equation (6) for wave-induced shear stress, f_w is an empirical friction factor depending on physical bed roughness (k_b) and the near-bottom excursion amplitude, $A_b = u_b/\omega$. Bed roughness has been calculated as 0.0025 m for Cleveland bay by (Lou and Ridd 1997). f_w is calculated in the Matlab routine (Appendix D) as it is in (Grant and Madsen 1982) using a method by Jonsson (1966) which gives:

$$f_w = \left\{ \begin{array}{cc} 0.13(k_b/A_b)^{0.40}, & \left(\frac{k_b}{A_b}\right) < 0.08 \\ 0.23(k_b/A_b)^{0.62} & 0.08 < \frac{k_b}{A_b} < 1.00 \\ 0.23 & \frac{k_b}{A_b} > 1.00 \end{array} \right\}$$

15

In equation (4) for current-induced shear stress, the effective drag coefficient, C_{de} relates the maximum bottom shear stress to the maximum velocity due to the wave and currents in equation (2). The iterative procedure described below is applied in the Matlab routine (Appendix D) to calculate the effective drag coefficient (C_{de}) at reference height, z_r. (using 0.3 m for Cleveland Bay). In (Signell et al. 1990), the current reference height, z_r is chosen within the region of almost constant stress, yet still above the wave boundary layer ($z_r = 0.2\ m$). From Wright (1995) the effective drag coefficient is defined as,

$$C_{de} = \left(\frac{u_{*c}}{u_c}\right)^2$$

16

Rearranging this equation and making an initial guess of C_{de} (0.015 was chosen in Appendix D), enables the calculation of the steady (current-induced) shear velocity component u_{*c},

$$u_{*c} = \sqrt{C_{de} u_c}$$

17

Now, the turbulence inside the wave boundary layer is described by the combined wave-current shear velocity u_{*cw}, may be defined using equation (2) as,

$$u_{*cw} = \sqrt{\frac{\tau_{bmax}}{\rho}} = \left(\frac{1}{2}C_{de}\alpha\right)^{1/2} |u_b| \tag{18}$$

Substituting into equation (1), and then using equations (4) and (6) this becomes,

$$u_{*cw} = \sqrt{u_{*w}^2 + u_{*c}^2} \tag{19}$$

In the next step of the iterative procedure, the apparent bottom roughness k_{bc} is calculated. This component represents the level of turbulence due to the combination of the wave boundary layer and the actual physical bottom roughness k_b. This results in the current above the wave boundary layer being subject to a greater level of resistance due to the wave presence.

$$k_{bc} = k_b \left[24 \frac{u_{*cw}}{u_b} \frac{A_b}{k_b}\right]^{\beta} \tag{20}$$

where the near-bottom excursion amplitude $A_b = \frac{u_b}{\omega}$, and the exponent β is given by,

$$\beta = 1 - \frac{u_{*c}}{u_{*cw}} \tag{21}$$

The velocity profile in the constant stress region above the wave boundary layer may be determined using the Law of the Wall relation,

$$u = \frac{u_{*c}}{\kappa} \ln\left(\frac{z+h}{k_{bc}/30}\right)$$

22

where $z = -h + z_r$. The velocity profile is then substituted into equation (4). This produces a new estimate of the drag coefficient,

$$C_{de} = \left[\frac{\kappa}{\ln(30z_r/k_{bc})}\right]^2$$

23

This iteration is repeated until the estimates of the drag coefficient differ by less than 10^{-7}. Finally, the corrected C_{de} value is substituted into equation (4) to calculate current-induced shear stress.

3.3 Calculation of wave-induced shear-stress from pressure

The first step is to calculate significant wave height (H_{sig}) from raw pressure data. H_{sig} is given by,

$$H_{sig} = 4(m_0)^{1/2}$$

24

where m_0 is the variance of sea surface elevation. That is, the total energy of the wave system. Significant wave height was traditionally defined as the mean wave height (trough to crest) of the highest third of the waves ($H_{1/3}$). However, in more recent times (Tucker 1991) significant wave height has come to be known as (H_{sig}) where for typical sea states,

$$0.9\,H_{sig} < H_{1/3} < H_{sig}$$

25

H_{sig} can be estimated from a time series of surface elevation measurements, using the Tucker-Draper method (Tucker 1991)(pp 43, 50-54, 92-93). The *wave.sp* routine (obtained from (http://neumeier.perso.ch/matlab/waves.html#Tucker) uses the standard methods, as described in (Tucker 1991) to correct the attenuation of pressure variations with depth. The input arguments are the uncorrected water heights (m) above bed, as obtained from calibrated pressure-sensor data, height of the pressure sensor above bed (m) and sampling frequency (Hz).

3.4 Results

A Matlab program (resuspension.m) (Appendix D) outputs graphs of maximum bottom shear stress vs. wave period for any given significant wave height and depth in Cleveland Bay. The routine was constructed using the theory in (section 3.2) and in Appendices B and C. This program also outputs bottom orbital velocity (Appendix C(i)) and individual shear stress components, which are given in section (3.4).

Significant wave heights were calculated using the above method using over 2000 groups of 10 individual pressure measurements (i.e. ~13 days of data), the sensor height from the bed (0.3 m) and sampling frequency of 1 Hz (Figure 20)(Figure 21). The resultant H_{sig} *time series* was input into the program *resuspension.m* (Appendix D) alongside mean site depth (12.1 m), Cleveland Bay bottom roughness (z_0 = 0.0025 m) and mean current (u_c = 0.1 m/s) to generate a time series of wave-induced bottom shear stress (Figure 22). During periods of high turbidity, shear stress also increases.

These results show that in Cleveland Bay, wave-induced shear-stress is indeed a dominant driver of turbidity due to resuspension of bottom sediment. Low turbidity conditions produce shear-stresses that fall below the critical threshold (1 N/m^2) and conversely, during a high turbidity event, wave-induced shear stress exceeds the limit (Figure 22). A clear lag exists, where it takes some time for the turbidity to go down after the stress drops off. This may be attributed to the time it takes for the sediment to fall back out of suspension and would be dependent on grain size and flocculation. Orpin (1999) postulated that in Cleveland Bay, a shear stress of 1 N/m^2 would be enough to generate turbidity of 20 NTU. These results are in close agreement with this value. Although, even with much lower bottom stress values (0.1 N/m^2), appreciable resuspension can be observed (Figure 22).

The resultant average H_{sig} for each regime (high/low turbidity) was similarly utilized into the program (Appendix D), outputting graphs of maximum bottom shear stress vs wave period, for a given H_{sig} value (Figure 23). The dominant wave period for Cleveland Bay is highlighted (Tp = 4.9 s) as well as the critical shear-stress limit required for resuspension (1 N/m^2) (Orpin 1999). This limit is to be used cautiously, as the true value will be highly dependent on grain size and likely to vary over time. Mean H_{sig} values during normal and cyclonic conditions are taken from the literature and also used in the program (Appendix D) to generate shear stress curves (Figure 23). For high mean values of H_{sig} (i.e. high turbidity event, cyclonic conditions) the resultant shear stress contours show at the dominant wave period (4.9 s) resuspension should be occurring. Conversely, H_{sig} for low turbidity conditions produce shear stresses that are below the critical shear stress threshold for normal wave periods available in Cleveland Bay (Figure 23).

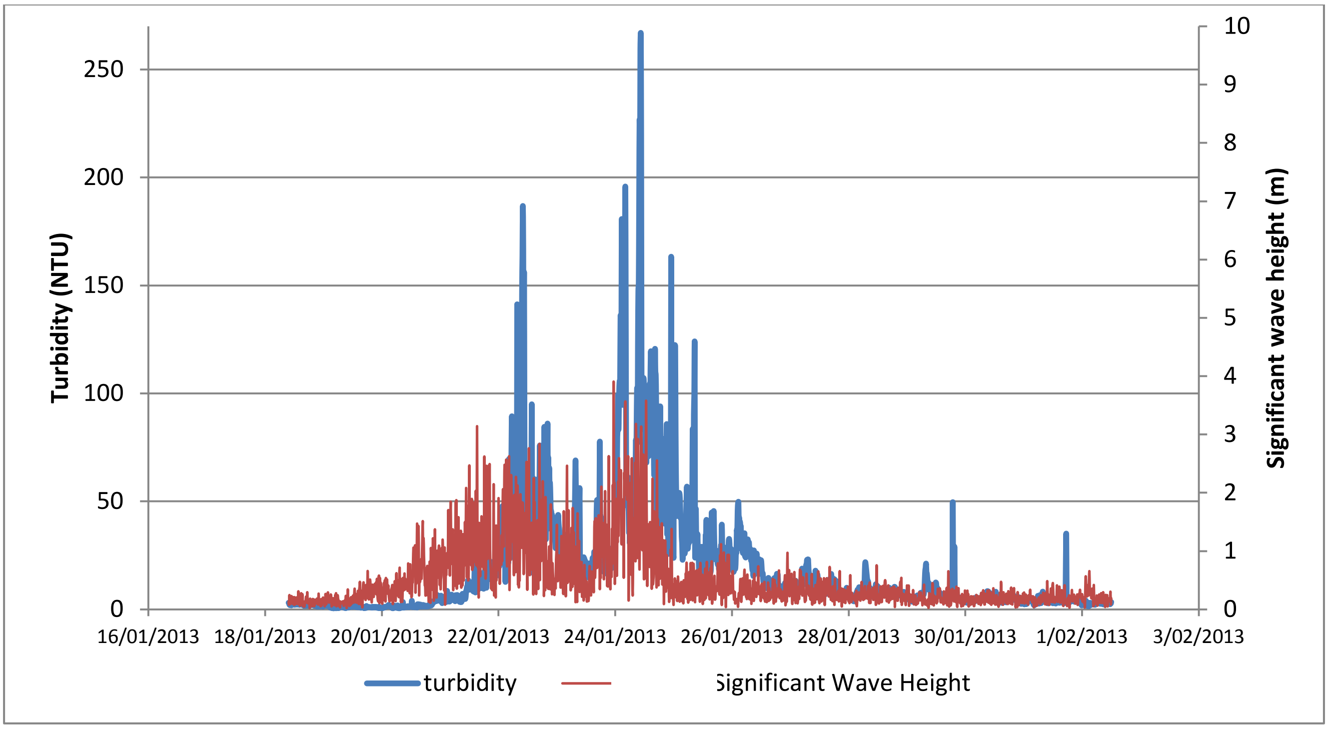

Figure 20 Calculated significant wave height and turbidity time series for the Cleveland Bay dataset. Each H_{sig} value is calculated from 10 individual pressure measurements, the sensor height from the bed (0.3 m) and sampling frequency of 1 Hz.

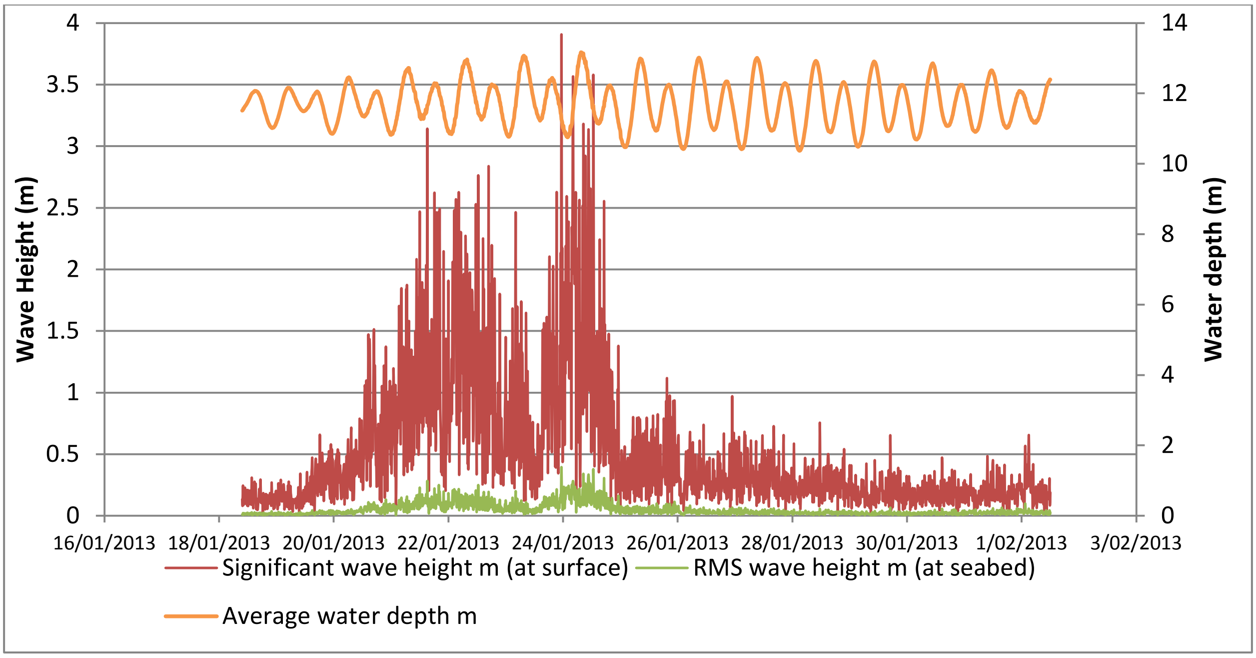

Figure 21 Significant wave height (m) and RMS wave height (m) calculated from calibrated pressure measurements (Average water depth (m)). Data from Cleveland Bay 2013.

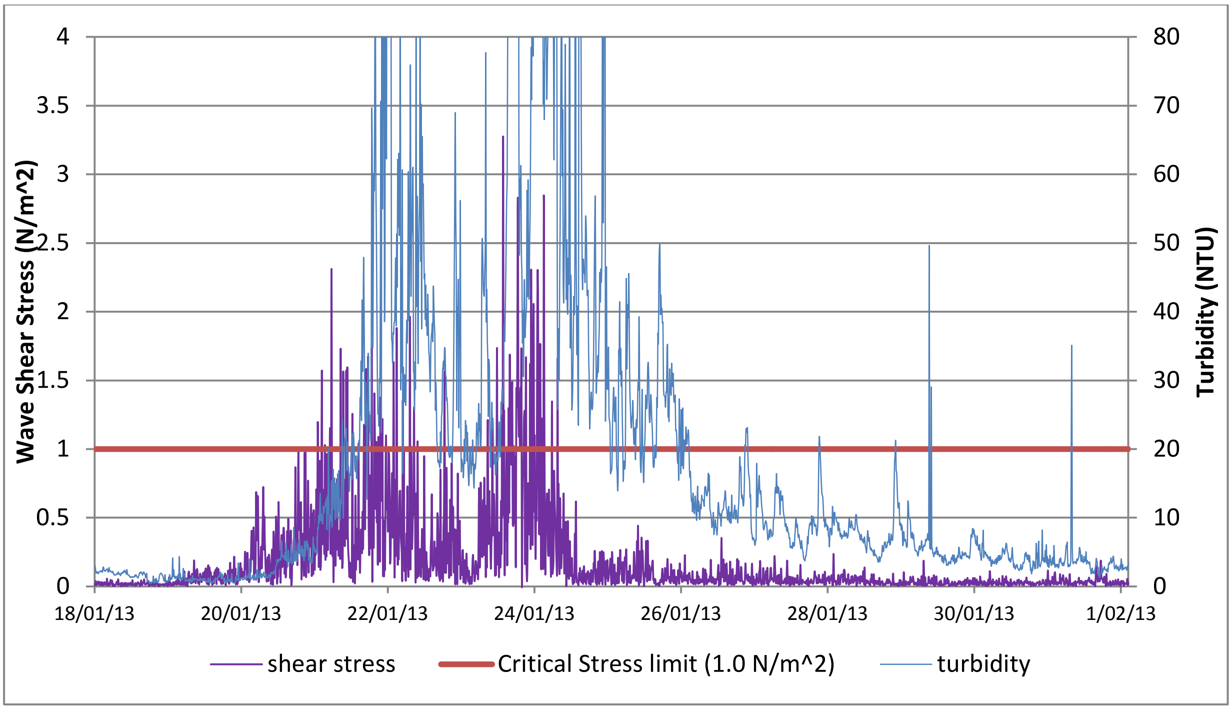

Figure 22 Calculated wave-induced bottom shear stress and concurrent turbidity time series for Cleveland Bay. Site specific constants include mean depth = 12 m, bottom roughness = 0.0025, mean current = 0.1 m/s and mean period = 4.9 s (Orpin 1999). Critical stress limit for resuspension shown (1 N/m^2) (Orpin 1999).

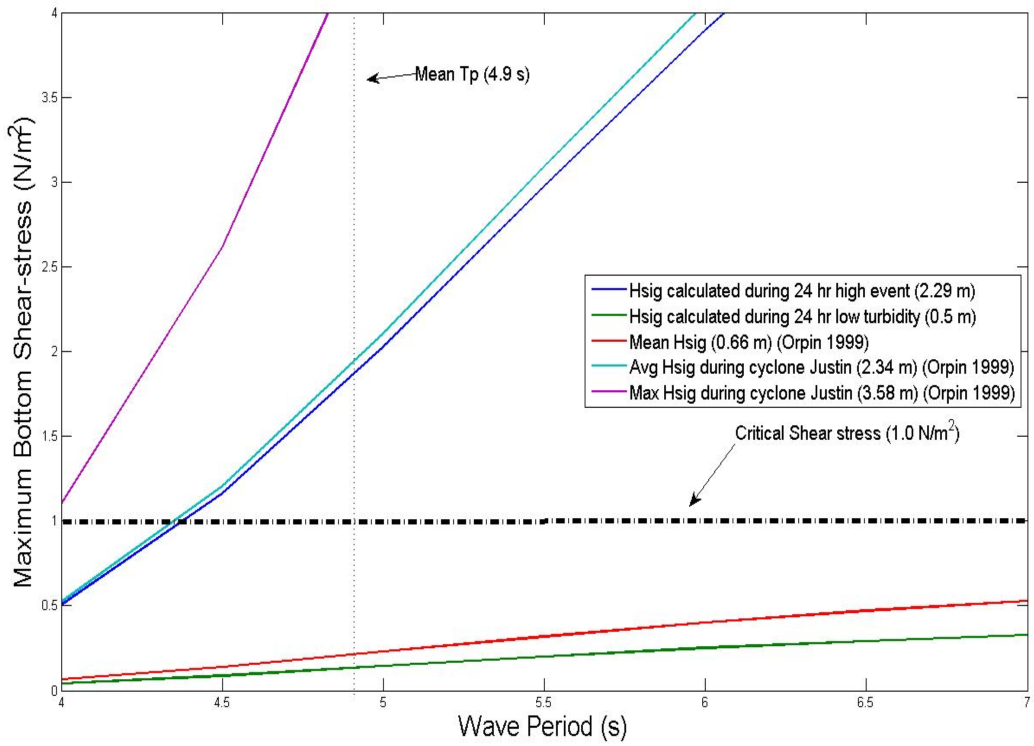

Figure 23 Maximum shear-stress calculated using various sig wave heights (H_{sig}) vs. wave period. H_{sig} of 2.29 m and 0.5 m are calculated from measured data during high and low turbidity event respectively. Other wave heights taken from the literature for mean turbidity (0.66 m) and a cyclonic event (2.34, 3.58 m) (Justin - Cat 0). Critical stress limit taken from the literature (1 N/m^2). Mean wave period in Cleveland Bay is 4.9 s. Results show during high turbidity events, bottom shear stresses exceed critical stress limit, for any realistic wave period.

3.5 Discussion

As a dominant turbidity driver, wave-induced shear stress was calculated from very coarse pressure measurements near the seabed, for the first time with instrumentation developed over the past 10 years with the Marine Geophysics Laboratory. These results still need to be independently tested but have led to preliminary shear stress investigations in consultancy work, which the author is currently involved in, alongside water quality monitoring projects such as dredge works in Barrow Island and Hay point. There is clearly scope for future research in this area and the next step will be independent verification of these findings.

REFERENCES

Anthony KRN, Ridd PV, Orpin AR, Larcombe P, Lough J (2004) Temporal variation of light availability in coastal benthic habitats: Effects of clouds, turbidity, and tides. Limnology and Oceanography 49:2201-2211

Cooper TF, Ridd PV, Ulstrup KE, Humphrey C, Slivkoff M, Fabricius KE (2008) Temporal dynamics in coral bioindicators for water quality on coastal coral reefs of the Great Barrier Reef. Marine and Freshwater Research 59:703-716

Fabricius KE, De'ath G, Humphrey C, Zagorskis I, Schaffelke B (2012) Intra-annual variation in turbidity in response to terrestrial runoff on near-shore coral reefs of the Great Barrier Reef. Estuarine, Coastal and Shelf Science 116: 57-65

Grant WD, Madsen OS (1979) Combined Wave and Current Interaction with a Rough Bottom. Journal of Geophysical Research 84:1797-1808

Grant WD, Madsen OS (1982) Movable Bed Roughness in Unsteady Oscillatory Flow. J Geophys Res 87:469-481

Larcombe P, Costen A, Woolfe KJ (2001) The hydrodynamic and sedimentary setting of nearshore coral reefs, central Great Barrier Reef shelf, Australia: Paluma Shoals, a case study. Sedimentology 48:811-835

Larcombe P, Ridd PV, Prytz A, Wilson B (1995b) Factors controlling suspended sediment on inner-shelf coral reefs, Townsville, Australia. Coral Reefs 14:163-171

Lou J, Ridd PV (1997) Modelling of Suspended Sediment Transport in Coastal Areas Under Waves and Currents. Estuarine, Coastal and Shelf Science 45:1-16

Orpin AR, Ridd PV (2012) Exposure of inshore corals to suspended sediments due to wave-resuspension and river plumes in the central Great Barrier Reef: A reappraisal. Continental Shelf Research 47:55-67

Orpin AR, Ridd PV, Stewart LK (1999) Assessment of the relative importance of major sediment-transport mechanisms in the central Great Barrier Reef lagoon. Australian Journal of Earth Sciences 46:883-896

Orpin AR, Ridd PV, Thomas S, Anthony KRN, Marshall P, Oliver J (2004) Natural turbidity variability and weather forecasts in risk management of anthropogenic sediment discharge near sensitive environments. Marine Pollution Bulletin 49:602-612

Signell RP, Beardsley RC, Graber HC, Capotondi A (1990) Effect of Wave-Current Interaction on Wind-Driven Circulation in Narrow, Shallow Embayments. Journal of Geophysical Research 95:9671-9678

Tucker MJ (1991) Waves in ocean engineering: measurement, analysis, interpretation. E. Horwood, New York

Waltham N, Mckenna S, York P, Devlin M, Campbell S, Rasheed MA, Da Silva E, Petus C, Ridd P (2015) Port of Mackay and Hay Point Ambiet Marine Water Quality Monitoring Program. Centre for Tropical Water and Aquatic Ecosystem Research, James Cook University

Wright LD (1995) Morphodynamics of Inner Continental Shelves. CRC Press, Boca Raton

Chapter 4. THE SEARCH FOR SECONDARY DRIVERS OF TURBIDITY

4.1 Abstract

Water turbidity and suspended sediment can influence the location and nature of coral reefs, particularly coastal reefs which may also be affected by land runoff as well as resuspension of bottom sediment. Wave-induced resuspension is presumed to be the dominant driver of turbidity at coastal sites; however, secondary factors such as water depth, distance to shore and distance to river may also contribute to water turbidity. In this chapter, previously published turbidity exceedance data (from 56 sites on the coastal Great Barrier Reef (GBR) also used in Chapter 1) were analysed for relationships between turbidity and these secondary oceanographic factors. Most deployment periods are not concurrent, which complicates inter-site comparison. However 35 sites in Cleveland Bay are grouped into four concurrent periods (1993, 2000, 2002 and 2004), enabling a more meaningful comparison. No significant relationship was found between the above factors and turbidity at 10, 50 and 90% exceedance levels. Similarly, no significant signal was attained using multiple linear regression and stepwise regression analyses, including interaction and quadratic factor combinations. Results indicate either turbidity at these sites is simply not driven by these factors, or that the driver is too weak to be measurable from these data.

4.2 Introduction

Australia's Great Barrier Reef (GBR) is the largest and most bio-diverse coral reef eco-system in the world, extending over 14 degrees of latitude (Maxwell 1968; Hopley 1982; Hopley et al. 2007). Water turbidity is a transient phenomenon which is spatially and temporally highly variable across the GBR. Turbidity in the inshore or coastal region of the GBR is a major focus for research due to land proximity, exposure to catchment runoff, dredging activities and coastal development (Furnas 2003).

It is well established that wave-induced resuspension of pre-existing bed sediment is the dominant driver of turbidity in coastal reef waters (Larcombe et al. 1995b; Larcombe et al. 2001; Anthony et al. 2004; Orpin et al. 2004; Cooper et al. 2008; Fabricius et al. 2012; Orpin and Ridd 2012). For much of the inner shelf, sediment resuspension is correlated to wave height, wave period and tidal range and also wind speed (Larcombe et al. 1995b; Fabricius et al. 2012). However, secondary drivers of turbidity are still not well understood in the coastal Great Barrier Reef (GBR) or in reefs around the world. The term 'driver' is defined here as a potential influencing factor of turbidity. Secondary influences/drivers may include factors such as distance to shore or river mouth and potentially water depth.

Riverine sediment delivery to the GBR has been increasing since European settlement, primarily due to anthropogenic effects on catchments (Moss et al. 1993; McCulloch et al. 2003a; Pandolfi et al. 2003; Orpin and Ridd 2012). Concern for the habitats and biological (especially benthic) communities on the GBR shelf has (perhaps incorrectly) led to the hypothesis that riverine sediment discharge is a significant driver of turbidity levels

(Wolanski et al. 2004; Brodie et al. 2005; Wolanski and De'Ath 2005; Wolanski et al. 2008; Lambrechts et al. 2010; De'ath et al. 2012; Fabricius et al. 2012). A recent paper examined the main determinants of inshore turbidity using 3 years of almost continuous turbidity data. Effective wave height was found to be the major driver (as is currently accepted) but secondary turbidity signals were also found for river distance and river discharge (Fabricius et al. 2012).

This paper aims to further address this issue by investigating the relationship of turbidity to several potential underlying factors, using nephelometer data obtained from a previous study by Macdonald et. al (2013). Potential factors include water depth, distance to shore and distance to river. This work is a broad investigation, focusing primarily on turbidity drivers not sediment regimes, although they are undoubtedly connected. A useful addition to this work would be a comprehensive sedimentary analysis; however corresponding sediment data are not readily available. A comparison of wave data to potential secondary factors would also be instructive. There is scope for such work to be done (see Chapter 3) however for most of these data, there is little or no corresponding wave information available.

4.2.1 Turbidity and suspended sediment

Turbidity measures the cloudiness of water is by detecting the light scattered at right angles to a beam of light that illuminates the water of interest. The scattering is predominantly caused by suspended material in the water column consisting of; sediment, algae, micro-organisms and other particulate matter. Turbidity is often closely related and 'calibrated' to suspended sediment concentration (SSC) (Larcombe et al. 1995b) but is also dependent upon a wide range of sedimentary variables, especially those related to grain size and type (Ludwig and Hanes 1990; Conner and De Visser 1992; Wolanski et al. 1994; Bunt et al. 1999).

Sediment is a normal and essential part of marine ecosystems and a natural relationship exists between silty and terrigenous sediments and many inshore coral reefs (Umbgrove 1947; Smithers and Larcombe 2003; Perry et al. 2008; Perry and Smithers 2009; Perry et al. 2009a; Browne et al. 2010; Perry and Smithers 2010). However, suspended sediment may act as a limiting factor to coral reef health in certain situations, primarily by reducing available light for photosynthesis, and being a source of material that subsequently settles onto the bed.

4.2.2 Dominant turbidity drivers

Wave energy is indisputably linked to sediment resuspension and thus turbidity (Orpin and Ridd 2012). A study on turbidity at an inshore fringing reef, in Nelly Bay, Magnetic Island by Orpin et al. (2004), noted the large range in turbidity, between 0.1 to >100 NTU over a 37 day period. Elevated turbidity events occurred simultaneously with high winds and associated high sea states, whereas during calm weather, turbidity levels were <1 NTU (Orpin et al. 2004). Whilst these and other studies inform us about the main driving factors behind changes in turbidity (i.e. sediment availability and hydrodynamic energy) and indicate that the turbidity regime in many places will have strong local controls, there remains relatively little information along the coastal GBR regarding secondary turbidity drivers.

Recently, major research undertaken by Fabricius et al. (2012) confirmed wave resuspension as the dominant turbidity driver and was the first study to document secondary turbidity drivers on the GBR (Fabricius et al. 2012). At any given wave height, wave period and tidal range, turbidity was found to be affected by river flow, rainfall and river distance. Fourteen reef sites were measured and for those nearest to rivers, mean turbidity was 10, 3 and 2-fold higher compared with the reefs furthest away in the Fitzroy, Burdekin and Whitsunday Regions, respectively. Turbidity was found to be unrelated to distance to river in the Wet Tropics Region.

4.2.3 Turbidity exceedance

Exceedance curves have been used previously in a study of the turbidity regime of reef-related sites in the GBR and Moreton Bay for a range of time intervals within a period of one and a half decades. The study by Macdonald (2013) used exceedance to demonstrate the strong spatial and temporal variability in water turbidity across inter/intraregional scales, as well as potentially contributing to refinement of water quality guideline values (Macdonald 2013). Exceedance was also used by Larcombe et al. (2001) to effectively demonstrate the bimodal turbidity regimes at Paluma Shoals and other inner shelf 'turbid' zone reefs. The resultant exceedance curves enabled inferences of repeated volumes of material resuspended and temporarily accumulated (Larcombe et al. 2001).

In this paper, exceedance curves are used in a similar fashion to Macdonald (2013) (chapter 2), by calculating T10, T50 and T90 exceedance values. However, here the values are analysed against potential secondary drivers as explained above. This is a useful method for searching for turbidity drivers, as it enables a large amount of data to be condensed and examined. Different exceedance regimes can be easily pinpointed by investigating the relevant percentage of time that a turbidity level exceeds.

4.3 Methods

An analysis is performed on previously published turbidity exceedance data, from 56 sites on the coastal Great Barrier Reef (GBR) (Macdonald et al. 2013) (Chapter 2). Relationships between turbidity and potential secondary oceanographic factors are investigated. Original turbidity measurements were gathered between 1993 and 2009, taken from 56 sites along the inner shelf of the GBRL (Table 4). Turbidity exceedance curves (the values for T_{10}, T_{50}, T_{90}, i.e. the turbidity value which 10%, 50% and 90% of the data exceed respectively) were published in Macdonald (2013). T_{50} values are used to examine median turbidity. T_{10} and T_{90} are used here to investigate turbidity extremes at either end of the scale (i.e. periods of very high and very low turbidity respectively). The data are utilised to investigate secondary drivers/influences of turbidity and determine in particular if the results match what is currently accepted in the literature to be the dominant/secondary turbidity and sediment drivers.

Cleveland Bay sites were investigated more thoroughly as much of these data were obtained concurrently across that region (Table 4). It was therefore possible to group sites into four deployment periods. This enabled a more meaningful comparison of data that were both geographically close (within 10 km) and obtained during the same time period.

4.3.1 Water depth

Latitude and longitude data were obtained from Macdonald (2013). Average water depths at site locations were then found using marine charts. Site depths are generalised and indicative only, as a full bathymetric survey was not performed. All sites are located on reef flats with the exception of sites: 8, 29, 30, 34, 35, 39 and 45 (Table 5). These data are compared with turbidity exceedances to examine whether a statistical relationship exists.

4.3.2 Distance to mainland and river

Site location data was obtained as above and distances were calculated from atlas measurements for each site (Table 5). Distance to mainland was examined rather than distance to shore (or island-shore) to ensure distance to island-shore would not affect data consistency. Distance to mainland may be a more meaningful variable, since it also correlates to river distance, whereas distance to island shore may be correlated to an increase in turbidity due mostly to the reduction in depth near the shoreline. Distance data were obtained from nautical chart measurements using decimal co-ordinates for each site (Table 4).

Distance to nearest river mouth was similarly obtained. Each river used was chosen as the largest river within that location. No preference was given to geographical positioning of the river within each location. Alexandra Shoals and Port Douglas were split into sub locations and the Mowbray River and Dickson's Inlet were used respectively (Table 4).

4.3.3 Multivariable Regression

The method of least squares provides estimates of the regression coefficients for a multiple linear regression model. These coefficients depict the part of each independent variable that is not related to the dependant variable prediction. The model then finds the plane of best fit to the data (Brown 2009a). The general model with *k* variables can be given as,

$$y_i = \beta_0 + \beta_1 x_{i1} + \beta_2 x_{i2} + \cdots + \beta_k x_{ik} + e_i, \qquad i = 1,2,3, \dots, n \tag{26}$$

A matrix model is then generated of the form,

$$Y = X\beta + \epsilon \tag{27}$$

where Y is an $n \times 1$ observation vector (in this case the T_{50} values for each site), X is an $n \times (k+1)$ predictor matrix and β is a $(k+1) \times 1$ vector of least squares estimators and ϵ is an $n \times 1$ random error vector. Assuming the variables, $x1, x2, \dots, xn$ are linearly independent, and rearranging the least squares normal equation, β may be obtained from,

$$\hat{\beta} = (X^T X)^{-1} X^T Y$$

28

Matlab software was used to compute the regression coefficients. In this case, vector Y represents measured turbidity at 50% exceedance and X is a $(n \times 4)$ matrix* consisting of a normalisation column and the three independent variables (water depth, distance to mainland and distance to river). The predicted T_{50} water turbidity (y) is generated from the specific model given as,

$$y_i = \beta_0 + \beta_1 x_{i1} + \beta_2 x_{i2} + \beta_3 x_{i3} + e_i \qquad i = 1,2,3, \dots, n^{**}$$

29

***where n = the number of sites, x_{i1} = depth, x_{i2} = distance to mainland and x_{i3} = distance to river*

4.3.3.1 Stepwise algorithm

Stepwise regression is a systematic algorithm that adds (based on entrance tolerance) and removes (based on exit tolerance) terms based on their statistical significance in a linear regression. Each step involves computation of the F-statistic and its corresponding p-value. Using the p-value, if the null hypothesis is rejected the term is added into the model (Emery and Thomson 1998; Brown 2009b).

4.4 Site locations

Turbidity data are obtained from Macdonald et al. (2013), who examined seven coastal GBR regions between Hay Point in Mackay, QLD and Princess Charlotte Bay in far North QLD

(Figure 24) and (Table 4). All sites are located at or adjacent to inshore coral reefs or coral communities. Sites are concentrated in the central section of the GBR, spanning both dry tropics wet tropics regions. The sites range from regions with significant human impact areas such as the Hay Point region to relatively undisturbed areas, such as the Princess Charlotte Bay region. See Macdonald et al. (2013) for a more complete description of regions.

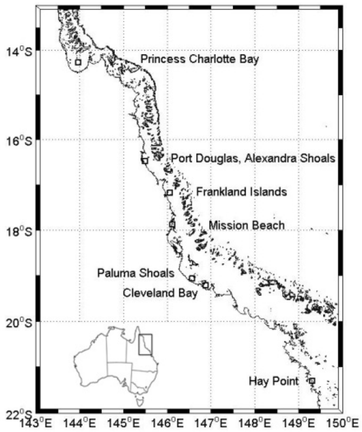

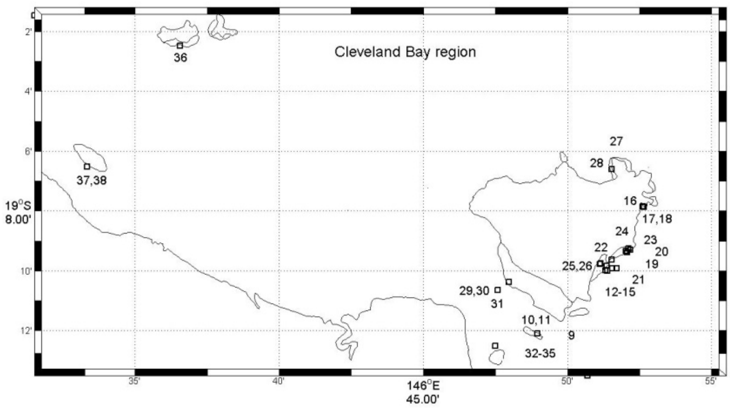

Figure 24 Map showing: 7 turbidity regions across the inshore Great Barrier Reef (top). Numbered sites within Cleveland Bay region (bottom) (see Table 4).

4.5 Data table

Table 4 Site Information taken from Macdonald et al. (2013).

Region	Nearest Major River	Site #	Site Name	days	Year	Lat	Long
Hay Point	Pioneer River	6	Slade Point	31	2008	-21.10	149.24
	"	7	Victor Island	31	2008	-21.32	149.32
	"	8	Roundtop Island	31	2008	-21.17	149.27
Cleveland Bay/Magnetic	Ross River	9	Middle Reef1	104	1993	-19.20	146.82
	"	10	Middle Reef2 0.7m	21	2009	-19.20	146.82
	"	11	Middle Reef2 2.2m	16	2009	-19.20	146.82
	"	12	Nelly Bay1	620	2001-2002	-19.17	146.86
	"	13	Nelly Bay2	589	2001-2002	-19.17	146.86
	"	14	Nelly Bay3	589	2001-2002	-19.17	146.86
	"	15	Nelly Bay4	589	2001-2002	-19.17	146.86
	"	16	Arthur Bay Edge	121	1993	-19.13	146.88
	"	17	Arthur Bay Deep1	121	1993	-19.13	146.88
	"	18	Arthur Bay Deep2	121	1993	-19.13	146.88
	"	19	Geoffrey Bay Edge	120	1993	-19.16	146.87
	"	20	Geoffrey Bay Deep	121	1993	-19.16	146.87
	"	21	Nelly Bay Seaward	37	2000	-19.16	146.86
	"	22	Bright Point	22	2000	-19.16	146.86
	"	23	Arcadia	37	2000	-19.15	146.87
	"	24	Bremner Point	37	2000	-19.16	146.87
	"	25	Nelly Bay ReefFlat a	14	2000	-19.16	146.85
	"	26	Nelly Bay ReefFlat b	14	2000	-19.16	146.85
	"	27	Horseshoe Bay2	88	2007	-19.11	146.86
	"	28	Horseshoe Bay1	116	1993	-19.11	146.86
	"	29	West Channel2a	28	2004	-19.18	146.79
	"	30	West Channel2b	28	2004	-19.18	146.79
	"	31	West Channel3	28	2004	-19.17	146.80
	"	32	West Channel5	12	2004	-19.21	146.79
	"	33	Virago Shoal	15	2004	-19.21	146.79
	"	34	West Channel7	15	2004	-19.21	146.79
	"	35	West Channel8	15	2004	-19.21	146.79

Paluma Shoals	Ross River	36	Rattlesnake Island	92	1993	-19.04	146.61
	"	37	Paluma Shoals1 0.9m	29	2009	-19.11	146.56
	"	38	Paluma Shoals1 1.7m	29	2009	-19.11	146.56
Mission Beach/Islands	Tully River	39	Mission Beach	39	2000	-17.88	146.11
	"	40	Dunk Island SW	39	2000	-17.95	146.14
	"	41	Thorpe Island	39	2000	-17.98	146.13
	"	42	Lugger Bay Shore	30	2003/2004	-17.96	146.10
	"	43	Bedarra Island	30	2003/2004	-18.01	146.15
	"	44	Lugger Bay Seaward	36	2003/2004	-17.96	146.10
	"	45	Clump Point	30	2003/2004	-17.87	146.12
	"	46	Thorpe Island2	31	2003/2004	-17.98	146.13
	"	47	Tam O Shanter Point	30	2003/2004	-17.96	146.10
Frankland Islands	Russel Mulgrave	48	Russel Island	23	2000	-17.22	146.09
	"	49	High Island1	13	2000	-17.15	146.00
	"	50	High Island SW4	40	2000	-17.16	146.00
	"	51	High Island5	40	2000	-17.16	146.00
Port Douglas / Alexandra Shoals	Dickson's Inlet	52	Port Douglas1	67	2004	-16.48	145.46
	"	53	Port Douglas2	65	2004	-16.48	145.46
	Mowbray River	54	Alexandra Shoals1	32	2000	-16.55	145.51
	"	55	Alexandra Shoals2	33	2000	-16.55	145.51
	"	56	Alexandra Shoals3	33	2000	-16.55	145.51
Princess Charlotte Bay	North Kennedy River	57	Obree Reef1	78	2001	-13.97	143.68
	"	58	Obree Reef3	75	2001	-13.97	143.68
	"	59	Obree Reef2	69	2001	-13.97	143.68
	"	60	June Reef1	47	2001	-14.29	143.77
	"	61	June Reef2	68	2001	-14.29	143.77
	"	62	Burkitt Island	48	2001	-13.93	143.78
	"	63	Cliff Island1	68	2001	-14.22	143.78
	"	64	Cliff Island2	48	2001	-14.21	143.77

4.6 Results

Water depth, distance to mainland and distance to river are calculated (where the necessary information is available) for each site and presented alongside exceedance values obtained from Macdonald et. al (2013) (Table 5).

Table 5 Mean turbidity, exceedance (T_{10}, T_{50}, T_{90}), depth, distance to mainland and distance to river data.

site #	mean turbidity (NTU)	T_{10} (NTU)	T_{50} (NTU)	T_{90} (NTU)	depth (m)	distance To mainland (km)	distance to river (km)
6	4.3	6.4	2.5	1.3	8.6	1.93	17.28
7	25	43.7	9.3	1.4	3	3.02	13.10
8	2.6	6.2	0.7	<0.5	7.5	7.07	9.79
9	9.1	19.2	5.3	2.3	4	4.31	7.71
10	1.7	3.7	0.8	<0.5	4	4.31	7.71
11	3	7.6	1.4	<0.5	4	4.31	7.71
12	1.9	3	0.9	<0.5	7.3	9.35	11.85
13	4.4	4	1	<0.5	7.6	9.24	11.86
14	1.8	3.3	1.3	<0.5	7.3	9.40	11.97
15	1.5	3	0.9	<0.5	7.3	9.47	12.02
16	6.2	12.8	3.7	1.7	8.8	12.63	15.80
17	5.3	12	3.1	1.2	12.8	12.62	15.81
18	6	12.3	3.1	1.2	12.8	12.62	15.81
19	7.3	16.1	3.4	1.5	7.3	6.85	12.80
20	12.5	23.5	3.7	1.3	7.3	10.20	12.40
21	14.9	47.1	3.9	1.5	7	8.75	11.46
22	10.8	20	2.1	0.7	8	9.37	11.73
23	3.2	5.5	1.9	1.6	8	10.31	12.75
24	8.9	22.3	2.4	<0.5	7	10.46	12.79
25	4.7	13.6	0.8	<0.5	2.5	10.46	12.79
26	8.5	22.5	2.9	0.5	2.5	10.46	12.79
27	3.3	9.4	1.1	<0.5	3.5	12.87	17.68
28	9.5	15.6	4.6	1.1	3.5	12.87	17.68
29	6.4	10.7	5.2	3	5.8	2.35	11.02
30	5.3	8.8	4.3	2.4	5.8	2.35	11.02
31	3.8	5.6	2.3	1.2	3	3.18	11.25
32	7.2	19	2.5	<0.5	2.7	3.80	8.18
33	5.3	13.7	2	<0.5	2.7	1.62	8.18
34	4.9	11.9	2.7	1	2.7	1.62	8.18
35	5.1	11.1	2.7	1.3	2.7	1.62	8.18

36	3.8	6.4	2.9	1.3	12.3	11.07	34.55
37	8.8	17.8	7.3	1.1	3	1.77	34.33
38	12.3	28.5	8	0.7	3	1.77	34.33
39	3.9	9.2	2.1	0.8	7.8	0.31	17.71
40	7	11.5	1.2	<0.5	8.5	5.05	12.77
41	2.8	7.5	1.2	<0.5	9.1	3.18	9.69
42	8	28.7	1.2	<0.5	0.3	0.30	4.52
43	5.3	7.1	3.9	1.6	6	6.47	8.34
44	8.5	27.4	2.1	1.1	2	0.90	4.78
45	2.4	7.1	0.8	<0.5	5	0.77	14.47
46	1.9	4.6	0.8	<0.5	3.1	3.11	6.09
47	3.9	9.4	1.8	0.7	2	0.25	4.18
48	1.3	2.5	<0.5	<0.5	16.4	11.88	12.19
49	3.1	8.9	<0.5	<0.5	18.3	4.50	8.33
50	0.8	0.8	<0.5	<0.5	18.3	4.30	8.12
51	1.2	0.8	<0.5	<0.5	18.3	4.53	8.20
52	13.3	23.3	11.4	4.1	2	0.60	0.61
53	7	12.1	6.5	2.1	2	0.23	0.46
54	10.3	23.9	5.2	<0.5	7.3	0.73	1.92
55	17.4	38.1	15.3	1.1	11	0.73	1.92
56	5.8	15.5	2.7	<0.5	7.3	0.73	1.92
57	2.8	4.9	2.2	0.9	4.1	3.66	64.60
58	2.3	4	1.7	0.9	4.1	3.56	64.60
59	3.6	8.2	2.2	<0.5	3.4	4.01	29.36
60	1	1.2	0.6	<0.5	9	13.93	65.23
61	1.7	4.6	0.5	<0.5	5	6.86	36.12

4.6.1 Turbidity and distance to mainland

Turbidity exceedances T_{10}, T_{50} and T_{90} are examined with distance to mainland (Figure 25). Exceedances are also examined for concurrent Cleveland Bay sites (Figure 26). As many of these sites were measured simultaneously they are able to be grouped into 4 deployment periods. The time periods are: 121 days ending in April 1993, 37 days ended in May 2000, 589 days ending in November 2002 and 28 days ended in May 2004. These four groups are compared to each other directly (Figure 26).

No relationship is found between turbidity exceedance and distance to mainland (Figure 25). Similarly, separation of the data into inshore and offshore groups (>4km from mainland) produces no relationship between turbidity and distance to mainland (Figure 25).

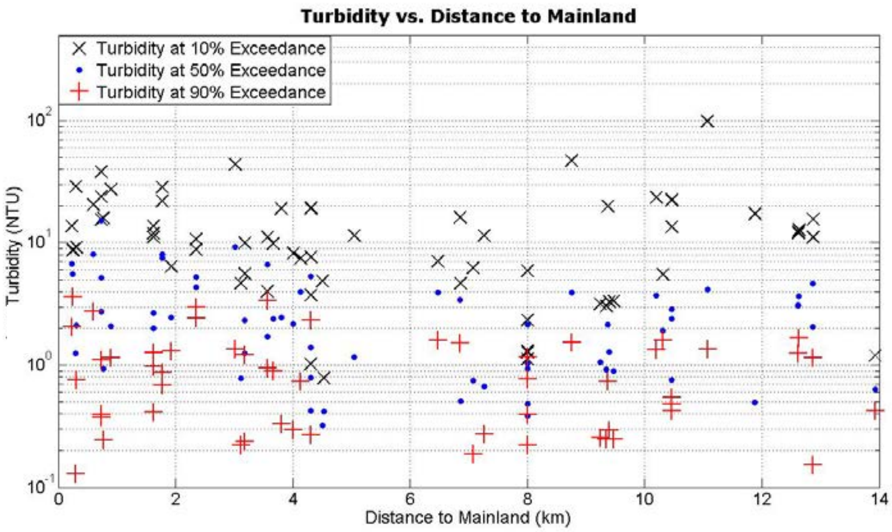

Figure 25 Turbidity (NTU) vs. distance to mainland (km) across all sites. Turbidity is displayed at 10 %, 50, % and 90 % Exceedance.

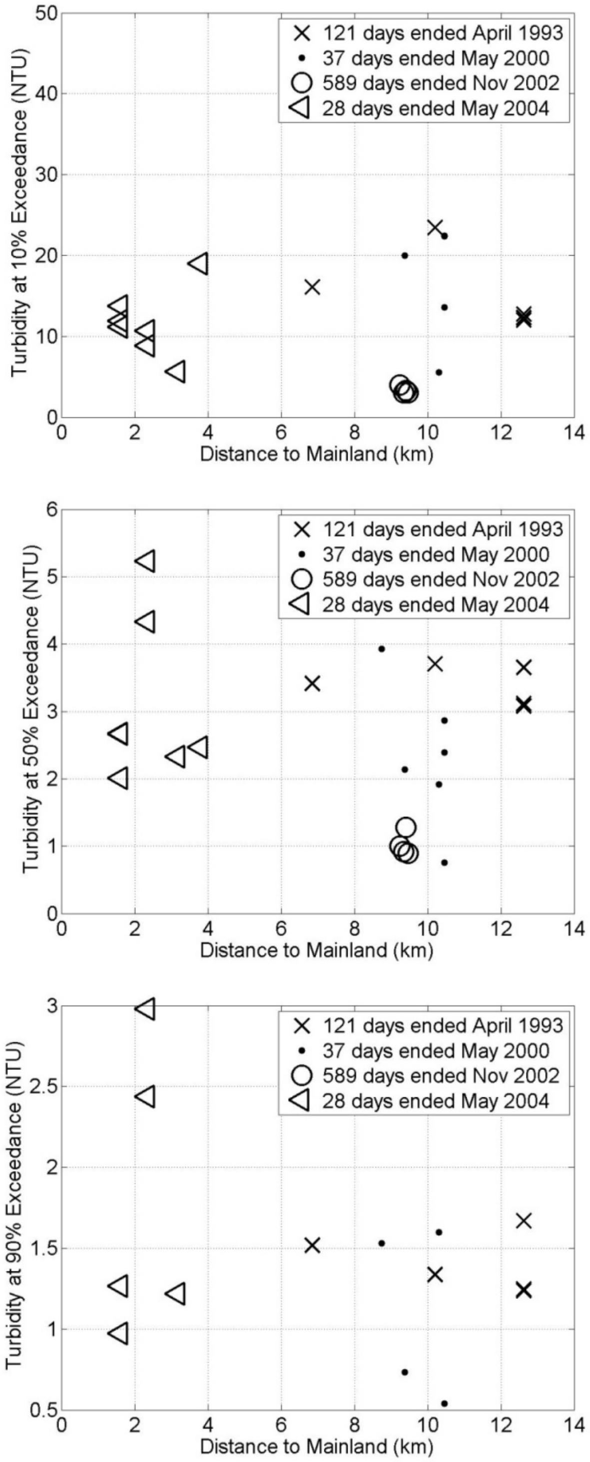

Figure 26 Cleveland Bay deployments showing turbidity exceedance vs distance to mainland at 10 % turbidity exceedance (top), 50 % turbidity exceedance (middle) and 90 % turbidity exceedance (bottom).

4.6.2 Turbidity and distance to river mouth

Turbidity exceedances, T_{50}, T_{10} and T_{90} are investigated in relation to distance to a major river mouth (Figure 27). The three exceedances are also separated into Cleveland Bay sites (Figure 28). Again, many of these sites were measured simultaneously and are able to be grouped into 4 deployment periods as above (121 days ending in April 1993, 37 days ended in May 2000, 589 days ending in November 2002 and 28 days ended in May 2004). These four groups are compared to each other directly (Figure 5). The same river is used for each region, with the exception of Port Douglas and Alexandra Shoals where Dickson's Inlet is used for the Port Douglas sites (Table 4, *sites 46, 47*) and the Mowbray River for the Alexandra Shoals sites (Table 4, *sites 48-50*). Once again a correlation between these measurements is not found.

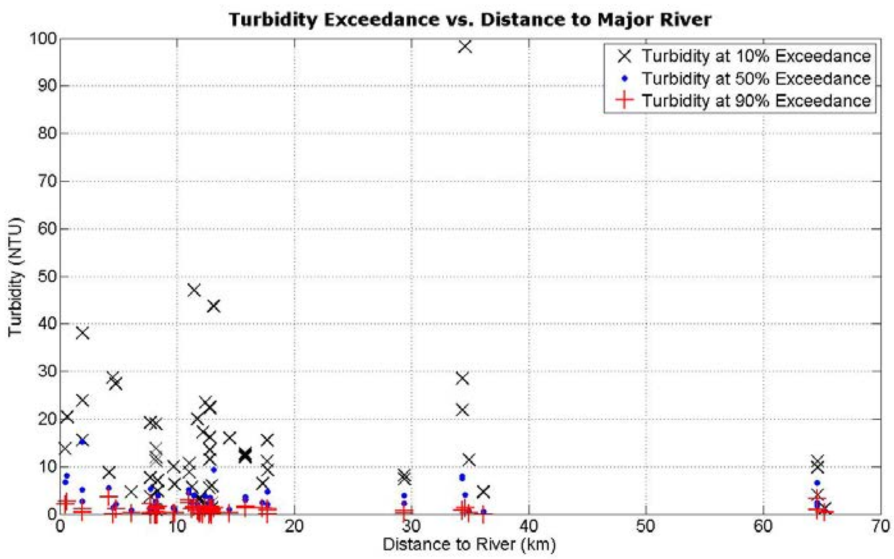

Figure 27 Turbidity (NTU) vs. distance to closest major river (km) across all sites. Turbidity is displayed at 10 %, 50, % and 90 % Exceedance.

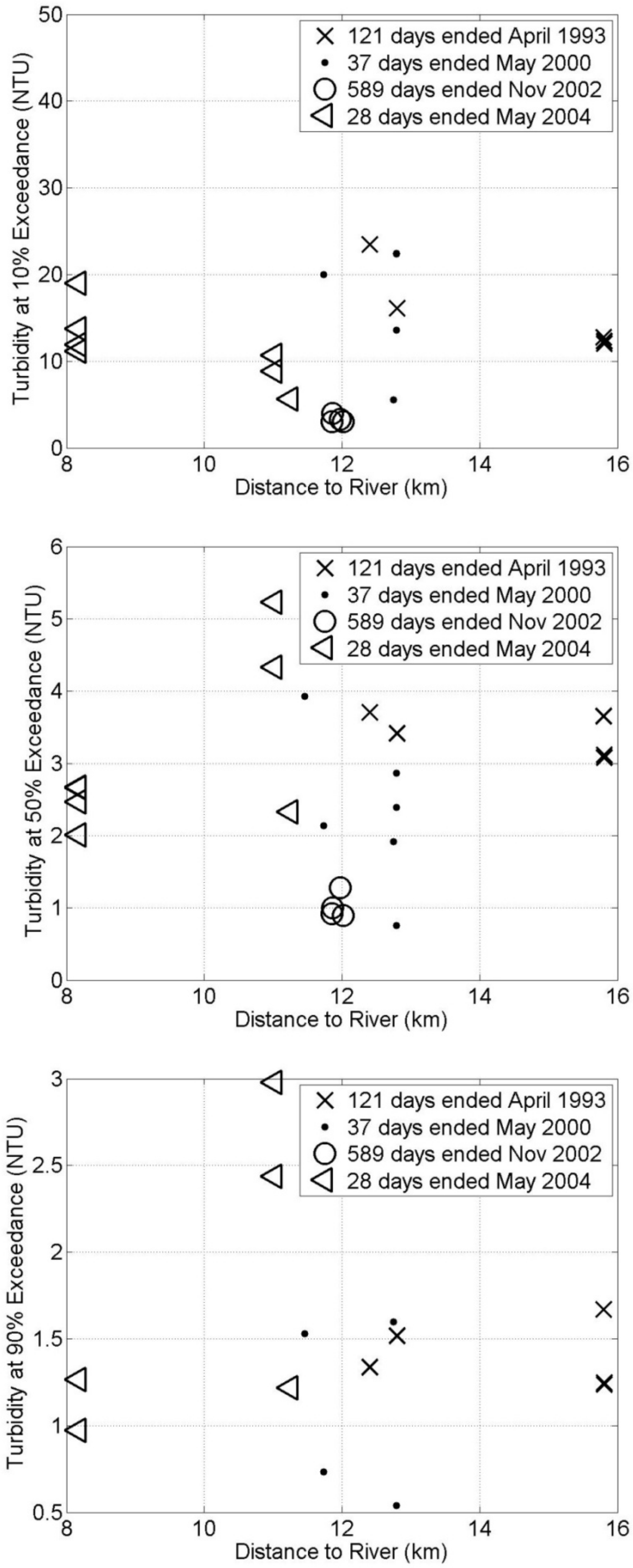

Figure 28 Cleveland Bay deployments showing turbidity exceedance vs distance to closest major river at 10 % turbidity exceedance (top), 50 % turbidity exceedance (middle) and 90 % turbidity exceedance (bottom).

4.6.3 Turbidity and water depth

Turbidity exceedances, T_{50}, T_{10} and T_{90} are investigated with average depth (Figure 29). The three exceedances are separated into Cleveland Bay sites (Figure 30) grouped into 4 deployment periods as above (121 days ending in April 1993, 37 days ended in May 2000, 589 days ending in November 2002 and 28 days ended in May 2004). Results show that for these data, turbidity exceedance vs. average water depth also does not hold a statistically significant correlation.

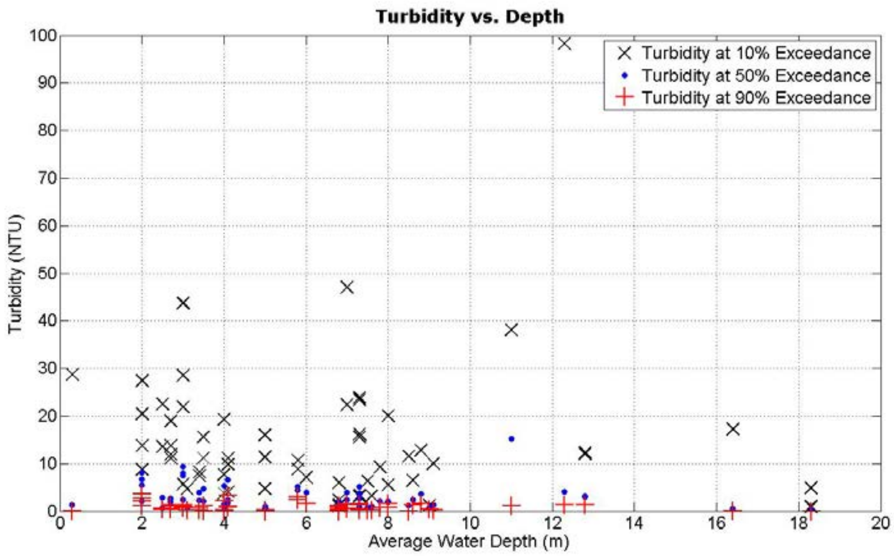

Figure 29 Turbidity (NTU) vs. average water depth (m) across all sites. Turbidity is displayed at 10 %, 50, % and 90 % Exceedance.

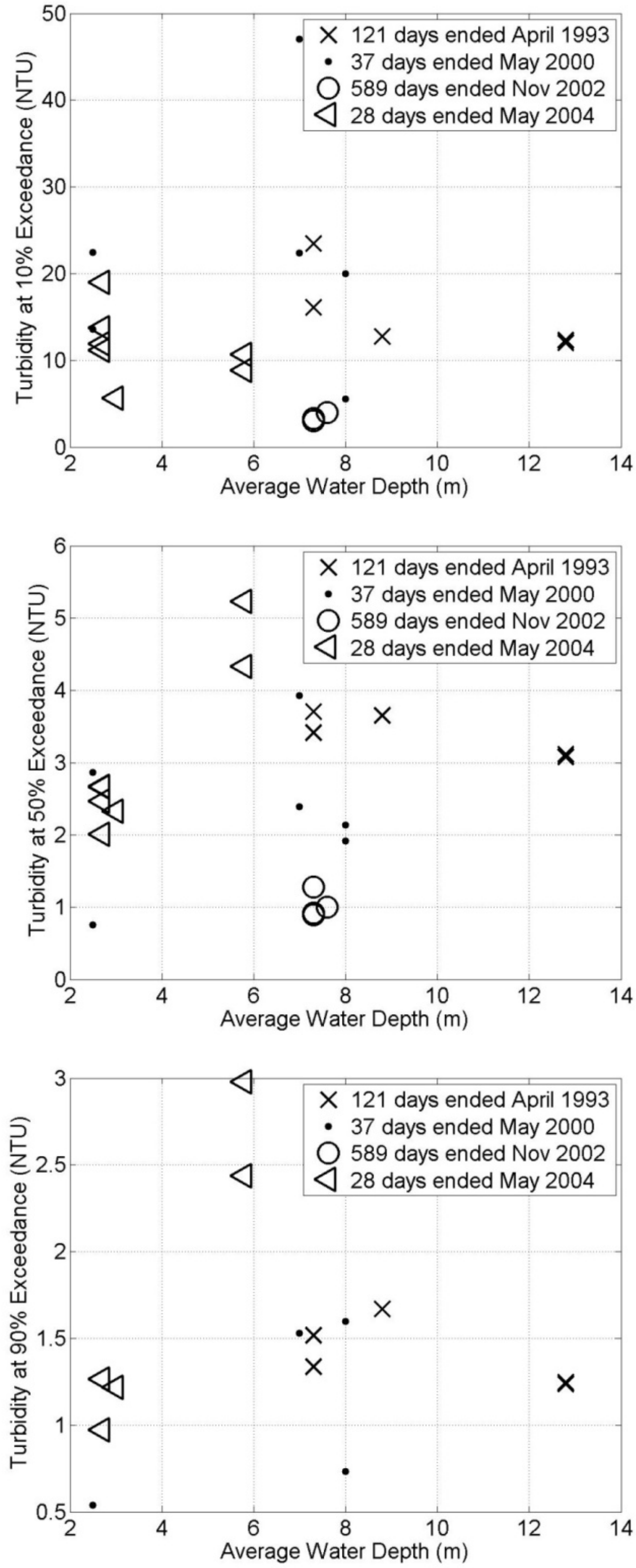

Figure 30 Cleveland Bay deployments showing turbidity exceedance vs average water depth at 10 % turbidity exceedance (top), 50 % turbidity exceedance (middle) and 90 % turbidity exceedance (bottom).

4.6.4 Region typing

Sites are grouped into three descriptive region types in an attempt to find a generalised correlation to turbidity. Type 1 denotes shore-attached fringing reefs such as, Paluma and Alexandra Shoals and Port Douglas (Figure 10). Type 1 are located mostly on open, relatively linear coastlines. Type 2 denotes sites that are located in muddy embayments such as Cleveland Bay (Figure 32) and Type 3 denotes sites that do not fit into either of the above categories (Figure 33). The total exceedance is presented for each type. This is calculated by appending all the turbidity data in each type and then producing a total exceedance curve from that data. This may have applications towards observing a general turbidity exceedance for particular location types.

All categories exhibit wide internal variability in turbidity. Across Type 1 the generalised turbidity regime is seen to decay slowly throughout low turbidity but becomes much steeper at around 5 NTU. The curve then flattens as it approaches 100 NTU (Figure 10). Across Type 2 the generalised turbidity regime follows an exponential decay curve until flattening out around 10 NTU (Figure 11). Across Type 3 very wide variation in turbidity is seen, with the generalised turbidity regime exceeding 1 NTU about 65% of the time. This type also follows an almost linear decay curve until flattening out around 10 NTU (Figure 12).

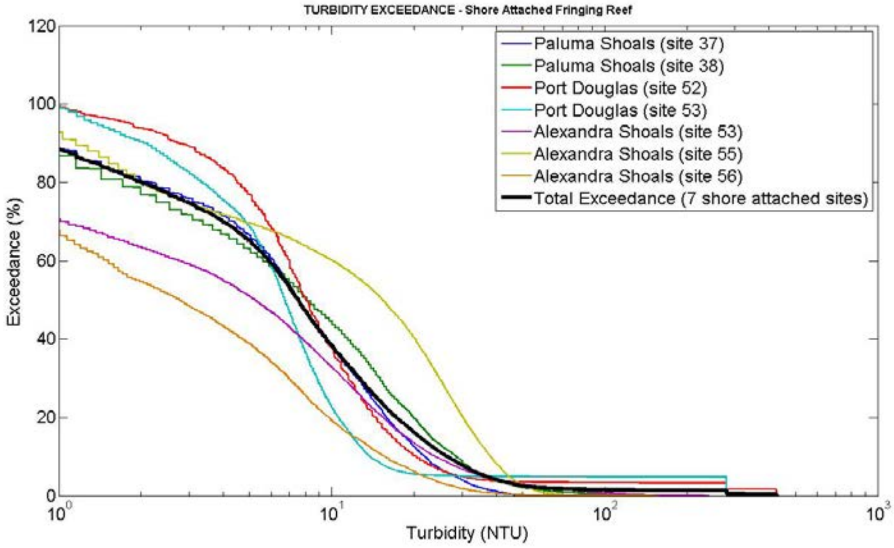

Figure 31 Exceedance curves grouped by type. Type 1: Shore-attached fringing reefs including Paluma Shoals, Alexandra Shoals and Port Douglas sites. Wide variation in turbidity is seen across this type.

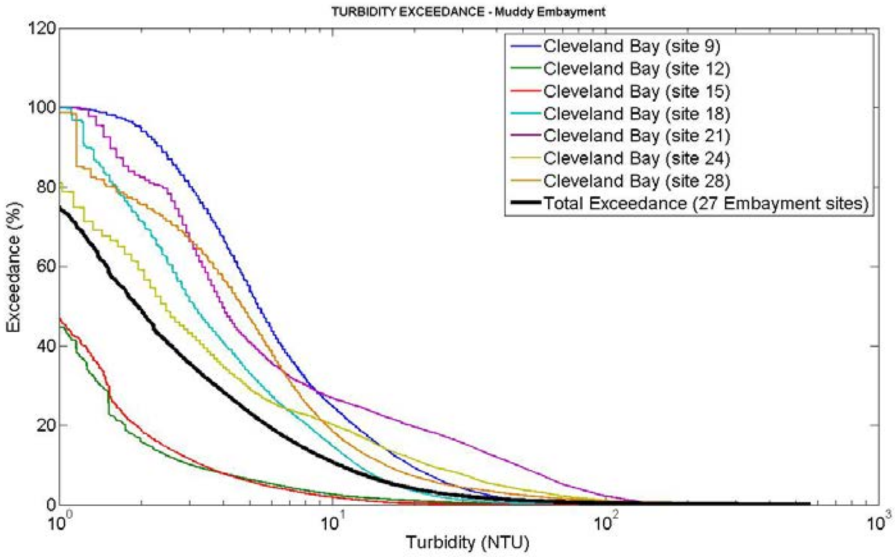

Figure 32 Exceedance curves grouped by type. Type 2: Muddy Embayment – all Cleveland Bay sites. Wide variation in turbidity is seen across this type and the generalised turbidity regime follows an exponential decay curve until flattening out around 10 NTU.

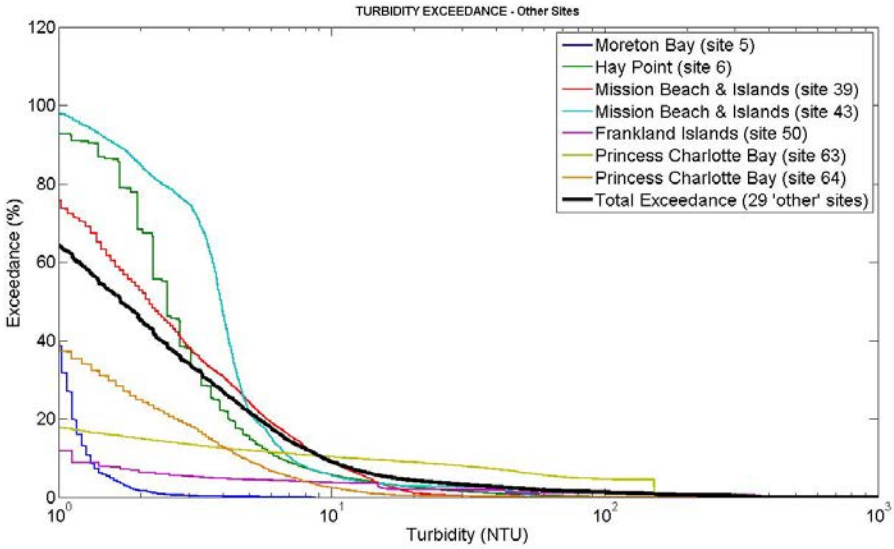

Figure 33 Exceedance curves grouped by type. Type 3: All other sites. Very wide variation in turbidity is seen with generalised turbidity regime exceeding 1 NTU about 65% of the time. The type also follows a weak linear decay curve.

4.7 Analysis

Simple linear regression does not describe a significant relationship between turbidity and any one of the independent variables tested. A multiple linear regression model was run in an attempt to evaluate the relationship between the dependant variable (water turbidity) with three independent variables, namely; water depth, distance to mainland and distance to river. A scatter plot of the measured turbidity versus the predicted values from the model shows no obvious correlation (Figure 34). This basic additive model is an exceptionally weak fit to the measured data. Here the R^2 value is 0.0534 and the *F*-statistic is 0.9214 with a corresponding *p*-value of 0.4375.

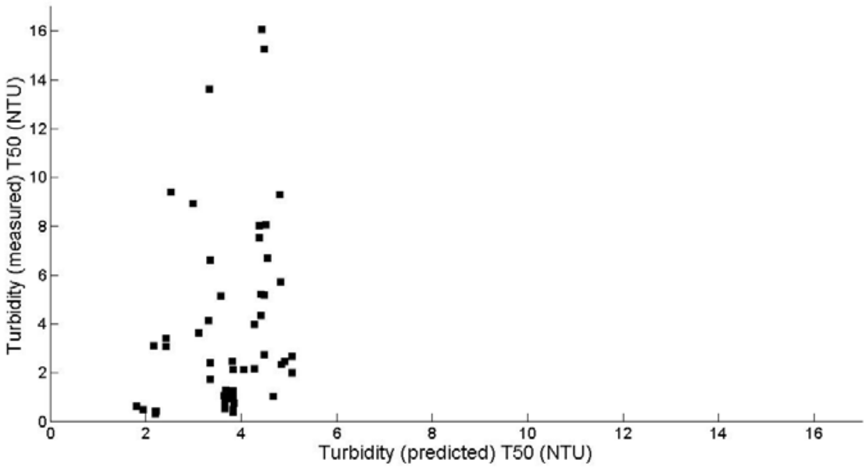

Figure 34 Measured median turbidity vs. multivariable linear regression model.

In an attempt to improve the model, interaction and quadratic terms, and their inverse terms are added to the independent variables, amounting to a set of 10 terms (Table 6). The Matlab stepwise regression function (*stepwisefit*) is implemented to determine the optimum combination (if any) of the terms in the model.

Table 6 Stepwise regression analysis of independent variables, depicting ten independent variables and the generated statistics.

Model term	Explicit term	Beta Coeff.	Std.Err.	Status	P-value
x_1	DEPTH^{-1}	0.4067	0.2788	Out	0.1498
x_2	$\text{DISTANCE TO SHORE}^{-1}$	0.0803	0.3995	Out	0.8414
x_3	$\text{DISTANCE TO RIVER}^{-1}$	0.392	0.3801	Out	0.3064
x_4	$(\text{DEPTH x DISTANCE TO SHORE})^{-1}$	0.1501	0.0869	Out	0.0894
x_5	$(\text{DEPTH x DISTANCE TO RIVER})^{-1}$	0.2081	0.77	Out	0.7878
x_6	$(\text{DISTANCE TO RIVER x DISTANCE TO SHORE})^{-1}$	0.0585	0.1206	Out	0.6296
x_7	$(\text{DEPTH x DISTANCE TO SHORE x DISTANCE TO RIVER})^{-1}$	0.1328	0.2432	Out	0.5871
x_8	DEPTH^{-2}	0.1549	0.0783	Out	0.0524
x_9	$\text{DISTANCE TO SHORE}^{-2}$	0.0753	0.029	In	0.0117
x_{10}	$\text{DISTANCE TO RIVER}^{-2}$	0.1944	0.1902	Out	0.3107

Based upon commonly used entrance and exit tolerances of 0.05 and 0.10 for p-values, stepwise regression accepts only one independent term for the model (distance to shore^{-2}). The best fit is produced using T_{90} as the dependant variable. The independent term is then substituted into the original program for linear regression to generate the following model,

$$y_i = \beta_0 + \beta_1 \left(\frac{1}{x_{i1}}\right)^2 + e_i$$

30

$$i = 1,2,3, \dots, n.$$

where n = the number of sites and x_{i1} = distance to shore

Further analysis of this regression model produces an R^2 value of 0.099, a F-statistic of 6.752 and a P-value of 0.012 (fitting into commonly accepted maximum P-value of 0.05). The stepwise model generates a marginally better fit to the measured data than the linear regression model, however the results are not statistically significant. It is likely that the goodness of P-value in this model is due to accuracy in modelling of the baseline turbidity data, however as the measured turbidity increases, the model fails to accurately predict T_{90} values (Figure 35).

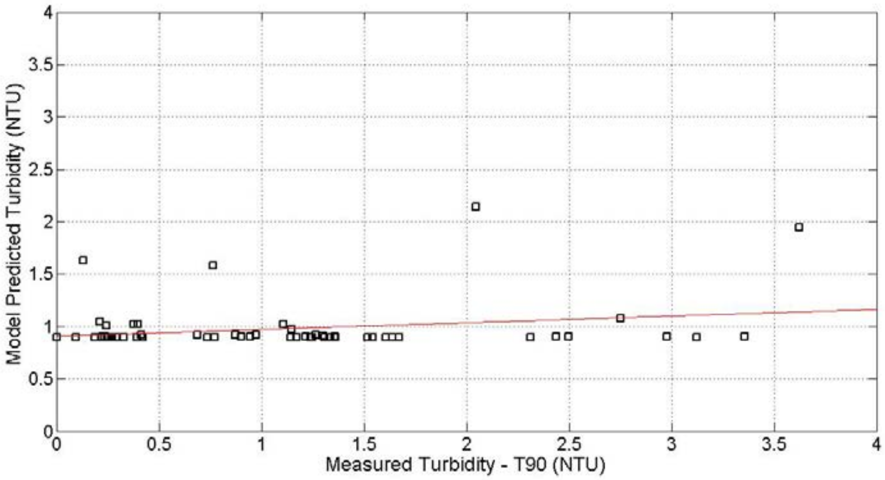

Figure 35 Stepwise linear regression model with inverted, quadratic term. Model R^2 value is 0.099 and P-value is 0.012. No physically significant linear correlation is found between measured turbidity and combinations of interaction and quadratic terms.

Two models are displayed using the Matlab colourmap function (Figure 36). The models are obtained using the stepwise regression method, but constrained to combinations of two independent initial variables (depth and distance to shore) and (depth and distance to river) respectively. For model 1 (Figure 36 top), the R^2 value is 0.059 and the P-value is 0.217 (Figure 36). For model 2 (Figure 36 bottom) the R^2 value is 0.044 and the P-value is 0.326. A P-value higher than 0.05 is not considered statistically significant (Emery and Thomson 1998; Brown 2009a).

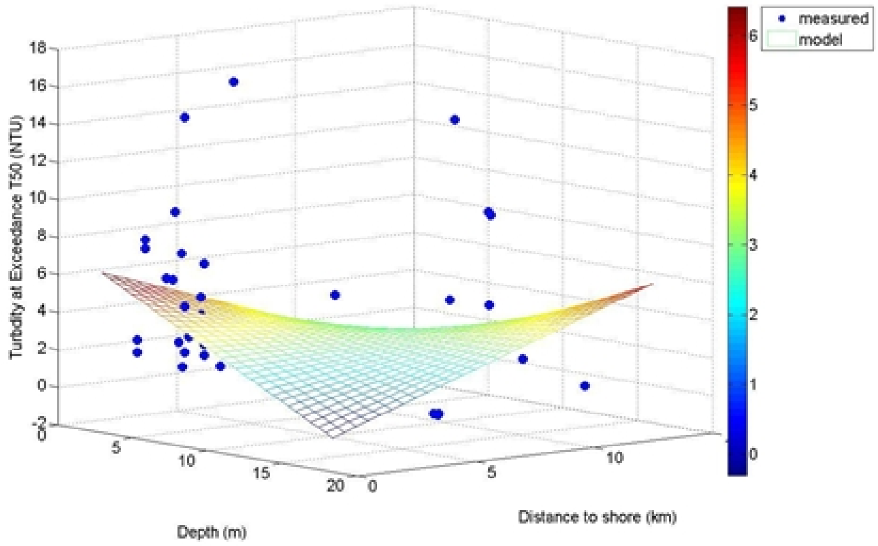

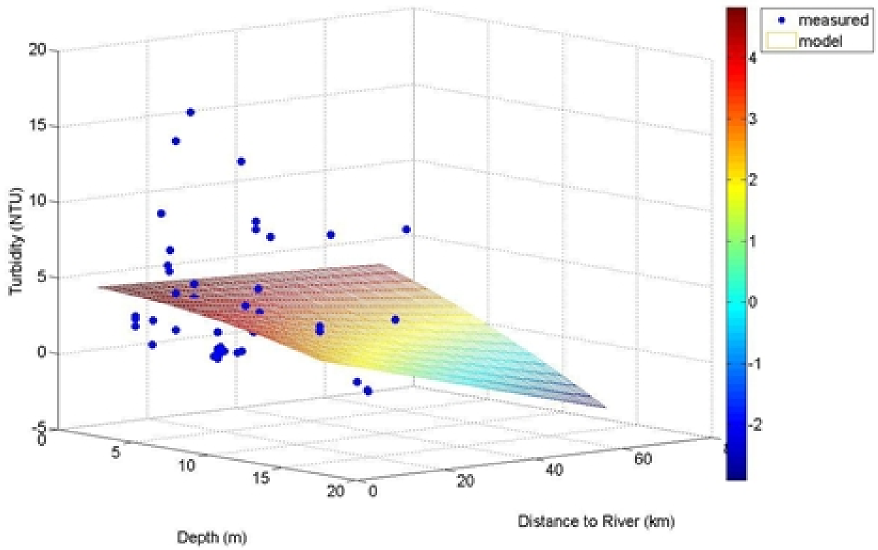

Figure 36 Measured turbidity (T50) vs. colourmap model generated from stepwise regression. Combining depth and distance to shore terms, (top). Combining depth and Distance to river terms (bottom).

If either of the above models were a good fit to the measured data, the turbidity scatter plot would sit closely within the plane of the colourmap model. What is shown instead is that the measured data is very much more dispersed than the model predicts. In other words, for these data, no statistically significant linear correlation is found between turbidity exceedance and the tested independent variables; water depth, distance to mainland or distance to major River. However, it is plausible and even probable that a non-linear correlation exists, thus highlighting the need for further investigation into the nature of such a correlation potential factors in inshore turbidity.

4.8 Discussion

This paper investigated the relationship of turbidity to several potential secondary factors. None of the investigated factors produced a statistical relationship to turbidity. No correlation is found between turbidity exceedance and distance to mainland or distance to river. Similarly turbidity exceedance vs. average water depth produces no statistically significant correlation (Figure 29). Several determinants of inshore GBR turbidity have recently been identified in a major study by Fabricius (2012). In that paper 3 years of almost continuous turbidity data were used to identify effective wave height was the major driver of turbidity with secondary signals found for river distance and river discharge (Fabricius et al. 2012). This was the first paper to document the effect of river discharge on turbidity in the GBR and as such, highlights the importance of future investigations into secondary drivers of turbidity in the coastal GBR.

4.8.1 Multivariable regression

Simple multiple linear regression and stepwise regression models were implemented to evaluate the relationship between water turbidity with three potential factors; water depth, distance to mainland and distance to closest major river. No significant linear correlation was found between turbidity exceedance and the independent variables. The stepwise model generates a marginally better fit to the measured data than the simple regression, however, the results are not considered to be statistically significant due to a low R^2-value of 0.099. Although this result may seem inconsequential, it may point to the difficulty in attributing geographical controls to a factor that exhibits such high spatial and temporal variability. Potentially, correlations could exist on other levels, as presented in a recent study of intra-annual turbidity variation (Fabricius et al. 2012). Within this study turbidity was significantly affected by river flow and rainfall. However this may be limited to a local correlation may be too weak to be observed in the broader scale, such as within the data presented here.

4.8.2 Region Typing

All three categorised types exhibited wide variability in turbidity. Although no dramatic distinction can be made in terms of variation there were some interesting differences across the generalised exceedance regimes. For the shore-attached type, turbidity is greater than 2 NTU for more than 80% of the time. The generalised turbidity regime is seen to decay slowly throughout low turbidity but becomes much steeper at around 5 NTU, indicating that the turbidity is greater than about 5 NTU, 60% of the time. The curve then flattens as it approaches 100 NTU, depicting higher turbidity over lower percentages of time. Within muddy embayment, the generalised turbidity regime depicts > 2 NTU about 70% of the time and follows a shallow exponential decay curve until flattening out around 10 NTU. For the "other" type, generalised turbidity is > 2 NTU for about 60% with an almost linear decay, until also flattening out around 10 NTU. Further investigation into site groups may lead to cross-site environmental similarities, although this was beyond the scope of this paper.

4.8.3 Concluding remarks

Despite widening concern in the literature that inshore reef turbidity is related to factors such as distance to shore, proximity to river mouth (Wolanski et al. 2004; Fabricius 2005; Wolanski and De'Ath 2005; Wolanski et al. 2008; Lambrechts et al. 2010) and water depth, these data indicate strong variability in turbidity with no statistically significant correlation to depth, distance to shore or distance to river. Importantly, this result does not preclude the implication made in many of these studies, however it highlights the need for more investigation into secondary drivers, particularly riverine related, as contributing factors to increased turbidity in the inshore GBR. For example, A recent paper showed that most of the sediment drops out of suspension very soon after leaving the Burdekin river mouth (Delandmeter et al. 2015). It should also be noted that comparisons between different data sets from different times of year must be performed with caution. As data in this study are from different times of year and subject to different events (such as cyclones, flooding), not all the datasets are long enough to average out the effects of these events. However, it is anticipated that effects from the shorter datasets are somewhat offset by the sheer number of sites presented. What is being demonstrated in this work, is that although secondary signals may exist on a level that cannot be observed here, turbidity is much more dependent on other driving factors such as wind and wave resuspension, and possibly tidal current and sediment size, type and distribution.

REFERENCES

Anthony KRN, Ridd PV, Orpin AR, Larcombe P, Lough J (2004) Temporal variation of light availability in coastal benthic habitats: Effects of clouds, turbidity, and tides. Limnology and Oceanography 49:2201-2211

Brodie J, Fabricius K, De'ath G, Okaji K (2005) Are increased nutrient inputs responsible for more outbreaks of crown-of-thorns starfish? An appraisal of the evidence. Marine Pollution Bulletin 51:266-278

Brown SH (2009a) Multiple Linear Regression Analysis: A Matrix Approach with MATLAB. Alabama Journal of Mathematics Spring/Fall 2009:3

Brown SH (2009b) Multiple linear regression analysis: a matrix approach with Matlab. Alabama Journal of Mathematics Spring/Fall:3

Browne NK, Smithers SG, Perry CT (2010) Geomorphology and community structure of Middle Reef, central Great Barrier Reef, Australia: an inner-shelf turbid zone reef subject to episodic mortality events. Coral Reefs 29:683-689

Bunt J, Larcombe P, Jago CF (1999) Quantifying the response of optical backscatter devices and transmissometers to variations in suspended particulate matter (SPM). Continental Shelf Research 19:1199-1220

Conner CS, De Visser AM (1992) A laboratory investigation of particle size effects on an optical backscatterance sensor. Marine Geology 108:151-159

Cooper TF, Ridd PV, Ulstrup KE, Humphrey C, Slivkoff M, Fabricius KE (2008) Temporal dynamics in coral bioindicators for water quality on coastal coral reefs of the Great Barrier Reef. Marine and Freshwater Research 59:703-716

De’ath G, Fabricius KE, Sweatman H, Puotinen M (2012) The 27–year decline of coral cover on the Great Barrier Reef and its causes. Proceedings of the National Academy of Sciences 109(44):17995-17999

Delandmeter P, Lewis SE, Lambrechts J, Deleersnijder E, Legat V, Wolanski E (2015) The transport and fate of riverine fine sediment exported to a semi-open system. Estuarine, Coastal and Shelf Science 167, Part B:336-346

Emery WJ, Thomson RE (1998) Data analysis methods in physical oceanography. Pergamon, New York

Fabricius KE, De’ath G, Humphrey C, Zagorskis I, Schaffelke B (2012) Intra-annual variation in turbidity in response to terrestrial runoff on near-shore coral reefs of the Great Barrier Reef. Estuarine, Coastal and Shelf Science 59:703-716

Furnas M (2003) Catchments and corals: terrestrial runoff to the Great Barrier Reef. Australian Institute of Marine Science, Townsville, Qld

Hopley D (1982) The geomorphology of the Great Barrier Reef: Quaternary development of coral reefs. John Wiley, New York

Hopley D, Smithers S, Parnell KE (2007) The geomorphology of the Great Barrier Reef: development, diversity, and change. Cambridge University Press, Cambridge

Lambrechts J, Humphrey C, McKinna L, Gourge O, Fabricius KE, Mehta AJ, Lewis S, Wolanski E (2010) Importance of wave-induced bed liquefaction in the fine sediment budget of Cleveland Bay, Great Barrier Reef. Estuarine, Coastal and Shelf Science 89:154-162

Larcombe P, Costen A, Woolfe KJ (2001) The hydrodynamic and sedimentary setting of nearshore coral reefs, central Great Barrier Reef shelf, Australia: Paluma Shoals, a case study. SEDIMENTOLOGY 48:811-835

Larcombe P, Ridd PV, Prytz A, Wilson B (1995b) Factors controlling suspended sediment on inner-shelf coral reefs, Townsville, Australia. Coral Reefs 14:163-171

Ludwig KA, Hanes DM (1990) A laboratory evaluation of optical backscatterance suspended solids sensors exposed to sand-mud mixtures. Marine Geology 94:173-179

Macdonald RK, Ridd PV, Whinney JC, Larcombe P, Neil DT (2013) Towards environmental management of water turbidity within open coastal waters of the Great Barrier Reef. Marine Pollution Bulletin 74:82-94

Maxwell WGH (1968) Atlas of the Great Barrier Reef. Elsevier, Amsterdam

McCulloch M, Fallon S, Wyndham T, Hendy E, Lough J, Barnes D (2003a) Coral record of increased sediment flux to the inner Great Barrier Reef since European settlement. Nature 421:727-730

Moss A, Queensland. Dept. of E, Heritage, Queensland. Dept. of Primary I (1993) A Preliminary assessment of sediment and nutrient exports from Queensland coastal catchments. Queensland Dept. of Environment and Heritage, Brisbane

Orpin AR, Ridd PV (2012) Exposure of inshore corals to suspended sediments due to wave-resuspension and river plumes in the central Great Barrier Reef: A reappraisal. Continental Shelf Research 47:55-67

Orpin AR, Ridd PV, Thomas S, Anthony KRN, Marshall P, Oliver J (2004) Natural turbidity variability and weather forecasts in risk management of anthropogenic sediment discharge near sensitive environments. Marine Pollution Bulletin 49:602-612

Pandolfi JM, Bradbury RH, Sala E, Hughes TP, Bjorndal KA, Cooke RG, McArdle D, McClenachan L, Newman MJH, Paredes G, Warner RR, Jackson JBC (2003) Global trajectories of the long-term decline of coral reef ecosystems. Science 301:955-958

Perry CT, Smithers S (2009) Stabilisation of intertidal cobbles and gravels by Goniastrea aspera: an analogue for substrate colonisation during marine transgressions? Coral Reefs 28:805-806

Perry CT, Smithers SG (2010) Evidence for the episodic “turn on” and “turn off” of turbid-zone coral reefs during the late Holocene sea-level highstand. Geology 38:119-122

Perry CT, Smithers SG, Johnson KG (2009a) Long-term coral community records from Lugger Shoal on the terrigenous inner-shelf of the central Great Barrier Reef, Australia. Coral Reefs 28:941-948

Perry CT, Smithers SG, Palmer SE, Larcombe P, Johnson KG (2008) 1200 year paleoecological record of coral community development from the terrigenous inner shelf of the Great Barrier Reef. Geology 36:691-694

Smithers S, Larcombe P (2003) Late Holocene initiation and growth of a nearshore turbid-zone coral reef: Paluma Shoals, central Great Barrier Reef, Australia. Coral Reefs 22:499-505

Umbgrove JHF (1947) Coral reefs of the East Indies. Geol Soc Am Bull 58:729-777

Wolanski E, De'Ath G (2005) Predicting the impact of present and future human land-use on the Great Barrier Reef. Estuarine, Coastal and Shelf Science 64:504-508

Wolanski E, Delesalle B, Gibbs R (1994) Carbonate mud in Mataiva Atoll, French Polynesia: Suspension and export. Marine Pollution Bulletin 29:36-41

Wolanski E, Richmond RH, McCook L (2004) A model of the effects of land-based, human activities on the health of coral reefs in the Great Barrier Reef and in Fouha Bay, Guam, Micronesia. Journal of Marine Systems 46:133-144

Wolanski E, Fabricius KE, Cooper TF, Humphrey C (2008) Wet season fine sediment dynamics on the inner shelf of the Great Barrier Reef. Estuarine, Coastal and Shelf Science 77:755-762

Chapter 5. LIGHT ATTENUATION AND VERTICAL TURBIDITY PROFILES

This chapter was submitted for publication in Marine Pollution Bulletin – July 2015

Macdonald R. K., et. Al (submitted 2015) *Light attenuation and vertical turbidity profiles in coastal waters of the Great Barrier Reef*, Marine Pollution Bulletin.

5.1 Abstract

Water turbidity has been thoroughly studied throughout Great Barrier Reef waters, mostly due to its influence on light availability for marine biota. However the relationship between turbidity and light has been almost ignored. Here vertical light and turbidity (T) profiles are obtained and linked for the first time, for inshore GBR locations. Attenuation coefficients (k_d) are calculated over water-column intervals, producing linear relationships between k_d and turbidity (R^2=0.91). Site-specific, average diffuse attenuation ($k_d^{AVG} = 0.43\ \mathrm{m}^{-1}$), clear-water ($k_d^{cl} = 0.3\ \mathrm{m}^{-1}$) and turbidity-based attenuation ($\alpha = 0.076\ \mathrm{m}^{-1}/\mathrm{NTU}$) components are calculated. Depth-averaged turbidity and seabed turbidity show linear relationships (R^2=0.96) and depth-averaged turbidity is 0.3-0.4 times seabed turbidity. A site-specific model predicting depth-averaged turbidity (T_{pred}) using light data correlates well to measured turbidity (T_{avg}); T_{pred} = 1.0(T_{avg}) and R^2=0.78 (Cleveland Bay), and T_{pred} = 0.77(T_{avg}) and R^2=0.68 at (Tully coast). The euphotic depth of Cleveland Bay is 10 m for a depth-averaged turbidity of 2.5 NTU.

5.2 Introduction

Light availability is a dominating survival factor for many marine organisms and plants and there is no exception for the Great Barrier Reef (GBR). Sunlight penetrates the upper layer of ocean (the Euphotic Zone) enabling photosynthesis to occur within the solar wavelength band 400-700 nm (photosynthetically active radiation (PAR))(Wright 1995). The depth of the euphotic zone depends upon water turbidity and varies with location (Wright 1995). Light attenuation in the GBR affects biota by reducing light penetration for photosynthesis and reducing visual range for sighted marine organisms (Davies-Colley and Smith 2001). The diffuse attenuation coefficient (k_d) is an apparent optical property related to light attenuation, that cannot be measured directly. However, it can be very useful, i.e. to obtain penetration depths for photosynthetic coral in GBR waters. k_d has a strong linear relationship to suspended particulate matter (SPM) and good predictions of k_d have been made previously from single depth light and SPM measurements in the literature (Devlin et al. 2008; Liu et al. 2010).

Considerable work has been done over the last two decades to document the variations in water turbidity and SPM for waters of the GBR. This has been partly to answer questions relating to the effect of increased sediment discharge into the GBR lagoon due to increased erosion from agricultural land (Larcombe et al. 1995a; Larcombe et al. 1995b; Neil 1996; Larcombe and Woolfe 1999a,b; Davies-Colley and Smith 2001; Neil et al. 2002; Orpin et al. 2004; Orpin and Ridd 2012). One of the primary influences of increased water turbidity is to reduce the light availability to biota throughout the water column and especially those on the seabed such as corals or seagrasses. Ironically the influence of turbidity on light reduction has received very little attention, even though it is potentially the most important stressor. The relationship between water turbidity and light attenuation coefficients is thus poorly documented with some notable exceptions, such as an important study by Anthony (2004) who was interested in the various drivers of light availability changes on a coral reef. The findings concluded that corals at the study site alternated between states of potential light limitation and light stress, with a 2–8-week periodicity that was caused mainly by turbidity variations (Anthony et al. 2004). Detailed study of the relationship between turbidity and light, and especially as it changes through the water column has thus been almost ignored. Although it is known that waves are by far the dominant driver of turbidity in the inshore GBR, the light-turbidity relationship warrants further investigation due to its fundamental link between the increased sediment discharge of sediment into the lagoon and potential light reductions seen by important ecosystems, and by organisms living within the water column.

Within coastal regions of the GBR (i.e. located within the 20 m isobath (Wright 1995; Cooper et al. 2008; Macdonald et al. 2013), SPM is a major influence on water turbidity, with minor influences being phytoplankton and dissolved organic matter / yellow substance (Furnas 2003). SPM is variable with depth and this variation can affect penetration depths and bottom production. Therefore, obtaining vertical profiles of water turbidity is important to understand how light changes throughout the entire water column. Direct measurements of turbidity are easily obtainable. However, for the GBR, these are generally only measured near the seabed (Fabricius et al. 2012; Macdonald et al. 2013). Restricting measurements to the benthos may not provide a complete picture, as a great deal of marine biota also inhabits the water column above the seabed. However, obtaining a depth profile of turbidity, and a depth averaged turbidity value, is complicated and potentially expensive, because multiple measurements and instruments are required. Coastal GBR turbidity also has high temporal variability; therefore a vertical turbidity profile can be difficult to model (Orpin and Ridd 2012).

We present the first vertical light and turbidity profile measurements collected together on the inshore GBR. These data allow all other bottom measurements to be extrapolated to depth averaged results and are hoped to broaden the current knowledge of the physics at play. To the author's knowledge, this is the first paper to properly link light attenuation and turbidity in the context of inshore GBR waters. The paper addresses the following questions: 1. What is the relationship between light attenuation coefficient and turbidity or coastal waters of the GBR? 2. What is the typical depth profile of turbidity in the coastal GBR? 3. Can light attenuation thus be used to predict water turbidity in the coastal GBR? 4. What is the euphotic depth limit for the coastal GBR?

5.3 Theory

5.3.1 Calculation of the diffuse attenuation coefficient (k_d)

Upon entering the water, downward directed light intensity is reduced by two distinct physical processes; absorption and scattering. Absorption completely removes the light, whereas scattering alters the direction of light propagation. This increases the probability that the light will eventually be absorbed by increasing the path length. In high turbidity regions, scattering is the dominant process and can cause the light to become isotropic. Absorption and scattering describe the attenuation of light through water by interacting in a nonlinear and complex fashion within the radiative transport equations (Mobley 1994). These equations cannot be solved analytically; however models exist which approximate numerical solutions (Mobley et al. 1993). In this work, it will be assumed that to first order, the general form of the downward directed irradiance decays as an inverse exponential with depth, i.e. in the absence of strong discontinuities in water optical properties PAR measurements (400-700 nm) can be well described by Beer-Lambert's Law,

$$I_z = I_{z0} e^{-k_d(z-z_0)}$$

31

where I_{z0} and I_z are the downward directed irradiances at an upper depth (z_0) and a lower depth (z) respectively, and k_d is the diffuse attenuation coefficient (averaged across the PAR waveband 400-700 nm) (Jerlov 1976; Kirk 1977). This approximation has been successfully applied to calculate k_d in ocean waters (Gordon 1989; Dennison et al. 1993; Kirk 1994). The equation for k_d is obtained by rearranging equation 31,

$$\boldsymbol{k_d = ln\left(\frac{I_{z0}}{I_z}\right)/(z - z_0)}$$

32

k_d may also be split into two components as follows,

$$k_d = k_d^{cl} + k_d^T$$

33

where k_d^{cl} is the light attenuation due to clear water (i.e. when turbidity is zero) and k_d^T is the light attenuation due *to* turbidity which is assumed to be a linear relationship i.e.

$$k_d^T = \alpha T$$

34

where *T* is water turbidity in nephelometric turbidity units (*NTU*) and α is a coefficient relating attenuation coefficient to turbidity. Ideally in conditions of low turbidity, light data should be obtained between the hours of 10 am and 2 pm to ensure irradiance angles are close to the solar zenith.

One aspect of this paper is to determine if light data can be used as a surrogate measure of water turbidity, because light is an easier, cheaper and more reliable parameter to measure than turbidity. Under the assumption that k_d^{cl} and α can be considered constant and if a surface light reading and a bottom light reading are available, the hypothesis to be tested in this work is that an average water turbidity can be inferred, using a combination of equations 32, 33 and 34 as follows,

$$T = \frac{\left[ln\left(\frac{I_0}{I}\right)/(z - z_0)\right] - k_d^{cl}}{\alpha}$$

35

5.3.2 Euphotic depth calculations

Euphotic or photic depth (Z_{eu}) is generally defined to be a measure of the depth where only 1 *%* of the surface irradiance remains (Wright 1995; Kleypas 1999; Devlin et al. 2008; Kirk 2010; Fabricius et al. 2012; Weeks et al. 2012; Fabricius et al. 2014). Most photo-autotrophic organisms cannot achieve positive net daily production below depths of this threshold. The definition of the euphotic depth as being 1 % of surface is equivalent to defining $Z_{eu} = 4.6/k_d$, assuming k_d is approximately constant with depth (Kirk 2010; Saulquin et al. 2013). Further, the mid-point of the euphotic depth (1/2 Z_{eu}) can be approximated as $2.3/k_d$ and corresponds to the depth at which downward irradiance is reduced to 10 % of the value just below surface (Kirk 2010). However, photic limits for coral reef are not well defined and significant differences between various authors exist in the literature. For example, Chalker (1981) suggests a photic band exists between 50-450 $\mu E\ m^{-2}s^{-1}$ using a range of I_k for individual coral, where I_k is a measure of coral adaption to light (Chalker 1981). This value is potentially much larger than the photic limit of 1% of the surface value which is 20 $\mu E\ m^{-2}s^{-1}$ for the GBR region where typical maximum surface irradiance is *ca.* 2000 $m^{-2}s^{-1}$.

5.4 Methods

5.4.1 Instrumentation

Four data loggers recording turbidity, light, pressure (depth) and temperature (Ridd and Larcombe 1994) were moored to give a vertical profile of these parameters (Figure 37). All four instruments are tethered to each other, utilising light frames and floats to maintain buoyancy. This enables instruments to be spaced at different depths throughout the water column. Typically, for a depth of 12 m the surface (first) instrument was floated to a large flashing buoy and sensors were located approximately 1 m from sea surface. The second instrument was located approximately 2 m below this and the third instrument approximately 4 m below the second. The seabed (fourth) instrument was approximately 4 m below the third and attached to a heavily weighted frame, with the sensors located approximately 40 cm from the bed. The turbidity and light sensors were programmed to self-clean every 120 minutes (Ridd and Larcombe 1994). Pressure measurements were converted to depth. Turbidity measurements have a potential zero error of 0.5 NTU. The light sensor measures downward directed light in the 400-700 nm wavelength region and has an approximately cosine angular response. The turbidity sensor is an optical fibre backscatter sensor (Ridd and Larcombe, 1994).

The four instruments allow three non-overlapping depth intervals for which attenuation coefficients can be calculated in the water column. A fourth depth interval, *viz* the entire water column, was also considered (Figure 37). The top instrument is at a constant distance from the surface because it is floating, whilst the other three instruments are at a constant distance from the seabed. At one site, instrument failure reduced the number of depth intervals that could be used.

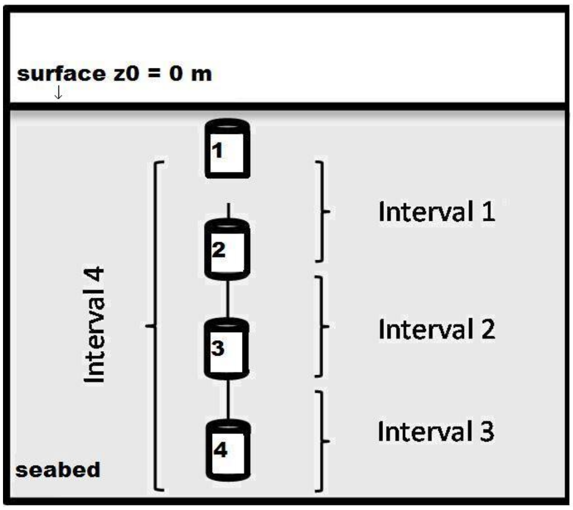

Figure 37 Schematic of instrument setup defining instrument numbers and intervals used in light attenuation calculations.

5.4.2 Sites and data collection

Turbidity measurements were obtained from three coastal sites in North Queensland Australia (Table 7). One site was located in Cleveland Bay (CB) and two sites were located along the coast between the Tully and Hull Rivers (T1 and T2).

5.4.2.1 Tully coast sites

The deployment at the Tully coast sites occurred over 24 days, from 20/02/2013 to 16/03/2013, during the wet season (austral summer). Instruments were deployed at two sites, T1 and T2, at less than 10 km far from Stingaree Reefs (Dunk Island), Timana Reef (Thorpe Island), and Richards Reef (Bedarra Island) (Figure 38). Each site consisted of four vertically connected loggers as presented in Figure 37. The seafloor sediment around the Tully and Hull River areas is predominantly terrigenoclastic and the main riverine sediment sources come from the Tully, Hull and Murray Rivers (Perry et al. 2009b). Nearby Dunk Island is primarily composed of granitic and metamorphic rocks. Fringing reef on the southern and western sides of the island is approximately 900 *m* wide (Hopley et al. 1983; Macdonald et al. 2013).

5.4.2.2 Cleveland Bay site

The deployment at Cleveland Bay occurred over 14 days, from 19/01/2013 to 01/02/2013, at a fringing reef of Magnetic Island. The site (CB) was located approximately 1 km off Bremner Point with depths of approximately 12 m (Figure 38). Magnetic Island is located about 10 km from the mainland coast, at the Cleveland Bay’s entrance, and has granitic formation. Cleveland Bay is a shallow embayment, partially sheltered from south easterly waves with a maximum depth of *ca.* 15 m (Orpin and Ridd 2012; Macdonald et al. 2013). Sediments in Cleveland Bay are mainly soft and silty and easily resuspended (Belperio 1979).

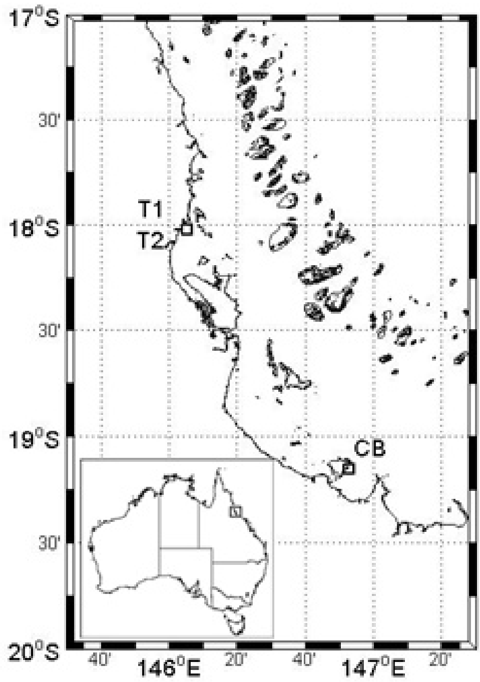

Figure 38 Section of North Queensland Coastline depicting portion of Great Barrier Reef and locations for quad-nephelometer deployments, Cleveland Bay (CB) and Tully coast (T1 and T2).

Table 7 Site locations for light attenuation study.

SITE NAME	**LABEL**	**LATITUDE**	**LONGITUDE**
Cleveland Bay	CB	-19.152433	146.880583
Tully coast Site1	T1	-18.023897	146.087294
Tully coast Site2	T2	-18.022658	146.089489

5.5 Results

5.5.1 Time series

Data from site T1 are highly representative of all deployments and shown in Figure 39 Synchronized tidal signals are observed in water depth data for all instruments except the surface instrument (1), which is floating (Figure 39a). Periods of high turbidity correspond with low light levels, and vice-versa (Figure 39 b-c). Examples of a low and high turbidity event are labelled (Figure 3b). High turbidity event at site CB is a 24 hour data segment taken from 24/01/2013. High turbidity event at T1 and T2 is a 12 hour data segment taken from 12/03/2013. High turbidity defined as NTU values that are consistently above 50 NTU. Low turbidity event for site CB is a 24 hour data segment taken from 20/01/2013. Low turbidity event at T1 and T2 is a 12 hour data segment taken from 02/03/2013. Low turbidity is defined as < 16 NTU.

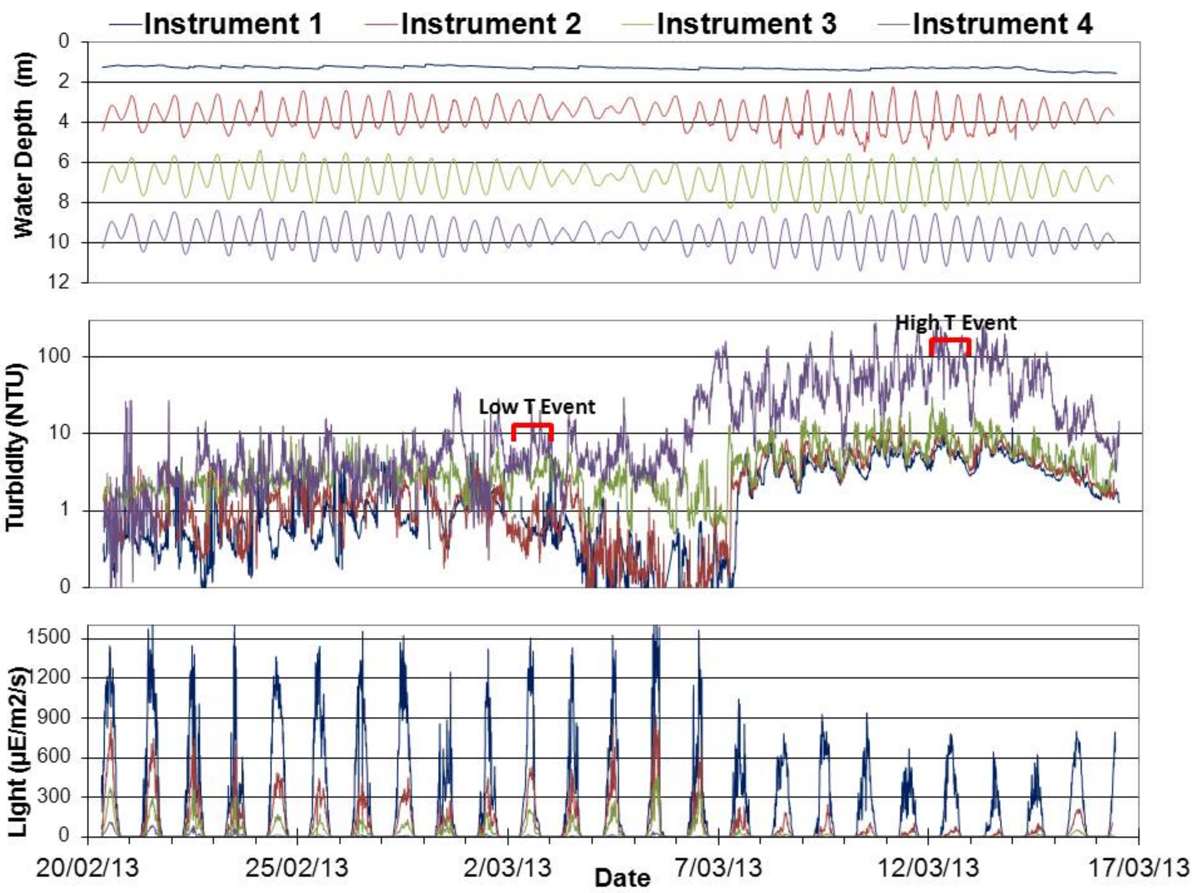

Figure 39 Time series data at Tully site T1. Top image: Water depth. Instrument 1 is located closest to the surface, followed by instruments 2 and 3. Instrument 4 is located closest to the seabed. Middle image: Turbidity (labelled with high and low turbidity event) nb. turbidity is plotted on a log scale. Bottom image: Light.

5.5.2 Relationship between k_d and turbidity

Concurrent light and depth data (near-surface and near-bed) was hourly averaged and taken between 10 am - 2 pm. These data were used to calculate diffuse attenuation coefficients (k_d) over various depth intervals throughout the water column (32). Depth-averaged turbidity was calculated by averaging turbidity data obtained from the four instruments along the water column (Figure 37). For the entire water depth, there is a strong linear relationship between T and k_d (R^2= 0.91) at site CB (Figure 40 a) and linear relationships at sites T1 and T2 (R^2 = 0.66 and 0.79, respectively, (Figure 40 b and c) The overall average diffuse attenuation coefficient (k_d^{avg}) is 0.43 m^{-1} for site CB, 0.53 m^{-1} for site T1 and 0.51 m^{-1}

for site T2 (average of all k_d values calculated over the entire water column i.e. interval 4 (Figure 40)). The clear-water-attenuation coefficients (k_d^{cl}) (a component of k_d defined in (33) for each site are obtained from the y-intercept of the fit to the graphs of k_d versus T (Figure 40 a-c). k_d^{cl} = 0.30 m^{-1} at CB (Figure 4a), k_d^{cl} = *0.41* m^{-1} at T1 (Figure 40 b) and k_d^{cl} = 0.40 m^{-1} at T2 (Figure 40 c). Values reported in the literature vary widely, due to the innate variability of ocean water turbidity. However for sites with similar turbidity, (k_d^{cl}) values are *ca 0.33 m-1* (Wright 1995).

The turbidity-attenuation coefficients (k_d^T) (a component of k_d defined in equation 4) are obtained by multiplying α (obtained from the slope of the fit (Figure 40)) with turbidity (T). At site CB, $\alpha = 0.076$ $m^{-1}NTU^{-1}$ (Figure 40 a) and at sites T1 and T2, α = 0.040 $m^{-1}NTU^{-1}$ and α = 0.037 $m^{-1}NTU^{-1}$ respectively (Figure 40 b and c). For CB, the value for α is almost double the values at sites T1 and T2. This is presumably a result of the different optical characteristics of the suspended material between the two regions.

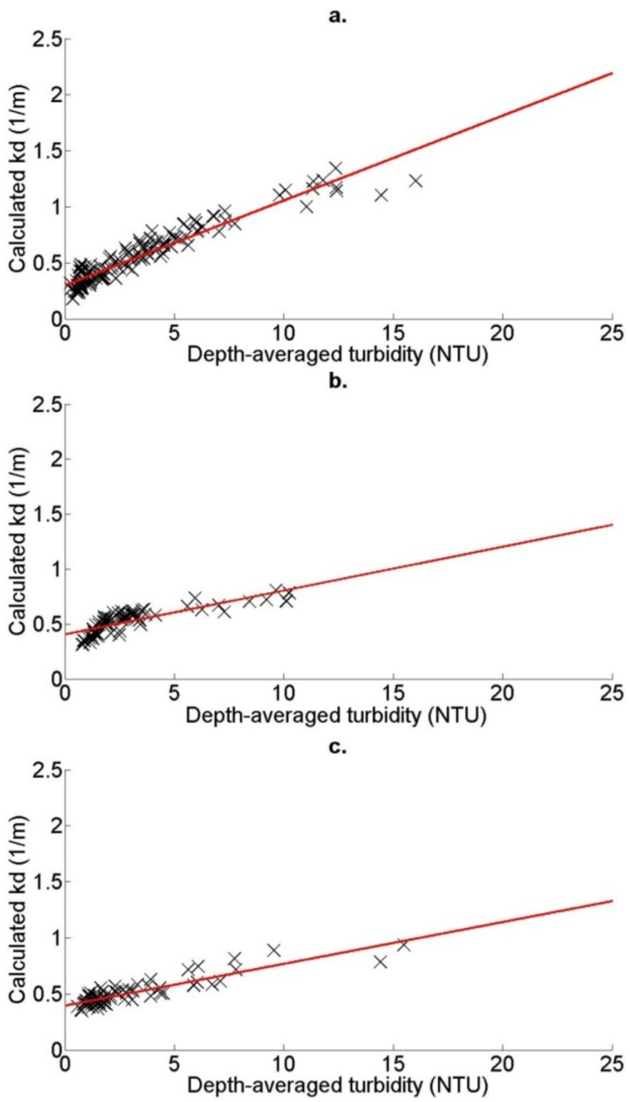

Figure 40 Light attenuation coefficients (calculated for depth interval 4) versus depth-averaged turbidity. Data are between 10am-2pm and hourly averaged. a: CB, $\alpha = 0.076\, m^{-1}/NTU$), $k_d^{cl} = 0.3\, m^{-1}$ and R^2 = 0.91. b: T1, $\alpha = 0.04\, m^{-1}/NTU$, $k_d^{cl} = 0.41\, m^{-1}$ and R^2 = 0.66. c: T2, $\alpha = 0.037\, m^{-1}/NTU$, $k_d^{cl} = 0.40\, m^{-1}$ and R^2 = 0.79.

Linear relationships are also found between k_d and T for water column sub intervals (Figure 41). Changes to slope and intercept are observed amongst the intervals, and throughout the different layers in the water column (Figure 41 a-c), again presumably as a result of differing optical properties of the suspended materials.

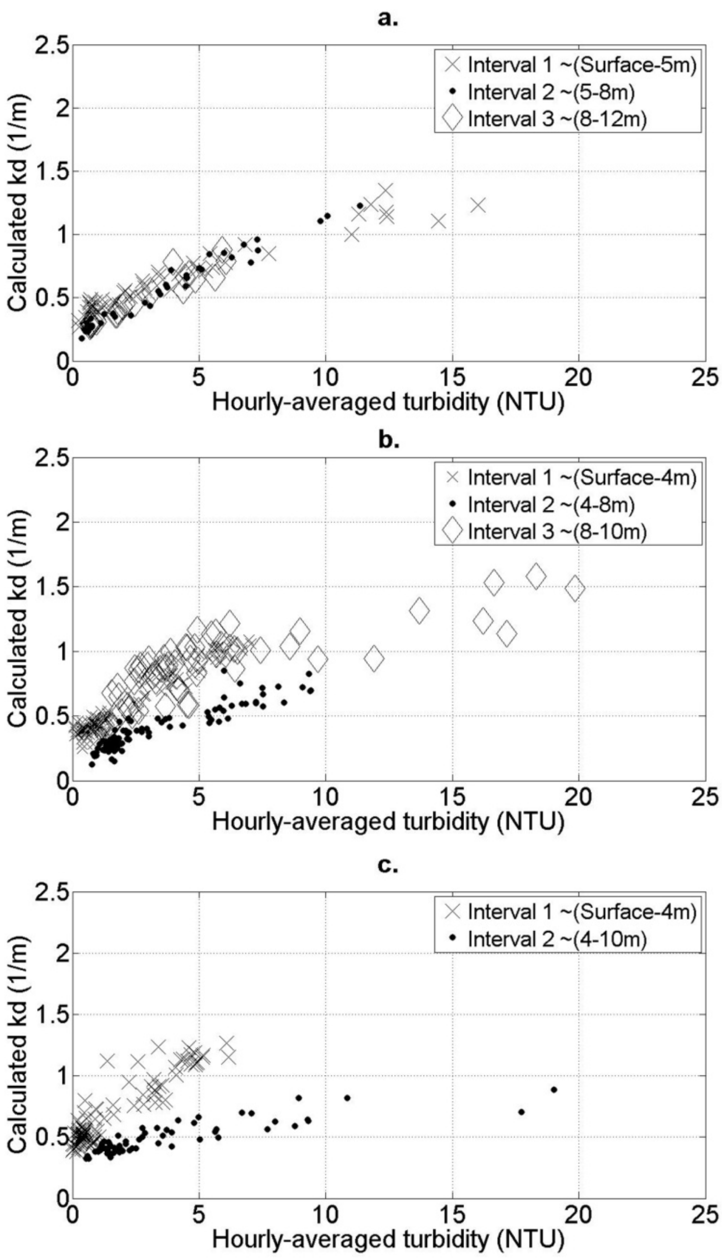

Figure 41 Light attenuation coefficients (calculated for depth intervals 1, 2 and 3) versus depth-averaged turbidity. Data are between 10am-2pm and hourly averaged. a: CB b: T1 c: T2.

5.5.3 Relationship between depth-averaged and seabed turbidity

A strong positive linear relationship was found between depth-averaged turbidity (T_{avg}) and seabed turbidity (T_{bed}) ($R^2 = 0.96, 0.99$ and 0.96 at CB, T1 and T2 respectively) (Figure 42 a-c).

Significantly, results show turbidity within water column to be between 0.3-0.4 times seabed turbidity across all sites (Figure 42 a-c).

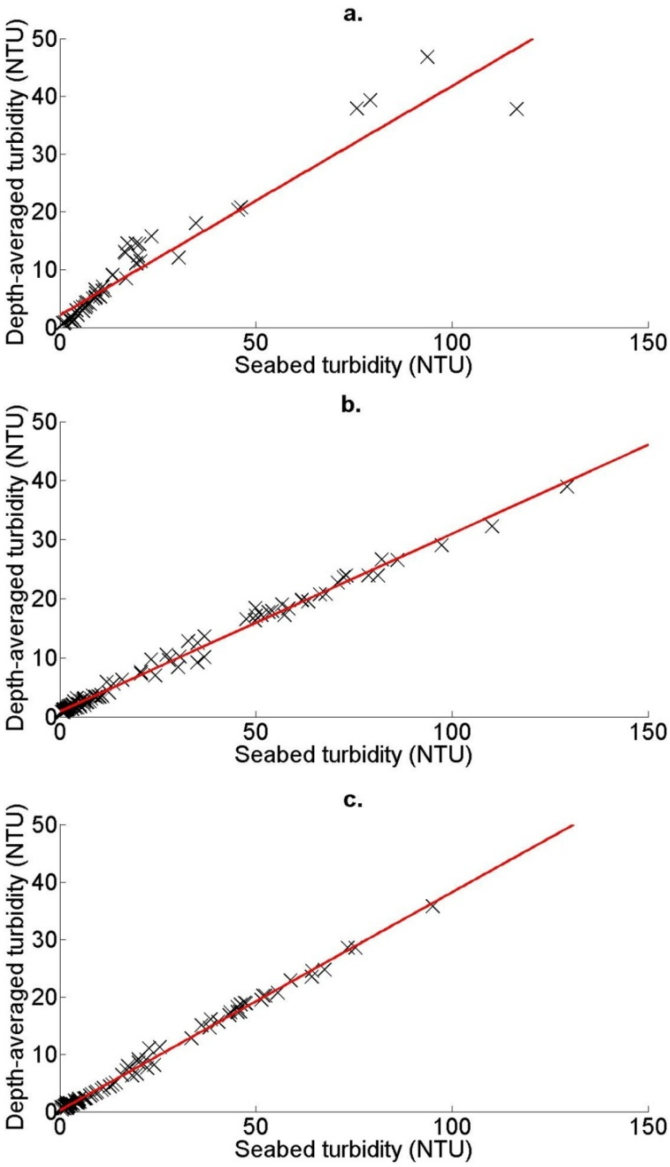

Figure 42 Depth-averaged turbidity (averaged over all four instruments) versus seabed turbidity. Data are hourly averages. a: CB, $T_{avg} = 0.40(T_{bed}) + 2.1$ and $R^2 = 0.96$. b: T1, $T_{avg} = 0.30(T_{bed}) + 0.92$ and $R^2 = 0.99$. c: T2, $T_{avg} = 0.38(T_{bed}) + 0.26$ and $R^2 = 0.99$.

There is an issue of autocorrelation when plotting depth-averaged turbidity vs seabed turbidity. This is because depth-averaged turbidity is derived from the sum of all four instrument readings including the seabed turbidity data, (Figure 42 a-c). Therefore it is expected to result in an inflated correlation coefficient, especially as the bottom turbidity reading is often considerably higher than readings from instruments higher in the water column. To investigate the extent of autocorrelation, the seabed measurement was removed from the depth-averaged turbidity calculation, i.e. the depth average of the top three instrument readings was used. The new correlation coefficients are R^2 = 0.75, 0.78 and 0.52 for CB, T1 and T2 respectively, i.e. there is a strong correlation between bottom turbidity and the turbidity in the upper part of the water column. However, whilst autocorrelation effects are acknowledged, it is considered to be a more useful physical representation to present depth-averaged turbidity data over the entire water column.

5.5.4 Use of light and depth data to infer turbidity

Using empirically derived attenuation coefficients for coastal waters of Cleveland Bay and the Tully coast, a model equation is defined which makes a prediction of depth-averaged turbidity (T_{pred}), given surface and seabed light and depth data. The model (T_{pred}) is derived in the theory section, equation (35) and redefined here as,

$$T_{pred} = \frac{\left[ln\left(\frac{I_0}{I}\right)/(z - z_0)\right] - k_d^{cl}}{\alpha} \tag{36}$$

In order to determine the values of the constants α and k_d^{cl}, a linear model of T_{pred} is trained on a segment of near-zenith, CB data (between the hours of 10am-2pm) (Figure 40 a). Time periods with light values < 0.5 $\mu E\ m^{-2}s^{-1}$ are omitted. This removes periods where the light is effectively completely attenuated and thus it is impossible to use the bottom light measurement to infer turbidity. T_{pred} training is presented (Figure 43 a) and T_{pred} versus measured depth-averaged turbidity (T_{avg}) is presented for each site (Figure 43 b-d). During training, T_{pred} constants are taken from CB attenuation calculations (Figure 40 a) ($\alpha = 0.076\, m^{-1}/NTU,\, k_d^{cl} = 0.3\, m^{-1}$). As is expected from training data, the model shows good agreement between measured and predicted data with and $R^2 = 0.90$.

There are not enough hourly averaged data-points within the (10am-2pm) data segment to both train and test the model. Therefore the above constants are applied to the remainder of CB data outside the period from 10am to 2 pm, i.e. it was applied to periods of lower sun angle (Figure 43 b). The model shows very good agreement between measured and predicted data with $T_{pred} = 1.0(T_{avg})$ and $R^2 = 0.78$. It should be noted that the unity slope of this prediction to two significant figures is a coincidence. Predictions of the Tully turbidity using coefficient derived from CB were not as successful with the model under-predicting depth-averaged turbidity by 0.39 % and 0.44 % for T1 and T2, respectively (Figure 43 c and d).

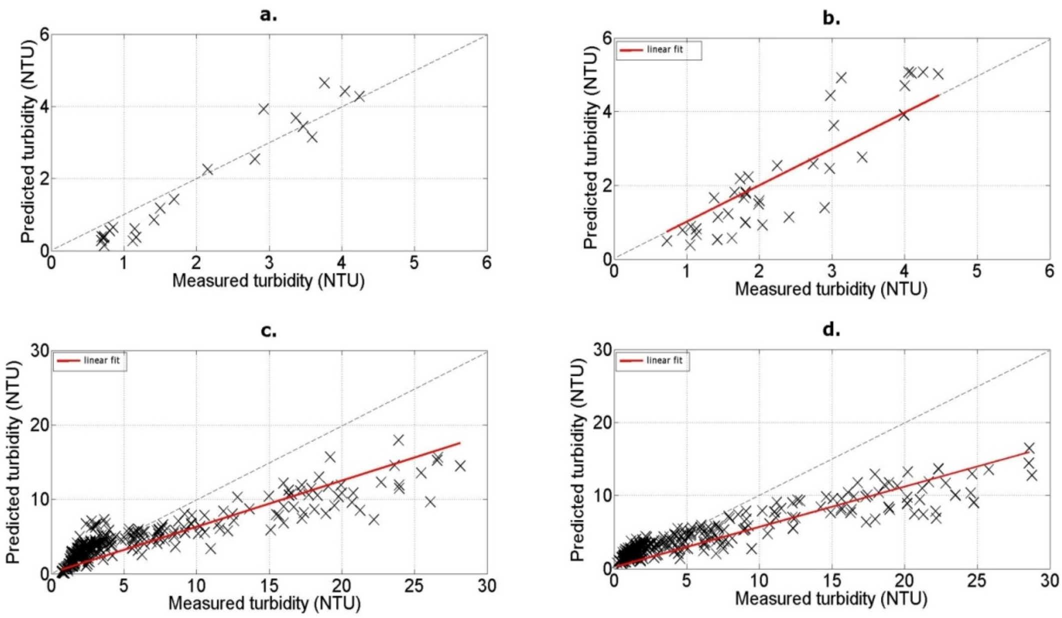

Figure 43 Predicted (depth-averaged) turbidity (T_{pred}) vs. measured (depth-averaged) turbidity (T_{avg}). Light data < 0.5 $\mu E\ m^{-2}s^{-1}$ are omitted. T_{pred} constants: $\alpha = 0.076\ m^{-1}NTU^{-1}$ and $k_d^{cl} = 0.3\ \mathrm{m}^{-1}$ calculated from CB data. a: (Training) CB data segment (10 am – 2 pm). b: Remainder of CB dataset (2pm-10am), T_{pred} = 1.0(T_{avg}) and R^2 = *0.77*. c: T1 dataset, T_{pred} = 0.61(T_{avg}) and R^2 = *0.64*. d: T2 dataset T_{pred} = 0.56(T_{avg}) and R^2 = *0.69*.

The under-prediction of T_{pred} values for sites T1 and T2 (Figure 43 c and d) was due to the use of coefficients from the CB site. When attenuation coefficients from the T1 site are used (Figure 40 b, $\alpha = 0.04\,\mathrm{m}^{-1}/\mathrm{NTU}$, $k_d^{cl} = 0.4\,\mathrm{m}^{-1}$) the model then produces better agreement between measured and predicted data: $T_{pred} = 0.77(T_{avg})$ and $R^2 = 0.68$. for T1 (Figure 44 a) and $T_{pred} = 0.65(T_{avg})$ and $R^2 = 0.78$ for T2 (Figure 44 b). However, this is still a considerable under-prediction.

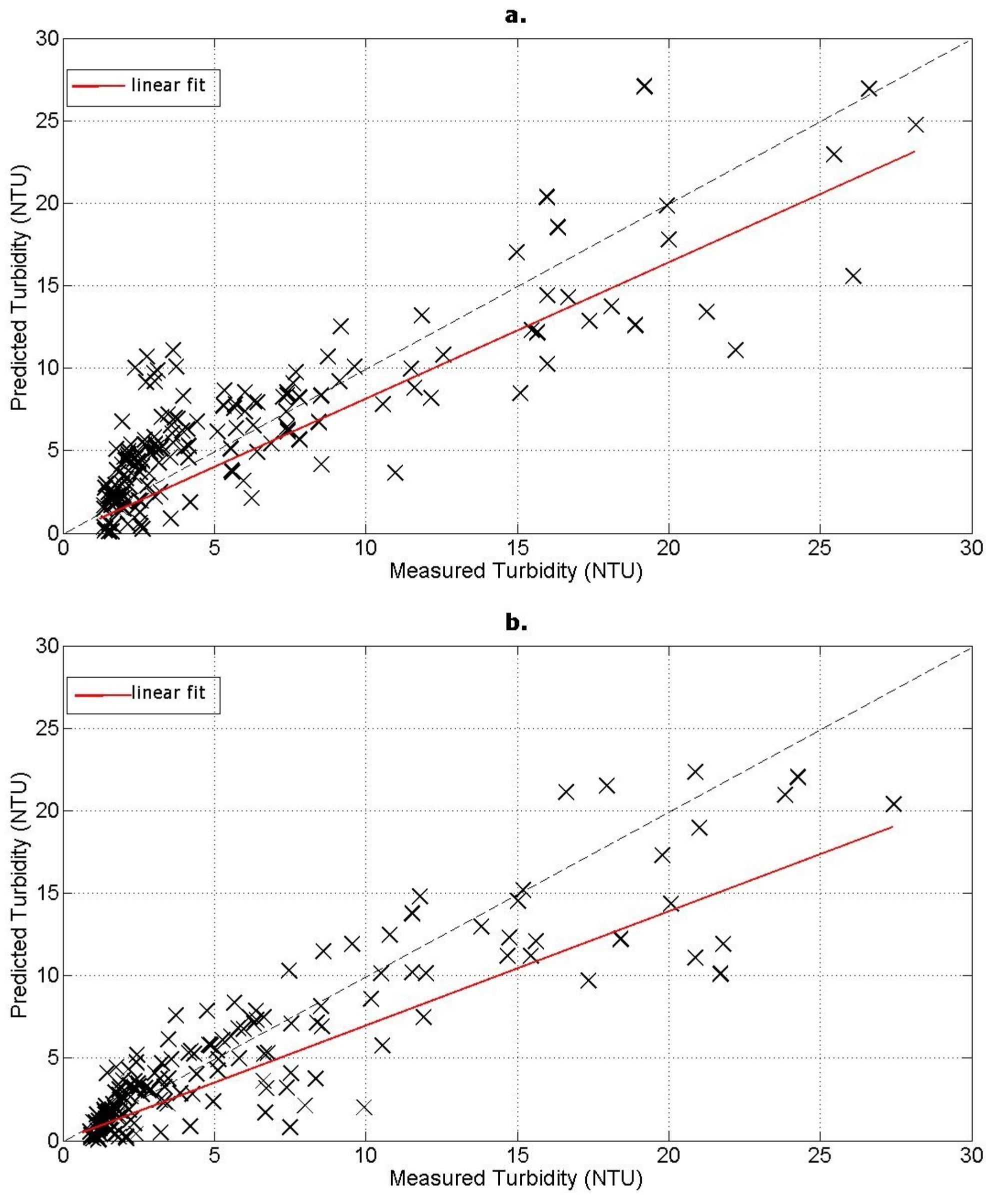

Figure 44 Predicted (depth-averaged) turbidity (T_{pred}) vs. measured (depth-averaged) turbidity (T_{avg}). Light data < 0.5 $\mu E\ m^{-2}s^{-1}$ are omitted. T_{pred} constants: $\alpha = 0.041\ \mathrm{m^{-1}/NTU}$ and $k_d^{cl} = 0.4\ \mathrm{m^{-1}}$ calculated from T1 data. a: T1 data segment (2 pm - 10 am), T_{pred} = 0.77(T_{avg}) and $R^2 = 0.68$. b: T2 data segment (2 pm – 10 am), T_{pred} = 0.65(T_{avg}) and $R^2 = 0.78$.

5.5.5 Coral photic depth thresholds for the coastal GBR

Using the calculated turbidity-attenuation coefficient for Cleveland Bay ($\alpha = 0.076$ m^{-1}/NTU), and the calculated attenuation due to clear water (k_d^{cl} = 0.3 m^{-1}), light-depth curves are presented with photic limits to examine light levels reaching marine organisms and depict potential coral mortality thresholds for Cleveland Bay (Figure 45). Light curves are modelled using Beer-Lamberts equation (equation 1), where I_0 is calculated from the average of surface light hourly maxima (from 10am-2pm) ($I_{0(maxima)}$ = 1925 $\mu E\ m^{-2}s^{-1}$) and photic limit is calculated as 1% of I_0 (Z_{eu}^{CB} = 19.25 $\mu E\ m^{-2}s^{-1}$). Theoretical depth-averaged turbidities are substituted into equation 1 to obtain each light curve.

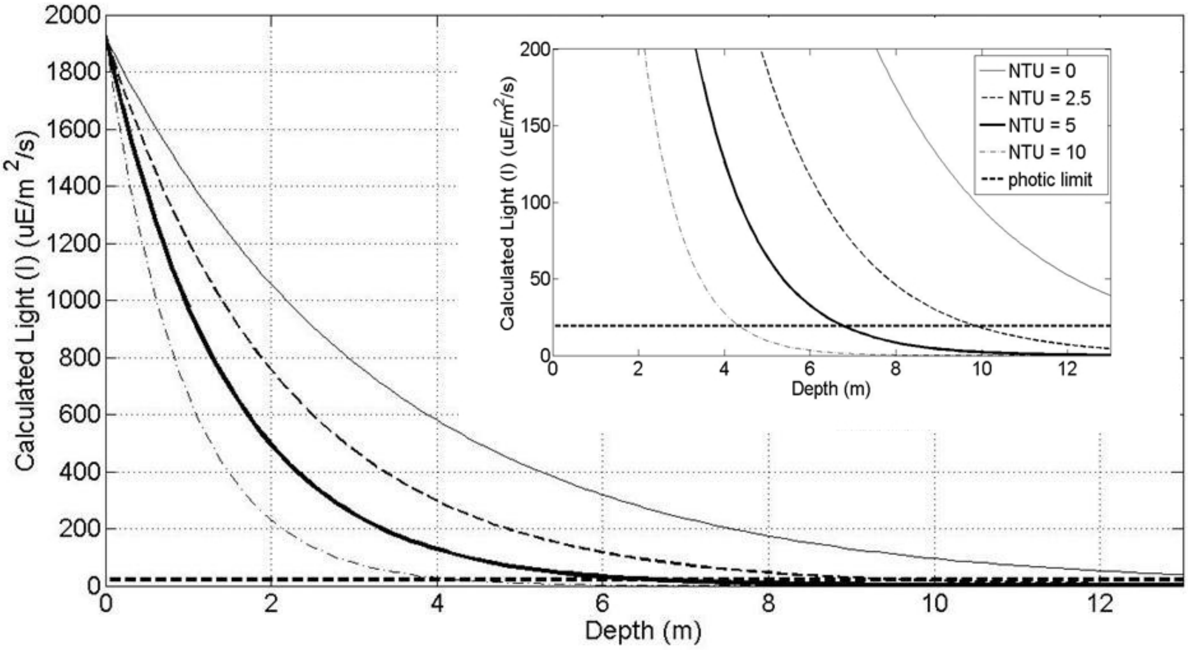

Figure 45 Irradiance curves for Cleveland Bay depicting euphotic depths for depth-averaged turbidities. Light curves are modelled (equation 1), I_0(maxima) = 1925 $\mu E\ m^{-2}s^{-1}$. Photic limit is 1% of I_0(maxima). Close-up inset: For depth-averaged turbidity of 2.5 NTU, photic depth is 10 m. For depth-averaged turbidity of 5 NTU and 10 NTU, photic depths are 6.7 and 4.3 m respectively.

For clear water (zero turbidity), the photic depth extends almost to the seabed for the whole bay, which has a maximum depth of approximately 13 m. A depth-averaged turbidity of 2.5 NTU (representing low turbidity levels (Figure 39)) produces a photic depth of 10 m. The mean, median turbidity across the entire CB dataset is 5 NTU, producing a photic depth limit of 7 m. Finally for a depth-averaged turbidity of 10 NTU (which is the mean depth-averaged turbidity for the entire CB dataset), the photic depth becomes 4 m (Figure 45).

5.6 Discussion

5.6.1 Attenuation coefficient as a function of turbidity

To the author's knowledge, this is the first study to link turbidity with light attenuation for the inshore Great Barrier Reef. As such, this work may be a useful extension on what we currently know about the connection between water quality and light attenuation. Examination of water turbidity, light and depth data reveals a positive linear relationship between depth averaged turbidity (*T*) and the calculated attenuation coefficient (k_d) across all sites; (R^2= 0.91) for CB site (Figure 40 a) and T1 and T2 ($R^2 = 0.66$ and *0.79* (Figure 40 b and c). The overall average diffuse attenuation coefficient (k_d^{avg}) is 0.43 m^{-1} for site CB, 0.53 m^{-1} for site T1 and 0.51 m^{-1} for site T2 (averaged over the entire water column (Figure 39 a-c)). These values are close to those previously reported for Cleveland Bay (K_d = 0.147-0.439 m^{-1}) (Anthony et al. 2004; Kirk 2010). Other examples of reported k_d values around Australia are; 0.4 m^{-1} (Swan River, WA) 0.55 m^{-1} (Lake Macquarie, NSW) 0.18 m^{-1} (Tasman Sea, NSW) (Kirk 2010).

The total attenuation coefficient is separated into the clear-water-attenuation coefficients (k_d^{cl}) and the turbidity-attenuation coefficients (k_d^{T}) and calculated for each site. For Cleveland Bay, k_d^{cl} = 0.30 m^{-1}. Values equivalent to k_d^{cl} reported in the literature for sites with similar turbidity/sediment levels are very close in value; *ca* $0.33\ m^{-1}$ (Wright 1995). For site CB, $\alpha = 0.076$ m^{-1}/NTU (Figure 40 a) and for sites T1 and T2, α = 0.041 m^{-1}/NTU and α =

0.037 m^{-1}/NTU respectively (Figure 40 b and c). Values of the attenuation component due to turbidity are not commonly referred to in the literature, so it is difficult to make a comparison with other work. Furthermore, as these values are highly site specific and dependant on sediment grain size etc., an intra-site comparison would unlikely be of significance.

5.6.2 Investigating turbidity and depth

Turbidity measurements are generally only obtained near the seabed (Fabricius et al. 2012; Macdonald et al. 2013). However the importance of not limiting measurements to the benthos must be taken into account, as a great deal of marine biota also inhabits the entire water column. Furthermore, how turbidity changes along the water column directly affects the availability of light on the seabed. We investigated how turbidity typically changes with depth at inshore GBR sites. Depth averaged turbidity levels are generally found to be between 0.3 and 0.4 times that of the seabed. The linear relationships between average and seabed turbidity are very strong (R^2 = *0.96, 0.99* and *0.96* for CB, T1 and T2 respectively) (Figure 42 a-c). This is a potentially very useful finding as most time series measurements of turbidity on the GBR are taken near the sea bed and this information can be used to extrapolate the depth averaged turbidity, and possibly depth averaged suspended sediment concentrations, for other sites of the GBR. It should be noted that measuring the turbidity profile is much more expensive than measuring bottom turbidity due to the requirement for more instruments and the fact that instruments placed near the water surface are more likely to be lost due to storms, boat strike and theft.

5.6.3 Predicting turbidity from light data

This paper presents a new method of predicting depth-averaged turbidity based upon measurements of light. The model equation is derived from Beer-Lamberts law and makes a prediction of water column (i.e. depth-averaged) turbidity (T_{pred}) between two light sensors placed at the surface and seabed. T_{pred} constants α and k_d^{cl} are initially obtained from calculations made on a segment of CB data (Figure 40 a). For the remainder of the CB dataset, the model shows very good agreement between measured and predicted data with $T_{pred} = 1.0(T_{avg})$ and an R^2 value of 0.78. However when T_{pred} (CB) coefficients are applied to T1 and T2 data (Figure 43 c and d), the model under-predicts average turbidity by 0.39% and 0.44% for T1 and T2. It was found that the under-prediction observed in T_{pred} for sites T1 and T2 (Figure 43 c and d) may be improved by obtaining site-specific coefficients from attenuation calculations (Figure 40 c). The model then shows better agreement between measured and predicted data: $T_{pred} = 0.77(T_{avg})$, with an R^2 value of 0.68 (Fig 10a.) for T1 and $T_{pred} = 0.65(T_{avg})$ with an R^2 value of 0.78, for T2 (Figure 44 b). However, this is still a considerable under-prediction. Due to constraints on available testing data, periods are included with low solar elevation (near sunrise and sunset) and it is thought that that this may cause the model to under-predict, due to the light travelling a slightly greater distance.

It is concluded that in an ideal situation, calculated light attenuation coefficients used in the predictive model should be site specific to reduce over/under prediction. Measuring light is generally easier than measuring turbidity as light sensors are less sensitive to fouling and other environmental factors which can reduce data recovery. Employing this method results in a much more cost effective and logistically simpler estimation of depth averaged turbidity at each site. There is also the advantage of being able to measure surface plumes which would likely be missed by a seabed turbidity sensor. A restriction of this model is that for very high turbidity conditions, the bottom light levels go to zero which produces an upper limit on the measurable turbidity. In addition no information about the turbidity can be found during the night or low light periods.

A comment should also be made on what the implications are of assuming a constant α and constant k_d^{cl} in the model. It is expected that the clear water attenuation component, k_d^{cl} should be essentially constant. It is defined as the contribution to attenuation when turbidity is zero and calculated as such. In coastal GBR waters, the remaining contributors to light attenuation (such as phytoplankton and dissolved organic matter) are considered to be negligible when compared to SPM (Furnas 2003). The second assumption in the model is that the turbidity component of attenuation $(k_d^T = \alpha T)$ is constant. However it is known that water-column turbidity is not homogeneous but varies spatially and temporally throughout the GBR. To mitigate this, the model works to predict a “depth-averaged” turbidity. Producing a single value of turbidity, averaged over the entire depth of the water column can be very useful, as it provides additional information to be used in conjunction with typical seabed or surface measurements, potentially producing a more complex representation of turbidity across the water column that was previously possible.

5.6.4 Coral photic depth thresholds

Light is a key resource for marine ecosystems, as it controls growth for the many groups of phototrophic organisms (Anthony et al. 2004). However, the role of light limits in shaping GBR ecosystems is not well understood (GBRMPA 2010). Aside from the commonly defined photic depth being 1% of surface irradiance (Kirk 2010), there are several other varying limits for coral growth cited in the literature between 50-450 $\mu E\ m^{-2}s^{-1}$ (Kleypas 1999). Inshore corals on the GBR are often exposed to intermittent periods of very low light, due to waves causing periods of sediment resuspension. Therefore these limits may not be as applicable to inshore corals (Dubinsky 1990; Larcombe et al. 1995b) (Conner and De Visser 1992; Logan et al. 2013).

The photic limit is calculated (as 1 % of surface light) to be 19.25 $\mu\mathrm{E}\ \mathrm{m}^{-2}\mathrm{s}^{-1}$ for the CB dataset. For zero turbidity, the photic depth extends to the seabed, however for conditions of low turbidity for Cleveland Bay (2.5 NTU), the photic depth is 10 m (Figure 45). This is likely to be a fair representation of coral depth limits in Cleveland Bay as hard coral colonies on Middle Reef are commonly observed and monitored at depths of 5 m (Schaffelke et al. 2009). Also hard coral cover and richness in the near-shore GBR peaks around 5-7 m (DeVantier et al. 2006). For depth-averaged turbidities of 5 NTU and 10 NTU, photic depths are calculated to be 7 m and 4 m respectively (Figure 45). By providing a depth-averaged alternative to mean seabed turbidity, this work contributes to current knowledge surrounding light attenuation in the GBR. In particular, regarding the interplay between variation in water clarity and mean photic depths.

It is well established that inshore corals can survive in turbid waters for some time, which may be due in part to temporal variations in turbidity as well as an increased ability to utilise suspended sediment as a food source (Anthony 2000). It is also well established that turbidity is temporally variable at coastal sites. Furthermore, the biological responses of coral vary with depth and species as well as duration of exposure to suspended particle matter (Anthony et al. 2004; Cooper et al. 2008). Therefore, interpreting photic depths for inshore coral communities must be done with great care, taking into account both median and mean turbidity values across the water column as well as changing temporal patterns in turbidity.

5.6.5 Extreme weather events

Extreme events such as monsoons and cyclones occur seasonally across the GBR. These acute events can result in river plumes and increased sediment resuspension, reducing light availability throughout the water column (GBRMPA 2012). This can lead to short term stress, increased vulnerability and potential mortality for reef organisms (Weeks et al. 2012). A recent paper by Fabricius (2014) used ten years of daily river load, oceanographic and MODIS-Aqua data to investigate changes in water clarity across a shallow 25,000 km^2 area of the central GBR shelf. Photic depth was found to be strongly related to river freshwater SSC and phosphorus loads ($R^2 = 0.65$ and 0.51, respectively). During seasonal river flooding, photic depth was found to be reduced. However these relationships were substantially weaker near the highly turbid coastal areas (Fabricius et al. 2014). Although these effects are normally short lived and self-limiting, further work into how extreme events affect light levels throughout the water column would contribute to the broader understanding of light attenuation in the inshore GBR. Unfortunately time limitations prevented such data acquisition during this study.

REFERENCES

Anthony KRN (2000) Enhanced particle-feeding capacity of corals on turbid reefs (Great Barrier Reef, Australia). Coral Reefs 19:59-67

Anthony KRN, Ridd PV, Orpin AR, Larcombe P, Lough J (2004) Temporal variation of light availability in coastal benthic habitats: Effects of clouds, turbidity, and tides. Limnology and Oceanography 49:2201-2211

Belperio AP (1979) The combined use of wash load and bed material load rating curves for the calculation of total load: An example from the Burdekin River, Australia. Catena 6:317-329

Chalker BE (1981) Simulating light-saturation curves for photosynthesis and calcification by reef-building corals. Marine Biology 63:135-141

Conner CS, De Visser AM (1992) A laboratory investigation of particle size effects on an optical backscatterance sensor. Marine Geology 108:151-159

Cooper TF, Ridd PV, Ulstrup KE, Humphrey C, Slivkoff M, Fabricius KE (2008) Temporal dynamics in coral bioindicators for water quality on coastal coral reefs of the Great Barrier Reef. Marine and Freshwater Research 59:703-716

Davies-Colley RJ, Smith DG (2001) Turbidity, suspended sediment, and water clarity: A review. Journal of the American Water Resources Association 37:1085-1101

Dennison WC, Orth RJ, Moore KA, Stevenson JC, Carter V, Kollar S, Bergstrom PW, Batiuk RA (1993) Assessing Water Quality with Submersed Aquatic Vegetation. Bioscience 43:86-94

DeVantier LM, De'ath G, Turak E, Done TJ, Fabricius KE (2006) Species richness and community structure of reef-building corals on the nearshore Great Barrier Reef. Coral Reefs 25:329-340

Devlin MJ, Barry J, Mills DK, Gowen RJ, Foden J, Sivyer D, Tett P (2008) Relationships between suspended particulate material, light attenuation and Secchi depth in UK marine waters. Estuarine, Coastal and Shelf Science 79(3):429-439

Dubinsky Z (1990) Evolution and zoogeography of coral reefs. In: Dubinsky Z (ed) Ecosystems of the World - Coral Reefs. Elsevier, Amsterdam; New York, pp1-9

Fabricius KE, Logan M, Weeks S, Brodie J (2014) The effects of river run-off on water clarity across the central Great Barrier Reef. Marine Pollution Bulletin 84:191-200

Fabricius KE, De'ath G, Humphrey C, Zagorskis I, Schaffelke B (2012) Intra-annual variation in turbidity in response to terrestrial runoff on near-shore coral reefs of the Great Barrier Reef. Estuarine, Coastal and Shelf Science 59:703-716

Furnas M (2003) Catchments and corals: terrestrial runoff to the Great Barrier Reef. Australian Institute of Marine Science, Townsville, Qld

GBRMPA (2010) Water quality guidelines for the Great Barrier Reef Marine Park. Great Barrier Reef Marine Park Authority, Townsville

GBRMPA (2012) Extreme Weather and the Great Barrier Reef, Govt. report http://www.gbrmpa.gov.au/managing-the-reef/threats-to-the-reef/extreme-weather/extreme-weather-and-the-great-barrier-reef-report

Gordon HR (1989) Can the Lambert-Beer law be applied to the diffuse attenuation coefficient of ocean water? Limnology and Oceanography 34:1389-1409

Hopley D, Slocombe AM, Muir F, Grant C (1983) Nearshore fringing reefs in north Queensland. Coral Reefs 1:151-160

Jerlov NG (1976) Marine optics. Elsevier Scientific Pub. Co, Amsterdam

Kirk JTO (1977) Attenuation of Light in Natural Waters. Aust J Mar Freshwater Res, 28:497-508

Kirk JTO (1994) Light and photosynthesis in aquatic ecosystems. Cambridge University Press, Cambridge [England]

Kirk JTO (2010) Light and Photosynthesis in Aquatic Ecosystems. Cambridge University Press, Cambridge

Kleypas JA (1999) Environmental Limits to Coral Reef Development: Where Do We Draw the Line? American Zoologist 39:146-159

Larcombe P, Woolfe KJ (1999a) Increased sediment supply to the Great Barrier Reef will not increase sediment accumulation at most coral reefs. Coral Reefs 18:163-169

Larcombe P, Woolfe KJ (1999b) Terrigenous sediments as influences upon Holocene nearshore coral reefs, central Great Barrier Reef, Australia. Australian Journal of Earth Sciences: An International Geoscience Journal of the Geological Society of Australia 46:141 - 154

Larcombe P, Woolfe KJ, Cooperative Research Centre for Ecologically Sustainable Development of the Great Barrier R (1995a) Great Barrier Reef: terrigenous sediment flux and human impacts. CRC Reef Research Centre, Townsville, Qld

Larcombe P, Ridd PV, Prytz A, Wilson B (1995b) Factors controlling suspended sediment on inner-shelf coral reefs, Townsville, Australia. Coral Reefs 14:163-171

Liu W-C, Wu R-S, Wu EM-Y, Chang Y-P, Chen W-B (2010) Using water quality variables to predict light attenuation coefficient: case study in Shihmen Reservoir. Paddy and Water Environment 8:267-275

Logan M, Fabricius K, Weeks S, Canto M, Noonan S, Wolanski E, Brodie J (2013) The Relationship between Burdekin River discharges and photic depth in the central Great Barrier Reef. Report to the National Environmental Research Program. Reef and Rainforest Research Centre Limited, Cairns 29pp

Macdonald RK, Ridd PV, Whinney JC, Larcombe P, Neil DT (2013) Towards environmental management of water turbidity within open coastal waters of the Great Barrier Reef. Marine Pollution Bulletin 74:82-94

Mobley CD (1994) Light and Water: Radiative Transfer in Natural Waters. Academic Press

Mobley CD, Gentili B, Gordon HR, Jin Z, Kattawar GW, Morel A, Reinersman P, Stamnes K, Stavn RH (1993) Comparison of numerical models for computing underwater light fields. Appl Opt 32:7484-7504

Neil DT (1996) Sediment concentrations in streams and coastal waters in the North Queensland humid tropics: Land use, rainfall and wave resuspension contributions. In: Hunter HM, Eyles AG, Rayment GE (eds) Downstream effects of land use. Dept. Natural Resources, Brisbane, pp97-101

Neil DT, Orpin AR, Ridd PV, Yu B (2002) Sediment yield and impacts from river catchments to the Great Barrier Reef lagoon. Marine and Freshwater Research 53:733-752

Orpin AR, Ridd PV (2012) Exposure of inshore corals to suspended sediments due to wave-resuspension and river plumes in the central Great Barrier Reef: A reappraisal. Continental Shelf Research 47:55-67

Orpin AR, Ridd PV, Thomas S, Anthony KRN, Marshall P, Oliver J (2004) Natural turbidity variability and weather forecasts in risk management of anthropogenic sediment discharge near sensitive environments. Marine Pollution Bulletin 49:602-612

Perry CT, Smithers SG, Johnson KG (2009b) Long-term coral community records from Lugger Shoal on the terrigenous inner-shelf of the central Great Barrier Reef, Australia. Coral Reefs 28:941-948

Ridd P, Larcombe P (1994) Biofouling control for optical backscatter suspended sediment sensors. Marine Geology 116:255-258

Saulquin B, Hamdi A, Gohin F, Populus J, Mangin A, d'Andon OF (2013) Estimation of the diffuse attenuation coefficient KdPAR using MERIS and application to seabed habitat mapping. Remote Sensing of Environment 128:224-233

Schaffelke B, Thompson A, Carleton J, Davidson J, Doyle J, Furnas M, Gunn K, Skuza M, Wright M, Zagorskis I (2009) Reef Rescue Monitoring Program Final Report of AIMS Activities 2008/2009. Australian Institute of Marine Science

Weeks S, Werdell P, Schaffelke B, Canto M, Lee Z, Wilding J, Feldman G (2012) Satellite-Derived Photic Depth on the Great Barrier Reef: Spatio-Temporal Patterns of Water Clarity. Remote Sensing 4:3781-3795

Wright LD (1995) Morphodynamics of Inner Continental Shelves. CRC Press, Boca Raton

Chapter 6. SPECTRAL IRRADIANCE ATTENUATION COEFFICIENTS

6.1 Introduction

In this chapter spectral Irradiance attenuation coefficients (spectral attenuation coefficients) are compared for inshore-offshore and shallow-deep waters of Cleveland Bay. This study is an extension of the light attenuation research detailed in Chapter 5. These original data collected PAR light as a variable and k_d was calculated as a single coefficient for each vertical water column intervals across the 400-700 nm waveband.

An exploratory field trip was carried out in September 2015 (Figure 46) utilising the HyperOCR Hyperspectral Radiometer to obtain light profiles across a spectrum of 137 individual wavelengths (from 300 ~ 800nm). Although a comprehensive time series of spectral light data is not yet available, these exploratory data were obtained to get a general idea of: how light attenuation coefficients vary a) across depth intervals, b) at inshore versus offshore locations, c) across 137 individual wavelengths and d) compared to PAR attenuation coefficients.

Figure 46 (The author) Rachael and (husband) Simon Macdonald performing exploratory research with hyperspectral radiometer, on the RV James Kirby in Cleveland Bay, September 2015.

The impact of suspended sediment on coral reefs has been widely studied (Belperio 1983; Rodgers 1990; Larcombe et al. 1995b; Fabricius 2005; Orpin and Ridd 2012), however light attenuation still remains poorly understood within the GBR. Photic depth is inversely related to light attenuation and is defined as the depth where only 1% of the surface radiance remains. Below this threshold, most photo-autotrophic organisms cannot achieve daily net positive production. Mean photic depth is defined as the depth of 10% of surface irradiance. This value has been recently investigated across the CB and Burdekin region using oceanographic and Modis-Aqua data (Fabricius et al. 2014).

Satellite data like MODIS-Aqua are routinely applied to mapping nearshore optical properties and a bio-optical algorithm for determining the photic depth using satellite radiances has been investigated in inshore regions of the GBR (Weeks et al. 2012). In this decadal study of photic depth, which is related inversely to light attenuation, from 2002-2012 using (MODIS-Aqua) satellite data (Weeks et al. 2012). This decadal (2002-2012) study showed wide spatial and temporal variability of water clarity, particularly within the inshore GBR. Although this work contributed greatly to the advancement of satellite remote sensing algorithms, it was noted that the capability of such models remain limited for optically shallow regions.

A recent laboratory-based study investigated how physical properties of sediment affect light availability. Results showed that fine grained and darker coloured sediment attenuates more PAR light than coarser, lighter coloured sediment particles. The attenuation coefficient for fine particles was found to be more than twice that for the coarse, particles (Storlazzi et al. 2015). Cleveland Bay bottom types are primarily fine, darker coloured, muddy sediment.

As far as the author is aware, there are little published data on light spectra within GBR waters, especially for turbid waters, such as those that are measured at close inshore locations.

6.2 Theory

6.2.1 Calculation of the spectral diffuse attenuation coefficients ($k_{d\lambda}$)

Absorption and scattering describe the attenuation of light through water by interacting in a nonlinear and complex fashion within the radiative transport equations (Mobley 1994). These equations cannot be solved analytically; however models exist which approximate numerical solutions (Mobley et al. 1993). As is assumed in Chapter 5, the general form of downward directed irradiance decays as an inverse exponential with depth; i.e. in the absence of strong discontinuities in water optical properties, spectral measurements can be well described by Beer-Lambert's Law,

$$I_z = I_{z0} e^{-k_{d\lambda}(z - z_0)} \tag{37}$$

where I_{z0} and I_z are the downward directed irradiances at an upper depth (z_0) and a lower depth (z) respectively, and $k_{d\lambda}$ is the diffuse attenuation coefficient (for a given wavelength, λ) (Jerlov 1976; Kirk 1977). This approximation has been successfully applied to calculate $k_{d\lambda}$ in ocean waters (Gordon 1989; Dennison et al. 1993; Kirk 1994). The equation for $k_{d\lambda}$ is obtained by rearranging equation (37),

$$\boldsymbol{k_{d\lambda} = ln\left(\frac{I_{z0}}{I_z}\right)\Big/(z - z_0)} \tag{38}$$

6.3 Methods

6.3.1 Location

Field work was performed during two trips over 20th – 21st September 2015, aboard the Research Vessel, James Kirby. A hyperspectral radiometer was deployed at 14 waypoints per trip, along two plotted courses across Cleveland Bay (Figure 47).

Cleveland Bay is a shallow embayment, partially sheltered from South Easterly waves with a maximum depth of *ca.* 15 m (Orpin and Ridd 2012; Macdonald et al. 2013). Sediments in Cleveland Bay are mainly soft and silty and easily resuspended (Belperio 1979). Data were collected at both inshore and offshore locations. GPS positioning data were recorded at each waypoint for Route 1 and Route 2 (Figure 47).

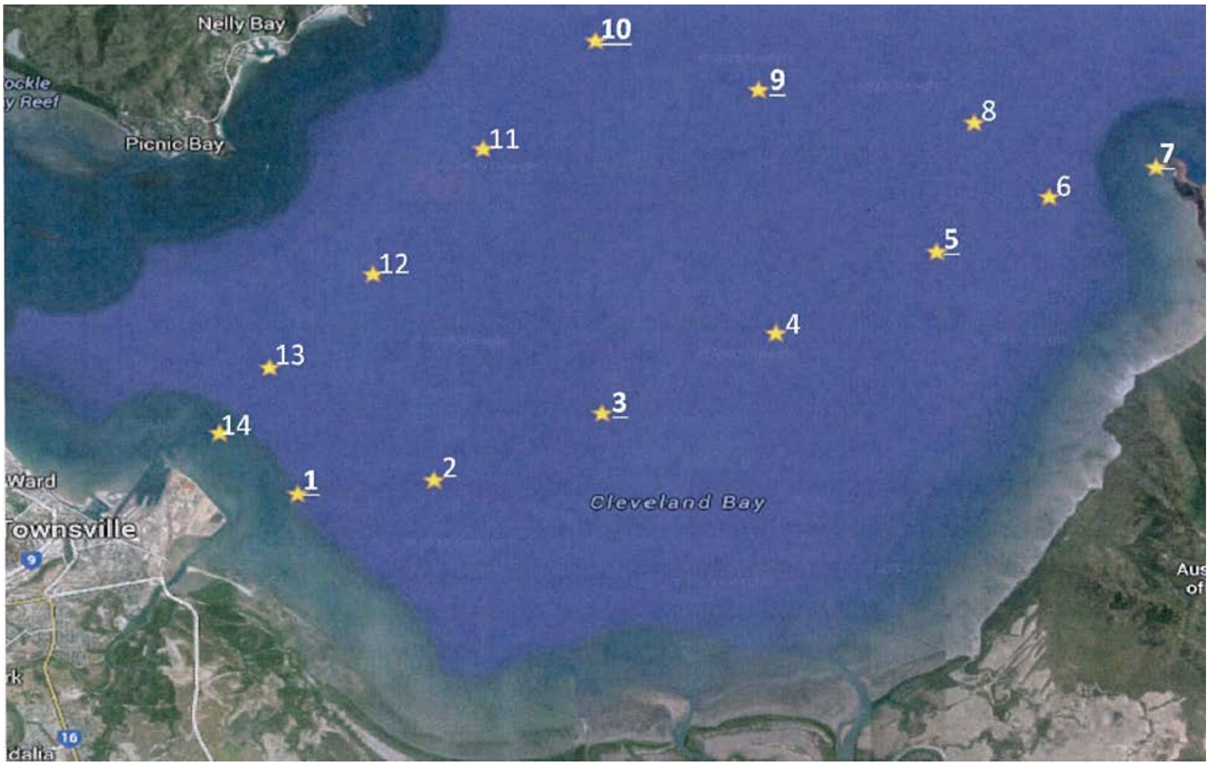

Figure 47 Routes 1 and 2 depicting data collection waypoints (light and depth) across Cleveland Bay.

6.3.2 Instrumentation

The hyperOCR is a stand-alone hyperspectral radiometer built by Satlantic, which records either irradiance (power projecting onto a surface per unit area) or radiance (power projecting onto a solid angle) over a maximum of 255 concurrent spectral channels, in an ocean environment. The standard spectral range is from 350-800 nm however this can be extended to 300-1200 nm. The detector is a multichannel silicon diode array with a 16-bit A/D converter and 25 bit dynamic resolution. The spectrometer has 3.3 nm/pixel spectral sampling with a spectral accuracy of 0.3 nm. This enables a wide range of light levels to be detected, and light is integrated over a pre-defined range of time intervals (Satlantic 2004).

The hyperOCR was held just below the water surface for one minute, logging irradiance/radiance values. It was then quickly lowered 2 m and a further minute of data were recorded. This was repeated until the instrument was on the sea bed. Depth was confirmed by vessel instrumentation and changes in surface lighting conditions were recorded throughout the measurements, such as increased cloud cover.

6.4 Results

6.4.1 Variation of attenuation coefficient with depth

Raw spectral irradiance is plotted versus wavelength for each depth for each site. Offshore sites 9 and 10 are displayed (Figure 48, Figure 49). These particular sites have a greater number of 2m intervals available, due to their depth and thus more observations were possible. Sub-surface irradiance (measurement taken with the instrument submerged just below the surface) demonstrates a rough bell shaped curve, with lower irradiance at the blue (~350 nm) end of the spectrum. The curve peaks at the approximate mid-point “green zone” of PAR (~500 nm) and then declines again towards the red end of the spectrum (~700 nm). Irradiance versus wavelength follows the same general shape, and can be seen to attenuate with each increasing depth interval, until it reaches the seabed (Figure 48, Figure 49).

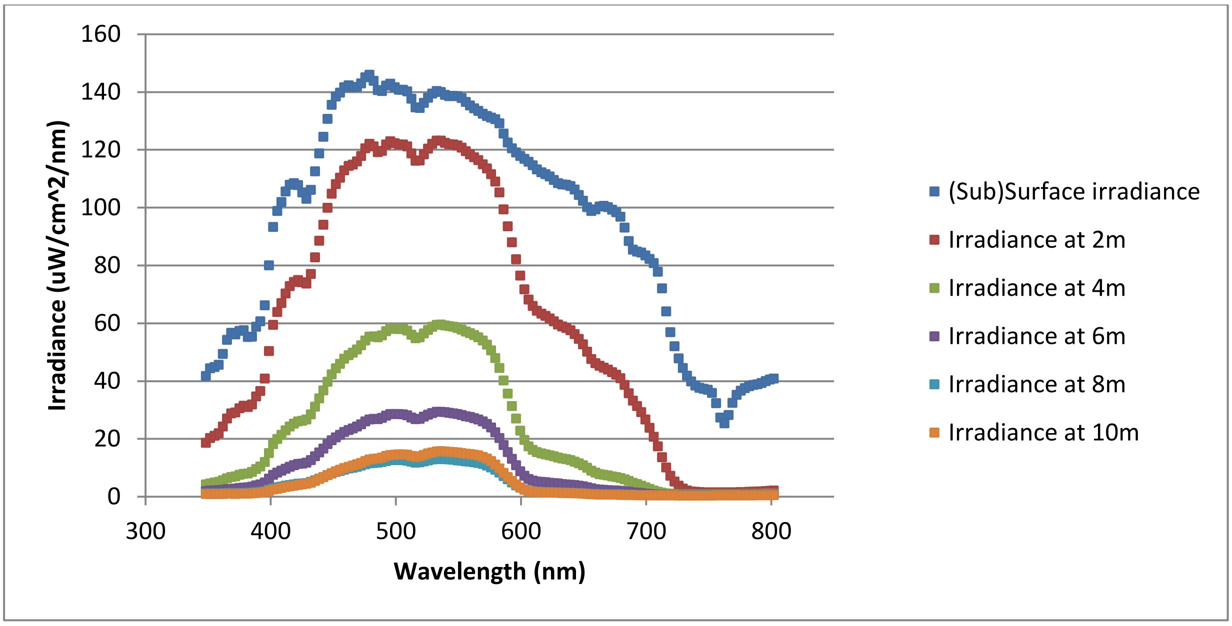

Figure 48 Measured irradiance uW/cm²/nm) vs wavelength (nm) for offshore site 10 in Cleveland Bay (total depth ~ 11m).

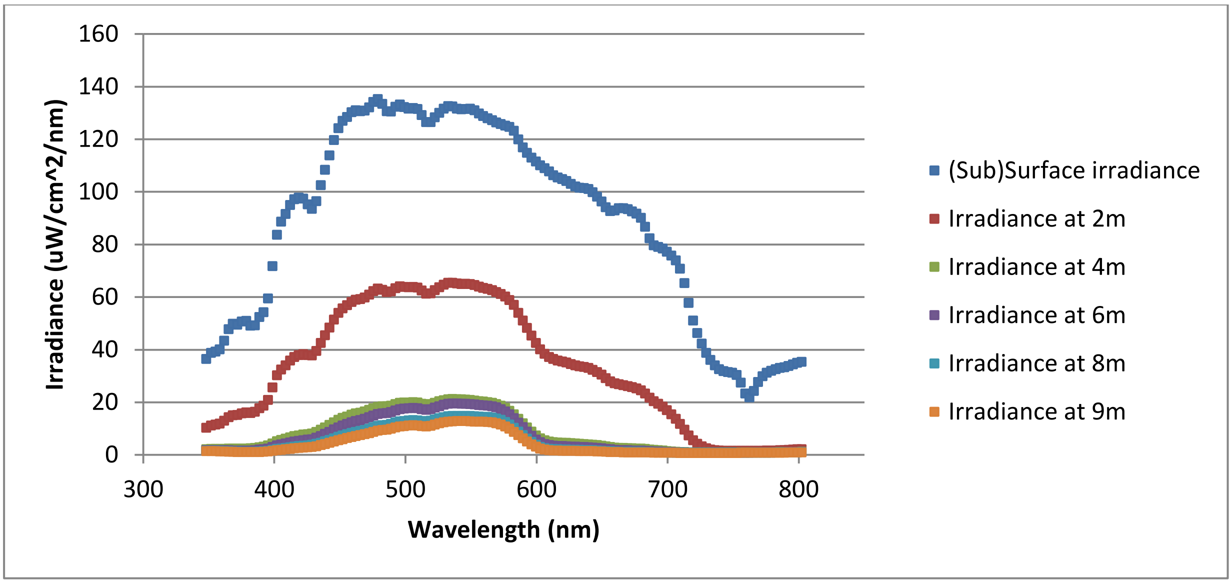

Figure 49 Measured irradiance uW/cm²/nm) vs wavelength (nm) for offshore site 9 in Cleveland Bay (total depth ~ 10m).

Using upper and lower raw irradiance and depth data, k_d is calculated over each depth interval (Equation 32). Each interval follows a similar shape, although at deeper intervals, for wavelengths greater than approximately 750 nm, attenuation falls to unusually low levels.

This is not likely to be a real feature of attenuation, but rather at the lower end of the depth interval, light levels are too low to be accurately measured by the instrument, thus resulting in an incorrect attenuation value. The red and blue ends of the spectrum are attenuated faster than the green/yellow region, which is exactly what is expected to occur (Figure 50, Figure 51).

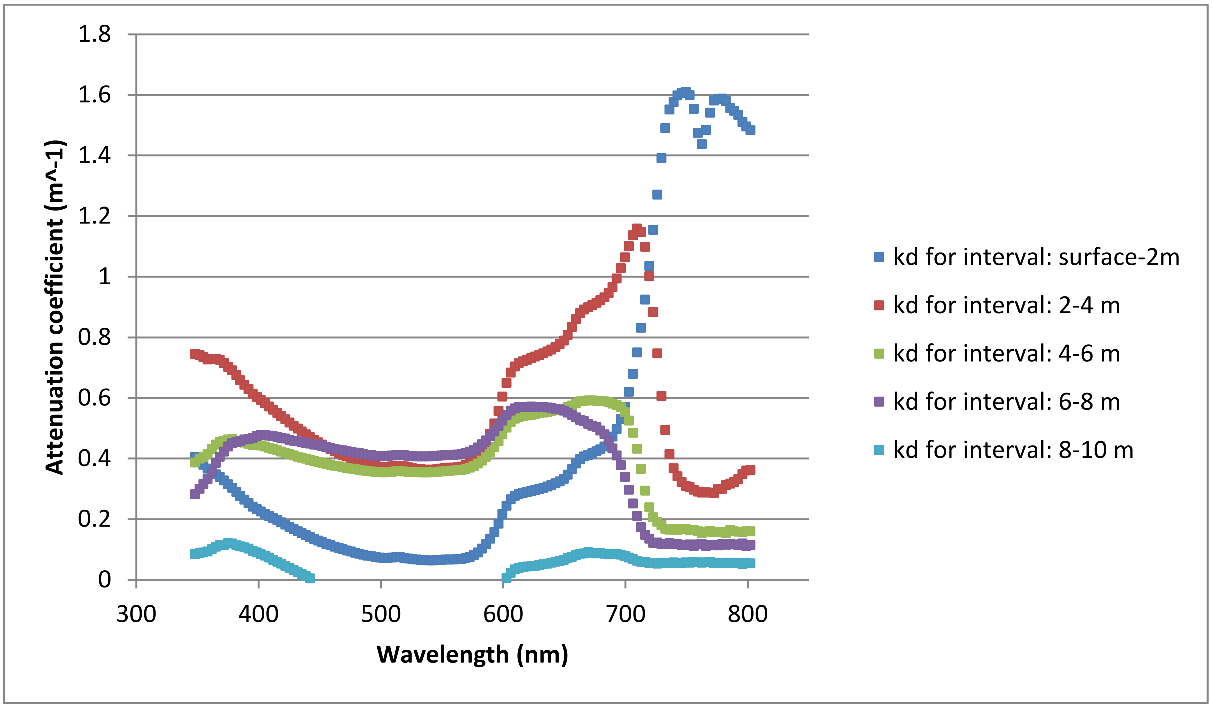

Figure 50 Attenuation coefficient vs. wavelength for offshore site 10 in Cleveland Bay (total depth ~ 11m). Kd is calculated over 2 m intervals from the surface to (near) seabed.

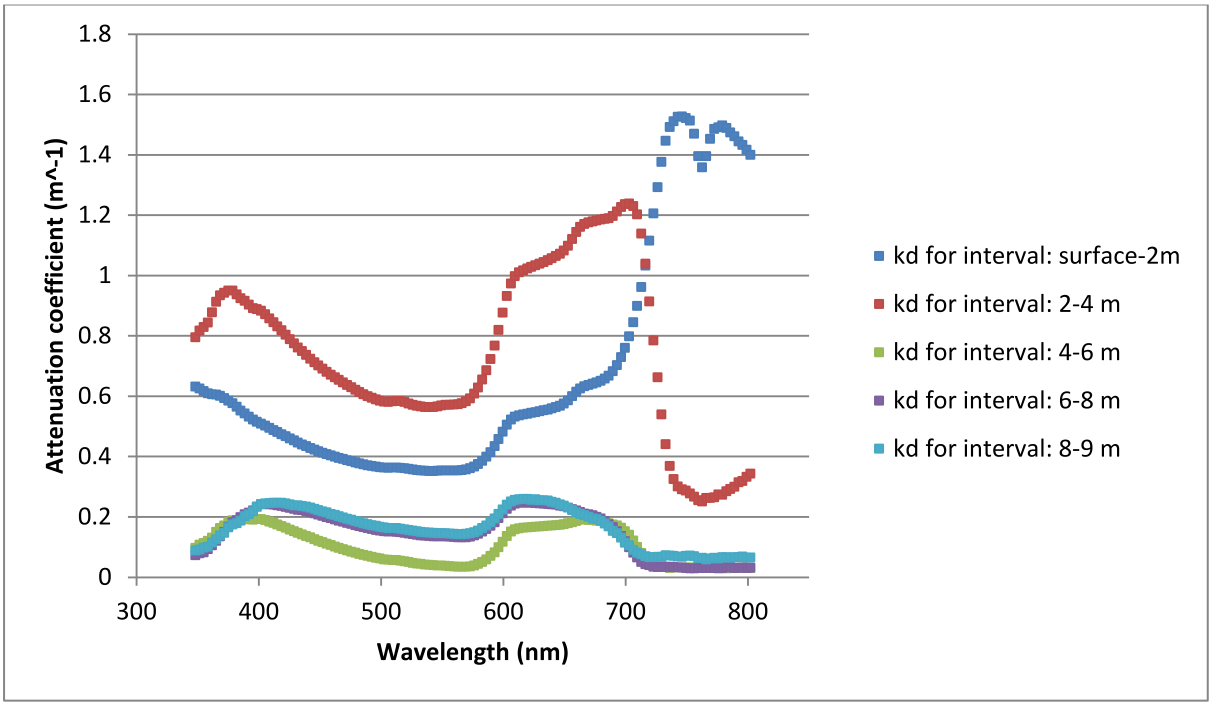

Figure 51 Attenuation coefficient vs. wavelength for offshore site 9 in Cleveland Bay (total depth ~ 10m). Kd is calculated over 2 m intervals from the surface to (near) seabed.

7.1.1.1 Depth profile of attenuation spectra

For sites 9 and 10, ten individual wavelengths across the entire spectrum were selected evenly across the dataset and used to calculate attenuation coefficients. These were plotted over depth in order to examine the variation with depth of discrete attenuation spectra (Figure 52, Figure 53). There is considerable variation across the entire spectrum for both sites although all attenuation spectra follow a similar profile with the exception of the 752 and 802 nm spectra for both sites. At the surface, for the (red) end of the spectrum, the coefficients are comparatively higher than other spectra, which is as expected as red light is the first to be lost as depth increases (Kirk 1977).

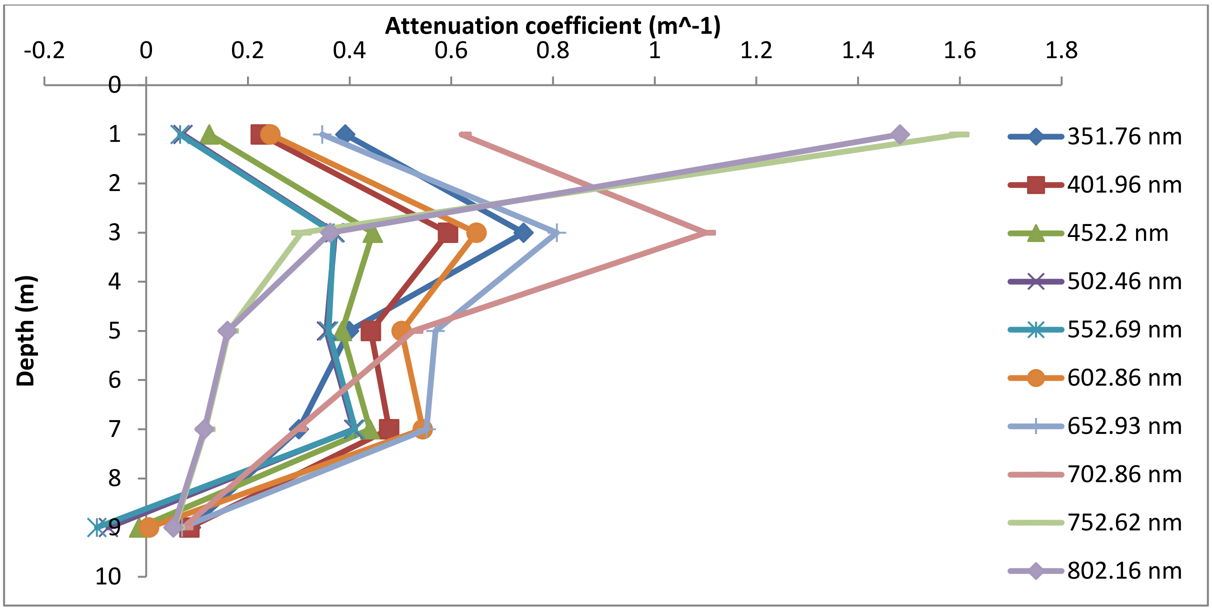

Figure 52 Attenuation coefficient vs depth for a selection of wavelengths at offshore site 10 (Cleveland Bay).

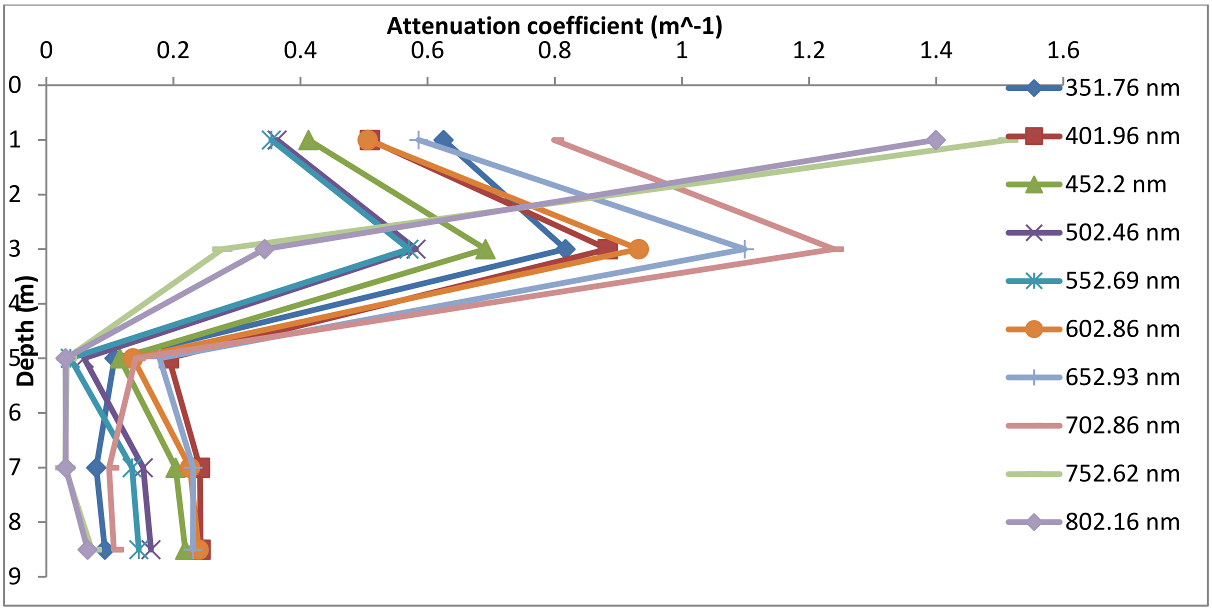

Figure 53 Attenuation coefficient vs depth for a selection of wavelengths at offshore site 9 (Cleveland Bay).

6.4.2 Variation of attenuation coefficient with site and wavelength

Inshore versus offshore comparison

Selections of inshore and offshore sites were compared for variations in attenuation coefficients. (Figure 54). Offshore sites exhibited little variation and closely followed the expected shape of the attenuation coefficient curve across the entire measured waveband.

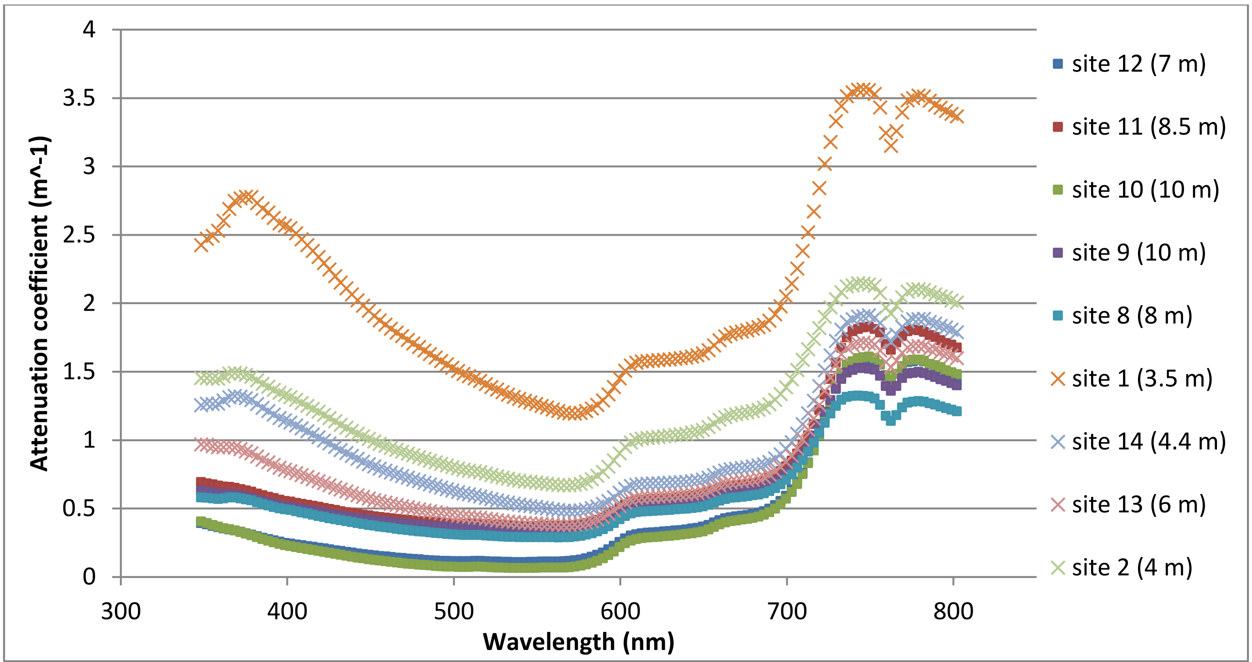

Figure 54 Attenuation coefficients (surface-2m) vs wavelength for both inshore and offshore sites. The general variation of k_d with wavelength is also observed.

Wavelength comparison

Attenuation coefficients are plotted for the interval surface-2m at a selection of deep/offshore sites, across the entire wavelength spectrum (Figure 54). This depicts how k_d changes over the spectrum from short to longer wavelength values, across sites of similar depth. For most of the sites, the red and blue coloured light is attenuated at almost the same time, leaving the green-yellow coloured light. The exception to this is site 1 which is located at the mouth of Ross River. Almost all of the blue light is attenuated first, which would explain the observed red-brownish tinge to the water at this site. Attenuation is also calculated over the 6-8 m interval for the same group of sites. Sites 8 9 and 10 all exhibit similar attenuation curves. A spurious curve is observed for site 11 (Figure 55) which cannot represent the real attenuation coefficients (negative values), but instead represents the inability of the instrument to accurately detect very low light at lower depths, thus causing errors in the calculation.

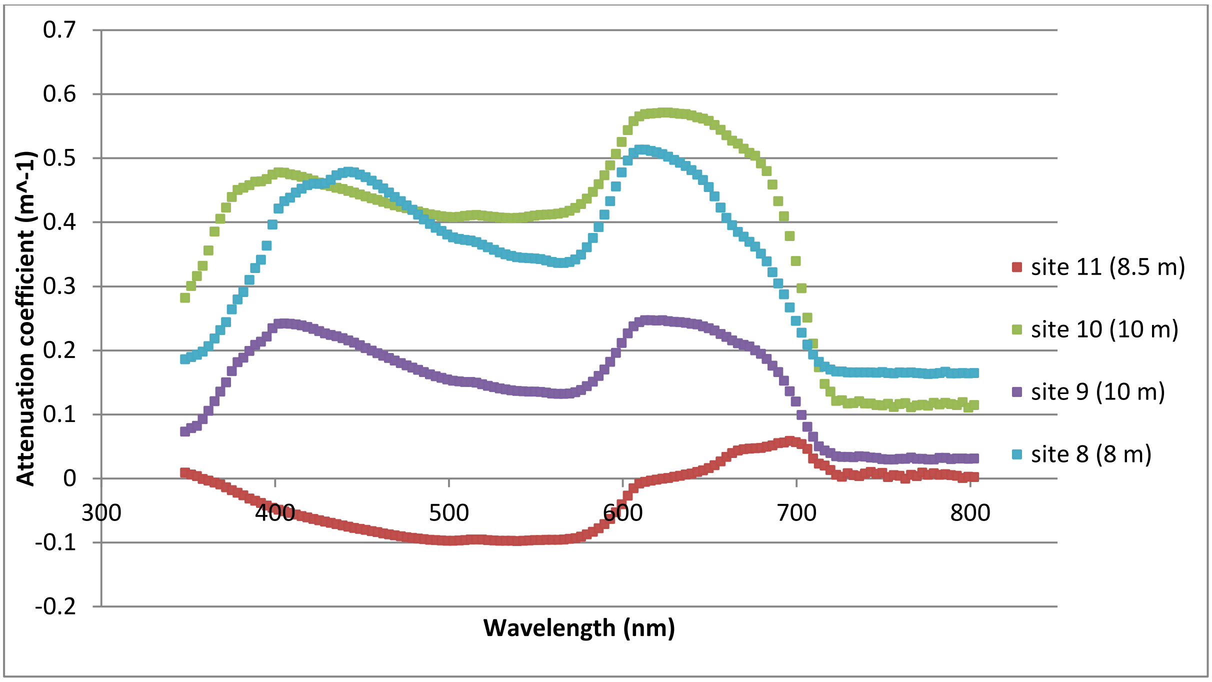

Figure 55 Attenuation coefficient for 6-8 m depth interval vs wavelength for several deep water/offshore sites. The general variation of k_d with wavelength is observed.

6.4.3 Comparing Attenuation Coefficients for PAR and depth

Concurrent light and depth data (near-surface and near-bed) were hourly averaged and taken between 10 am - 2 pm. These data were obtained from site CB (Cleveland Bay) and first used in Chapter 5 to calculate diffuse attenuation coefficients (k_{dPAR}) over various depth intervals throughout the water column (equation 32)(Figure 56). The overall average diffuse attenuation coefficient (k_{dPAR}^{avg}) is 0.43 m^{-1} for site CB. This value is the average of all k_{dPAR} values calculated over the entire water column. It is difficult to extract features of k_d with depth, due to variation of turbidity over the 14 day data set (Figure 56). A 3-day subset of low turbidity is extracted, and analysed for attenuation features over depth (Figure 57). The result confirms that the attenuation coefficient in clear, low turbidity waters of Cleveland Bay is approximately 0.3 m^{-1}, validating the clear water attenuation component for this region as calculated in Chapter 5. However since the profile is only sampled over 4 depth positions in the water column, the results are coarser than those obtained using the instantaneous profiler.

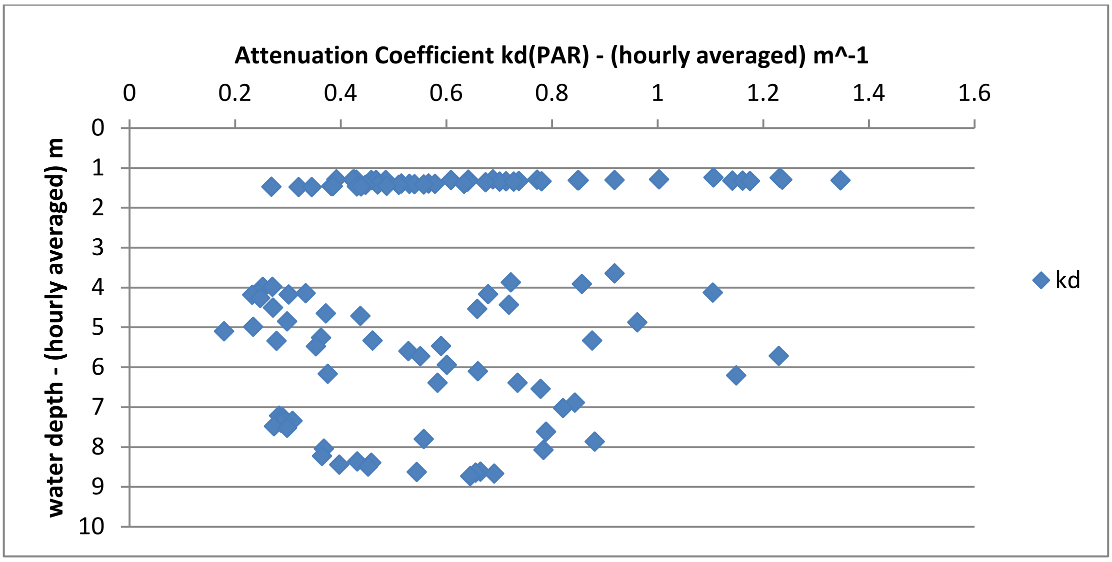

Figure 56. Water depth (hourly averaged) versus attenuation coefficient k_{dPAR}. k_{dPAR} is calculated using hourly averaged light and depth data, over 3 depth intervals and appended (Chapter 5).

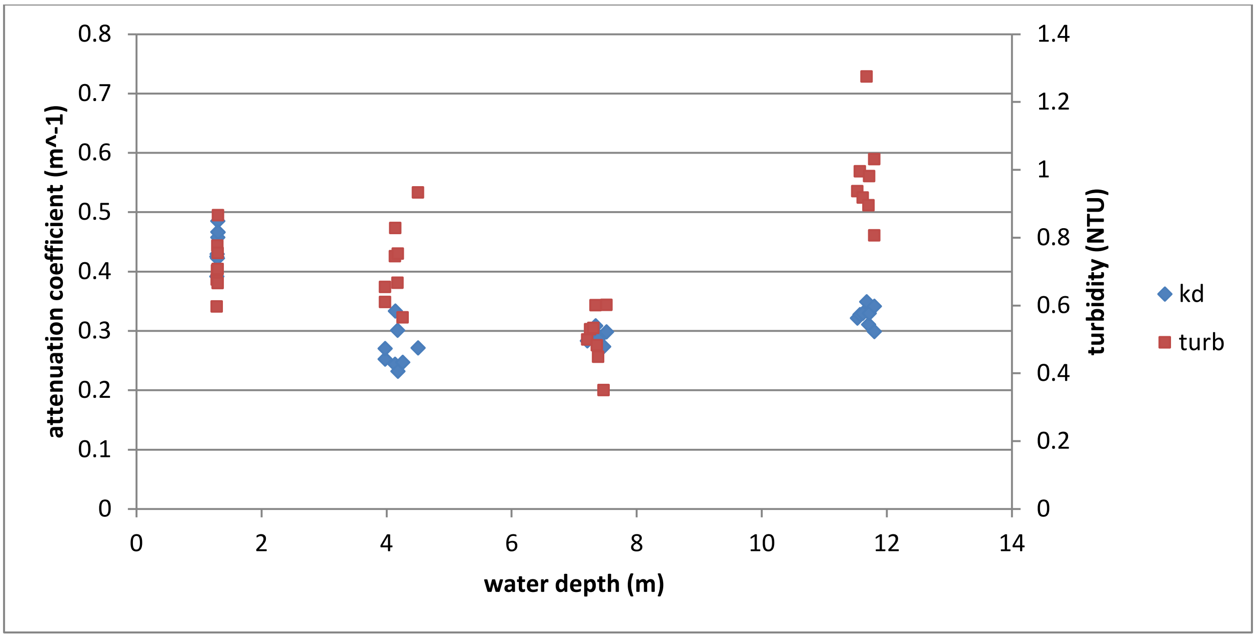

Figure 57 PAR Attenuation coefficient and turbidity (both hourly averaged) vs. water depth for 3 days of "low turbidity" conditions (data taken from 10am-2pm only). January 2013. The turbidity regime is similar to that during the spectral radiometry dataset (September 2015) (although turbidity measurements were not obtained on this later field trip). Attenuation coefficients approximate 0.3 m^-1 as calculated for the clear water component in Chapter 5.

6.5 Discussion

Exploratory light profiles were measured across a spectrum of 137 individual wavelengths (from 300 ~ 800nm). Research was conducted as preliminary investigations of: how light attenuation coefficients vary a) across depth intervals, b) at inshore versus offshore locations, c) across 137 individual wavelengths and d) compared to PAR irradiance. Using upper and lower raw irradiance and depth data, k_d was calculated over each depth interval (Equation 32). Selections of inshore and offshore sites were compared for variations in attenuation coefficients. (Figure 54). Offshore sites exhibited little variation and closely followed the expected shape of the attenuation coefficient curve across the entire measured waveband. That is, attenuation coefficients were lowest for green/yellow light and similar values for blue and red light, with the red light value tending to be slightly higher than the blue.

In the original PAR light study (Chapter 5), the clear-water component of attenuation (k_d^{cl}) was calculated for Cleveland Bay to be k_d^{cl} = 0.30 m^{-1}. Values equivalent to k_d^{cl} reported in the literature for sites with similar turbidity/sediment levels are very close in value; *ca* $0.33\,m^{-1}$ (Wright 1995). This value was able to be validated here by comparing with attenuation coefficients calculated by individual spectra, at offshore sites. For example, the lowest attenuation coefficients obtained at offshore sites (sites 8-12) were calculated to be between 0.2-0.4 m^{-1} This result shows the calculated clear water attenuation coefficient (k_d^{cl} = 0.30 m^{-1}) to be valid over the green/yellow area of the spectrum, with slightly higher values occurring at the blue and red end of the spectrum.

REFERENCES

Belperio AP (1979) The combined use of wash load and bed material load rating curves for the calculation of total load: An example from the Burdekin River, Australia. Catena 6:317-329

Belperio AP (1983) Terrigenous sedimentation in the central Great Barrier Reef lagoon: a model from the Burdekin region. BMR Journal of Australian Geology and Geophysics 8:179-190

Dennison WC, Orth RJ, Moore KA, Stevenson JC, Carter V, Kollar S, Bergstrom PW, Batiuk RA (1993) Assessing Water Quality with Submersed Aquatic Vegetation. Bioscience 43:86-94

Fabricius KE (2005) Effects of terrestrial runoff on the ecology of corals and coral reefs: Review and synthesis. Marine Pollution Bulletin 50:125-146

Fabricius KE, Logan M, Weeks S, Brodie J (2014) The effects of river run-off on water clarity across the central Great Barrier Reef. Marine Pollution Bulletin 84:191-200

Gordon HR (1989) Can the Lambert-Beer law be applied to the diffuse attenuation coefficient of ocean water? Limnology and Oceanography 34:1389-1409

Jerlov NG (1976) Marine optics. Elsevier Scientific Pub. Co, Amsterdam

Kirk JTO (1977) Attenuation of Light in Natural Waters. Aust J Mar Freshwater Res, 28:497-508

Kirk JTO (1994) Light and photosynthesis in aquatic ecosystems. Cambridge University Press, Cambridge [England]

Larcombe P, Ridd PV, Prytz A, Wilson B (1995b) Factors controlling suspended sediment on inner-shelf coral reefs, Townsville, Australia. Coral Reefs 14:163-171

Macdonald RK, Ridd PV, Whinney JC, Larcombe P, Neil DT (2013) Towards environmental management of water turbidity within open coastal waters of the Great Barrier Reef. Marine Pollution Bulletin 74:82-94

Mobley CD (1994) Light and Water: Radiative Transfer in Natural Waters. Academic Press

Mobley CD, Gentili B, Gordon HR, Jin Z, Kattawar GW, Morel A, Reinersman P, Stamnes K, Stavn RH (1993) Comparison of numerical models for computing underwater light fields. Appl Opt 32:7484-7504

Orpin AR, Ridd PV (2012) Exposure of inshore corals to suspended sediments due to wave-resuspension and river plumes in the central Great Barrier Reef: A reappraisal. Continental Shelf Research 47:55-67

Rodgers CS (1990) Responses of coral reefs and reef organisms to sedimentation. Marine Ecology Progress Series 62:185-202

Satlantic L (2004) Operation Manual for the HyperOCR, Halifax, Nova Scotia

Storlazzi C, Norris B, Rosenberger K (2015) The influence of grain size, grain color, and suspended-sediment concentration on light attenuation: Why fine-grained terrestrial sediment is bad for coral reef ecosystems. Coral Reefs 34:967-975

Weeks S, Werdell P, Schaffelke B, Canto M, Lee Z, Wilding J, Feldman G (2012) Satellite-Derived Photic Depth on the Great Barrier Reef: Spatio-Temporal Patterns of Water Clarity. Remote Sensing 4:3781-3795

Wright LD (1995) Morphodynamics of Inner Continental Shelves. CRC Press, Boca Raton

Chapter 7. CONCLUDING REMARKS

In this work, the largest turbidity dataset across the Great Barrier Reef (GBR) was assembled, using exceedance curves and derivatives. More than 800,000 data points across 61 reef sites were analysed to redefine typical inshore turbidity regimes. Results were compared with SSC trigger values and turbidity was found to be above the 2 mg l^{-1} limit more than half the time, at 31 sites. These results and the comparison between pristine reference sites and those of higher human activity, highlight the question of using a single SSC trigger value, for the entire open coastal region.

As a dominant turbidity driver, wave-induced shear stress was calculated from very coarse pressure measurements near the seabed, for the first time, with instrumentation developed over the past 10 years by the Marine Geophysics Laboratory. These initial results are promising and pending independent testing of this new method, mean shear stress investigations can now be implemented on much of the historic and future data, which are being used on environmental monitoring work, for dredge operation on the Queensland and Western Australian coast.

An exploration of secondary drivers of turbidity was presented. Conclusions are that although some contribution to turbidity from riverine sources is likely, the effect of rivers was too small to be measurable for the data investigated. Importantly, more research in the area of secondary turbidity drivers is essential to continuing projects in GBR-catchment management.

Certainly, more work needs to be carried out with respect to quantifying turbidity levels contributed by inshore secondary drivers. This would contribute to the understanding of these processes and importantly future refinement of management protocols, for the continuing protection and monitoring of the health of the inshore Great Barrier Reef.

Vertical profiles of light and turbidity were obtained and light attenuation was mathematically linked to turbidity for the first time, *for inshore GBR locations*. A site-specific model predicting depth-averaged turbidity using PAR light was implemented with good success. This new method of measuring turbidity using light data is useful, as light is a far easier, cheaper and more reliable parameter to obtain than turbidity. Turbidity data are also generally only obtained near the seabed and obtaining depth profiles for any reasonable deployment time is complex. Strong linear relationships between depth-averaged turbidity and seabed turbidity were discovered to be 0.3-0.4 times seabed turbidity at all sites. This was an important finding which may be extrapolated to obtain depth-averaged values for all other (near) seabed turbidity data in the GBR. New predictions of photic depths in Cleveland Bay were made from depth-averaged turbidity and may provide an improved estimate than current values, which are typically calculated using (near) seabed turbidity.

Spectral attenuation coefficients were obtained as an extension to the light study (which utilised PAR). Results were obtained over 137 individual wavelengths at inshore/offshore locations, for various depths and compared to PAR attenuation. Attenuation coefficients followed the expected pattern along the colour spectrum, with loss of red light occurring before blue and finally green-yellow. Importantly, results from offshore Cleveland Bay sites were able to validate the value of attenuation coefficient ($k_d = 0.3\ m^{-1}$) in this region, due to clear seawater alone. In the original light study, this value was calculated using PAR irradiances and used with success as a new method of measuring depth-averaged turbidity in coastal waters.

This work has contributed to a broader understanding of light and turbidity in waters of the coastal Great Barrier Reef. Future work in this field could involve refinement of new measurement methods outlined here, as well as continued development and application to marine monitoring programs. In order to properly understand sediment hydrodynamics within the coastal GBR, the “nature of the supply of sediment” which was beyond the scope of this work would be good direction to head this research in the future. Although this work has a strong local focus, much of the findings hold great potential to incorporate research in waters outside of the Great Barrier Reef. Coastal waters worldwide that require knowledge of the dynamic relationship between suspended sediment and light would markedly expand the scope of this research.

Appendix A – The Inner Continental Shelf

The continental shelf is a primary source of coastal sediments and conditions the physical oceanographic processes that drive coastal behaviour. The inner shelf is the region immediately seaward of the surf zone – where waves frequently agitate the bed. On most peri-continental shelves, this region extends offshore to approximately 30m deep. The inner shelf links the realms of the land margin to the mid shelf and the outer shelf. The outer shelf edge marks the boundary of the upper continental slope and deep sea.

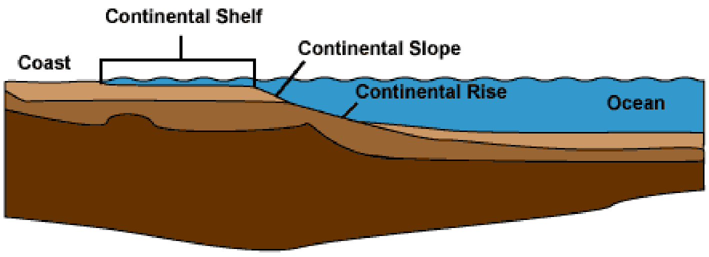

Fig 58 Depiction of the continental shelf.

The outer portions of most shelves were subject to surf zone processes in the geologically recent past. However at present, the physical coupling between the outer and inner shelves is weak. Correspondingly, the inner shelf is strongly contiguous with beaches and surf zones, as well as with estuaries, river mouths and tidal inlets. The inner shelf facilitates cross marginal passage of particulate matter and also modulates the processes (hydrodynamic forces) that drive surf zone and estuarine processes (Wright 1995).

Sediment transport processes are more intense on the inner shelf than the mid and outer. This is partly due to the shallow depth, which means most waves reach the seabed.

Additionally, the inner shelf is friction dominated. The surface and bottom boundary layers overlap and often take up the entire water column. This means that the frictional effects of winds blowing across the sea surface are directly transmitted to the bed. The micro-morphology of the bed causes drag effects on the flow and in these shallow cases, this can extend all the way up the water column to the sea surface. The bottom agitating forces are strongest at the surf zone and become less intense toward the mid shelf (Wright 1995).

Waves typically contribute the most to resuspension of inner shelf sediments off the seabed, however other flows also come into play in lifting sediments across and along the shelf. The mean currents are responsible for sediments being diffused to elevations significantly above the wave boundary layer. Important transport phenomena that cause fluxes of sediment particles include

- Wind-driven along-shelf and across-shelf (upwelling and downwelling) flows
- Surface gravity waves
- Tidal currents
- Internal waves
- Infragravity oscillations
- Buoyant plumes (positive and negative)
- Wave driven surf zone processes

From deep water to the surf zone, the relative intensities of the different flows change dramatically. For example, in the surf zone, radiation-stress gradients associated with breaking waves force the dominant flows. Further seaward from the surf zone, the breaking process is no longer important and the currents are wind driven or tidal. Over the outer shelf the most important process are geostrophic flows and here, frictional forces and wave-induced bottom orbital velocities are unimportant. Over the inner shelf however, frictional forces become dominant, the boundary layers of the surface and bottom often take up the entire water column (Nittrouer and Wright 1994; Wright 1995).

A brief account of oceanographic theory is given in Appendix B. The main contributor to suspended sediment is wind driven surface gravity waves. This is via bed stress on the inner shelf. A first order, linear treatment of surface gravity waves is derived using Airy theory (Appendix B). Orbital motion at varying depths is covered as well as the non-linear aspects of surface gravity waves. Examples are given showing bottom orbital velocity calculations for a range of depths, wavelengths, periods and amplitudes (Appendix C). Shear stresses within the bottom boundary layer are treated with a derivation from first principles and stress contours depicting the maximum bottom shear stress as well as the individual wave and current related components (Appendix C). This is undertaken through a Matlab based program, written as an oceanographical tool to investigate bottom orbital velocities and bottom shear stresses for a range of input variables. The source code for this program is provided (Appendix D).

Appendix B – Linear Wave Theory

Surface gravity wave propagation – Basic theory

Wind generated surface gravity waves are the main contributor to suspended sediment via bed stress on the inner shelf. To first order, the behaviour of small amplitude waves can be described using linear wave theory (Airy Theory). Small amplitude waves (Stokes waves) are waves that are small with respect to the depth of the water and also have small water surface angles. Using Airy theory, the propagation of gravity waves on a homogeneous fluid surface is described in terms of a 2-dimensional potential flow.

The fluid domain is bound by a horizontal, impermeable bottom (the seabed) at $z = -h$ and by a free surface at $z = \eta(x, t)$. Here η is the perturbation above mean sea-level. The vertical co-ordinate, z is positive in the up direction and the mean surface elevation is at $z = 0$. The free surface elevation, $\eta(x, t)$ is a sinusoidal function of position, x and time, t. It is given as,

$$\eta(x, t) = a\cos(kx - \omega t)$$

39

where a is wave amplitude, and wave number k is,

$$k = \frac{2\pi}{\lambda}$$

40

and angular frequency ω is,

$$\omega = \frac{2\pi}{T} = 2\pi f$$

41

where T is the wave period and f is wave frequency. The phase speed / celerity C_ϕ is given by,

$$C_\phi = \frac{\omega}{k} = \frac{\lambda}{T} = \frac{g}{\omega}\tanh kh$$

42

where λ is the wavelength. Wave height, H is given by,

$$H = 2a$$

43

Assumptions

Here four assumptions are made. Firstly, that the flow is incompressible. The continuity equation is given in differential form as,

$$\frac{\partial \rho}{\partial t} + \nabla \cdot (\rho u) = 0$$

44

However since we assume an incompressible flow, the density is constant and this equation is simplified to,

$$\nabla \cdot \bar{u} = 0$$

45

meaning the divergence of wave velocity, $\bar{u}$ is zero. It follows that the potential, ϕ has to satisfy the Laplace equation,

$$\nabla^2 \phi = 0$$

46

i.e.,

$$\frac{\partial^2 \phi}{\partial x^2} + \frac{\partial^2 \phi}{\partial z^2} = 0$$

47

The second assumption is that the flow is irrotational, meaning the vorticity $\bar{v}$ is zero, i.e.,

$$\nabla \times \bar{v} = 0$$

48

Thirdly, we assume that the flow is inviscid and lastly, that there are no currents or other motions. Using potential theory and the above assumptions, enables a very good approximation of the fluid interior flow for waves on a liquid surface.

Mathematical Formulation:

The velocity potential, $\phi(x, z, t)$ is related to the components of flow velocity, u_x and u_z by,

$$u_x = \frac{\partial \phi}{\partial x}$$

49

and

$$u_z = \frac{\partial \phi}{\partial z}$$

50

Starting from first principles we take the Navier-Stokes equations which describe the conservation of linear momentum,

$$\frac{D\bar{u}}{Dt} = \bar{F} - \frac{\nabla p}{\rho} + \upsilon \nabla^2 \bar{\mathrm{u}}$$

51

and from assumptions above, the divergence of wave velocity is zero ($\nabla \cdot \bar{u} = 0$). The material derivative taken along a path moving with velocity, $\bar{u}$ is given by,

$$\frac{D\bar{u}}{Dt} = \frac{\partial \bar{u}}{\partial t} + (\bar{u} \cdot \nabla)\bar{u}$$

52

A sinusoidal wave field produces the potential flow solution to the flow and pressure field,

$$\nabla^2 \phi = \frac{\partial^2 \phi}{\partial \mathrm{x}^2} + \frac{\partial^2 \phi}{\partial \mathrm{z}^2} = \nabla^2 \psi = \frac{\partial^2 \psi}{\partial \mathrm{x}^2} + \frac{\partial^2 \psi}{\partial \mathrm{z}^2} = 0$$

53

where as defined above, ϕ is the velocity potential and here, ψ is the Stream Function. These equations are orthogonal everywhere, i.e.,

$$\frac{\partial \phi}{\partial x} = \frac{\partial \psi}{\partial z}$$

54

and

$$\frac{\partial \psi}{\partial x} = \frac{\partial \phi}{\partial z}$$

55

Three boundary conditions are imposed on equation (53):

Boundary condition (BDC) 1:

There is no flow though the bottom boundary (i.e. the bed is impermeable),

$$\frac{\partial \phi}{\partial z} = 0 \quad at\ z = -h$$

56

Boundary condition 2:

A parcel of fluid at the surface must remain at the surface i.e.,

$$-\frac{\partial \eta}{\partial t} - u_x \frac{\partial \eta}{\partial x} + u_z = 0$$

57

Substituting u_x and u_z from equations (49) and (50) and rearranging, the second BDC becomes,

$$\frac{\partial \eta}{\partial t} + \frac{\partial \phi}{\partial x}\frac{\partial \eta}{\partial x} = \frac{\partial \phi}{\partial z} \quad at\ z = \eta$$

58

Boundary condition 3:

The pressure on the surface (i.e. the atmospheric pressure) remains constant. Using the Bernoulli's equation for unsteady potential flow we find,

$$\frac{\partial \phi}{\partial t} + \frac{\Theta(\mathrm{x,t})}{\rho} + \frac{1}{2}\nabla\phi \cdot \nabla\phi + g\eta = F(t)$$

59

where pressure, $P = \Theta(x, t)$ at $z = \eta$, and ρ is fluid density.

However since we have constant pressure, let $P = 0$. The second term above then goes to zero. Also Laplace's Equation (equation 46) allows the third term above to also go to zero making the third BDC,

$$\frac{\partial \phi}{\partial t} + \mathrm{g\eta} = 0 \quad \mathrm{at\ z = \eta}$$

60

The solution to equation (53) can be expressed by a Fourier series. Using Airy wave theory, we take the first term of this series to approximate the velocity potential as,

$$\phi(x, z, t) = a\frac{g}{w}\frac{\cosh k(z+h)}{\cosh kh}\sin(kx - \omega t)$$

61

And the water surface elevation from equation (39) is now given in the form,

$$\eta(x, t) = \frac{H}{2} sin\frac{2\pi}{\lambda}kx - \omega t.$$

62

Now, phase speed/celerity is given in the form,

$$C_{\phi}^{2} = \frac{g\lambda}{2\pi} tanh\frac{2\pi h}{\lambda}.$$

63

This can be described in terms of ω in the linear dispersion relation,

$$\omega^2 = gk\tanh(kh)$$

64

Appendix C - Orbital Wave Motion and Shear Stress Theory

Orbital wave motion – Basic theory

At the sea surface we describe a propagating wave however, underneath the surface the fluid particles are in orbital motion (Figure 59). Within these bidirectional paths there is no net translation over a complete wave cycle, meaning zero net mass transport. By Airy theory, in very deep water, these oscillatory motions are closed circular curves. In shallow water however, the fluid particles follow elliptical paths, becoming flatter as they approach the seabed. The orbital diameter also decreases with depth. The properties of linear gravity waves simplify when considering deep water and shallow water waves. Intermediate depths are defined (where, $\frac{\lambda}{20} < h < \frac{\lambda}{2}$). Here, both the water depth and the wave period significantly influence the linear wave solution. At intermediate depths, orbital velocities near the bed play an important part in sediment transport initiation.

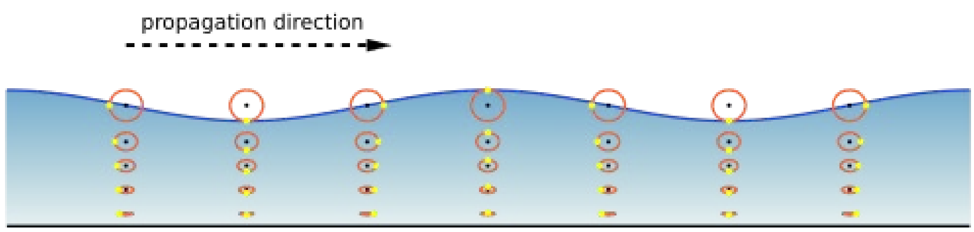

Figure 59 Fluid particles in orbital motion

Orbital velocities consist of horizontal and vertical components however, the vertical component vanishes near the bed. The maximum orbital velocities there are given by,

$$\bar{u}_{bmax} = \frac{a\omega}{\sinh(kh)}.$$

65

The general linear expression of horizontal orbital velocity, $\bar{u}_{xo}$ is given by,

$$\bar{u}_{xo} = a\omega \frac{\cosh k(z+h)}{\sinh kh} \cos(kx - \omega t)$$

66

and vertical orbital velocity, $\bar{u}_{zo}$ is,

$$\bar{u}_{zo} = a\omega \frac{\sinh k(z+h)}{\sinh kh} \sin(kx - \omega t).$$

67

i) Deep water waves

For deep water (assume infinite water depth), short waves, where wave height is greater than half one wavelength (i.e. $h > \frac{\lambda}{2}$), the phase speed is not influenced by depth. This is the case for most wind generated waves on the ocean surface. The velocity potential here may be simplified to,

$$\phi = a\frac{g}{\omega} e^{kz} \sin(kx - \omega t)$$

68

The phase speed becomes,

$$C_\infty = \frac{g}{\omega} = g\frac{T}{2\pi}$$

69

And wavelength is,

$$\lambda_\infty = g\frac{T^2}{2\pi}$$

70

The orbital velocities are also simplified to become,

$$\bar{u}_{xo} = a\omega e^{\omega z}\sin(kx - \omega t)$$

71

and,

$$\bar{u}_{zo} = a\omega e^{\omega z}\cos(kx - \omega t)$$

72

ii) Shallow water waves

In shallow water (long waves) where wave height is smaller than $\frac{\lambda}{20}$, the phase speed is no longer a function of wavelength and is dependent on water depth. The velocity potential here may be further simplified to,

$$\phi = a\frac{g}{\omega}\sin(kx - \omega t)$$

73

the phase speed becomes,

$$C = \sqrt{gh}$$

74

and wavelength is,

$$\lambda = T\sqrt{gh}$$

75

the orbital velocities in shallow water then simplify further to,

$$\bar{u}_{xo} = \frac{Ca}{h}\cos(kx - \omega t)$$

76

and as mentioned above,

$$\bar{u}_{zo} = 0$$

77

iii) Intermediate depths

In all other cases, where $\frac{\lambda}{20} < h < \frac{\lambda}{2}$ both the water depth and the period have a significant influence on the solutions. In this case equation (63) is used and is typically solved graphically.

iv) Graphing bottom orbital velocity

Wind generated waves will induce orbital motion at the bed when the water depth is less than half the wavelength. In shallow water, simple approximations of bottom orbital velocities from linear theory have proven relatively accurate (Wiberg and Sherwood 2008). As above, for a small amplitude monochromatic wave, the vertical orbital velocity goes to zero as *z* goes to *h*. From equation (66) we have the general expression for horizontal orbital velocity. Let the term $\cosh k(z+h)$ go to 1 and substitute $H = 2a$ and $\omega = \frac{2\pi}{T}$. The horizontal orbital velocity at the bottom (*z = h*) is then given as,

$$u_{xo} = \frac{H\pi}{T\sinh(kh)}\cos(kx - \omega t)$$

78

This orbital velocity varies as a sinusoid through a wave period. The bottom orbital velocity, u_b is the maximum of this oscillation and is found when the absolute value of $\cos(kx - \omega t)$ goes to 1, i.e.

$$u_b = \frac{H\pi}{T\sinh(kh)}$$

79

and substituting $H = 2a$ and $\omega = \frac{2\pi}{T}$, this becomes,

$$u_b = \frac{\omega a}{\sinh(kh)}$$

80

Equation (79) shows that u_b is directly proportional to wave height, *H* and inversely proportional to depth, *h.* In order to solve this equation for u_b, we first need to address the linear dispersion relation equation (64) in order to solve for wave number, *k*. Substituting $\omega = \frac{2\pi}{T}$ and rearranging for *k*, we find equation (64) becomes,

$$k = \frac{4\pi^2}{gT^2\tanh(kh)}$$

81

This equation is non-linear in terms of k and thus has no analytical solution. We are able to numerically approximate a solution using the Newton-Raphson iterative method,

$$x_{n+1} = x_n - \frac{f(x_n)}{f'(x_n)}$$

82

This firstly involves defining the dimensionless variables,

$$x = \frac{\omega^2 h}{g}$$

83

$$y = kh$$

84

$$F_b = \frac{U_b^2 \, h}{a^2 g}$$

85

This follows the approach taken in (Soulsby 1987). Equation (80) for U_b then becomes (after use of equation (64), the dispersion relation),

$$F_b = \frac{2y}{\sinh(2y)}$$

86

And the dispersion relation becomes,

$$x = y\tanh(y)$$

87

A Matlab program using the above functions, obtains the required k approximation after three iterations. A graph of u_b as a function of period, T is plotted over a range of depths, periods and amplitudes.

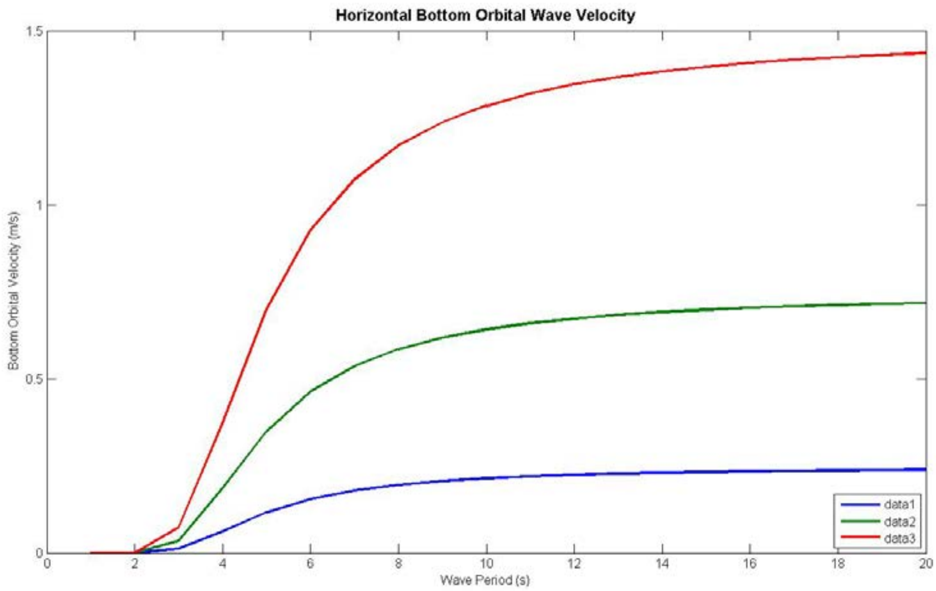

Figure 60 Horizontal Bottom Orbital Velocity Vs. Wave Period - For a depth of 10 m and Wave Heights of 0.5, 1.5 and 3 m respectively.

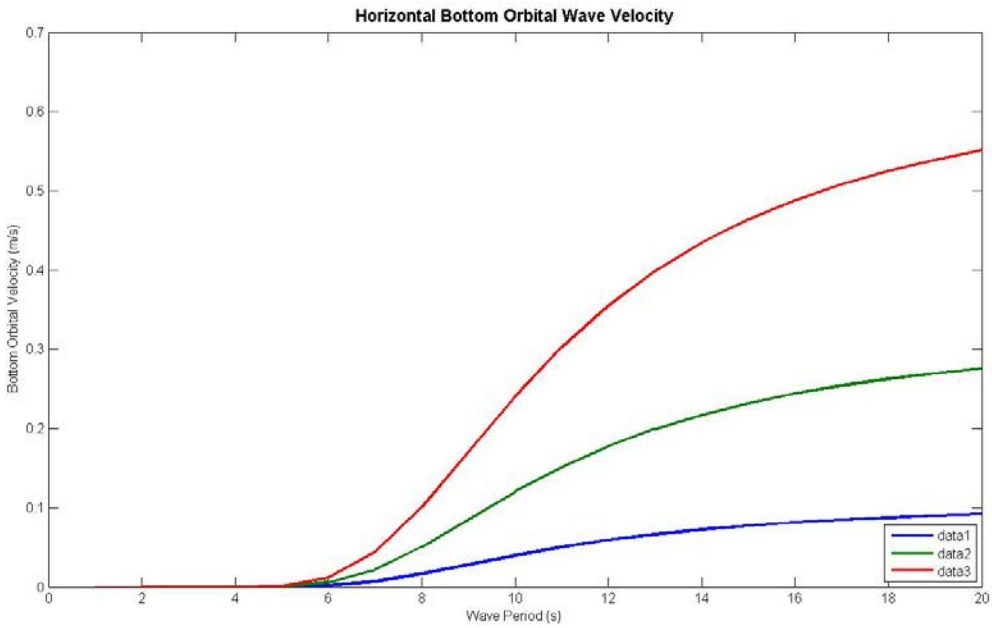

Figure 61 Horizontal Bottom Orbital Velocity Vs. Wave Period - For a depth of 50 m and Wave Heights of 0.5, 1.5 and 3 m respectively.

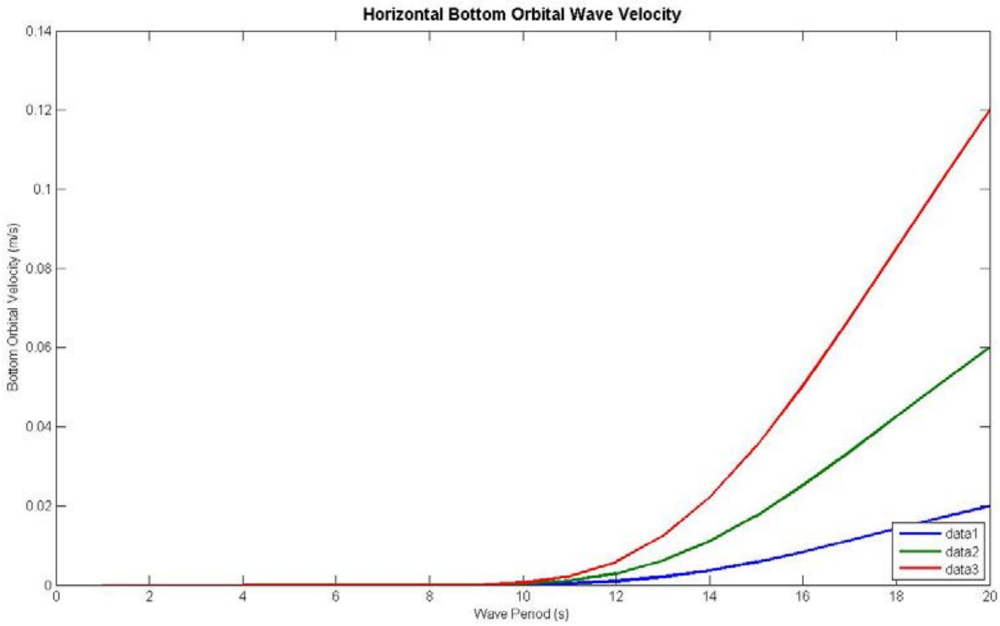

Figure 62 Horizontal Bottom Orbital Velocity Vs. Wave Period - For a depth of 200 m and Wave Heights of 0.5, 1.5 and 3 m respectively.

In shallow water the orbital velocities are predominantly driven by depth and when $\sinh(kh) \approx kh$, the bottom orbital velocity becomes,

$$u_b = a\sqrt{g/h}$$

88

This result can be derived from equation (76) above, the horizontal orbital velocity for a shallow water wave. Letting the $\cos(kx - \omega t)$ term go to 1 as before, we find,

$$u_b = \frac{Ca}{h}$$

89

And from the equation for celerity, C for a shallow water wave we then have,

$$u_b = \frac{(\sqrt{gh})a}{h}$$

90

Shear stress - basic theory

To begin a theoretical treatment of shear stress, it is first examined as a component of stress as performed in (Wright 1995). Stress, τ consists of 3 normal stress components $(\tau_{xx}, \tau_{yy}, \tau_{zz})$ and 6 tangential shear stress components $(\tau_{xy}, \tau_{xz}, \tau_{yx}, \tau_{yz}, \tau_{zx}, \tau_{zy})$. The final two shear stress components, $\tau_{zx}\ and\ \tau_{zy}$ involve the vertical transfers via friction of across and along-shelf momentum. At the bed there are equivalent transfers across the sediment-water interface. These components, τ_{bx} and τ_{by} are the shear stresses that cause the movement of sediment. In regions of the boundary layer that are fully turbulent, the shear stresses are equivalent to the Reynolds stress;

$$\tau_{zx} = -\rho\langle w'u'\rangle$$

91

and

$$\tau_{zy} = -\rho\langle w'v'\rangle$$

92

where u', v' and w' are the turbulently fluctuating components of flow along the x, y and z axes. This can be expressed in terms of the eddy viscosity, ξ and mean currents, $u_c\ and\ v_c$,

$$\tau_{zx} = \rho\xi_{zx}\frac{du_c}{dz}$$

93

and

$$\tau_{zy} = \rho\xi_{zy}\frac{dv_c}{dz}$$

94

There is a thin viscous sub layer adjacent to the bed where flows are slow and molecular viscosity, ν becomes important. (Here, $\nu \sim \xi$) therefore,

$$\tau_{zx} = \rho(\nu + \xi_{zx})\frac{du_c}{dx}$$

95

and

$$\tau_{zy} = \rho(\nu + \xi_{zy})\frac{dv_c}{dx}$$

96

Guided by a theoretical model first presented by Grant and Madsen (1979), the maximum bottom shear stress is derived here from first principles. Assuming Coriolis and convective accelerations are negligible, the fluid motion associated with a combined wave and current (inside and outside the wave boundary layer) is given as,

$$\frac{\partial u}{\partial t} = -\frac{1}{\rho}\nabla p + \frac{\partial}{\partial z}\frac{\tau}{\rho}$$

97

where the pressure, p is given as,

$$p = p_w + p_c$$

98

and the velocity, u is given as,

$$u = u_w + u_c$$

99

The subscripts w and c in equations (98) and (99) refer to the wave induced (unsteady) and current induced (steady) components. This derivation remains valid under the condition that the current values are of the same order of magnitude as the wave orbital velocity values.

The flow kinematics are related to turbulent shear stress by a turbulent eddy viscosity term, ξ. Assuming steady and unidirectional flow, in the region close to the boundary, the eddy viscosity varies linearly with distance from the shear boundary where,

$$\xi = \kappa u_* z.$$

100

Here, κ is Von Karman's constant. This describes the logarithmic velocity profile of a turbulent fluid flow near a boundary, which has no slip. (i.e. the fluid has zero velocity at a solid boundary). κ = 0.41 for clear water, z is the vertical co-ordinate (positive in the upward direction from the boundary) and u_* is the characteristic shear velocity that represents the flow turbulence level. It is given in its generic form using generic shear stress, τ by,

$$u_* = \sqrt{\frac{\tau}{\rho}}$$

101

Using equation (101), the stress divergence in (97) is expressed below as a linear function of velocity,

$$\frac{\partial}{\partial z}\left(\frac{\tau}{\rho}\right) = \frac{\partial}{\partial z}\left(\epsilon\frac{\partial u}{\partial z}\right)$$

102

Substituting equations (102), (99) and (98) into (97) we obtain,

$$\frac{\partial u_w}{\partial t} = -\frac{1}{\rho}\nabla p_c - \frac{1}{\rho}\nabla p_w + \frac{\partial}{\partial z}\epsilon\frac{\partial u_w}{\partial z} + \frac{\partial}{\partial z}\epsilon\frac{\partial u_c}{\partial z}$$

103

From this linear governing equation, we obtain two equations. One concerns the steady current motion and one concerns the unsteady wave motion. Now, two distinct boundary layers exist for the combined wave and current flow. A relationship must be defined between the shear stress and the velocity field, in the region near the seabed.

For turbulent flows due to pure wave motion, as well as unidirectional steady flows, Bottom friction is generally modelled using a quadratic drag law. Again, this is the approach taken by Grant and Madsen (1979). The instantaneous boundary shear stress, τ_b is related to the combined wave and current velocity field, u_{cw} by the following equation,

$$\tau_b = \frac{1}{2}\rho C_{de}(u^2 + v^2)\left[\frac{u}{(u^2 + v^2)^{1/2}}, \frac{v}{(u^2 + v^2)^{1/2}}\right]$$

104

where C_{de} is the effective drag coefficient, associated with the combined wave and current flow (known in Grant and Madsen (1979) as the wave-current friction factor, f_{cw}). In the above equation, u and v are the x and y components of horizontal velocity and,

$$\left[(u^2 + v^2)^{1/2}\right] = |u_{cw}|$$

105

Assuming that the direction of wave propagation is in the positive x direction, u and v are defined as,

$$u = (\sin\theta + (|u_c|/|u_b|)\cos\phi_c)|u_b| \equiv g_x|u_b|$$

106

and

$$v = ((|u_c|/|u_b|)\sin\phi_c)|u_b| \equiv g_y|u_b|$$

107

where $|u_c|$ is the magnitude of the steady current velocity at reference height above the bed and ϕ_c is the angle made by u_c with the direction of wave propagation. This angle only needs to be defined from 0° to 90° in accordance with linear wave theory. $|u_b|$ is the maximum near-bottom orbital velocity as derived previously in this section (equation 80). The maximum orbital velocities there are given by,

$$\bar{u}_b = \frac{a\omega}{\sinh(kh)}.$$

108

Where the general linear expression of horizontal orbital velocity, $\bar{u}_{xo}$ is given by,

$$\bar{u}_{xo} = a\omega \frac{\cosh k(z+h)}{\sinh kh} \cos(kx - \omega t)$$

109

and vertical orbital velocity, $\bar{u}_{zo}$ is,

$$\bar{u}_{zo} = a\omega \frac{\sinh k(z+h)}{\sinh kh} \sin(kx - \omega t).$$

110

i) Constant shear stress contours

Using a Matlab routine (Appendix D), similar to a method detailed in (Orpin 1999), constant shear stress contours are produced on graphs of varying wave height profile vs. period (Figure 63, Figure 64, Figure 65). The constants used to calculate wave number and bottom orbital velocity are; reference height $z_r = 0.2\ m$, current c = 0.35 m/s, bottom roughness $k_b = 0.01\ m$ to correspond to an initial drag coefficient of $C_{de} = 1.5 \times 10^{-3}$ at 1m above the bed when there are no waves.

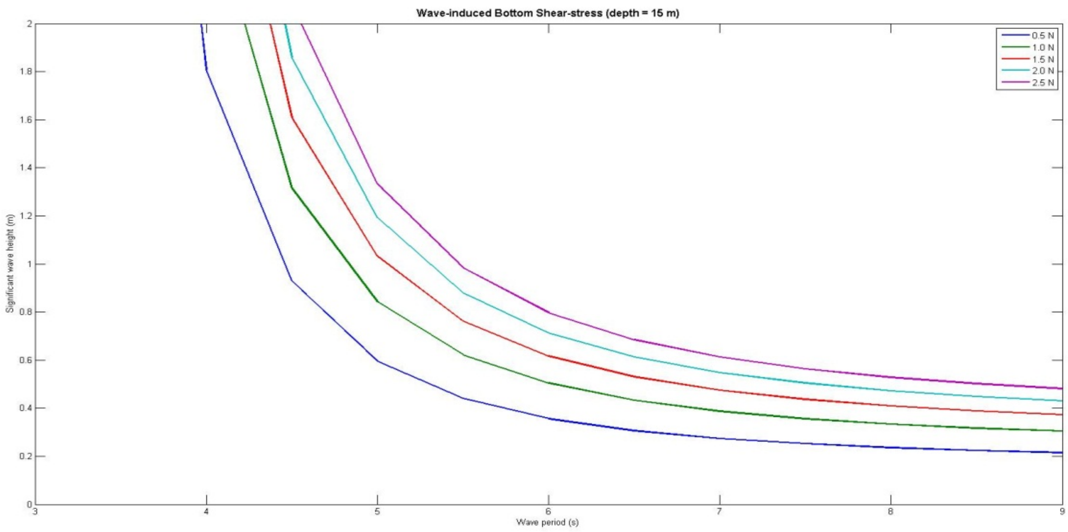

Figure 63 Constant wave-induced bottom shear stress theoretical contours. Significant wave height vs. Wave period.

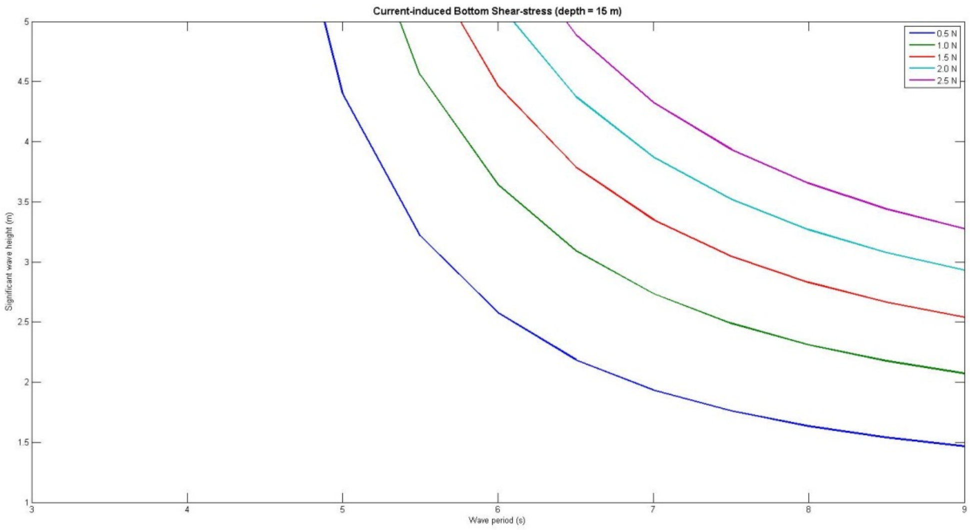

Figure 64 Constant current-induced bottom shear stress theoretical contours. Significant wave height vs. Wave period.

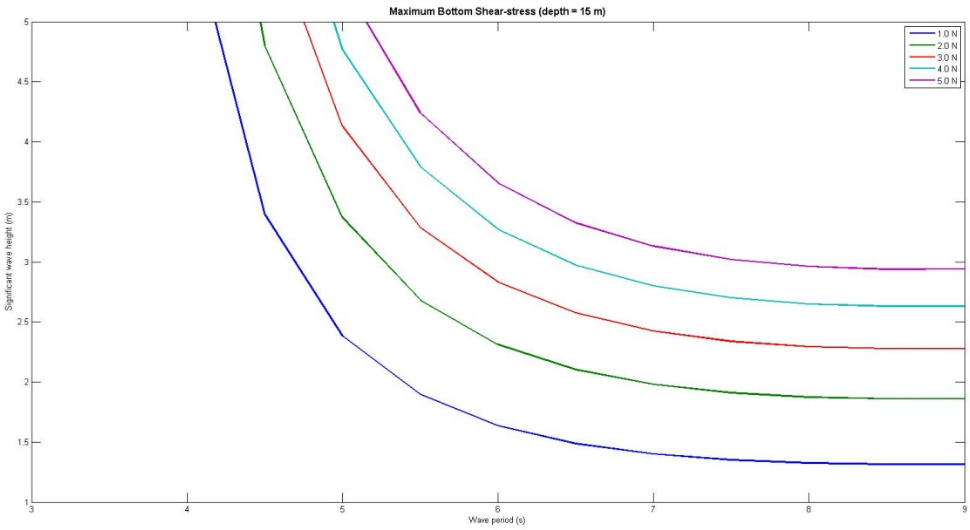

Figure 65 Constant maximum bottom shear stress theoretical contours. Significant wave height vs. Wave period.

Appendix D – Matlab Programs:

resuspension.m (see Chapter 3)

This raw data has been removed

This raw data has been removed

This raw data has been removed

This raw data has been removed

This raw data has been removed

This raw data has been removed

This raw data has been removed

This raw data has been removed

This raw data has been removed

This raw data has been removed

This raw data has been removed

This raw data has been removed

This raw data has been removed

This raw data has been removed

This raw data has been removed

This raw data has been removed

This raw data has been removed

This raw data has been removed

This raw data has been removed

This raw data has been removed

This raw data has been removed

This raw data has been removed

This raw data has been removed

Appendix E - Light Attenuation Theory and Derivations

Introduction

In this section, equations for light attenuation are derived from first principles, incorporating how turbidity varies as a function of depth (Jerlov 1976; Kirk 1977). These equations were used to formulate the model T_{pred} introduced in (Chapter 5), where site-specific attenuation coefficient, α is calculated and then using light, depth and turbidity data, used in an empirical model which approximates depth-averaged turbidity.

The process of light attenuation refers to the combination of absorption and scattering that acts to diminish the intensity of light. Underwater light is attenuated by water itself as well as dissolved and suspended particulate substances. The two main optical properties of water are the absorption and scattering coefficients. These coefficients combine to make up the total attenuation, which is dependent on several parameters. The water quality parameters considered optically important are; coloured dissolved organic matter (yellow substance) (Kirk 1994) and suspended particulate matter (SPM). SPM can be broken into categories of; fixed suspended solids (such as clay, silt and sand) and volatile suspended solids; such as, phytoplankton chlorophyll-a and non-pigmented organic detritus.

(i) The scattering coefficient

The main contributors to the scattering coefficient are suspended particles including sediment and plankton. The water also scatters light itself, however this effect is small compared to that from suspended particles.

(ii) The absorption coefficient:

Water: Water absorbs visible light. It absorbs more strongly at the red end of the spectrum. Water itself is a blue-coloured liquid and strongly scatters blue light. Pure fresh water has similar absorption properties to seawater. The addition of salts does not affect absorption of visible light. Water is the greatest contributor to light absorption in the oceans (i.e. as opposed to sediment, phytoplankton etc.)

Yellow substance: However in inland and coastal waters a very important contributor to absorption is the dissolved yellow substance in the water. This substance is mainly composed of polymerized oxidized phenolics from plant breakdown products. It causes high variability in absorption, whereas absorption by water alone is always constant. The concentrations of yellow substance vary greatly between regions. Its concentration is also temporally variable in inland waters. It is comparatively low in coastal water and negligible in the open ocean.

Phytoplankton: Another significant factor in absorption is phytoplankton. The part of absorption caused by phytoplankton, $a_{phytoplankton}$ is given by the equation,

$$a_{phytoplankton} = n * (absorption\ cross\ section)$$

111

Where n is the number of algal cells per unit volume and the absorption cross section is the amount of light (of wavelength, λ) that an algal cell will remove from a light beam per unit area. The absorption cross section depends on the pigment, size and shape of the algal cells.

Suspended sediment: The final major contributor to absorption is that of suspended sediment, which consists of sand, silt, clay and other minerals and particles in the water column. Not much research has been done on characterizing this contribution to absorption in the ocean.

(iii) Total Attenuation and the attenuation coefficient

The attenuation coefficient, k_d is a combination of the absorption and scattering coefficients. For the purposes of this study, no attempt was made to calculate the absorption and scattering contributions separately as this becomes a complex issue, particularly in shallow coastal waters. Another difficulty lies in differentiating the relative contributions between water, yellow substance, suspended sediment and phytoplankton to overall light attenuation in water. A recent study by Devlin (2009) showed that the attenuation coefficient can be well approximated (to within 3% accuracy) by just using SPM (i.e. suspended sediment and phytoplankton) calculated k_d. Therefore, for the purposes of the light attenuation study (Chapter 5), k_d is approximated by using the contributions from clear water and SPM and not yellow substance, although there is scope to include this in the model for further research.

Derivations of irradiance

Once light enters the water it is attenuated by two distinct physical processes: absorption and scattering. Absorption completely removes the light, whereas scattering alters the direction of light propagation. This increases the probability that it will eventually be absorbed by increasing the path length. Absorption and Scattering describe the attenuation of light through water by interacting in a nonlinear and complex fashion within the radiative transport equations. These equations cannot be solved analytically but there have been numerous models written to solve them numerically.

The general form of underwater irradiance has been shown by numerous field measurements to decay as an inverse exponential to depth. To first order and in the absence of strong discontinuities in water quality, PAR (Photosynthetically Active Radiation) measurements (400-700 nm) can be well described by Beer-Lambert's Law,

$$I_z = I_{z0} e^{-k_d (z - z_0)} \tag{112}$$

where I_{z0} and I_z are the irradiances at depths z_0 (let it be water surface i.e. $z_0 = 0$ m) and z, and k_d is the diffuse attenuation coefficient for PAR. The Beer Lambert law combines Lambert's Law and Beer's law to state that absorbance is correlated to both the sample thickness and concentration. We shall derive from first principles a conceptual version of the law and then take the equation further as a real-case examination.

Let us first imagine an infinitesimally thin slab of area, A and thickness, dz and illuminate it at right angles by a parallel beam of monochromatic light. We assume the particles in the layer (of concentration, N) have an absorption cross section, σ perpendicular to the path of light. Also assume dz is small enough that the particles in the layer do not obstruct each other when viewed along the z axis, which is parallel to the direction of light.

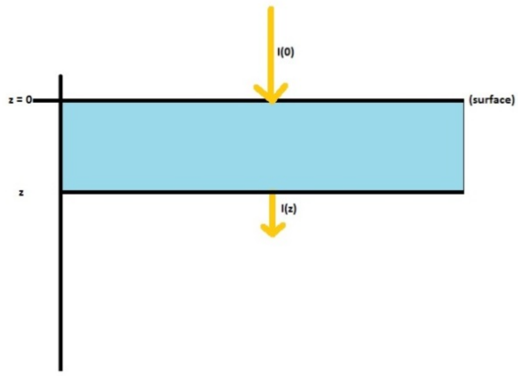

Figure 66 Diagram showing attenuation of monochromatic light beam.

Some of the light will be absorbed, most of the rest will be transmitted and a very small amount will be scattered, mostly in the forward direction. The fraction of radiant flux / photons that is absorbed divided by the layer thickness, dz is the absorption coefficient, a. The fraction of radiant flux that is scattered divided by dz is the scattering coefficient, b. However, in this simplified case we shall negate scattering and assume only absorption occurs to attenuate the light beam.

(i) Case 1: SPC not dependant on depth (derivation of Beer-Lambert's Law)

This case is used in (Chapter 5) to predict turbidity given light data. Let I be the light intensity entering the layer, dI is the change in light intensity upon exiting the layer. In other words, the intensity entering the slab, I will be reduced by a factor, β giving the intensity leaving the slab, dl

$$dI(z) = \beta I(z)$$

113

The fraction of photons absorbed, β is the total area of the particles divided by the total area of the slab i.e.

$$\beta = \frac{\sigma AN\, dz}{A} = \sigma N\, dz = -\kappa\, dz$$

114

we constrain β from $-1\ to\ 0$ and define κ as the attenuation coefficient. Now substituting into equation (113) and rearranging we obtain the simple differential equation,

$$\frac{dI(z)}{dz} = -\kappa\, I(z)$$

115

Rearranging to solve we have,

$$\frac{dI(z)}{I(z)} = -k\, dz$$

116

And taking the integral of both sides from *z = 0* to some depth, *z* we find,

$$\int_{z=0}^{z} \frac{1}{I(z)} dI(z) = -\int_{z=0}^{z} \kappa \, dz$$

117

taking the limits,

$$\ln I(z) - \ln I(0) = -\kappa z$$

118

and expressing as,

$$ln\left(\frac{I(z)}{I_0}\right) = -\kappa z$$

119

Then taking the exponent of both sides we obtain the solution,

$$\frac{I(z)}{I_0} = e^{-\kappa z}$$

120

or in the usual form as Beer-Lamberts law,

$$I = I_0 e^{-\kappa z}$$

121

We know that κ is a function of concentration, i.e.

$$\kappa = \sigma N$$

122

By substituting equation 122 into equation 121 we obtain,

$$I = I_0 e^{-\sigma N z}$$

123

(ii) Case 2: Concentration as a linear function of depth

In this case we let I represent the intensity across the PAR waveband entering the ocean surface at $z = 0$, dI is the change in PAR light intensity at some depth, z. We assume here that the concentration of particles, N is a function depth so that for a simple linear case, N may be given as

$$N = \gamma z + \delta$$

124

(where δ accounts for the concentration at the surface at $z = 0$ and γ is some coefficient of depth)

Therefore substituting into equation (122),

$$\kappa_{zlinear} = \sigma(\gamma z + \delta)$$

125

And letting $k_\gamma = \sigma\gamma$ and $\kappa_\delta = \sigma\delta$ we have,

$$\kappa_{zlinear} = \kappa_\gamma z + \kappa_\delta$$

126

Now we obtain a new differential equation,

$$dI(z) = \kappa(z)I(z)dz$$

127

Rearrange to solve,

$$\frac{dI}{I} = -\kappa_\gamma z + \kappa_\delta \, dz$$

128

$$\int_{z=0}^{z} \frac{1}{I} dI = \int_{z=0}^{z} -(k_\gamma z - \kappa_\delta) \, dz$$

129

$$\ln I(z) - \ln I(0) = \left[\frac{-\kappa_\gamma z^2}{2} + \kappa_\delta z\right] + \left[\frac{-\kappa_\gamma 0^2}{2} + \kappa_\delta z\right]$$

130

$$ln\left(\frac{I}{I_0}\right) = \frac{-\kappa_\delta \kappa_\gamma z^2}{2} + \kappa_\delta z + C$$

131

With the new solution,

$$I = I_0 e^{\left(\frac{-\kappa_\delta \kappa_\gamma z^2}{2} + \kappa_\delta z + C\right)}$$

132

(iii) Case 3: Concentration as an exponential function of depth

We assume here that the concentration of particles, N is a decaying exponential function of depth so that N is be given as

$$N = e^{-(\gamma z+\delta)}$$

133

Therefore substituting into equation (122) we have,

$$\kappa_{zexp} = \sigma e^{-(\gamma z+\delta)}$$

134

Now we obtain a new differential equation,

$$dI(z) = \kappa_{zexp} I(z) dz$$

135

Rearrange to solve,

$$\frac{dI}{I} = \sigma e^{-(\gamma z+\delta)}\, dz$$

136

$$\int_{z=0}^{z} \frac{1}{I} dI = \int_{z=0}^{z} \sigma e^{-(\gamma z+\delta)}\, dz$$

137

$$\int_{z=0}^{z} \frac{1}{I} dI = \int_{z=0}^{z} \sigma e^{-\gamma z} e^{\delta}\, dz$$

138

$$\int_{z=0}^{z} \frac{1}{I} dI = \sigma e^{\delta} \int_{z=0}^{z} e^{-\gamma z}\, dz$$

139

$$\int_{z=0}^{z} \frac{1}{I} dI = \sigma e^{\delta} \int_{z=0}^{z} (e^{z})^{-\gamma} \ dz$$

140

$$\ln I(z) - \ln I(0) = \frac{-\sigma e^{\delta}}{\gamma} \ \ ([(e^{z})^{-\gamma}] - \ [(e^{0})^{-\gamma}])$$

141

$$ln\left(\frac{I}{I_0}\right) = \frac{-\sigma e^{\delta}}{\gamma}((e^{z})^{-\gamma} - 1)$$

142

With the analytical solution,

$$I = I_0 e^{\left\{\frac{-\sigma e^{\delta}}{\gamma}((e^{z})^{-\gamma}-1)\right\}}$$

143

We now have three theoretical cases of how suspended sediment concentration may vary with depth. Case 1 has been implemented in (Chapter 5). Case 2 and 3 have the potential to be investigated for future work with application to real light data. Applications may be held for situations where the concentration of sediment with depth is unusual, such as during a river plume.

REFERENCES

Grant WD, Madsen OS (1979) Combined Wave and Current Interaction with a Rough Bottom. Journal of Geophysical Research 84:1797-1808

Jerlov NG (1976) Marine optics. Elsevier Scientific Pub. Co, Amsterdam

Kirk JTO (1977) Attenuation of Light in Natural Waters. Aust J Mar Freshwater Res, 28:497-508

Kirk JTO (1994) Light and photosynthesis in aquatic ecosystems. Cambridge University Press, Cambridge [England]

Nittrouer CA, Wright LD (1994) Transport of particles across continental shelves. Rev Geophys 32:85-113

Soulsby RL (1987) Calculating bottom orbital velocity beneath waves. Coastal Engineering 11:371-380

Wiberg PL, Sherwood CR (2008) Calculating wave-generated bottom orbital velocities from surface-wave parameters. Computers and Geosciences 34:1243-1262

Wright LD (1995) Morphodynamics of Inner Continental Shelves. CRC Press, Boca Raton

REFERENCES

Abal EG, Dennison WC (1996) Seagrass depth range and water quality in southern Moreton bay, Queensland, Australia. Marine and Freshwater Research 47:763-771

Anthony KRN (2000) Enhanced particle-feeding capacity of corals on turbid reefs (Great Barrier Reef, Australia). Coral Reefs 19:59-67

Anthony KRN, Fabricius KE (2000) Shifting roles of heterotrophy and autotrophy in coral energetics under varying turbidity. Journal of Experimental Marine Biology and Ecology 252:221-253

Anthony KRN, Ridd PV, Orpin AR, Larcombe P, Lough J (2004) Temporal variation of light availability in coastal benthic habitats: Effects of clouds, turbidity, and tides. Limnology and Oceanography 49:2201-2211

Belperio AP (1979) The combined use of wash load and bed material load rating curves for the calculation of total load: An example from the Burdekin River, Australia. Catena 6:317-329

Belperio AP (1983) Terrigenous sedimentation in the central Great Barrier Reef lagoon: a model from the Burdekin region. BMR Journal of Australian Geology and Geophysics 8:179-190

Belperio AP (1988) Terrigenous and carbonate sedimentation in the Great Barrier Reef province. Elsevier, Amsterdam

Brodie J, Fabricius K, De'ath G, Okaji K (2005) Are increased nutrient inputs responsible for more outbreaks of crown-of-thorns starfish? An appraisal of the evidence. Marine Pollution Bulletin 51:266-278

Brown BE (1997) Disturbances to reefs in recent times. In: Birkeland C (ed) Life and Death of Coral Reefs. Chapman and Hall Inc., New York, pp354-385

Brown SH (2009a) Multiple Linear Regression Analysis: A Matrix Approach with MATLAB. Alabama Journal of Mathematics Spring/Fall 2009:3

Brown SH (2009b) Multiple linear regression analysis: a matrix approach with Matlab. Alabama Journal of Mathematics Spring/Fall:3

Browne NK, Smithers SG, Perry CT (2010) Geomorphology and community structure of Middle Reef, central Great Barrier Reef, Australia: an inner-shelf turbid zone reef subject to episodic mortality events. Coral Reefs 29:683-689

Browne NK, smithers SG, Perry CT (2012) Coral reefs of the turbid inner-shelf of the Great Barrier Reef, Australia: an environmental and geomorphic perspective on their occurrence, composition and growth. . Earth-Science Reviews 115:1-20

Bryce S, Larcombe P, Ridd PV (1998) The relative importance of landward-directed tidal sediment transport versus freshwater flood events in the Normanby River estuary, Cape York Peninsula, Australia. Marine Geology 149:55-78

Bunt J, Larcombe P, Jago CF (1999) Quantifying the response of optical backscatter devices and transmissometers to variations in suspended particulate matter (SPM). Continental Shelf Research 19:1199-1220

Capelin M, Kohn P, Hoffenberg P (1998) Land use, land cover and land degradation in the catchment of Moreton Bay. The University of Queensland, School of Marine Science, Brisbane

Chalker BE (1981) Simulating light-saturation curves for photosynthesis and calcification by reef-building corals. Marine Biology 63:135-141

Chartrand KM, Rasheed MA, Sankey TL (2008) Deepwater seagrass dynamics in Hay Point - measuring variability and monitoring impacts of capital dredging: Final Report. Ports Corporation of Queensland 43

Conner CS, De Visser AM (1992) A laboratory investigation of particle size effects on an optical backscatterance sensor. Marine Geology 108:151-159

Cooper TF, Ridd PV, Ulstrup KE, Humphrey C, Slivkoff M, Fabricius KE (2008) Temporal dynamics in coral bioindicators for water quality on coastal coral reefs of the Great Barrier Reef. Marine and Freshwater Research 59:703-716

Davies-Colley RJ, Smith DG (2001) Turbidity, suspended sediment, and water clarity: A review. Journal of the American Water Resources Association 37:1085-1101

De'ath G, Fabricius K (2008) Water Quality of the Great Barrier Reef: Distributions, Effects on Reef Biota and Trigger Values for the Protection of Ecosystem Health

De’ath G, Fabricius KE, Sweatman H, Puotinen M (2012) The 27–year decline of coral cover on the Great Barrier Reef and its causes. Proceedings of the National Academy of Sciences

Delandmeter P, Lewis SE, Lambrechts J, Deleersnijder E, Legat V, Wolanski E (2015) The transport and fate of riverine fine sediment exported to a semi-open system. Estuarine, Coastal and Shelf Science 167, Part B:336-346

Dennison WC, Orth RJ, Moore KA, Stevenson JC, Carter V, Kollar S, Bergstrom PW, Batiuk RA (1993) Assessing Water Quality with Submersed Aquatic Vegetation. Bioscience 43:86-94

DeVantier LM, De’ath G, Turak E, Done TJ, Fabricius KE (2006) Species richness and community structure of reef-building corals on the nearshore Great Barrier Reef. Coral Reefs 25:329-340

Devlin MJ, Barry J, Mills DK, Gowen RJ, Foden J, Sivyer D, Tett P (2008) Relationships between suspended particulate material, light attenuation and Secchi depth in UK marine waters

Dubinsky Z (1990) Evolution and zoogeography of coral reefs. In: Dubinsky Z (ed) Ecosystems of the World - Coral Reefs. Elsevier, Amsterdam; New York, pp1-9

Dunbar G (2003) Massive siliciclastic discharge to slopes of the Great Barrier Reef Platform during sea-level transgression: constraints from sediment cores between 15°S and 16°S latitude and possible explanations. Sedimentary Geology 162:141-158

Dunbar GB, Dickens GR, Carter RM (2000) Sediment flux across the Great Barrier Reef Shelf to the Queensland Trough over the last 300 ky

Dupont L (2003) Development of an in-situ fluorometer for the study of organic materials on a fringing reef. James Cook University,

Emery WJ, Thomson RE (1998) Data analysis methods in physical oceanography. Pergamon, New York

Fabricius KE (2005) Effects of terrestrial runoff on the ecology of corals and coral reefs: Review and synthesis. Marine Pollution Bulletin 50:125-146

Fabricius KE, Wolanski E (2000) Rapid smothering of coral reef organisms by muddy marine snow. Estuarine, Coastal and Shelf Science 50:115-120

Fabricius KE, Logan M, Weeks S, Brodie J (2014) The effects of river run-off on water clarity across the central Great Barrier Reef. Marine Pollution Bulletin 84:191-200

Fabricius KE, De'ath G, Humphrey C, Zagorskis I, Schaffelke B (2012) Intra-annual variation in turbidity in response to terrestrial runoff on near-shore coral reefs of the Great Barrier Reef. Estuarine, Coastal and Shelf Science 59:703-716

Furnas M (2003) Catchments and corals: terrestrial runoff to the Great Barrier Reef. Australian Institute of Marine Science, Townsville, Qld

GBRMPA (2010) Water quality guidelines for the Great Barrier Reef Marine Park. Great Barrier Reef Marine Park Authority, Townsville

GBRMPA (2012) Extreme Weather and the Great Barrier Reef, Govt. report http://www.gbrmpa.gov.au/managing-the-reef/threats-to-the-reef/extreme-weather/extreme-weather-and-the-great-barrier-reef-report

Gilmour J (1999) Experimental investigation into the effects of suspended sediment on fertilisation, larval survival and settlement in a scleractinian coral. Marine Biology 135:451-462

Goatley CHR, James Cook University. School of M, Tropical B (2013) The ecological role of sediments on coral reefs.

Gordon HR (1989) Can the Lambert-Beer law be applied to the diffuse attenuation coefficient of ocean water? Limnology and Oceanography 34:1389-1409

Grant WD, Madsen OS (1979) Combined Wave and Current Interaction with a Rough Bottom. Journal of Geophysical Research 84:1797-1808

Grant WD, Madsen OS (1982) Movable Bed Roughness in Unsteady Oscillatory Flow. J Geophys Res 87:469-481

Hopley D (1982) The geomorphology of the Great Barrier Reef: Quaternary development of coral reefs. John Wiley, New York

Hopley D, Smithers S, Parnell KE (2007) The geomorphology of the Great Barrier Reef: development, diversity, and change. Cambridge University Press, Cambridge

Hopley D, Slocombe AM, Muir F, Grant C (1983) Nearshore fringing reefs in north Queensland. Coral Reefs 1:151-160

Jerlov NG (1976) Marine optics. Elsevier Scientific Pub. Co, Amsterdam

Johnson PR, Neil DT (1998) The corals of Moreton Bay: living with extremes. The University of Queensland, School of Marine Science, Brisbane

Kirk JTO (1977) Attenuation of Light in Natural Waters. Aust J Mar Freshwater Res, 28:497-508

Kirk JTO (1994) Light and photosynthesis in aquatic ecosystems. Cambridge University Press, Cambridge [England]

Kirk JTO (2010) Light and Photosynthesis in Aquatic Ecosystems. Cambridge University Press, Cambridge

Kleypas JA (1999) Environmental Limits to Coral Reef Development: Where Do We Draw the Line? American Zoologist 39:146-159

Lambrechts J, Humphrey C, McKinna L, Gourge O, Fabricius KE, Mehta AJ, Lewis S, Wolanski E (2010) Importance of wave-induced bed liquefaction in the fine sediment budget of Cleveland Bay, Great Barrier Reef. Estuarine, Coastal and Shelf Science 89:154-162

Larcombe P, Woolfe KJ (1999a) Increased sediment supply to the Great Barrier Reef will not increase sediment accumulation at most coral reefs. Coral Reefs 18:163-169

Larcombe P, Woolfe KJ (1999b) Terrigenous sediments as influences upon Holocene nearshore coral reefs, central Great Barrier Reef, Australia. Australian Journal of Earth Sciences: An International Geoscience Journal of the Geological Society of Australia 46:141 - 154

Larcombe P, Woolfe KJ, Cooperative Research Centre for Ecologically Sustainable Development of the Great Barrier R (1995a) Great Barrier Reef: terrigenous sediment flux and human impacts. CRC Reef Research Centre, Townsville, Qld

Larcombe P, Costen A, Woolfe KJ (2001) The hydrodynamic and sedimentary setting of nearshore coral reefs, central Great Barrier Reef shelf, Australia: Paluma Shoals, a case study. Sedimentology 48:811-835

Larcombe P, Ridd PV, Prytz A, Wilson B (1995b) Factors controlling suspended sediment on inner-shelf coral reefs, Townsville, Australia. Coral Reefs 14:163-171

Liu W-C, Wu R-S, Wu EM-Y, Chang Y-P, Chen W-B (2010) Using water quality variables to predict light attenuation coefficient: case study in Shihmen Reservoir. Paddy and Water Environment 8:267-275

Logan M, Fabricius K, Weeks S, Canto M, Noonan S, Wolanski E, Brodie J (2013) The Relationship between Burdekin River discharges and photic depth in the central Great Barrier Reef. Report to the National Environmental Research Program. Reef and Rainforest Research Centre Limited, Cairns 29pp

Lou J, Ridd PV (1997) Modelling of Suspended Sediment Transport in Coastal Areas Under Waves and Currents. Estuarine, Coastal and Shelf Science 45:1-16

Ludwig KA, Hanes DM (1990) A laboratory evaluation of optical backscatterance suspended solids sensors exposed to sand-mud mixtures. Marine Geology 94:173-179

Lybolt M, Neil D, Zhao J, Feng Y, Yu K-F, Pandolfi J (2011) Instability in a marginal coral reef: the shift from natural variability to a human-dominated seascape. Frontiers in Ecology and the Environment 9:154-160

Macdonald RK, Ridd PV, Whinney JC, Larcombe P, Neil DT (2013) Towards environmental management of water turbidity within open coastal waters of the Great Barrier Reef. Marine Pollution Bulletin 74:82-94

Maxwell WGH (1968) Atlas of the Great Barrier Reef. Elsevier, Amsterdam

McCulloch M, Fallon S, Wyndham T, Hendy E, Lough J, Barnes D (2003a) Coral record of increased sediment flux to the inner Great Barrier Reef since European settlement. Nature 421:727-730

McCulloch M, Fallon S, Wyndham T, Hendy E, Lough J, Barnes D (2003b) Coral record of increased sediment flux to the inner Great Barrier Reef since European settlement

Mobley CD (1994) Light and Water: Radiative Transfer in Natural Waters. Academic Press

Mobley CD, Gentili B, Gordon HR, Jin Z, Kattawar GW, Morel A, Reinersman P, Stamnes K, Stavn RH (1993) Comparison of numerical models for computing underwater light fields. Appl Opt 32:7484-7504

Moore KA, Neckles HA, Orth RJ (1996) Zostera marina (eelgrass) growth and survival along a gradient ofnutrients and turbidity in the lower Chesapeake Bay. Marine Ecology Progress Series 142:247-259

Moss A, Queensland. Dept. of E, Heritage, Queensland. Dept. of Primary I (1993) A Preliminary assessment of sediment and nutrient exports from Queensland coastal catchments. Queensland Dept. of Environment and Heritage, Brisbane

Neil DT (1996) Sediment concentrations in streams and coastal waters in the North Queensland humid tropics: Land use, rainfall and wave resuspension contributions. In: Hunter HM, Eyles AG, Rayment GE (eds) Downstream effects of land use. Dept. Natural Resources, Brisbane, pp97-101

Neil DT (1998) Moreton Bay and its catchment: landscape and seascape, development and degradation. The University of Queensland, School of Marine Science, Brisbane

Neil DT, Orpin AR, Ridd PV, Yu B (2002) Sediment yield and impacts from river catchments to the Great Barrier Reef lagoon. Marine and Freshwater Research 53:733-752

Nittrouer CA, Wright LD (1994) Transport of particles across continental shelves. Rev Geophys 32:85-113

Orpin AR, Ridd PV (2012) Exposure of inshore corals to suspended sediments due to wave-resuspension and river plumes in the central Great Barrier Reef: A reappraisal. Continental Shelf Research 47:55-67

Orpin AR, Ridd PV, Stewart LK (1999) Assessment of the relative importance of major sediment-transport mechanisms in the central Great Barrier Reef lagoon. Australian Journal of Earth Sciences 46:883-896

Orpin AR, Ridd PV, Thomas S, Anthony KRN, Marshall P, Oliver J (2004) Natural turbidity variability and weather forecasts in risk management of anthropogenic sediment discharge near sensitive environments. Marine Pollution Bulletin 49:602-612

Palmer SE, Perry C, Smithers SG, Gulliver P (2010) Internal structure and accretionary history of a nearshore, turbid-zone coral reef: Paluma Shoals, central Great Barrier Reef, Australia. Marine Geology 276:14-29

Pandolfi JM, Bradbury RH, Sala E, Hughes TP, Bjorndal KA, Cooke RG, McArdle D, McClenachan L, Newman MJH, Paredes G, Warner RR, Jackson JBC (2003) Global trajectories of the long-term decline of coral reef ecosystems. Science 301:955-958

Perry CT, Smithers SG (2006) Taphonomic signatures of turbid-zone reef development: examples from Paluma Shoals and Lugger Shoal, inshore central Great Barrier Reef, Australia. Coral Reefs 28:941-948

Perry CT, Smithers S (2009) Stabilisation of intertidal cobbles and gravels by Goniastrea aspera: an analogue for substrate colonisation during marine transgressions? Coral Reefs 28:805-806

Perry CT, Smithers SG (2010) Evidence for the episodic “turn on” and “turn off” of turbid-zone coral reefs during the late Holocene sea-level highstand. Geology 38:119-122

Perry CT, Smithers SG, Johnson KG (2009a) Long-term coral community records from Lugger Shoal on the terrigenous inner-shelf of the central Great Barrier Reef, Australia. Coral Reefs 28:941-948

Perry CT, Smithers SG, Johnson KG (2009b) Long-term coral community records from Lugger Shoal on the terrigenous inner-shelf of the central Great Barrier Reef, Australia. Coral Reefs 28:941-948

Perry CT, Gulliver P, Palmer SE, Smithers SG (2010) Internal structure and accretionary history of a nearshore, turbid-zone coral reef: Paluma Shoals, central Great Barrier Reef, Australia. Marine Geology 276:14-29

Perry CT, Smithers SG, Gulliver P, Browne NK (2012) Evidence of very rapid reef accretion and reef growth under high turbidity and terrigenous sedimentation. Geology 40:719-722

Perry CT, Smithers SG, Palmer SE, Larcombe P, Johnson KG (2008) 1200 year paleoecological record of coral community development from the terrigenous inner shelf of the Great Barrier Reef. Geology 36:691-694

REEFPLAN (2013) Reef water quality protection plan 2013 - For the Great Barrier Reef World Heritage Area and adjacent catchments. In: Cabinet DoPa (ed). Reef Water Quality Protection Plan Secretariat, Brisbane

Ridd P (2010) A Review of the Exposure of Corals to Suspended Sediments in the inshore Great Barrier Reef. School of Engineering and Physical Sciences, James Cook University, Townsville, QLD

Ridd P, Larcombe P (1994) Biofouling control for optical backscatter suspended sediment sensors. Marine Geology 116:255-258

Rodgers CS (1990) Responses of coral reefs and reef organisms to sedimentation. Marine Ecology Progress Series 62:185-202

Sahl LE, Marsden MAH (1987) Shelf sediment dispersal during the dry season, Princess Charlotte Bay, Great Barrier Reef, Australia. Continental Shelf Research 7:1139-1159

Satlantic L (2004) Operation Manual for the HyperOCR, Halifax, Nova Scotia

Saulquin B, Hamdi A, Gohin F, Populus J, Mangin A, d'Andon OF (2013) Estimation of the diffuse attenuation coefficient KdPAR using MERIS and application to seabed habitat mapping. Remote Sensing of Environment 128:224-233

Schaffelke B, Thompson A, Carleton J, Davidson J, Doyle J, Furnas M, Gunn K, Skuza M, Wright M, Zagorskis I (2009) Reef Rescue Monitoring Program Final Report of AIMS Activities 2008/2009. Australian Institute of Marine Science

Signell RP, Beardsley RC, Graber HC, Capotondi A (1990) Effect of Wave-Current Interaction on Wind-Driven Circulation in Narrow, Shallow Embayments. Journal of Geophysical Research 95:9671-9678

Smithers S, Larcombe P (2003) Late Holocene initiation and growth of a nearshore turbid-zone coral reef: Paluma Shoals, central Great Barrier Reef, Australia. Coral Reefs 22:499-505

Soulsby RL (1987) Calculating bottom orbital velocity beneath waves. Coastal Engineering 11:371-380

Stafford-Smith MG (1993) Sediment-rejection efficiency of 22 species of Australian scleractinian corals. Marine Biology 115:229-243

Storlazzi C, Norris B, Rosenberger K (2015) The influence of grain size, grain color, and suspended-sediment concentration on light attenuation: Why fine-grained terrestrial sediment is bad for coral reef ecosystems. Coral Reefs 34:967-975

Trimarchi S, Keane J (2007) Port of Hay Point apron area and departure path capital dredging project: environmental review. Ports Corporation of Queensland, Brisbane

Tucker MJ (1991) Waves in ocean engineering: measurement, analysis, interpretation. E. Horwood, New York

Umbgrove JHF (1947) Coral reefs of the East Indies. Geol Soc Am Bull 58:729-777

Waltham N, Mckenna S, York P, Devlin M, Campbell S, Rasheed MA, Da Silva E, Petus C, Ridd P (2015) Port of Mackay and Hay Point Ambiet Marine Water Quality Monitoring Program. Centre for Tropical Water and Aquatic Ecosystem Research, James Cook University

Weeks S, Werdell P, Schaffelke B, Canto M, Lee Z, Wilding J, Feldman G (2012) Satellite-Derived Photic Depth on the Great Barrier Reef: Spatio-Temporal Patterns of Water Clarity. Remote Sensing 4:3781-3795

Wiberg PL, Sherwood CR (2008) Calculating wave-generated bottom orbital velocities from surface-wave parameters. Computers and Geosciences 34:1243-1262

Wolanski E, De'Ath G (2005) Predicting the impact of present and future human land-use on the Great Barrier Reef. Estuarine, Coastal and Shelf Science 64:504-508

Wolanski E, Delesalle B, Gibbs R (1994) Carbonate mud in Mataiva Atoll, French Polynesia: Suspension and export. Marine Pollution Bulletin 29:36-41

Wolanski E, Richmond RH, McCook L (2004) A model of the effects of land-based, human activities on the health of coral reefs in the Great Barrier Reef and in Fouha Bay, Guam, Micronesia. Journal of Marine Systems 46:133-144

Wolanski E, Fabricius KE, Cooper TF, Humphrey C (2008) Wet season fine sediment dynamics on the inner shelf of the Great Barrier Reef. Estuarine, Coastal and Shelf Science 77:755-762

Wright LD (1995) Morphodynamics of Inner Continental Shelves. CRC Press, Boca Raton